Investigating Mechanical Interactions of Cells with Their Environment

by

Sara Molladavoodi

A thesis
presented to the University of Waterloo
in fulfillment of the
thesis requirement for the degree of
Doctor of Philosophy
in
Mechanical Engineering

Waterloo, Ontario, Canada, 2015

Author's Declaration

I hereby declare that I am the sole author of this thesis. This is a true copy of the thesis, including any required final revisions, as accepted by my examiners.

I understand that my thesis may be made electronically available to the public.

Abstract

Recent studies have shown that cells not only respond to chemical signals such as growth factors or chemoattractants, but they are also capable of detecting mechanical stimuli and responding to them. The process during which these mechanical stimuli are detected and transferred to chemical signals, that cells can process, is called mechanotransduction. The mechanical stimuli that can affect cells can be either an external stimulus applied to cells, such as shear flow or cyclic compression and tension, or they can be linked to the mechanical properties of their substrates. One of the mechanical properties of a substrate that can affect cellular behavior is known to be stiffness, mostly measured by elastic modulus. Stiffness influences a wide variety of cellular behaviour such as cell shape, adhesion to substrate, proliferation, and differentiation.

Anchorage dependent cells are in direct contact with their environment, which then leads to complicated interactions. These interactions can be both biological and mechanical. In the current research, the mechanical interactions are often called the "mechanical responses" of cells. For anchorage-dependent migrating cells, mechanical responses can be the substrate deformations induced by the forces generated by cells also called cell traction forces. These mechanical responses can be studied in three levels of complexity. The first level is when cells are cultured on a 2D matrix and responses are also studied in 2D. The second level of complexity is when cells are cultured on a 2D matrix and the biological behaviour of cells, such as growth or migration, is studied in 2D, however, the mechanical responses of cells are studied in 3D, meaning that not only in plane deformation and forces are studied, but out of plane ones are also assessed. The third level of complexity is when cells are cultured inside a 3D matrix and both biological responses and mechanical responses are studied in 3D.

In the current research, the second level of complexity is chosen. After testing different types of materials, polyacrylamide (PAAm) was chosen as the model biomaterial. Following mechanical characterization of PAAm samples, substrates were prepared with three different elastic moduli. Both biological responses and mechanical responses of human corneal epithelial cells (HCECs) were studied. For biological responses, cell viability, activation, adhesion molecules, apoptosis and migration behaviour were studied. For mechanical responses, confocal microscopy in junction with image processing technique, digital volume correlation (DVC), was used to measure cell induced deformations.

It was found that elastic modulus, as a mechanical stimulus, affects not only biological behaviour of cells, but also their mechanical behaviour. Decreasing elastic modulus led to significantly lower migration speed of HCECs, slightly higher number of apoptotic cells as well as significantly higher number of necrotic cells. Furthermore, while no significant changes in adhesion molecules occurred, dramatic

changes in cytoskeleton structure was seen on cells cultured on compliant matrices. Also, the DVC code was capable of detecting both in plane and out of plane deformations from confocal images. It was found that substrate elastic modulus can change the pattern of displacements on compliant substrate compared to stiff ones. Results of the present study suggest that the deformation pattern and magnitude does not change over the body of cells and that they are rather similar in the leading edge and trailing edge. Deformation under the nucleus was also assessed and for compliant and stiff substrates were present while no deformation was found under the cells cultured on medium stiffness substrates. It was also speculated that mechanical interaction of HCECs with their substrates can be more complicated than currently known and cells seem to be able to exert moments on their substrate as well as forces.

Results presented in this thesis demonstrate that HCECs are sensitive to substrate stiffness and elastic modulus can affect their behaviour. Furthermore, considering the complexity of HCECs mechanical interaction with their substrates, it is critical to study both biology and mechanics for full comprehension of cellular interaction with the ocular environment.

Acknowledgements

I would like to express my sincere gratitude to my supervisors, Dr. HJ Kwon, Dr. John Medley, and Dr. Maud Gorbet. Not only did they give me the opportunity of doing this research, but also supported me endlessly throughout the years and patiently thought me both research and life lessons. I will forever be indebted by their guidance.

I would like to acknowledge my thesis examining committee members, Dr. Craig Simmons from University of Toronto, Dr. Wayne Brodland, Dr. Hamid Jahed, and Dr. Naveen Chandrashekar from University of Waterloo for taking the time to review my thesis and provide valuable feedback.

I would also like to acknowledge Natural Sciences and Engineering Research Council of Canada (NSERC; Discovery Grants of my supervisors), University of Waterloo and the Department of Mechanical and Mechatronics Engineering for financial support of the project.

I would like to extend special thanks to technical staff at confocal facilities at University of Waterloo, especially Dale Weber and Adrienne Boone, for assisting me to perform my complicated and out of norm experiments.

My PhD research allowed me to experience the excitement of working on a multidisciplinary area. I was fortunate enough to work with many talented, determined, and truly inspiring individuals in different research labs with different academic backgrounds that made my experience in UW extraordinary and fulfilling. I would like to thank my colleagues in Material Interaction with Biological Systems (MIBS) lab, Laura Doody, Dr. Tidimogo Gaamangwe, Sara Luck Williams, (soon to be Dr.) Cameron Postnikoff, (again, soon to be Dr.) Rob Pintwala, Shahabedin Eslami, and Saman Mohammadi who were always willing to selflessly help me. I wish you guys all the best in all aspects of your life. Special thanks to biointegrative mechanics lab members specifically Yougun Han, Jiwon Lee, and Tong Liu for their assistance. I have also made lifelong friends through my research, Allan Rogalsky, Homeyra Pourmohammadali, and Zeinab Jahed. I thank you guys for all the long discussions we had and for always being full of ideas and creativity.

Here is where the words fall short. I cannot thank my family enough. Mom, dad, I am here today because of you. Thank you for always having faith in me, even when I didn't believe in myself, for always inspiring me to work hard and be passionate, and for constantly encouraging me to be a better person. My brother and his wife, Saeid and Somayeh. You are my role models and best friends, and I know, no matter what happens, I can count on you. Thank you for always being there for me. My husband's parents, Reza and Shirin, thank you for your constant support and words of encouragement.

The biggest thank you goes to my husband, Nima, who is the nicest, the most honest and the most patient person I have ever met in my life. You are more than a friend to me in this journey, and you know I couldn’t have done this without you. Thanks for giving me courage and confidence, for your endless support, for your patience, and for motivating me, everyday, to look forward no matter what happens.

*To **Nima***

Table of Contents

List of Figures

List of Tables

List of abbreviations

2D	Two-dimensional
3D	Three-dimensional
AFM	Atomic force microscopy
APS	Ammonium persulfate
CCD	Charged couple device
CFM	Confocal fluorescence microcopy
CRM	Confocal reflectance microscopy
CS	Correlation size
DIC	Digital image correlation
DMA	Dynamic mechanical analyzer
DVC	Digital volume correlation
ECM	Extracellular matrix
FAK	Focal adhesion kinase
FBS	Fetal bovine serum
FGF	Fibroblast growth factor
FNCC	Fast Normalized Cross-Correlation
fps	Frames per second
GAG	Glycosaminoglycan
GPCRs	G protein-coupled receptors
GS	Grid size
GTA	glutaraldehyde
IBS	Irritable bowel syndrome
IRM	Interference reflection microscopy
MAP	Mitogen-activated protein
MLCK	Myosin light-chain kinase
PAAm	Polyacrylamide
PLLA	Poly (L-Lactic acid)
ROCK	Rho-associated kinases

SEM	Scanning electron microscopy
SR	Search ratio
SSD	Sum-of-squared differences
TEMED	Tetramethylethylenediamine
TGFβ	Transforming growth factor beta
UV	Ultraviolet
Vol	Volume
Wt	Weight

Glossary of terms

Angiogenesis: Formation of new blood vessels from existing ones is called angiogenesis.

Cascade: A cascade is a series of consecutive reactions that product of one step is used at the following step. There are several different kinds of cascades such as coagulation cascade, and enzymatic cascade. In this thesis mainly signal transduction cascades are considered. Signal transduction cascade is the series of events that result in interpreting of a signal by cell, whether it is chemical, physical or mechanical.

Chemoattractant: Chemotaxis is the process of cell migration as a result of a chemical signal. Chemoattractant is the chemical substance including chemotaxis.

Chromatin: DNA and several other proteins make a complex that has genetic information in it. This complex is called chromatin and it exists in the cell nucleus.

Cross-correlation: CC is a method for measuring similarity level of two sets of signals using mathematical equations.

Cytosol: The liquid inside a cell is called cytosol.

Durotaxis: The process of cell movement as a result of a mechanical stimulus is called durotaxis.

Ectodomain: Proteins on the cell walls are sometimes extend from inside the cell all the way to the outside of the cell. The section of the protein that is outside is called ectodomain.

Filopodia: Protrusions on the cell membrane that contain parallel fibers of actin filaments are called filopodia. Filopodia are mainly involved in exploring the environment during cell migration.

Fourier transform: Fourier transform is a mathematical computation technique and an image processing tool that maps images from spatial domain to frequency domain. This mapping significantly decreases computational load.

Growth factor: Growth factors are proteins that stimulate cells for higher growth rate, division and also differentiation.

Kinase: A kinase is an enzyme that can transfer phosphate groups from one molecule to another [1].

Ligand: Generally speaking, ligand is a molecule that can bind to another one and make a large complex. This complex usually serves a specific purpose. In the present research, ligand usually refers to an ECM component.

Lipid bilayer: Lipid bilayer is the cell wall that separates the inside and outside of a cell.

Lamellipodia: Lamellipodia are flat protrusions on the cell surface during migration that contain network of actin filaments. They are mostly involved in directional migration.

Mechanotransduction: The process during which cells can detect mechanical stimuli and transfer it to chemical signals is called mechanotransduction.

Morphogenesis: Formation of a multicellular organism is called morphogenesis. It is one of the fundamental processes during embryonic development.

Phenotype: The collection of detectable characteristics of an organism makes that organism's phenotype. For a specific cell type, any behaviour, such as biological, physical, mechanical and chemical contribute to that cell's phenotype.

Receptor: A protein that collects stimuli for cells is a receptor. It resides either inside the cell or on the surface. Upon stimulus collection by a receptor, cell responds to it accordingly.

Stem cell niche: The matrix that stem cells live in is called stem cell niche. Stem cells collect a large portion of the information they need from their niche.

Transfection: The process of genetically introducing a protein into the cells, so that cells express a desired property, is called transfection.

Voxel: A unit of 3D volume image, similar to pixel in 2D, is called voxel.

Chapter 1: Introduction

In the human body, cells are either in contact with a solid three-dimensional (3D) substrate and/or interact with bodily fluids. Specifically, in a tissue, native cells live in a 3D substrate called the extracellular matrix (ECM). ECM not only provides structural support for cells, it also provides information to them. Cells collect this information and respond to it accordingly. The information can come from both the chemical constituents of the ECM and the physical and mechanical properties of this substrate.

It has been recently shown that cells have the ability to detect mechanical stimuli and respond to them through a process called mechanotransduction [2]. A wide range of mechanical stimuli, including shear stress due to flow [3,4], tensile and compressive stresses [5], and even mechanical properties of the substrate cells live on\in [2], can affect cellular behaviour. Also, a broad variety of cellular behaviour, such as proliferation [6], differentiation [7], and also migration [8], can be affected by these mechanical stimuli. This broad variety of signal types and also cellular behaviour emphasizes the importance of mechanotransduction in regulating biological processes. In the present thesis, the main focus is on cell migration.

As one of the vital processes in the human body, cell migration in the ECM has been the subject of numerous studies in the past. During migration, cells push and pull their substrate and, as a result, deform it and exert mechanical forces that are called cell traction forces. The idea of measuring these mechanical

responses, in single cell level, was started more than three decades ago when substrate wrinkling was assumed to be an indication of cell induced deformation [9]. Since then, technological advancements have allowed the development of many different methods to measure cell mechanical behaviour. One of the most common measurement methods is called cell traction force microscopy. In this method, cells are cultured on/in a flexible substrate and allowed to migrate over a certain period of time. During migration, cells induce deformation on the substrate and these deformations can be measured by microscopy techniques. One method for measuring these deformations is to load the flexible substrate with fluorescent microbeads. Displacements of these beads is then measured and considered cell-induced deformation [10]. Using the deformation and substrate mechanical properties, cell traction forces can then be calculated using constitutive equations governing the mechanical properties of the substrate [11].

These measurements can be performed in three levels of complexity. The first and easiest level is when cells are migrating on a two-dimensional (2D) surface and cell responses (biological and mechanical) are also studied in 2D. In this case cell migration is occurring in 2D and deformation and force measurements are also in 2D. This is the most common and most studied level of investigation. The second level is when cells are cultured on a 2D substrate and therefore biological responses from cells results from 2D interactions, however, mechanical responses are measured in 3D. In this case not only in-plane deformation and forces are calculated, but also out-of-plane (third dimension) measurements are performed. The third complexity level and the most complicated one is when cells are embedded in a 3D matrix, and both biological and mechanical responses are measured in 3D as well. This is the most realistic case when compared to the behaviour of most cells *in vivo*. It is critical to note that both second and third levels are recent approaches and have not been fully investigated yet. The fact that cells are able to apply a force in 3D, even when they are cultured on a 2D surface, has been a recent finding [11–14]. Encapsulation of cells in a 3D matrix and measuring 3D responses, for a single cell, has only started to emerge very recently [15].

While the number of studies is still limited, the current research highlights the important role of mechanics in cellular behaviour. However, very little is known about the behaviour of different cell types and there is a significant need for developing more specific methods. Implementing various engineering techniques, along with knowledge of biological sciences, can lead to more efficient and comprehensive measurement methods. This can guide us to a better understanding of all aspects of cellular behaviour.

In the present thesis, mechanical interactions of cells with their environment were studied. The effect of substrate stiffness, as a mechanical stimulus for cells and its influence on biological responses was

investigated as well as its influence on mechanical behaviour. For the experimental investigation, the second level of complexity was chosen. Furthermore, for the mechanical effect of cells on their substrate, cell-induced deformation by cells was measured using a recent method called digital volume correlation (DVC). This method enables us to estimate cell-induced displacements and strains in 3D while cells are cultured on a 2D surface of a substrate.

1.1 Hypothesis

The present thesis hypothesizes that mechanical interaction of cells with their environment can be investigated effectively through studying both biological and mechanical responses. Two main research questions and hypotheses were addressed in the present thesis:

1. *Research question:* Do corneal epithelial cells respond to stiffness of their substrate?
   Hypothesis: Substrate stiffness is a mechanical stimulus and cells respond to it.
2. *Research question:* Is studying biological behaviour of cells enough?
   Hypothesis: Studying mechanical responses of cells as well as biological responses can reveal further aspects of cellular behaviour.

Implementing engineering techniques, using confocal microscopy paired with theoretical calculations by image processing methods, enable us to explore these new aspects of cellular behaviour.

1.2 Objectives

In this thesis, the 3D mechanical and biological responses of cells cultured on 2D surfaces were investigated. There were three main objectives:

1. Choosing a suitable model substrate material that has controlled properties and permits cell viability, attachment and migration.
2. For the chosen substrate and the selected cells, investigating the viability, growth, adhesion molecule expression, apoptosis and migration patterns as biological responses.
3. Determining the cell-induced deformations as the mechanical response of cells using confocal microscopy and image processing techniques.

1.3 Significance

It is now well known that biological responses from cells are intertwined with the mechanics of the environment, but how mechanics affect biological behaviour is still unclear.

Investigating cellular behaviour from both biological and mechanical perspective is a rather new approach of understanding cellular behaviour. This understanding can be applied in clinical research to improve therapeutic strategies various processes and conditions such as wound healing or cancer.

1.4 Thesis organization

Following introduction to the present thesis in Chapter 1, Chapter 2 provides background information needed to understand the current research as well as reviewing the previous studies in this field. Chapter 3 addresses the first objective of the thesis and various substrate materials are discussed. As the material is chosen, its characterization is also presented in this chapter.

The Chapter 4 addresses the second objective and presents the results related to the biological response of cells in addition to a considerable discussion. Chapter 5 presents the study on the cell mechanical responses and thus addresses the third objective with an emphasis on the protocols used as well as significant discussion. Chapter 6 presents the conclusions of this thesis and outlines the contributions that thesis has made to the cell biomechanics field along with recommendations for future work.

Chapter 2: Background and Literature review

The focus of this chapter is to describe some basic concepts needed for understanding the current research as well as reviewing the previous studies on the mechanical and biological interaction of cells.

2.1 The Extracellular matrix (ECM)

2.1.1 Introduction and Functions

The extracellular matrix (ECM) is the substance that hosts all tissue cells in the body. Most of these tissue cells are anchorage dependent: in order to survive, they need to adhere to a surface; i.e. most of these cells cannot survive when suspended in a fluid. The ECM is the substrate that cells anchor on to perform their vital activities, such as migration, proliferation, and differentiation. However, this is only one of the ECM functions. Following are the roles of ECM in the human body:

1. **Structural and mechanical support:** ECM provides a substrate and structural support that tissue cells need to perform their activities [16,17]. The ECM also gives its integrity to the tissue of different organs. Depending on the tissue and its specific functions, the ECM can have a variety of compositions and mechanical functions. For example, in the articular cartilage, the ECM is rich in water, electrolytes, as well as collagen and proteoglycans. Through this unique structure, the

cartilage is then able to support lubrication in synovial joints, which also leads to its exceptional load bearing capacity [18,19]. At the same time, the ECM of bones is also composed of collagen and proteoglycans, but the presence of minerals such as hydroxyapatite and calcium phosphate (which represent about 50% of its volume and 75% of its weight) gives this tissue its distinctive strength and rigidity [18]. The ECM also has specific compositions in order to be the suitable substrate for different cell types such as endothelial cells in the lining of blood vessels that are exposed to blood shear flow. The ECM also supports the growth of nerves and lymphatic vessels and provide nutrients to tissue cells [20].

2. **Controlling cellular behaviour through chemical composition:** The ECM can also be a reservoir of many chemical signals that affect the biological behaviour of different cells [16,21], such as growth factors like transforming growth factor β (TGFβ) [22] and fibroblast growth factor (FGF), [23] as well as ECM associated proteins such as fibronectin [24] or tenascin [25]. The ECM not only provides the chemical factors to cells, but also affects the distribution and release of these factors and proteins [25].

3. **Controlling cellular behaviour through physical and mechanical properties**[1]**:** The ECM, not only can influence cellular behaviour via its chemical components, but also its physical and mechanical properties affect cells [16]. The ECM is in a dynamic state as cells are constantly degrading and remodeling it, thus parameters such as microstructure and density are not constant. Furthermore, ECM properties can change due to various diseases. For example, during tumor formation, collagen crosslinking density is changed and this can affect ECM properties and therefore cell behaviour [26,27].

2.1.2 Composition

The ECM in different tissues is made up of similar components. However, the relative amount of these components can vary drastically [1]: the composition and the state of the ECM is tailored to the function of that specific tissue/organ.

Generally, the ECM consists of a fibrous network of collagen molecules surrounded by a mixture of other proteins such as glycosaminoglycans, proteoglycans, and also other glycoproteins such as laminin, tenascin, and fibronectin [28]. These proteins are often large multi-domain molecules (100-1000 kDa

[1] The effect of mechanical properties of ECM on cellular behavior will be discussed later in this chapter.

[28]), and have asymmetric shape. A few of the well-known molecules will be discussed in the following paragraphs.

Collagen exists in the largest amount in the ECM. It represents about 25% of the total protein mass in mammalian bodies [1]. Collagen molecules have a triple helical structure in which three chains (called α chain) are twisted around each other. These molecules are long, stiff and make a fibrous structure when seen under a microscope [29].

Glycosaminoglycans (GAGs) are polysaccharide molecules that are much too stiff to bend and fold, so they occupy large volumes compared to their mass. Hyaluronic acid (or hyaluronan) is a well-known GAG molecule, which plays an important role in bearing compressive forces in joints [1]. It is also important in embryonic development. Usually, GAG molecules are covalently bonded to a core protein and form proteoglycans [1,28] to make exceptionally long molecules.

Other components of the ECM are glycoproteins, which, similar to integrin molecules, are involved in cell adhesion to substrate [1]. One of these molecules is fibronectin that is actively involved in cell-matrix interactions [1,28].

Another important component of the ECM is elastin. This molecule provides elasticity to tissues and its relative amount can change from a few percent in the skin to about 50% dry weight in the aorta [1] and almost 70% in some ligaments [30]. This elasticity gives the tissue the ability to go through cycles of repetitive deformations. Since this molecule is very hydrophobic, it is one of the most durable proteins in the body [30].

2.1.3 ECM involvement in biological processes

The ECM has important roles in mammalian cellular behaviour and plays a crucial role in many biological processes. Selected activities with ECM involvement are discussed here. It is essential to note that processes discussed here are complicated and most of them are intertwined with each other in a way that is impossible to separate them.

The first cellular activity that is directly affected by the ECM is cell migration. Cell migration plays a crucial role in many physiological processes such as the immune system response, wound healing, inflammation, angiogenesis, embryonic development, and metastasis. Cell migration is a highly complex process in which several proteins get involved and different cascades are activated at subsequent time points. There are many different parameters that can affect the cell migration process (migration mechanism or speed). These parameters can be classified as matrix-associated factors and cell-associated

factors [31]. Matrix-associated factors are physical, chemical, and mechanical properties of the ECM: Dimensionality of ECM (2D vs. 3D), its density, microstructure and pore size, topography, composition, and also stiffness can influence cell migration [31]. At the same time, cell-associated factors such as cell type and function, cell-cell junctions (through cadherins, as the main component), and cell-matrix adhesions are the parameter that can change cell migration patterns [31]. In 3D, during cell migration, cells have to migrate through gaps and pores. Depending on the physical (pore size) and mechanical (stiffness) properties of matrix, cells either get deformed or start to remodel their matrix (either degrading[1] or deforming) to find their path [32–34]. The other parameter that can affect cell migration is the strength of cell adhesion to matrix. There is an optimum for adhesion strength in terms of migration speed: very low as well as very high adhesion strengths are not favorable for cell migration [35].

Metastasis is another process that has close relation with ECM. During metastasis, cancer cells lose their adhesion, migrate through the ECM and invade healthy organs. They can also be transported to distant organs by nearby blood or lymph vessels [36–38].

ECM properties and components can also directly affect angiogenesis (the process of new blood vessel formation) which is highly related to tumor growth. In this process, it is not only crucial for the ECM to provide the necessary molecules (such as growth factors and cytokines), it also needs to provide a substrate for blood vessels to form in [39–41]. It should be mentioned that not all the molecules provided by the ECM help the angiogenesis process, some of them can actually inhibit the process [39].

Differentiation is another process that is affected by the ECM. Generally, two types of parameters can affect stem cell differentiation: “intrinsic” factors that are parameters from the cell itself and “extrinsic” factors that are from the environment around the cells [42]. Again, not only can the components of the ECM affect the differentiation, but the physical and mechanical properties of the ECM can affect this process [43]. Stem cells cultured on stiff substrate tend to differentiate to osteoblasts and cells on softer substrates tend to differentiate to chondrocytes [7]. Mechanical forces on the substrate can also influence stem cell differentiation [44]; for example, shear force on human bone marrow derived stem cells has been reported to induce chondrogenesis.

Embryonic development [16], morphogenesis [45], and homeostasis are other biological processes that are controlled, to some extent, by the information delivered by the ECM.

[1] Matrix degradation by cellular agents is called proteolysis.

2.1.4 ECM to cytoskeleton: Focal adhesions and integrins

2.1.4.1 Cytoskeleton

All eukaryotic cells have a skeleton that gives them shape as well as mechanical and supportive functions. This skeleton is called the cytoskeleton. There are three main types of filaments in the cytoskeleton [1]: intermediate filaments, microtubules and actin filaments. Actin filaments are flexible fibers made of actin monomer. The actin monomers are arranged in a way that the actin filaments form a "two-stranded α-helical" structure. These two filaments (protofilaments) can make linear structures, 2D grids or 3D networks.

The cytoskeleton is a complex and dynamic structure in which filaments can disassemble and reassemble due to different chemical signals and mechanical stimuli. Besides the aforementioned filaments, there are many proteins in the cytoplasm that help the cell structure to be dynamic. These proteins are called motor proteins. The motor protein that can interact with the actin filaments also referred to as "stress fibers" is myosin [1]. Interaction of myosin with actin stress fibers in muscle cells causes the muscle contraction. In the last few decades, it has been shown that myosin interaction with actin fibers can also happen in non-muscle cells. Myosin is an elongated protein that consists of a long heavy chain (with two coiled α helices) and four light chains [1]. The light chains are arranged in a way that the two light chains are on each α helix of the heavy chains. Also, there is one N-terminus on each light chain heads, which plays an important role during interaction of myosin with actin. However, there is also another myosin molecule with just one head[1], which is called Myosin I and the myosin with two heads is called Myosin II. During myosin II and actin filaments interaction, myosin II attaches to actin filament and starts to move along the fiber. The movement is accompanied by ATP hydrolysis and fabrication of ADP and requires attaching and detaching of myosin to the filament, thus generating force and contraction. Myosin activity can be controlled by myosin light chain kinase (MLCK) [1]. This kinase can change myosin conformation from bent to extended state through phosphorylation.

2.1.4.2 Focal adhesions and integrins

Cells are attached to the substrate at spots that are called focal adhesion. Focal adhesions are extremely complex, dynamic and sensitive structures that anchor cells to their supporting substrate. Abercrombie *et al.* [46] first detected focal adhesions by interference reflection microscopy (IRM) in 1971. They consist

[1] This molecule has been specifically seen in amoeba.

of about 160 molecules with over 700 links between them [47]. Some of these molecules inherently belong to focal adhesions, while others are recruited in different processes at different time points [47]. Among them, integrins intrinsically belong to focal adhesion and play actually the main role in focal adhesions.

Integrins are heterodimer molecules consisting of α and β subunits that non-covalently form the molecule [48]. To date, 18 different α subunits and 8 different β subunits have been identified and their combinations form 24 different integrins [48–50]. These molecules stretch from inside the cell, the cytoplasm, all the way to the outside of the cell, the ECM, "integrating" these two environments [51]. They were first identified as glycoprotein molecules linking actin filaments of the cell to the fibronectin component of the ECM and the name "integrin" was proposed back in 1986 [52]. Integrins can detect many different types of ligands: molecules dissolved in the ECM as well as the ones attached to the ECM [49]. The 24 possible pairs of α and β subunits lead to integrin molecules with different binding capabilities [53]. Therefore, specific integrins can bind to specific ECM components (ligands); for example, $\alpha_3\beta_1$ and $\alpha_5\beta_1$ bind to fibronectin [50,53] and $\alpha_2\beta_1$ and $\alpha_3\beta_1$ can bind to collagen and laminin [50]. Both α and β subunits of the integrin ectodomains have several sections and flexible links exist between these sections, giving the molecule exceptional properties. The α subunit has four main sections: calf 2, calf 1, thigh and seven bladed β-propeller [48] (Figure 2-1). Just 18 out of 24 integrins have an extra domain between second and third blade of the β-propeller (α-I domain) which distinguishes their structure and functions from the other integrin molecules [54]. The β leg, on the other hand, has seven sections and therefore is more flexible than the α leg [48] (Figure 2-1). The ligand-binding site exists between the α and β subunits.

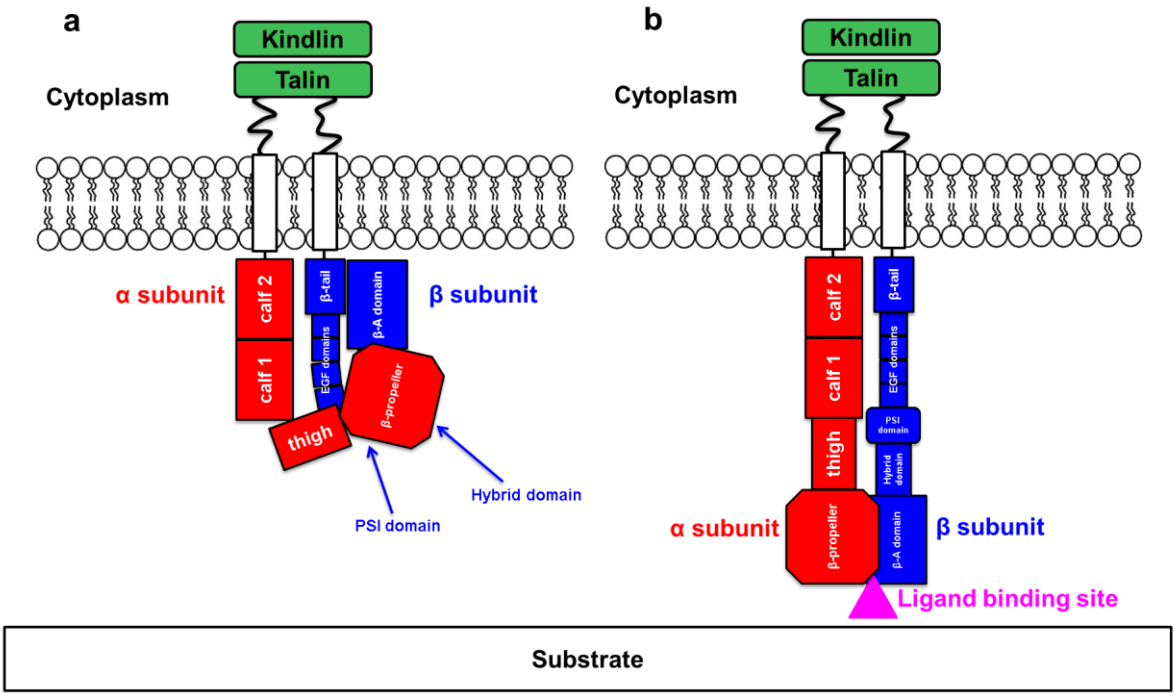

Figure 2-1: Schematic of integrin structure in a) not activated b) activated state, adapted from [48,49,53,55].

Integrins can adopt three distinct conformations: inactive or bent (low affinity), medium affinity, extended or active (high affinity) [55–57]. Two models have been proposed for explaining the process of changing conformation: the switchblade model [58–61] and the deadbolt model [49]. In the inactive state, the integrin α chain is bent at the "knee" which is the link between calf-1 and the thigh and this bent covers and hides the β chain [53] (Figure 2-1a). The other flexible link in the α subunit is between the thigh and β-propeller [48,53]. During the activation process, the salt bridge between the two intercellular subunits breaks by binding of the talin protein to the β molecules at specific sites [48,62,63] (Figure 2-1b). Since talin has both actin and integrin binding sites [64,65], it is one of the crucial molecules for communication between integrins and actin. In talin-deficient *Drosophila Melanogaster*[1], integrins are not able to attach to the actin filaments [66]. Kindlin is another protein that can affect the activation process in the same manner as talin [67–69]. Following this separation, the bent in the integrin ectodomain extends. This extension can be accompanied by up to 80^0 change in the angle [58,70–72]. Following this "switchblade" extension, the ligand binding site gets exposed and the integrin molecule becomes capable of binding to ECM ligands [73]. Besides the extension, there is evidence that twisting

[1] Commonly known as fruit fly or vinegar fly.

sections of the molecule relative to each other might also happen [73]. The activation process is highly dynamic and occurs very rapidly.

The switchblade model can explain the switch between bent and extended states, while the deadbolt model describes more subtle changes in the conformation [48]. Another mechanism that controls integrin's conformational change is the presence of three metallic cations: Mn^{2+}, Mg^{2+} and Ca^{2+} [58,74]. It is believed that there are cation-binding sites at the interface of α and β subunits [49]. Depending on the presence and concentration of these ions, integrin conformation and therefore affinity can be affected. For example, the presence of Mn^{2+} can promote integrin activation [71] and the ratio of Mg^{2+} to Ca^{2+} can change the ability of integrin β1 to bind to fibronectin [75].

Although these models are relatively consistent and can explain most of the observations, there are controversial findings as well. The switch from closed to open conformation is not necessarily needed for integrins to bind to their ligands. This was observed for $\alpha_V\beta_3$ both bound to soluble fibronectin in presence of Mn^{2+} [71] and also bound to the RGD sequence in bent conformation [76]. Furthermore, there is evidence that the inactive $\alpha_5\beta_1$ integrin might have an extended molecular shape and not the bent conformation [77]. It is important to understand that the reactions are extremely specific and depend on the type of integrin, ligand as well as the cells (being primary or immortalized cells) involved in the process.

Integrins play several roles in cells. They not only can be a key player in the inside-out signaling process, but they can also collect information from the outside environment and send it to the inside of the cell for processing the information. This is known to be the outside-in signaling duty of integrins. Therefore, integrins can contribute to many different signaling cascades [78].

Integrin clustering and activation on the cell surface is the first step in the focal adhesion formation process at the leading edge of the cell, following lamellipodium extension. Lamellipodia are flat protrusions containing network of actin filaments and are involved in cell migration. Ligand binding is accompanied by focal adhesion kinase (FAK) activation and engagement of several other adapter molecules [53]. Small "initial adhesions" form on the surface following ligand binding [53], which contain actin and talin [64]. Following engagement of vinculin [79], they might grow into dot-like structures called nascent focal adhesions or focal complexes. Focal complexes are small structures (about 1 μm) [53,80] that mainly form under lamellipodia [81,82]. During lamellipodia extension, actin filaments form and this formation is followed by actin network movement toward the center of the cell. This movement is called "retrograde flow" [83]. At this leading edge, focal complex formation is believed

to be dependent on a the G-protein named Rac [84]. There are different possibilities that can explain Rac activity toward focal complex formation, one of which being through actin polymerization and reacting with the ARP2/3 complex [85].

Focal complexes can further mature into focal adhesions. During the maturation of focal complexes, several molecules get recruited one after the other in an orderly manner. For example, paxillin is known to be important in focal complexes but not focal adhesions [80,86,87] and zyxin is an important molecule in focal adhesions [88]. Stable focal adhesions have elongated shape and their survival depends on presence of mechanical forces. Integrins in these adhesions are bound to ECM ligands on one side and are attached to actin filament on the other side by the actin binding molecules talin, α-actinin [82], and vinculin [79,89]. The adapter protein talin is not only important in integrin activation [63] and also clustering, it also plays an important role in attaching the integrins to actin filaments [65,79,90]. In fact, it was reported that talin-deficient fibroblasts are not able for form focal adhesions and their lamellipodia are unstable [90]. The path to mature focal adhesion and the differences between focal complexes and focal adhesions is summarized in Figure 2-2.

One of the important molecules involved in focal adhesion formation is the GTPase protein called Rho [85]. Rho can affect focal adhesion formation through two different pathways. It can bind to Dia1 and promote actin polymerization [91]; forces generated in the process can help focal adhesion growth. It can also activate Rho-associated kinases (ROCK) [92] and trigger myosin II contractility. There is evidence that these two pathways have to be active at the same time to affect actin filaments and focal adhesion [93,94].

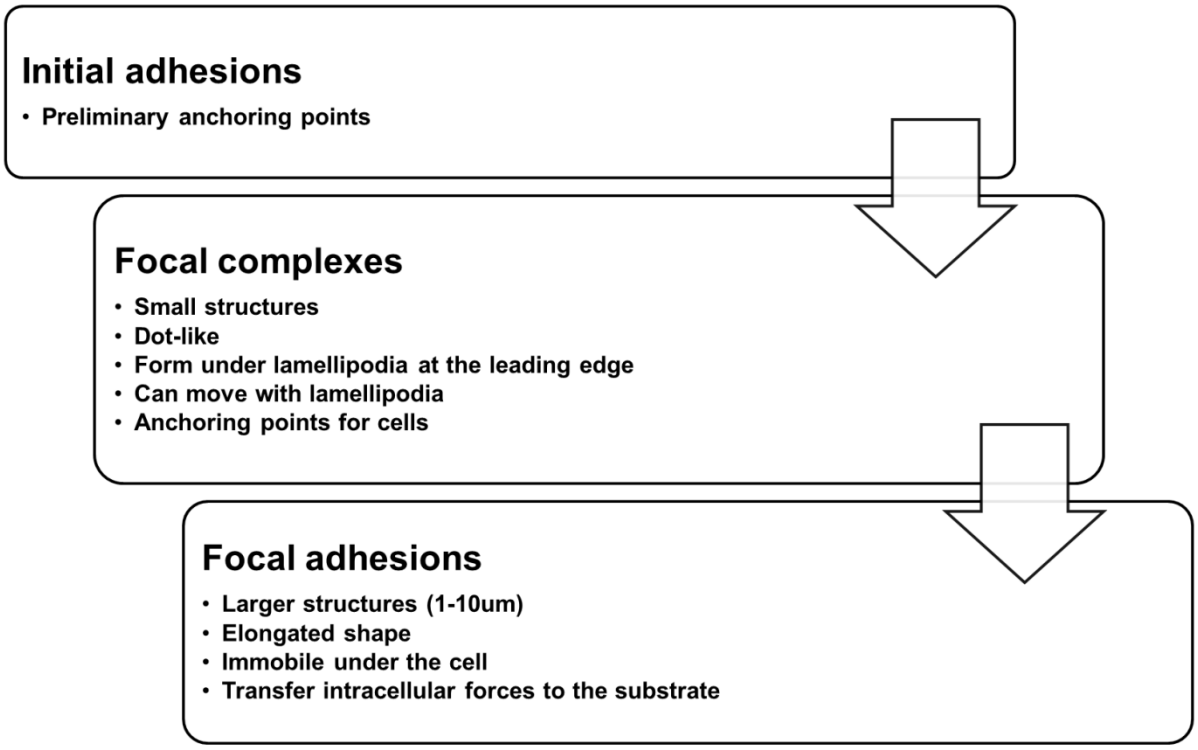

Figure 2-2: Path to mature focal adhesions formation.

Focal complex maturation to focal adhesions also depends on the presence of mechanical forces. These mechanical forces can be either intracellular forces generated by myosin II activity on actin filaments or they can be externally applied. It was reported that by inhibiting Rho or ROCK activity (therefore disrupting force generation through blocking myosin II activity), focal adhesion formation was disrupted [95]. An interesting phenomenon with focal adhesions is that for cells with inhibited Rho or Rho-assisted kinase activity, focal adhesions can form again by applying external forces [95,96]. The same behaviour was seen in cells with blocked myosin activity [97]. It is also worth mentioning that focal adhesions can directly apply forces to their substrate as well because of their engagement with actin fibers and myosin activity.

Focal adhesions are fairly well studied for cells cultured on 2D substrates. However, more ambiguities are present with 3D cultures. Even the existence of structures similar to focal adhesions is a matter of controversy in the literature [98]. Fraley et al. [99] has reported that molecules similar to those involved in 2D focal adhesions exist in cells cultured in 3D ECM. However, these exist mainly inside the cytoplasm and do not form focal adhesions. Fraley et al.also reported that, while focal adhesions do not

fully form in 3D cultures, these molecules still control cell migration. On the other hand, there are also reports indicating the existence of adhesion spots similar to focal adhesions that occur in 3D EDM [100–103]. It has been suggested that this controversy stems from the visualization of these structures [98,102]. It has also been reported that, like 2D substrates, 3D ECM properties, such as density, can provide information to cells and regulate their behavior [100,104].

2.2 The machinery of cell

2.2.1 Mechanotransduction: where biology meets mechanics

In the physiological environment, chemical signals from the ECM include signaling molecules, growth factors, or chemoattractants and can induce specific cell behaviour such as differentiation, proliferation, or directional migration[1]. Nowadays, it is well recognized that cells not only respond to chemical signals but also to mechanical stimuli. Cells can sense mechanical stimulus and convert it to chemical signals through a process called mechanotransduction.

One source for mechanical stimuli can be the external forces applied to the cells. Depending on the function of the tissue, these forces can vary over a broad range of magnitudes and types: endothelial cells on the inner layer of blood vessels experience shear forces from blood flow [3,4]; during cardiac cycle, cells feel shear, compressive and tensile stresses [53]; in bone and cartilage, cells are under cyclic stresses of both tension and compression [105]; and forces in tendons can increase up to 9kN [106].

In vitro, many strategies have been developed to externally apply force and mechanically stimulate cells: exposing cells to shear stress using liquid with specific flow rate [3,4], substrate stretching [5], utilizing microneedles [107], atomic force microscopy [108], optical tweezers [109], magnetic twisting cytometry [110], and magnetic tweezers [111]. Some of these methods apply a localized force and can help understanding the behaviour at the cellular level as opposed to the tissue level.

The other source for mechanical stimulus for cells can be mechanical properties of the environment that they are cultured on/in. One of the mechanical properties of the substrate acting as a stimulus for cells is the stiffness of the substrate [6,8,112]. Recently for viscoelastic hydrogels, loss modulus was identified as an important mechanical property affecting cell behaviour [113]. The first study on response of cells to the mechanical properties of the substrate was performed by Pelham and Wang in late 90s [112], whereby polyacrylamide gels with tunable mechanical properties were used for mechanotransduction applications.

[1] The directional migration of cells in response to chemoattractants is called chemotaxis.

It was shown that cells on stiffer substrates were more spread and elongated while cells cultured on softer substrates were more irregular in shape and less elongated [112]. It was also found that cells migrated faster on softer substrates (0.55 μm/min) compared to stiffer substrates (0.06 μm/min) [112]. Moreover, focal adhesions of cells on softer substrates were reported to be irregular and unstable compared to stiffer substrates on which focal adhesions were stable and elongated. This stability was believed to be due to the increase in tyrosine phosphorylation [112].

It is well established that cells cultured on a 2D substrate are more likely to migrate towards the stiff substrate. This behaviour was first named durotaxis by Lo *et al.* in 2000 [8]. Durotaxis also has been reported for cells migrating in 3D collagen matrices [114]. Recently, it has been reported that mesenchymal stem cells (MSCs) are able to detect different stiffness gradient patterns and respond to them differently [115]. In this study, regardless of the pattern, MSCs consistently moved towards the stiffer side. Evans *et al.* [6] reported that for polydimethylsiloxane (PDMS) substrates, cell attachment was unaffected by variation in substrate stiffness; however, cell spreading and proliferation were higher on stiffer substrates. Furthermore, stem cell differentiation has been shown to be affected by changing substrate stiffness, and cells cultured on stiffer substrates displayed osteogenic markers [6]. These results were in agreement with the behaviour of the preosteoblast cell line, MC3T3, cultured in 3D collagen glycosaminoglycans substrates [116]. Interestingly, cell stiffness can also be altered by substrate stiffness; increasing the substrate stiffness can increase the cell stiffness as measured by atomic force microscopy (AFM) [117–119]. Actomyosin light chain phosphorylation has been reported to regulate these mechanical changes in the cytoskeleton [120]. Cell stiffness can also be affected by metastatic capability in some cell lines. Coughlin and Fredberg reported that highly metastatic kidney cancer cells have higher stiffness compared to the ones with milder metastatic capability [121]. While studies have proven that fibroblasts proliferate more in collagen gels with higher stiffness [122], Miron-Mendoza *et al.* [123] found that for fibroblasts cultured in collagen gels, increasing stiffness with glutaraldehyde crosslinking did not affect cell spreading and migration. Substrate stiffness was shown to play an important role in tissue formation, where cells on the soft substrates tend to aggregate and form the tissue, whereas cells on stiff substrates start to move away from each other [124]. Furthermore, recently, McGrail *et al.* [125] showed that ovarian carcinoma cells show higher malignancy, including higher chemoresistance, when cultured on softer substrates.

It is worth noting that cells not only respond to the mechanical properties of the substrate, they can also respond to ligand density tethered to the substrate [126,127] and also pattering on the surface of the

matrix [128,129]. Recently, research on mammary epithelial cells revealed that ligand density and stiffness together influence malignant phenotypes in cells [130]. It is worth mentioning that, there is an optimum level to stiffness sensitivity. Keeping the ligand density constant, cells on extremely soft substrates and also extremely stiff substrates have shown slow migration speeds. This was specifically reported for smooth muscle cells [131].

2.2.2 Mechanotransduction mechanisms

It is believed that mechanotransduction is an outside-in and inside-out signaling loop [2]. There is a systematic order of events that happen during this loop [53]. First, cells sense the stimulus. This step involves transferring this stimulus to the inside of cells for processing. This is the outside-in portion of the loop. The second step is the processing of this received information that occurs inside the cell. In the last step, cell behaves/responds according to the processed information, which is the inside-out signaling portion of the loop.

There has been a significant amount of research and speculation on the mechanisms involved in this process. Depending on the cells involved and the type of mechanical stimulus, such as the load type, the mechanism can be different. Due to the complicated nature of the processes and pathways involved in mechanotransduction, not all the links are fully known; furthermore, intracellular mechanisms are often interconnected and complex. A few of the known mechanisms are briefly introduced below.

2.2.2.1 Mechanotransduction through ion channels

The cell lipid bilayer has the ability to transport many different kinds of molecules into the cytosol. Depending on the type of molecule, its size and charge, the lipid bilayer is more permeable to some molecules than others. In general, the smaller the molecule, and the more hydrophobic it is, the more permeability there is for that molecule [1]. For hydrophilic and large molecules and any molecules that the lipid bilayer is not permeable to, specific proteins exists on the lipid bilayer that either bind to the molecule or transport it in, or they "open channels" for them to pass into the cytosol [1]. Ions such as Na^+, K^+, Ca^{2+} or Cl^- are transported through the membrane by these proteins. These proteins, called ion channels, are extremely selective, and they open and close very rapidly to let the ion into the cytosol [1]. Some of these ion channels are also known to be mechanosensitive [53].

There are two categories of mechanosensitive ion channels: stretch-sensitive ion channels and flow-sensitive ion channels [53]. As mentioned earlier, one of the methods to externally apply a force to cells is

by applying a force to the substrate that cells are cultured on/in. As can be inferred from their name, stretch-sensitive ion channels are activated by stretching of the substrate [53] and the cell membrane becomes permeable to ions: K^+, Ca^{2+} and Ba^{2+} stretch-sensitive channels have been reported in different types of cells [132–134]. This flux of ions with different charges inside and outside the cell can cause very small, yet effective, currents that allow the cells to react and respond to the mechanical stimulus. Ca^{2+} ion channels have also been shown to be important in cell response to change in the substrate stiffness [135]. The pathway in this case was related to myosin activity through Myosin Light Chain Kinase (MLCK) [136]. Flow-sensitive ion channel activation, such as Ca^{2+} [137], K^+ [138], and Cl^- [139], has been previously reported in different types of endothelial cells.

2.2.2.2 Mechanotransduction through the cell membrane

G-protein coupled receptors (GPCRs) are cell-surface proteins that are involved in many signaling cascades; for example our senses of smell, sight and, in some cases, taste depend in part on these membrane associated proteins [1]. There is a wide variety of GPCRs and more than 700 of them exist in humans [1]. Some of these signaling pathways can depend on more than one of these receptors; adrenaline interacts with 9 different GPCRs [1]. These molecules are believed to be involved in signaling cascades for mechanotransduction [53]. Generally, G-proteins can be activated through ligand binging [140]. When GPCRs are in active conformation, they can bind to ECM ligands. This binding triggers signaling cascades starting with activating G-proteins. It is worth noting that there is evidence that G-proteins are involved with integrins and it is believed that the G-protein mediated pathways can be simultaneously active with the integrin-cytoskeleton mediated pathway [141].

There are also other ways that G-proteins can be activated. G-proteins can become activated within seconds of applied external forces, such as shear force [142] through these receptors. Although there are studies that report GPCRs are somewhat involved in the process [143], G-protein activation can happen even without ligand binding [144,145]. G-proteins also have the ability to become activated even without engagement of GCPRs. In this case, the cell membrane is directly involved in G-protein activation [146,147].

It is worth noting that besides membrane associated proteins, cell lipid bilayer properties, such as membrane fluidity [146,148], free volume [149], and polarity [53] can also be involved in mechanotransduction pathways.

2.2.2.3 Mechanotransduction through focal adhesion and cytoskeleton

Generally, a few elements are involved in mechanotransduction process: the inside of cell, the cytoskeleton, the extracellular matrix, the molecule that connects these two, also, the stimulus from outside, and the molecules that process the information [53]. As mentioned before, focal adhesions are anchoring spots of cells to their substrate. Despite being very complicated, the main molecule involved in these structures is integrin. Integrins are bound to ECM ligands outside the cell and attached to actin filaments through adapter molecules inside the cell. So, not only do they connect and sense the stimuli, they can transfer cell responses as well [78].

Numerous signaling molecules are involved in both sensing the mechanical stimuli and responding to it. For example, paxillin is one of these molecules that localizes in focal adhesion sites and interact with integrins [87]. The level of phosphorylation of these molecules determines their activity, which can change through stimuli received from ECM [53]. Forces generated in cells as a result of actin filament polymerization in lamellipodia are another parameter that can be changed by mechanical stimulus through MLC activity. Other molecules such as talin and kindlin, that affect integrin activation, can be another source for focal adhesion mechanosensitivity. p130CAS is another component of focal adhesions that can go through substantial conformational changes by mechanical force [150]. These conformational changes can expose binding sites that are naturally hidden. Rho and ROCK pathways are also reported to be involved in this process [95]. The Mitogen-activated protein (MAP) kinase pathway regulates integrin activation [151] and thus can be involved in mechanotransduction as well. It was also shown that for human mesenchymal stem cells, RhoA and its effector RhoA kinase (ROCK) control calcium ions fluctuation in cytoplasm, on substrate with different stiffnesses, and therefore, control stem cells behaviour [152].

Another source for changes in focal adhesion can be the forces that focal adhesion feels. As mentioned before, focal adhesion assembly (cell adhesion) is affected by forces applied to adhesion sites. These forces can be generated by the cell or the forces from the environment.

As one of the cell cytoskeleton filaments, microtubules are also involved in mechanotransduction pathways. Like actin filaments, there are motor proteins that interact with microtubules to control filaments growth. CLIP-170 is the protein that interacts with microtubule filaments [53]. Microtubule filaments growing end are involved in lamellipodia during cell migration. The GTPase involved in reaction of proteins and microtubule filaments is called IQGAP1 [153]. This GTPase affects Rac1 activity, and Rac1 can control the cell leading edge activity [153,154].

2.2.2.4 Nuclear mechanotransduction

In eukaryotic cells, the nucleus occupies about 10% of the cell volume [1]. It is separated from the cytosol by a membrane called nuclear envelope [1]. The nuclear envelope has two membranes: the inner membrane and the outer membrane. There is another layer inside the inner membrane called nuclear lamina. The nuclear lamina mechanically supports the nuclear envelope and is made of intermediate filaments [1,53]. There are holes at repeated intervals in the nuclear envelope called nuclear pores. These pores facilitate the transfer of molecules between nucleus and cytosol.

There are two types of studies regarding mechanical properties investigation of cell nucleus [53]: the ones that study the cell nucleus in the natural state of cell and the others that measure properties of isolated nucleus. Nuclei isolation can be performed by either mechanical or chemical techniques [155]. Mechanical isolation is removing the parts of the cell using a micropipette while during chemical isolation the cytoplasm is chemically dissolved and the nucleus is left isolated. The results from these studies vary by cell type and measurement method but the universal result is that the cell nucleus is much stiffer than the cell [155–157]. It was also found that nuclear lamina can act as a load bearing layer that brings structural integrity to the nucleus [158]. At the same time, chromatin is believed to have viscous behaviour that "flows" under mechanical load [159]. When adherent cells are detached from their substrate, the nucleus changes shape and become rounder. There are two possibilities, either the nucleus is under stretch in an adherent cell or when floating, nucleus changes to a round shape due to hydrostatic pressure. In both cases, it can be concluded that nucleus is under constant mechanical loading [160,161]. It is worth noting that mechanical properties of cells are viscoelastic and highly nonlinear [162,163].

It is believed that the nucleus is connected to the cytoskeleton via protein complexes called linker of nucleus and cytoskeleton (LINC). These complexes contain proteins called SUN and nesprin and connect microtubules and actin filaments to nuclear lamina and lamina-associated proteins [164]. This will allow close connections between nucleus and cytoplasm components; for example, force transfer from microtubules to nucleus [165] or signal transfer from nucleus to cytoplasm.

External forces applied to cells can mechanically deform the nucleus and changes its shape. Also, it is believed that the nucleus shows stiffening behaviour under mechanical load, meaning applying mechanical force, such as shear force, can increase the stiffness of the nucleus and decrease its height [166,167]. It was reported that 3T3 fibroblasts showed cytoskeleton reorganization and increased nucleus movement under shear [168]. Also, endothelial cells nuclei not only showed compressed and elongated shape under shear, they also showed higher stiffness. This was assumed to be due to structural remodeling

of the nucleus under shear and nucleus was suggested to be one of the "load-bearing organelles" of the cells [166]. At the same time, changes in the shape of cells and nuclei can affect cell phenotype [169,170]. There is also some evidence that the mechanical forces can directly affect gene transcription. As mentioned before, forces applied to cells can be transferred to the nucleus through cytoskeleton filaments such as microtubules. This force transfer can affect DNA conformation inside the cell [170]. Experiments on DNA show conformational changes upon force exertion [171]. Conformational changes of DNA can expose some gene transcription factor while hide other ones [170]. There is also another possibility that transferred forces can rearrange genes inside the nucleus [170]. This rearrangement can be due to changes in the nucleus shape.

Nuclear transcription factor relocation is another mechanotransduction mechanism involving the nucleus. It has been reported that Yes-associated protein (YAP) and transcriptional coactivator with PDZ-binding motif (TAZ), commonly referred to as YAP/TAZ, relocate from the cytoplasm to nucleus when cells are cultured in rigid substrates compared to soft ones [172]. YAP was also reported to affect cancer cells matrix remodeling [173].

2.2.3 Clinical relevance

There is a wide range of diseases that can be caused by the inability of cells to properly regulate mechanotransduction pathways. These conditions might arise from cells not being able to detect mechanical stimuli or properly process the information collected from the ECM and forces exerted on them [174]. Changes in ECM condition, including mechanics, can be another reason for clinical conditions [174]. During metastasis, tumor cells need to squeeze through the ECM to invade healthy organ. Since the ECM mechanical properties can change in cancer [175], as a result of tissue stiffening, this affects cell behaviour through mechanotransduction pathways. Also, cancer cells themselves might have altered mechanical properties, which affects their behaviour and can influence the progression of disease [38,176,177]. Tissue stiffening can also occur during wound healing (after an injury while tissue scar is forming) [178] and fibrosis [179].

Mechanotransduction has been shown to impact cardiovascular diseases as well [180]. For example, during cardiac cycle, there is a phase where muscles relax and ventricles are filled with blood. This phase is called the diastole. Diastolic heart failure is a cardiovascular condition that is accompanied by increased stiffness in the ventricular muscle [181]. At the same time, there is evidence that substrate stiffness affects cardiac myocytes [182] and cardiac fibroblasts [183] behaviour. Besides cancer and cardiovascular

conditions, to name a few, mechanotransduction can have effect on achalasia [174], liver [184] and kidney diseases [174,185], asthma [186,187], chronic back pain [174], and irritable bowel syndrome (IBS) [174].

The visible path from these observations to achievable clinical therapies is yet to be determined, however, the influence of mechanotransduction in these conditions is undeniable.

2.3 Mechanical interaction

2.3.1 Cell migration mechanisms

Involvement of cells with the ECM in native tissue, and their substrate *in vitro*, during migration is one of the instances where mechanical interaction plays a key role. Therefore, it is important to understand different cell migration modes.

Cell migration can be divided into two main categories: collective cell migration and single cell migration. Each of these mechanisms is vital for specific processes, for example collective cell migration is one of the main mechanisms during embryonic morphogenesis [188] and single cell migration has been addressed as one of the processes during metastasis [36]. During metastasis, cancer cells lose their adhesion, migrate through tissue and invade the healthy organs. They can also be transported to distant organs by nearby blood or lymph vessels [36–38].

Single cell migration can occur by be either amoeboid or mesenchymal. Amoeboid migration is associated with movement of round or "blebby" cells that do not make mature stress fibers and focal adhesions during migration [31,189]. These cells usually migrate fast and lack formation of the pseudopodia during migration [31]. During mesenchymal cell migration, specialized cell-matrix adhesions and stress fibers are formed and cell shape is "fibroblast-like" during migration [31]. In 2D, that is when cells are cultured on a surface, three distinct stages can be recognized during mesenchymal cell migration: initially, the cell polarizes in response to a stimulus/signal, and protrusions called lamellipodia (more flat protrusions containing network of actin filaments) and filopodia (containing parallel fibers of actin filaments) are formed in the cell membrane. Lamellipodia are mostly involved in directional migration whereas filopodia role in migration cycle is exploring the environment around the cell[1] [190]. Formation of these protrusions is usually driven by actin polymerization [190]. Actin polymerization happens on the cell surface through actin-related proteins or ARPs, which are generally

[1] Lamellipodia and filopodia are usually called pseudopodia.

called ARP 2/3 complex. It should be mentioned that cell cytoplasm has relatively high concentration of actin monomers, which can be recruited for actin polymerization [1]. Profilin is the protein that binds to actin monomers and helps the monomers to attach to the growing actin polymer chain during polymerization [1]. In response to the signals from lamellipodia and filopodia, new adhesion sites (focal adhesions) are formed in the leading edge, and in the last step, the cell rear detaches from the substrate [31]. It is believed that migration in 2D surfaces is a cyclic process in which these three steps repeat [189].

However, it is not known whether the same exact mechanism can be extended to 3D matrices or not. It is reported that cells in 3D culture either not show distinct focal adhesions or the focal adhesions are small and have a very short life [191,192]. Fraley *et al.* [99] investigated both 2D and 3D migration of wild-type HT1080 cells and found that pseudopodia that formed in 3D were neither similar to filopodia nor lamellipodia. These pseudopodia were long, thin, and long lasting, and cell speed was dependent on growth rate and number of protrusions. It was also shown that for the same cell line, 2D migration pattern did not correlate with 3D migration behaviour; in fact, the migration mechanism was found to be totally different in 3D [99]. Lobopodial migration is another mechanism cells might use for migration inside 3D substrates [193,194]. Petrie *et al.* [194] reported this mechanism and showed that lobopodia are "large, blunt, cylindrical protrusions". They also claimed that switch between lamellipodia-dependent and lobopodia-independent migration mode occurs based on the degree of linear elastic behaviour of the ECM substrate [194]. In case of a linear elastic substrate, cells migrate by lobopodia dependent migration mechanism [194].

During cell migration in three dimensions, cells have to migrate through gaps and pores. Depending on the physical (pore size) and mechanical (stiffness) properties of matrix, cells either get deformed or start to remodel (either degrading or deforming) the matrix that they are in to find their path [32,33]. The way that cells respond to their matrix also depends on the migration mode that they follow. Cells that adopt mesenchymal mode of migration (such as fibroblasts) are able to proteolytically degrade the matrix. However, cells that migrate by amoeboid mode of migration (such as lymphocytes) move faster and do not degrade the matrix as much [195]. The other parameter that can affect cell migration is the adhesion strength. Migration speed and adhesion strength have a biphasic relation; very low adhesions strength as well as very high adhesion strength are not favorable for cell migration [35].

2.3.2 Cell-induced deformation and traction forces

Due to the anchorage dependency attribute of tissue cells, cells are in direct contact with their environment at focal adhesions. While cells are migrating, focal adhesions disassemble and reassemble to drag the cells forward. During this dynamic process, cells start to push and pull the substrate they have anchored on, which is associated with mechanical deformation and thus forces (l, as well as forces developed during the process). These mechanical forces are called cell traction forces.

It is believed that cell traction forces are a result of myosin II activity and interaction of it as a motor protein with actin or "stress fibers" of cells that can be transmitted to the substrate via focal adhesions[1]. This hypothesis was studied using a myosin II inhibitor, which decreases the activity of this molecule by binding to it. Upon addition of myosin II blocker, deformation of substrate was decreased, indicating that myosin II activity is one of the origins of cell traction force generation [11,196]. Furthermore, upon inhibition of myosin light chain phosphatase (thus increasing myosin light chain phosphorylation) traction forces were shown to increase [196]. For endothelial cells during initial attachment and spreading, cell traction forces start to appear before actin stress fiber and focal adhesion formation [197].

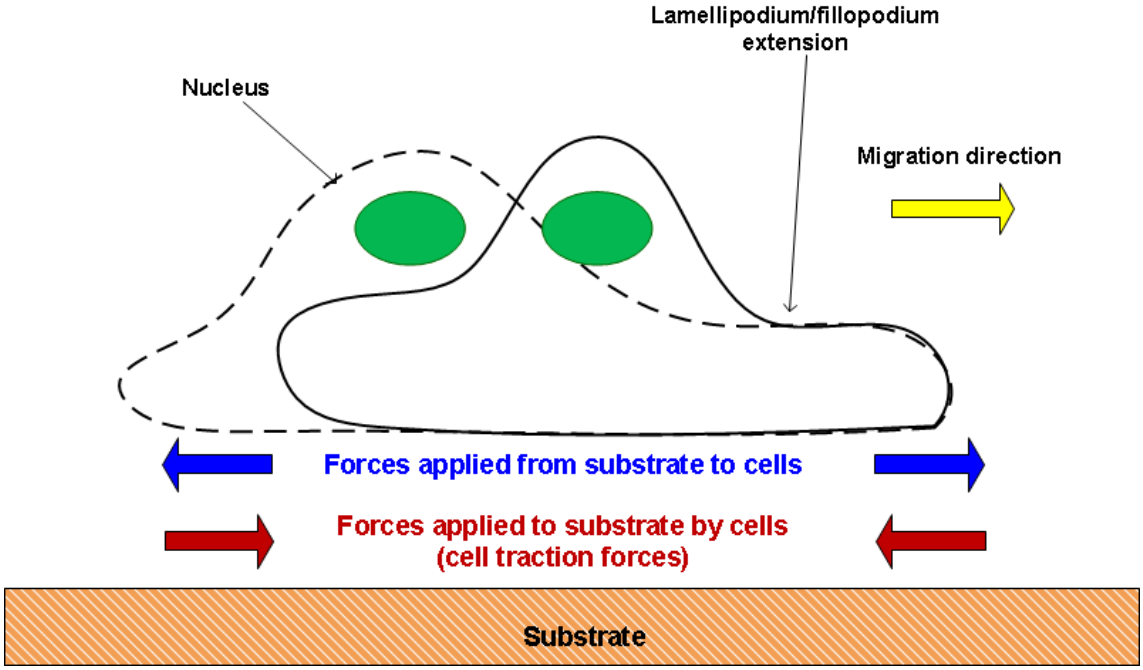

Figure 2-3: Schematic showing a single migrating cell, as well as forces developed during the process.

[1] More details about the mechanism were discussed in section 2.1.4.

Cell induced deformation and traction forces have mostly been studied in 2D; so, most of the studies have found in-plane forces. However, cells in the ECM are in a 3D matrix and are in contact with the surrounding matrix over their whole body, which shows the obligation of more accurately 3D cell traction force measurements. In a study done by Kraning-Rush *et al.* [176], the mechanism of cell traction force generation in 2D and 3D were studied for the metastatic breast adenocarcinoma cells, cultured on polyacrylamide gels, and also embedded in collagen type I. In this research, it was found that in 2D, inhibiting actin and microtubule polymerization, as well as stabilizing microtubules resulted in a decrease of cell traction forces exerted by cells on their substrate. Also, increasing myosin activity, by inhibiting myosin light chain phosphatase, increased the force. In 3D, collagen fiber reconfiguration was considered as the indicator of the change in cell behaviour, however, no forces were reported for the 3D study. It was found that the overall behaviour of cells and the role of microtubules and actin are similar in both 2D and 3D [176].

Furthermore, studies have been done on the effect of metastatic capability of cells on cell migration and force generation. In contrast to defined regions of high traction forces on the edge of lamellipodium in normal cells, transformed cells show weak scattered regions of traction forces [177]. Investigating cell lines with different metastatic capability (but same origin) revealed that, although stress fibers are normal, the increasing metastatic capability increases traction forces. It was also shown that changing matrix from 2D surface to 3D matrix have more effect on cells with higher metastatic capability [38].

2.3.3 Measurement methods

Although forces developed due to the collective migration of chick embryo fibroblasts were reported in 1969 [198], cell induced deformation and traction force measurement of a single cell was not reported until 1980 [9]. Harris *et al.* [9] used a silicone membrane (which was set on a bed of liquid silicone) and cultured cells on that membrane. Wrinkles on the membrane were the indication of deformation on the surface and also forces that cells generated while moving. Forces were inaccurately quantified through implementation of microneedles with known "flexibility". This study was the precursor of the well-known method called cell traction force microscopy (CTFM). The fundamental drawback of this method was the chaotic nature of the wrinkles, which made it impossible to accurately calculate forces caused by cells. Thereafter, studies were performed to optimize the silicone system. More controlled properties were achieved through UV irradiation and the system was utilized for measuring forces during cell division of fibroblasts [199]. Moreover, Lee *et al.* [200] incorporated latex microbeads on the crosslinked surface and

deformation was quantified through bead displacement. It was reported by Lee *et al.* [200] that, although lamellar extension can be seen in the leading edge of an epithelial fish keratocyte, no cell traction force can be seen, suggesting that cell traction force is not needed in the leading edge for movement of this cell line. It was believed that force generation in these cells could be a result of the balance between actin cytoskeleton strength and cell-substrate adhesion.

After introducing polyacrylamide gel with adjustable mechanical properties by Pelham and Wang [112], and also, developing new methods for fabricating novel substrates [201,202], several studies were performed to develop methods for accurate mechanical interaction measurements of both deformation and forces. These measurement methods can be divided into two main categories[1] (Figure 2-4):

1. Cell populated gel based techniques
2. Microscopy based techniques

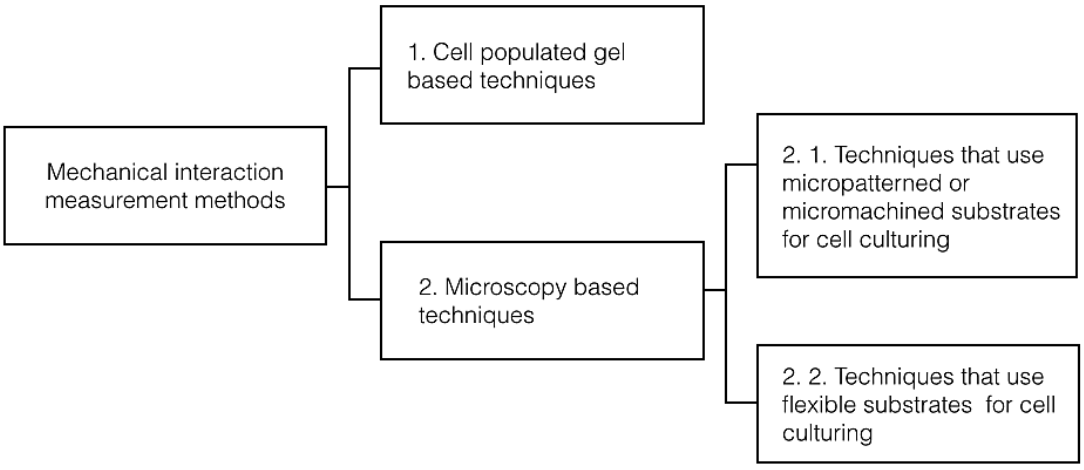

Figure 2-4: Mechanical interaction measurement methods classification.

1. Cell populated gel based techniques

This method is for macroscopic measurement of 3D cell induced deformation and traction forces and the gel that is mainly used is collagen. In this method, collagen is mixed with cells and due to the fact that cells exert forces on the gel, the construct start to contract. One of the first studies that reported the contraction was done by Bell *et al.* [203] . By measuring the contraction of the construct, forces can be quantitatively calculated [204]. Incorporating 10^6 human skin fibroblasts into collagen type I caused 50 - 80% contraction in 24 hours. Also, Sun *et al.* [205] reported that, for fibroblasts, 2×10^5 cells/ml can cause 12% contraction after 24 hours. For measuring the forces, constructs were restrained at both ends and the

[1] It should be mentioned that there are other classifications of CTF measurement methods available in literature [338].

forces developed were measured and cell traction forces were reported as F/t, where F is the tension developed in the material and t is the time required to develop that tension, which was found to be 87 ± 16 %. With the same method, Campbell *et al.* [206] reported more accurate forces as 2nN per cell.

2. Microscopy based techniques

Microscopy based techniques are mainly called Cell Traction Force microscopy (CTFM). CTFM is a versatile method that can be used both for 2D and 3D deformation and force measurements. Generally, this method consists of the following steps: at first, a flexible substrate or a micropatterned surface is chosen, then, following cell culturing, cell-induced deformation is measured, and finally, traction forces are calculated from cell-induced deformation.

Depending on the substrate or basically ``force sensor`` used, CTFM can be categorized into two main groups as follows (Figure 2-4):

2. 1. Techniques that use micropatterned or micromachined substrates for cell culturing

These methods are mostly used for 2D measurements. Micropatterned and micomachined substrates are usually fabricated through lithography techniques. The other method that has been used for fabricating a novel force sensor was moiré fringe fabrication [207]. These substrates are made of either pads that are connected to cantilever beams with known stiffness [208] or arrays of vertical beams that are called pillars [97,201,209–211]. In the case of pads, displacement of pads can be considered cell induced deformation and force can be calculated from these displacements (as a result of cell migration) and stiffness of cantilever beam [208]. In the case of pillars, it was reported that each pillar can be assumed as an ideal spring and force can be calculated with spring equations [202]. Moreover, there are other studies that assumed cell traction forces bend each pillar and force can be calculated through beam bending equations [196,201,209].

This technique has also been used to measure cell traction forces at each focal adhesion point in non-migrating fibroblasts [97]. Forces were calculated by solving an ill-posed equation and it was reported that there is a linear relationship between the force on each focal adhesion and the size of that focal adhesion. Although forces change on different focal adhesions (the order of force is about 10 nN and the peak is at 30 nN), the stress on different focal adhesions with different sizes was almost constant and the magnitude was 5.5 ± 2 nm/μm^2 [97]. For Madin-Darby canine kidney (MDCK) cells, maximum stress exerted by cells on a single pillar was 3.8 ± 0.1 nN/μm^2 [201]. The average value, considering all pillars under the cell, was also reported to be 0.06 nN/μm^2 [201]. Moreover, forces resulting from MDCK cell

sheets were also measured and it was found that cells in the subconfluent layer exerted more mechanical force than cells in a confluent layer [201].

It was also reported that migrating cells exert rearward forces on the leading edge and forward forces on the rear end [196,201]. Using PDMS pillars, relationship between fibronectin assembly and forces exerted by cells was studied and it was found that although the magnitude of force does not affect fibronectin fibril size, direction of traction force guide the direction of fibronectin assembly [196].

As it was mentioned earlier, micromachined substrates are mostly used for 2D cell traction force measurement and migration. However, recently, Doyle *et al.* [212] disclosed that cells cultured on a micropatterned one-dimensional lines on glass coverslip, start to migrate on the line and behave similarly to the cells cultured on 3D matrices. This can be the beginning of the development of new methods for understanding 3D mechanical interaction of cells with their environment.

2. 2. Techniques that use flexible substrates for cell culturing

The advantage of this method is that it can be used for both 2D and 3D mechanical interaction studies. In the first step, a biomaterial with specific properties is chosen and cells are cultured on a substrate or in a matrix. The second step, which is measuring deformation, is performed by incorporating fluorescent markers in the substrate material. When cells migrate, displacement of the markers is believed to be the deformation caused by cell traction force [10]. The third and final step is calculating the force field from the deformation field.

In order for cells to deform the substrate, the substrate should have specific mechanical properties. One of the most common materials that is used for both 2D and 3D deformation and traction force measurement, is polyacrylamide gel. This material is fully elastic, incompressible, chemically neutral [112], and when coated with ECM proteins such as collagen I [112], or fibronectin [3], or even synthetic molecules such as arginine-glycine-aspartic acid-serine (RGDS) [35], acceptable cell attachment can be seen. The other material that can be used is Polydimethylsiloxane (PDMS) [213]. Since it is harder to control mechanical properties of PDMS, this material is mostly used for fabricating micropillars as the force sensor. Gelatin has also been reported for measuring traction forces of fish epithelial keratocytes [214]. Silicone gels were also recently utilized for neurons cells traction force studies [215].

Fluorescent marker tracking, for deformation measurement, is performed by analyzing micrographs of the substrate. Consecutive micrographs are needed for deformation measurement: a micrograph of the substrate while forces are exerted and a micrograph of the substrate in a relaxed state of substrate upon

removal of cells from it. There are two main techniques for tracking fluorescent markers; one is single particle tracking method [15,216–218], also known as particle tracking velocimetry (PTV) [13], during which individual beads are tracked to measure their displacements. The second method for displacement measurement is digital volume correlation (DVC) that is based on image processing techniques. This method has been also called particle image velocimetry (PIV) [177]. In this method, micrographs are divided to smaller subsets and displacements are measured by cross correlating these smaller volumes. It was also reported by Sabass *et al.* [219] that the combination of the two methods as well as utilization of two differently colored markers lead to a higher resolution deformation field.

The last step, which is calculating force from the displacement, depends on the cell traction force measurement mode and the material that was used. For substrates like polyacrylamide and PDMS, in case of 2D cell traction force measurement, displacement and force can be related through the Fredholm integral equation of first kind. Also, fluorescent beads displacements are supposed to be much smaller than the thickness of the substrate, so the substrate can be considered as elastic half-space. In this technique, which is called inverse method [220], finding force from displacement is an ill-posed inverse integral problem. Due to complexity, an ill-posed problem is highly sensitive to noise, and does not have a unique and continuous solution [219]. It is noteworthy that all displacements and forces are measured in 2D. Ill-posed problems can be solved with different regularization techniques, which is addition of an extra assumption to the problem to make it solvable. Fourier transform traction cytometry (FTTC), traction reconstruction with point forces (TRPF), and boundary element method (BEM) are a few methods that have been used for finding force from displacement [219]. In a research done by Sabass *et al.* [219], the above mentioned methods were compared, and it was found that, depending on the regularization method chosen for solving the equation, each of the methods has advantages and disadvantages. Finite element method was the other way of force calculation [221]. Linear elastic theory is probably the most used assumption for force calculations, however, recently, Toyjanova *et al.* [222] reported that using large deformation assumption leads to more accurate results, specifically, in Schwann cells.

Another method for measuring cell traction forces from displacement is the forward method [220]. In the forward method, once discrete bead displacements are calculated, continuous displacement field is determined by interpolation. Differentiating this function leads to strain field computation and forces can be then calculated directly from the strain field.

Since 2009, studies have been performed on finding cell traction forces in 3D by cell traction force microscopy. Hur *et al.* [13] reported that for bovine aortic endothelial cells (BAEC) cultured on polyacrylamide gel coated with fibronectin, "the cell edge experiences an upward or pulling up force, whereas the cell nucleus experiences a downward or pushing down force". In this study, forces were calculated with a particle tracking algorithm and the software ABAQUS was used for solving FEM equations. It was found that the ratio of the force in the z direction to the force in x or y direction was ~0.6, which showed that the vertical force was not negligible. Using Digital Volume Correlation (DVC) algorithm, Franck *et al.* [223] reported that, for 3T3 fibroblasts, the ratio of the force in the z direction to the force in x and y direction was ~1.6 and ~ 5, respectively. Also, Delanoë-Ayari *et al.* [14] found that there is a linear relationship between normal force and in-plane forces for *Dictyostelium* Cells. 3D force magnitude and pattern has also been the subject of different studies. It has been reported that the trailing edge transfers the largest forces [11,14] and under the cell is also involved in force transmission to the substrate and at certain time points large displacements can be seen beneath the nucleus [11]. Also, Ayari and Rieu reported that cells push against the substrate under the nucleus and pull the substrate at the rear of the cell [14]. The same pattern (large forces in the leading edge) was also reported by the studies on 2D force pattern [10]. In this case, cells are moving because of the forces generated in the lamellipodium, and these forces drag the cell forward [10]. A very recent study by Legant *et al.* [15] reported that for fully spread cells, no forces can be seen under nucleus. It was also reported that at focal adhesions, cells are capable of exerting rotational moments. 3D forces were also shown to be present during cell division in 3D matrices [224].

Recently, a new level of 3D cell traction force measurement has emerged, where CTFM is done on cells that are cultured inside a 3D flexible substrate, and forces are also measured in three dimensions [225,226]. Legant *et al.* [225] reported that similar to 2D surfaces, in 3D matrices, highest traction forces can be found at the tip of long and thin pseudopodia. In this study, 3D images taken with confocal microscope coupled with FEM were used for finding cell traction forces [225]. In this research, polyethylene glycol (PEG) based synthetic polymer was used as the biomaterial for cell encapsulation. This is the newest measurement method and the closest to native tissue mechanisms.

In summary, based on these recent findings, traction force microscopy method can be divided into three different levels of complexity. The first level (2D method) is when cells are cultured on a 2D substrate and 2D deformations and forces are measured. The second level of complexity follows the finding of 3D forces that cells are able to apply while cultured on a 2D substrate (2.5 method [15]). The third level and

the most complicated one is when cells are cultured in 3D substrate and 3D responses are investigated. Although recent findings have revealed new information regarding mechanical responses of cells, there are still many more unanswered questions and ambiguities that need to be addressed. Creating more knowledge to further expand the field is necessary: studying different and new types of cells, further studying the behaviors, and understanding the underlying mechanisms are among the subjects that need further investigation.

2.3.4 Concluding remarks

Literature suggests that research on mechanical interaction of cells with their environment, specifically 3D cell-induced deformation, is at the early stages of development and studies are trying to develop more accurate methods to measure mechanical responses of cells. These studies need to be expanded to also include various cell lines toward clinical implications. Simultaneous studying of biological and mechanical responses can further help the route to practical solutions, and since there is a lack of such comprehensive studies, more knowledge in area needs to be gained.

In this thesis, the topic of mechanical interaction of cells with their substrate was approached from both the perspectives of biological responses from cells and the mechanical responses from them. Combining both approaches can lead to better understanding of mechanical interaction of cells with their surrounding and it can further broaden the knowledge in this area.

Chapter 3: Search for a suitable model substrate: investigating properties

To study mechanical interaction of cells with their environment, choosing the right biomaterial, as the model environment, is the very first step in the experimental procedure. To use a material for this purpose, it has to have specific properties:

1. Biocompatibility: Although biocompatibility has a broad definition, in the current application, cytotoxicity is one of the main concerns. A material that is not cytotoxic, which is desirable, is chemically inert in cell culture medium and does not contain or release any cytotoxic components.

2. Suitable cell attachment: In the present research, all cell lines used are anchorage dependent cells; therefore, it is crucial to choose a material that provides a proper substrate for cells to attach to. In case of no cell attachment, it is crucial to be able to treat the surface of the substrate to allow the attachment to occur.

3. Controlled mechanical properties: It is important to choose a material with properties comparable to native tissue. It is also crucial to consider that deformation induced by cells and forces exerted by them are extremely small, thus the material stiffness should be in the range that cells are able to deform. As an example, Swiss Albino 3T3 fibroblasts are able to deform

polyacrylamide gels with an elastic modulus up to 9 kPa [223]. NIH 3T3 fibroblasts have also been reported to deform PEG based 3D hydrogels with elastic modulus ranging 0.6-1 Pa [225].

In the current research, to find the right biomaterial, several options were studied. In this chapter selected ones are discussed.

3.1 Poly (L-Lactic acid)[1]

Poly (L-Lactic acid) is a synthetic polymer that is often used as a tissue engineering scaffold. There are several different methods for fabricating tissue engineering scaffolds with desired properties. The method chosen here is thermally induced phase separation (TIPS). Two different TIPS protocols were utilized to prepare PLLA with different microstructures: Fibrous (F-TIPS) and porous (P-TIPS). Mechanical properties were tested and cell viabilities in different microstructures were studied.

3.1.1 Materials and methods

3.1.1.1 Sample Preparation

The 3 wt%, 5 wt%, and 7 wt% Poly(L-lactic acid) (PLLA; Resomer grade, Boehringer Ingelheim, Germany) samples were fabricated by both F-TIPS and P-TIPS methods:

1. F-TIPS: PLLA was dissolved in Tetrahydrofuran (THF; Sigma Aldrich, Canada) at 60-70^{0}C. Samples were then placed in the freezer at -25^{0}C for two hours. Frozen samples were placed in water for the solvent to be exchanged with water, which is a non-solvent, for two days. Water was changed twice a day.
2. P-TIPS: PLLA was dissolved in a mixture of 1,4-dioxane (Sigma Aldrich, Canada) and distilled water (the ratio of 1,4-dioxane to distilled water was 87/13 [227]) at 60-70^{0}C. The solution was poured in an aluminum mold to be immediately placed into liquid nitrogen. After samples were completely frozen in liquid nitrogen for two hours, samples were placed in ethanol for two days for the solvent to be replaced with ethanol which is a non-solvent in this method. Ethanol was changed twice a day.

After the exchange process, samples of both groups were freeze-dried for another two days to make dry samples.

[1] Results of this work were published as a journal paper [313]. The full journal paper with further details of experiments and results can be found in Appendix A.

3.1.1.2 SEM investigations

To study PLLA samples prepared by different methods, freeze-dried samples were characterized using scanning electron microscopy (JSM-6460, JEOL, Japan) at 20 KV. For SEM observations, samples were fractured in liquid nitrogen and coated with a 10 nm layer of gold.

3.1.1.3 Mechanical behaviour characterization: simple compression

Stress-strain behaviour was investigated by simple compression test using a universal material testing machine (Texture analyser.xt Plus, Stable Micro Systems, New Jersey) with a 50 N load cell (Figure 3-1).

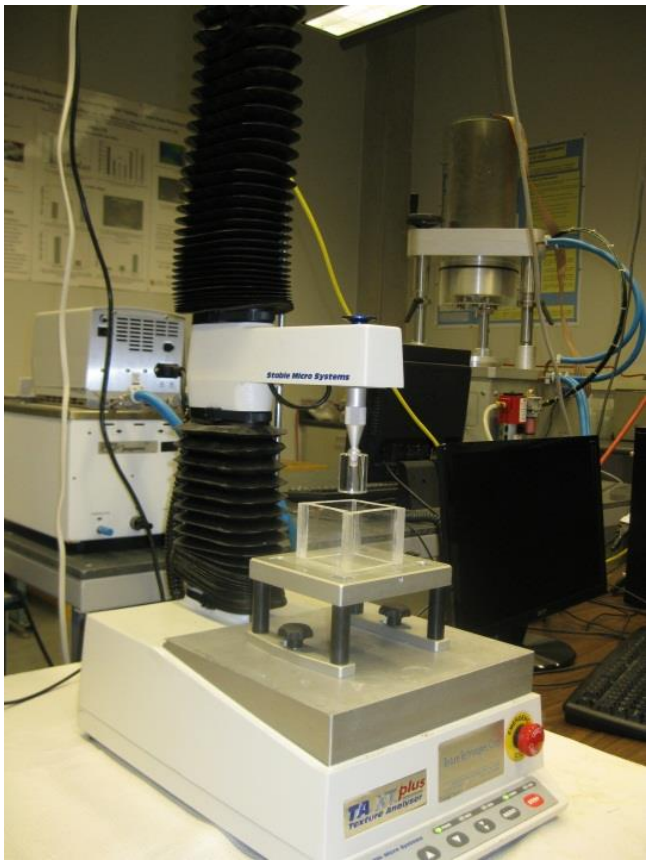

Figure 3-1: Instrument used for simple compression test of PLLA samples.

3.1.1.4 Cell culturing and viability measurements

The MG63 cell line (human osteosarcoma fibroblast) (ATCC, Manassas, VA), derived from a 14 year old male, was maintained in MEM cell culturing medium (Minimum Essential Medium Eagle, ATCC, Manassas, VA) supplemented with 10 % fetal bovine serum (FBS), and 1 % penstrep (Invitrogen, Carlsbad, CA), which is a mixture of 5,000 units of penicillin (base) and 5,000 µg of streptomycin

(base)/ml, at 37 ^{o}C, 5 % CO_2, and 95 % humidity incubator. Cell culture medium was changed every two to three days.

Prior to cell culturing, all PLLA samples were sterilized by 70% Ethanol. In order to study cellular behaviour, cells were fluorescently stained with the LIVE/DEAD cell viability kit (Invitrogen, Carlsbad, CA) following manufacturer's protocol and imaged by confocal microscope.

3.1.1.5 Confocal microscopy

Confocal microscopy was performed by taking images of fluorescently labeled cells with an inverted laser scanning confocal microscope (LSM 510 meta, Carl Zeiss, Germany) using an argon laser (488nm) and an HeNe laser (543nm).

3.1.2 Results and discussion

3.1.2.1 Microstructural investigation

As shown in Figure 3-2, the microstructures resulting from F- and P-TIPS methods are significantly different. F-TIPS yielded fibrous structure that better resembles native ECM microstructure, whereas P-TIPS produced foam like porous microstructure.

Typical TIPS consists of the following major steps: dissolving PLLA in a suitable solvent, freezing the solution, exchanging the solvent with a non-solvent and finally drying the sample (mostly by freeze-drying) [228]. During both F-TIPS [229,230] and P-TIPS [231–235] polymer solution goes through liquid-liquid phase separation, however, use of different solvents and cooling temperatures result in drastically different microstructures. The difference in final microstructures might have resulted from the different mechanisms of pore formation occurring during the fabrication process. Similar microstructures for both F- [229] and P-TIPS [227,233] methods have been previously reported.

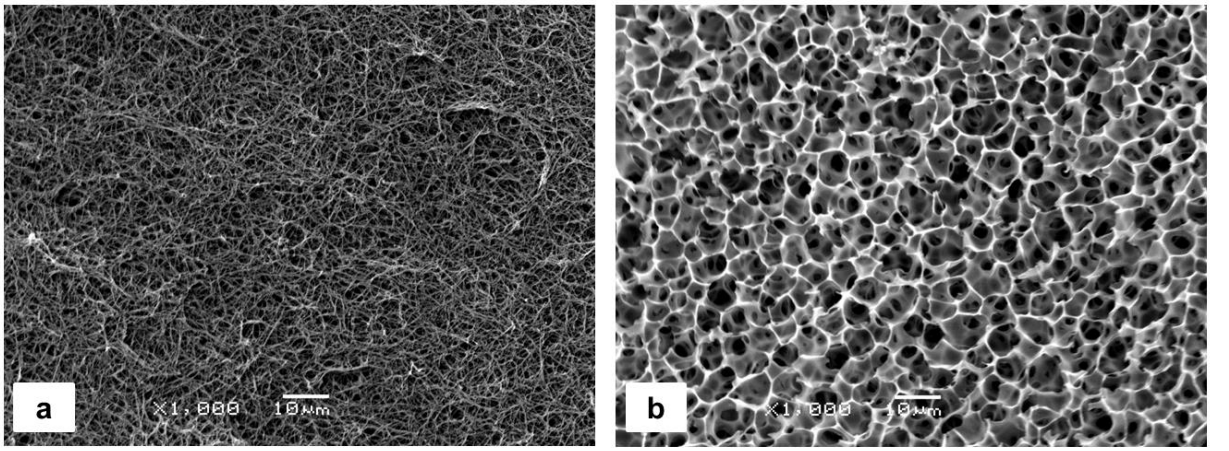

Figure 3-2: SEM micrographs of typical structures fabricated by a) 5F-TIPS, and b) 5P-TIPS.

3.1.2.2 Mechanical characterization of Poly(L-lactic acid)

For the mechanical characterization of PLLA structures, the elastic modulus was measured by simple compression test and the results are presented in Table 3-1. It can be seen that P-TIPS samples generally have higher elastic modulus values than F-TIPS samples. In F-TIPS samples, which had a fibrous structure, deformation mechanism could be related to deformation, slipping and eventually breaking of fibers, whereas, in P-TIPS samples with a porous structure, pore walls deformed during mechanical loading. Since fiber diameters were smaller than pore wall thicknesses, fibrous structures were more flexible than porous structures. Moreover, fibers were loosely connected by flexible junctions as opposed to the pore walls rigidly interconnected together. Both methods led to structures with relatively large elastic moduli that were significantly higher than the appropriate range for cell traction force microscopy.

Table 3-1: Elastic moduli of PLLA samples with various concentrations, prepared by both F- and P-TIPS methods

Polymer concentration (wt%)	Fabrication method	Elastic modulus Avg ± std dev (kPa)
3	F-TIPS	202 ± 75
	P-TIPS	1527 ± 580
5	F-TIPS	780 ± 97
	P-TIPS	6145 ± 1338
7	F-TIPS	1204 ± 51
	P-TIPS	7541 ± 1166

3.1.2.3 Cell viability assessment

In order to see if cells can live within PLLA scaffolds, cells were cultured in structures and cell viability was assessed using the LIVE/DEAD cell viability kit (Invitrogen, Carlsbad, CA). Results are shown in Figure 3-3. The green staining identified live cells with high nonspecific esterase activity. The live cell dye can penetrate inside the cell and following interactions with estrases, calcein AM green fluorescent molecules allow the live cells to appear as green. On the other hand, dead cells with ruptured plasma membrane allowed penetration of ethidium homodimer (the dead cell dye) and appeared red. It can be seen that although dead cells can be found in the structures, majority of cells could survive inside both structures.

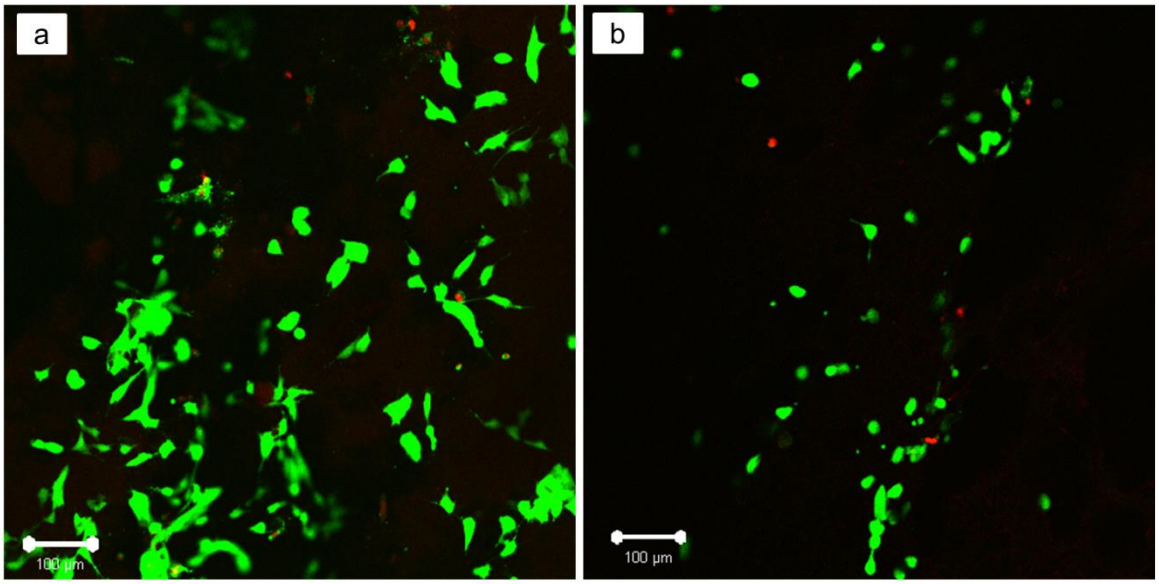

Figure 3-3: Fluorescently stained cells by Live\dead cell viability kit in a) 5F-TIPS, b) 5P-TIPS specimen.

3.1.3 Concluding remarks

TIPS can be used for fabrication of substrate with different microstructures. As a biodegradable and biocompatible polymer, cells can survive in different PLLA structures fabricated by F-TIPS and P-TIPS. However, the high elastic modulus limits the application of this material for investigating cellular mechanical interaction.

3.2 Collagen

As the main constituents of connective tissue, different types of collagen have been extensively used to study cell-ECM interactions over the years. This natural biogel was investigated to determine if it could fulfill the essential requirements of this study.

3.2.1 Materials and methods

3.2.1.1 Sample preparation

3D collagen gels were prepared by diluting the high concentration type I rat tail collagen (BD Biosciences, NJ, USA) solution in 0.02N acetic acid. Dilution was done by addition of 1N sodium hydroxide, 10X PBS (VWR, PA, USA) and cell culturing grade water. Since collagen samples start to gel at room temperature, sample preparation was done aseptically on ice. Diluted collagen solution was

poured in a Teflon mold and incubated at 37^0C for 45 minutes. Stock solution concentrations ranged from 8 to 11 mg/ml and the final samples concentrations ranged from 2.5 mg/ml to 5 mg/ml.

For confocal microscopy samples, carboxylate-modified fluorescent microspheres (1μm diameter, excitation/emission wavelengths of 580/605 nm) were mixed with collagen solutions prior to gelation. Samples were placed in 35 mm glass bottom dishes (MatTek, Ashland, MA) (Figure 3-4) to perform microscopy.

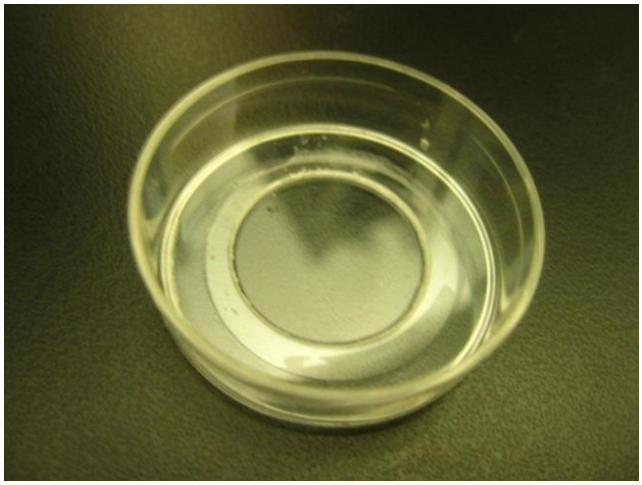

Figure 3-4: 35 mm glass bottom MatTek dishes used for confocal microscopy.

3.2.1.2 Cell culturing, fluorescent staining, and transduction

Swiss Albino 3T3 fibroblast cells were maintained at 37 ^{0}C, 5 % CO_2, and 95 % humidity in complete growth medium, Dulbecco's Modified Eagle Medium (DMEM) (Invitrogen, CA, USA) supplemented with 10 % FBS (VWR, Radnor, PA) and 1 % penstrep (Invitrogen, Carlsbad, CA), which is a mixture of 5,000 units of penicillin (base) and 5,000 μg of streptomycin (base)/ml.

In order to image cells, calcein AM was used with excitation/emission of 495/515 nm. However, since calcein exits cell cytoplasm after 3-4 hours. In order to track cells during migration, cells were transduced overnight using CellLight® Actin-GFP, BacMam 2.0 (Invitrogen, CA, USA) to express green fluorescent protein (GFP) on actin filaments, following manufacturer's protocol. Excitation/emission wavelengths of GFP are 485/520 nm.

3.2.1.3 Mechanical behaviour characterization: viscoelastic properties

The dynamic mechanical analyzer (Q800, TA instruments, New Castle, DE) (Figure 3-5a) was used to investigate viscoelastic properties of collagen samples. Tests were performed by submersion compression

clamp (Figure 3-5b) at 37^0C and complete cell culture medium (DMEM supplemented with 10 % FBS and 1 % penstrep) was used as the immersion medium.

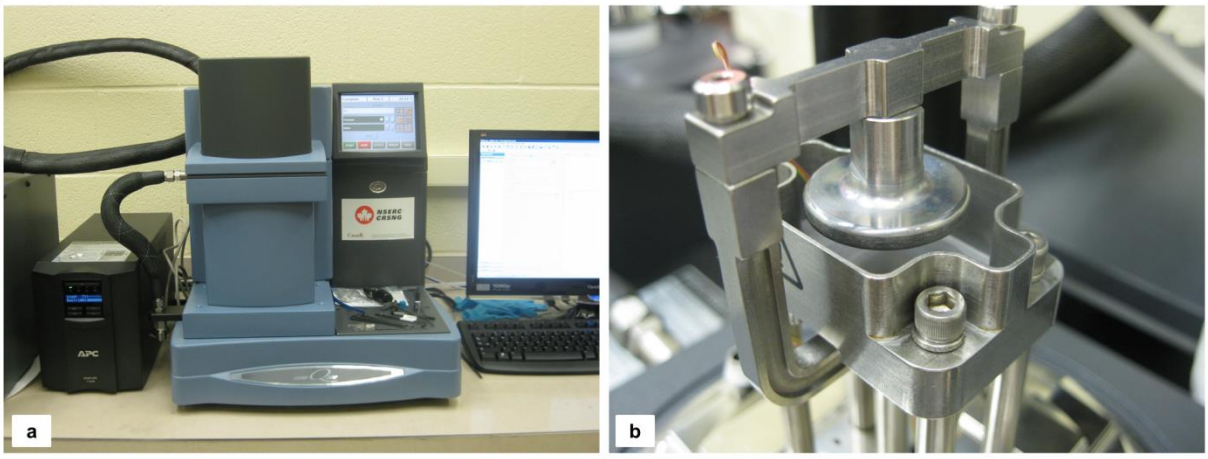

Figure 3-5: a) Dynamic mechanical analyzer b) Submersion compression clamp used for characterizing collagen samples.

3.2.1.4 Confocal microscopy

Inverted confocal laser scanning microscope (CLSM; Zeiss, LSM 510 meta) was used to both image collagen microstructure and to perform live cell imaging. The following objective lenses were utilized: 10x/0.45 water immersion, 40x/1.2 water immersion, 63x/1.4 oil immersion. During time-lapse imaging, the confocal microscope was equipped with a micro-incubator (Biosciences Tools, CA, USA), so that the temperature was kept at 37^0C (Figure 3-6). Also CO_2 (5%) and humidity (95%) were controlled to ensure the appropriate environment for cells.

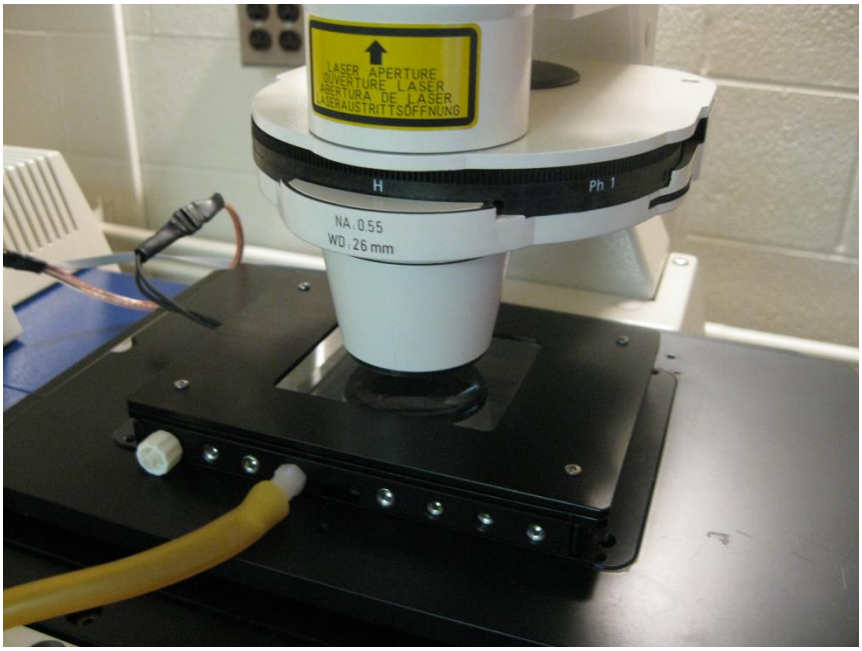

Figure 3-6: Micro-incubator on the confocal microscope stage.

Two confocal microscopy techniques were used to image cells:

1. Confocal fluorescence microscopy (CFM): During CFM, in order to image cells, samples were illuminated by Argon laser with a wavelength of 488 nm and the emitted light (with wavelength of 515 or 520) was detected by the photomultiplier tube. HeNe laser with a wavelength of 543 nm was used for imaging fluorescent microspheres.
2. Confocal reflectance microscopy (CRM): Collagen samples were illuminated by Argon laser with a wavelength of 488 nm and the photomultiplier tube detected the same wavelength.

3.2.2 Results and discussion

3.2.2.1 Mechanical characterization

In order to mechanically characterize collagen gels and study their viscoelastic properties, the dynamic compression test in a submersion compression clamp was performed using the dynamic mechanical analyzer (DMA). In this test, effect of amplitude (which shows the influence of strain) and frequency (which shows the influence of strain rate) as device parameters, and collagen concentration as sample property, were investigated. Depending on the test, either frequency or amplitude was kept constant to assess the effect of the other factor.

The first test investigated the effect of collagen concentration on storage (Figure 3-7a) and loss (Figure 3-7a) moduli for sample concentrations of 2.5 mg/ml and 5 mg/ml. As expected, increasing collagen concentration led to an increase in storage and loss moduli of the gel. Thus, it was beneficial to keep the concentration as low as possible for the cells to easily deform the gel. On the other hand, since the collagen samples were generally weak, decreasing collagen concentration made handling of the samples more difficult. So, the optimum sample concentration was chosen to be 2.5 mg/ml. In this case, storage modulus was measured to be about 1 kPa. The similar trend has been reported for collagen samples in the literature [236].

It can also be seen from Figure 3-7 that increasing frequency led to negative loss modulus. Two reasons might have caused the negative modulus. One cycle of dynamic test consists of both loading and unloading. For higher frequencies, collagen sample did not have enough time to recover during unloading, so the sample might have lost contact with the platen, which is applying the force. Also, since the dynamic compression test was performed in cell culture medium, higher frequencies caused larger volume of liquid to move during the test. Therefore, the forces applied due to the movement of larger volume of liquid might have been detected as a sample response.

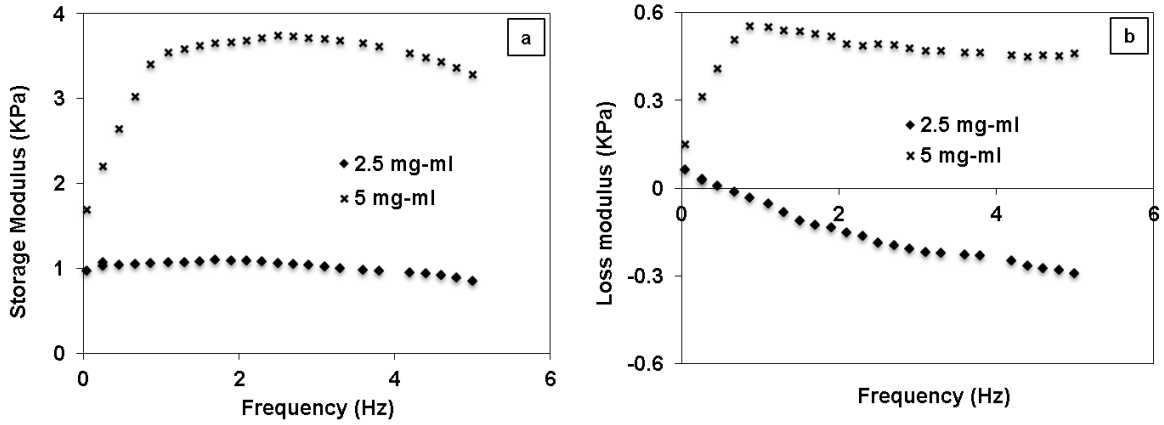

Figure 3-7: Effect of collagen concentration on a) storage, and b) loss moduli, amplitude = 50μm.

In order to find out the suitable frequency for measuring mechanical properties of a sample with concentration of 2.5 mg/ml, effect of frequency on storage (Figure 3-8a) and loss (Figure 3-8b) moduli at two different amplitudes was investigated. According to these results, loss modulus had negative values for frequencies higher than ~ 0.5 Hz. Therefore, the final frequency was chosen to be 0.1 Hz.

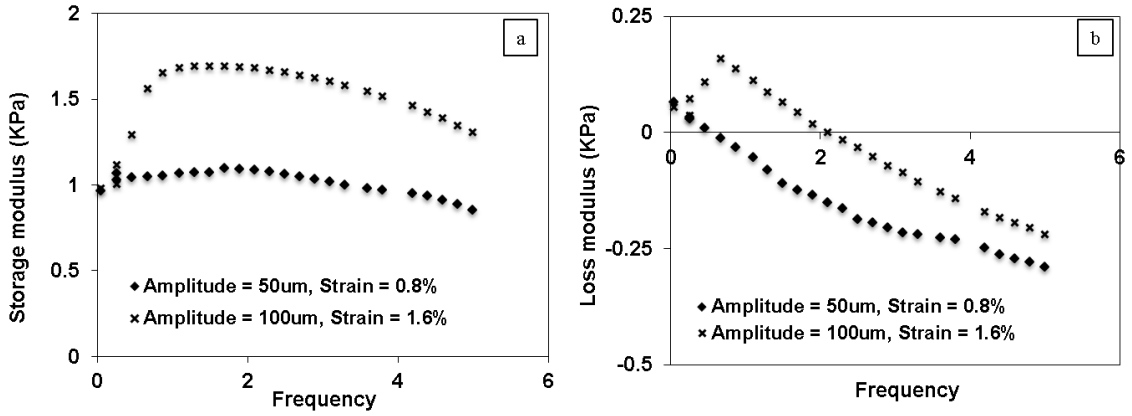

Figure 3-8: Effect of frequency on a) storage and b) loss moduli, concentration = 2.5 mg/ml.

With the frequency of 0.1 Hz, the effect of strain (amplitude) on storage and loss moduli was studied. Figure 3-9a shows the change of storage and loss moduli with strain. Also, Figure 3-9b is the stress strain curve of this sample. In this graph, stress was the maximum stress at each cycle of the test with the corresponding amplitude (strain). Also, tan δ, which is defined as the ratio of storage and loss modulus, was calculated to range from 0.07 to 0.09.

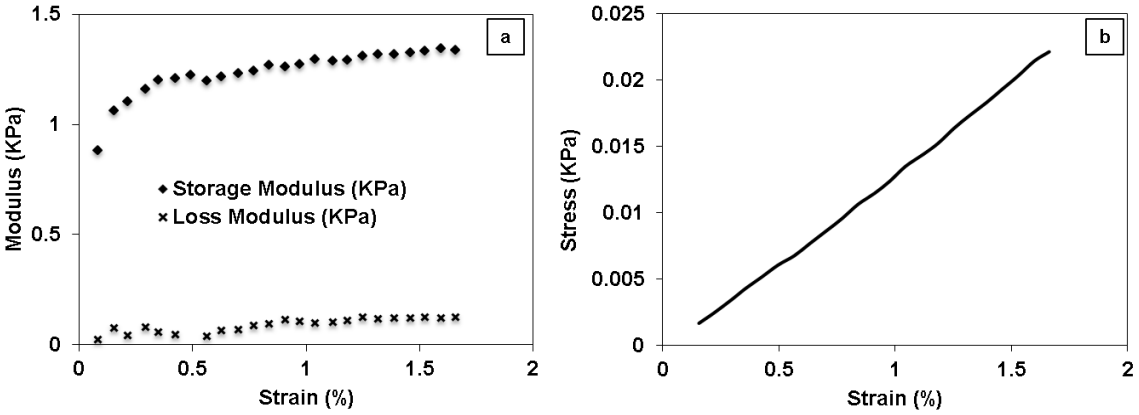

Figure 3-9: a) Effect of amplitude (strain) on storage and loss modulus, b) stress strain curve, small strains, frequency = 0.1 Hz.

In Figure 3-9, maximum strain was ~ 1.7% and in this range of strain, storage modulus change was not significant. However, increasing strain resulted in a different behaviour (Figure 3-10).

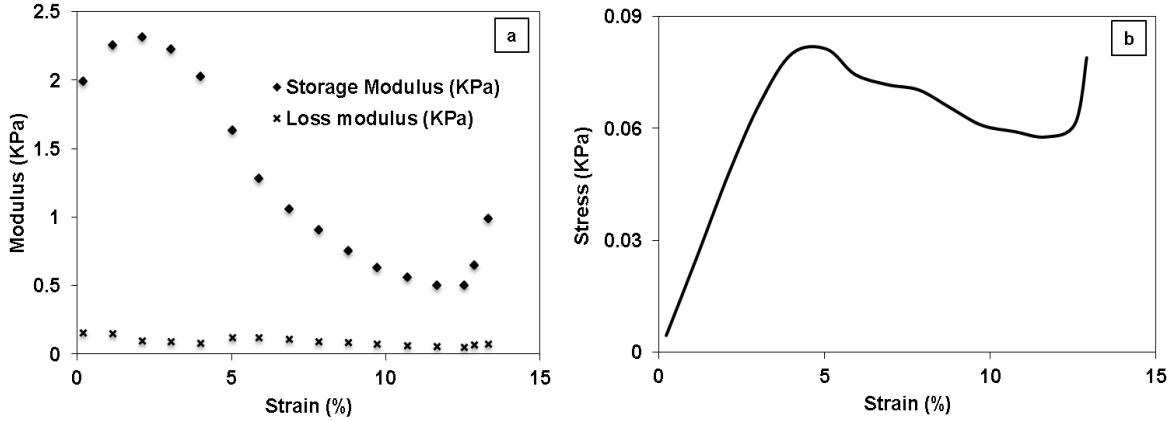

Figure 3-10: a) Effect of amplitude (strain) on storage and loss modulus, b) stress strain curve, large strains, frequency = 0.1 Hz.

Collagen belongs to a group of polymers that are called semi-flexible polymers and can be described by polymer theory. According to polymer theory, filaments can be categorized into three groups based on two characteristic parameters: persistence length l_p and contour length l_v [237]. Persistence length is the characteristic mechanical property of a filament and is defined as "the typical length scale for decay of tangent-tangent correlation" [237]. If $l_p \ll l_v$, the filament is flexible; if $l_p \gg l_v$, the filament is rigid; and if the two lengths are comparable, the filament is semiflexible. Most biopolyemrs which are interconnected structure of filaments, such as collagen, actin, and fibrin, lie in this category [237,238]. This group of polymers has unique properties, such as negative normal stress in shear, and strain stiffening at moderate strains during shear [238]. There are different theories for explaining the strain stiffening: Storm *et al.* [237] described it by entropic behaviour of individual filament. Onck *et al.* [239] related this property to microstructural changes during the deformation. According to this theory, during shear, filaments start to rotate to the direction of deformation and change their mode of deformation from bending to stretching, and due to much higher mechanical properties of filaments in tension, polymer mechanical properties increases. It was also proven that filaments undulation can postpone the onset of stiffening.

It can be seen in Figure 3-10a that storage modulus is decreasing in the range of ~ 3% to ~ 13% rather than increasing. This decrease is seen in Figure 3-10b as well, where a decrease is seen in stress-strain curve in the same strain range. This response can be explained by the Onck *et al.* [239] theory. During compression test, collagen filaments experience more undulation rather than stretching, so, the possibility of filaments going through bending mode of deformation as opposed to stretching mode of deformation

can be an expected phenomenon. The significant increase in storage modulus, strain stiffening, which is starting at ~ 14% strain, can also be attributed to microstructural changes. Increase in mechanical properties during compression test has been previously reported for trabecular bones, in which this increase was related to densification at larger strains [240].

3.2.2.2 Confocal microscopy

The basic confocal micrographs were images of cells. Figure 3-11 shows cell morphology at three different magnifications. These cells were cultured on a glass bottom dish (Figure 3-4) and were stained by calcein. Cell length was measured to be ~ 50μm.

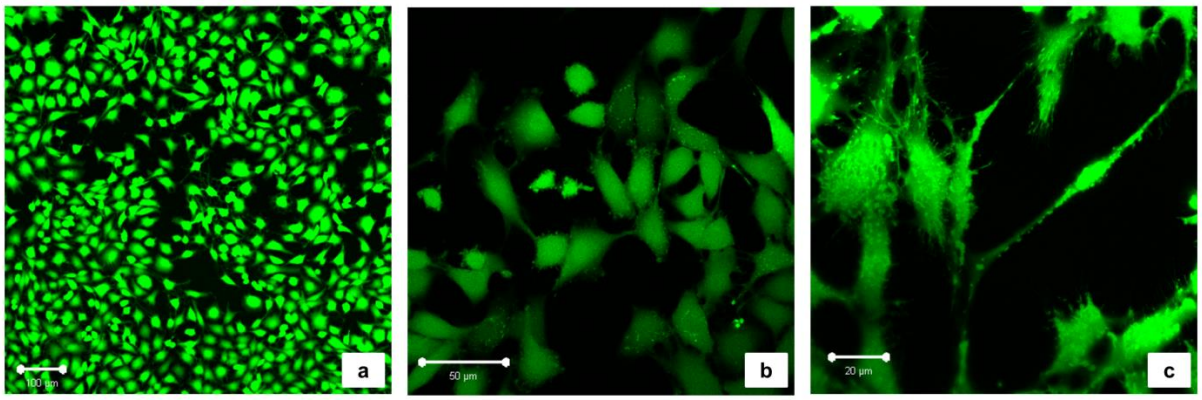

Figure 3-11: 3T3 fibroblast cells stained with calcein AM at a) 10x, b) 40x, and c) 63x objective lens magnification.

3D images of cells cultured in collagen samples with two concentrations of 2.5 mg/ml (Figure 3-12a) and 5 mg/ml (Figure 3-12b) were also taken by confocal microscope. Each image consists of micrographs of cells taken at different planes and the final 3D image is formed by stacking the slices on the top of each other.

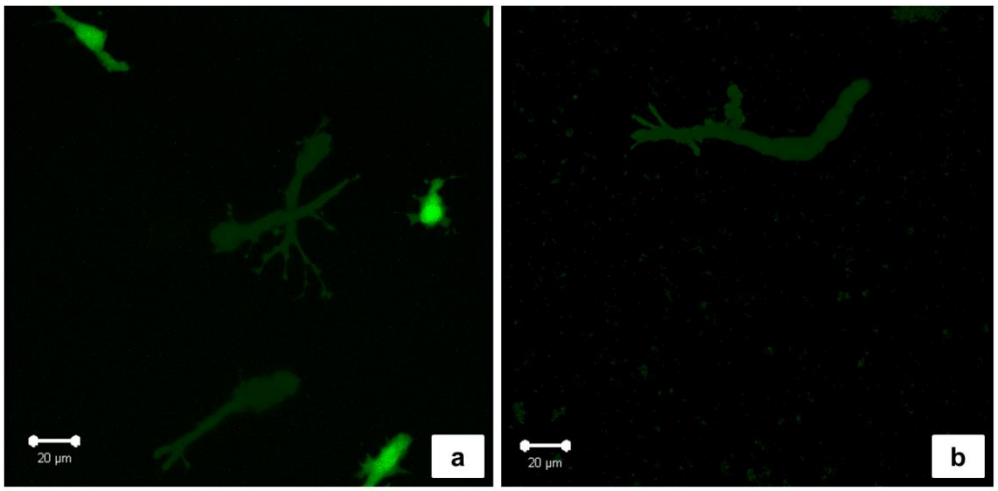

Figure 3-12: Cells cultured in collagen with different concentrations a) 2.5mg/ml, b) 5 mg/ml, stained with calcein and imaged by 40x, water immersion objective lens.

When cells are cultured in a 3D matrix, whether migrating or not, they are in contact with their environment in all three dimensions. Whereas cells cultured on a 2D surface are in contact with the surrounding just on their basal plane. Thus, in order to perform their vital activities (such as migration), they change their morphology in a way that they can squeeze in the pores of the matrix. At the same time, they also try to adapt to their surrounding by remodeling or proteolysis of the matrix [32]. As shown in Figure 3-12 it can also be assumed that the single cell in the collagen matrix with higher concentration had a more elongated shape than the cells in a collagen with lower concentration.

For simultaneous confocal microscopy of substrate and cells, two approaches were taken:

1. The first approach is the conventional traction force microscopy method where fluorescent microbeads are added to substrate [10]. To do so, images of both beads (Figure 3-13a) and also cells and beads, simultaneously, (Figure 3-13b) were taken.

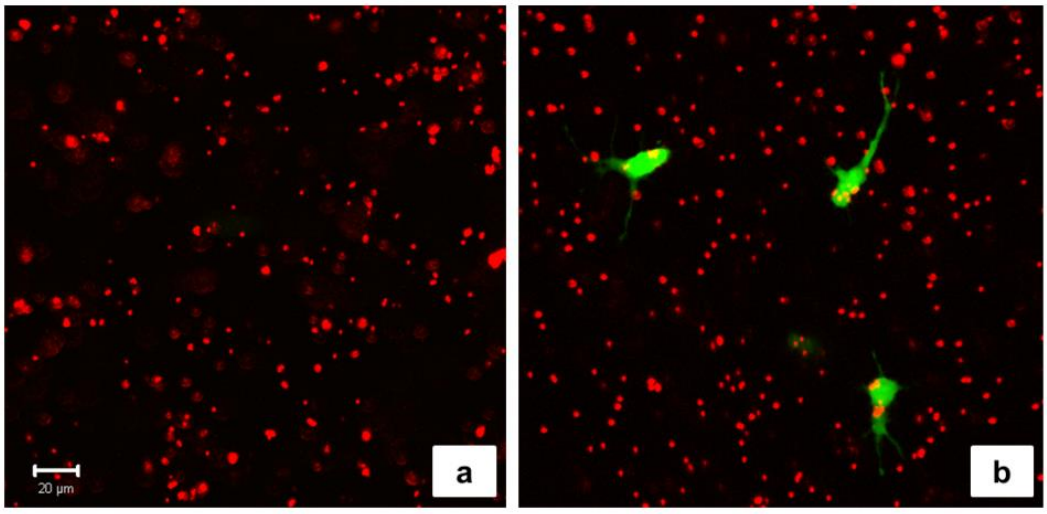

Figure 3-13: Confocal micrographs of a) 1vol% of fluorescent microspheres in a matrix of collagen with concentration of 5 mg/ml, b) simultaneous imaging of 2.5 mg/ml collagen sample, containing 1vol% of fluorescent microspheres and cells stained by calcein.

2. Another approach is by visualizing collagen fibers by CRM and simultaneous imaging of collagen fibers and cells. Figure 3-14a and b shows collagen fibers at two different magnifications.

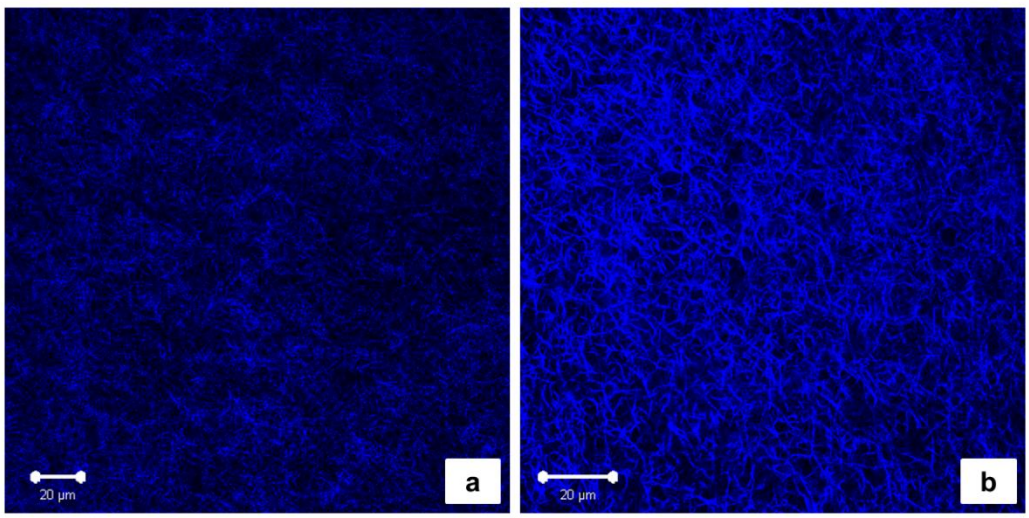

Figure 3-14: Confocal micrograph of collagen fiber in a sample with concentration of 2.5mg/ml collagen at magnification of a) 40x, b) 63x.

An image of cells cultured in collagen is presented in Figure 3-15. In this image, collagen fiber realignment in the direction of cells, as an indication of matrix remodeling, can be seen (white arrows). Karning *et al.* [50] has previously reported similar results and believed that this matrix reorganization can be an indication of traction forces in the matrix. Thus, cells in collagen matrices have the ability to not

only deform the matrix and realign the fibers, they can also degrade the collagen fibers [241] or even deposit ECM to the matrix [242]. The versatile nature of interactions between cells with collagen makes it complicated to just isolate cell-induced deformations and cell traction forces.

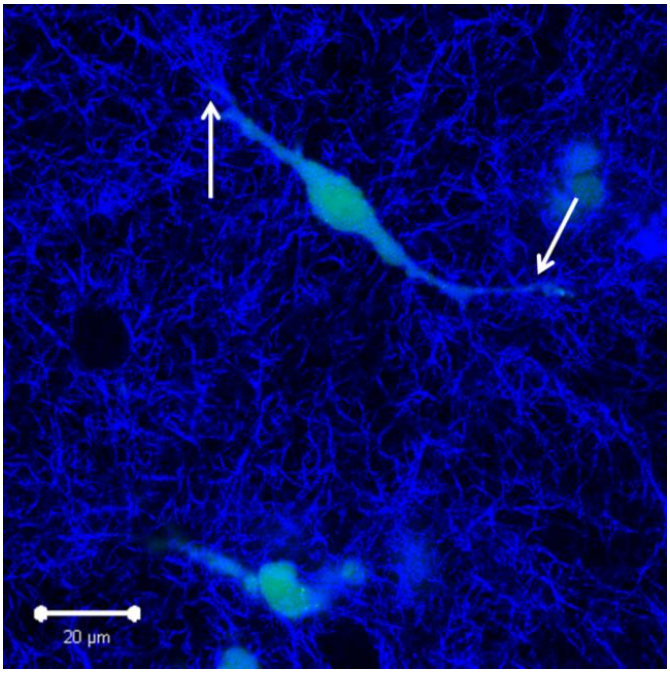

Figure 3-15: Confocal micrograph of cells in a collagen matrix, concentration = 2.5 mg/ml, 63x objective lens magnification.

3.2.2.3 Time lapse imaging

Time lapse imaging to study cell migration was the next step in the experimental studies. A typical time lapse imaging result can be seen in Figure 3-16. The main issue and the biggest problem with live cell imaging of collagen/cell constructs was the fact that no migration was seen for cells cultured in collagen matrices. This may have been a result of the high collagen concentration, however, concentrations lower than 2.5 mg/ml were extremely delicate and almost impossible to handle. So, this problem did not allow the use of collagen for cell migration studies. Phototoxicity, photobleaching, and microscope's focus drift were also the other challenges involved in time lapse imaging in these experiments[1].

[1] These challenges will be discussed in detail in 5.2.3.

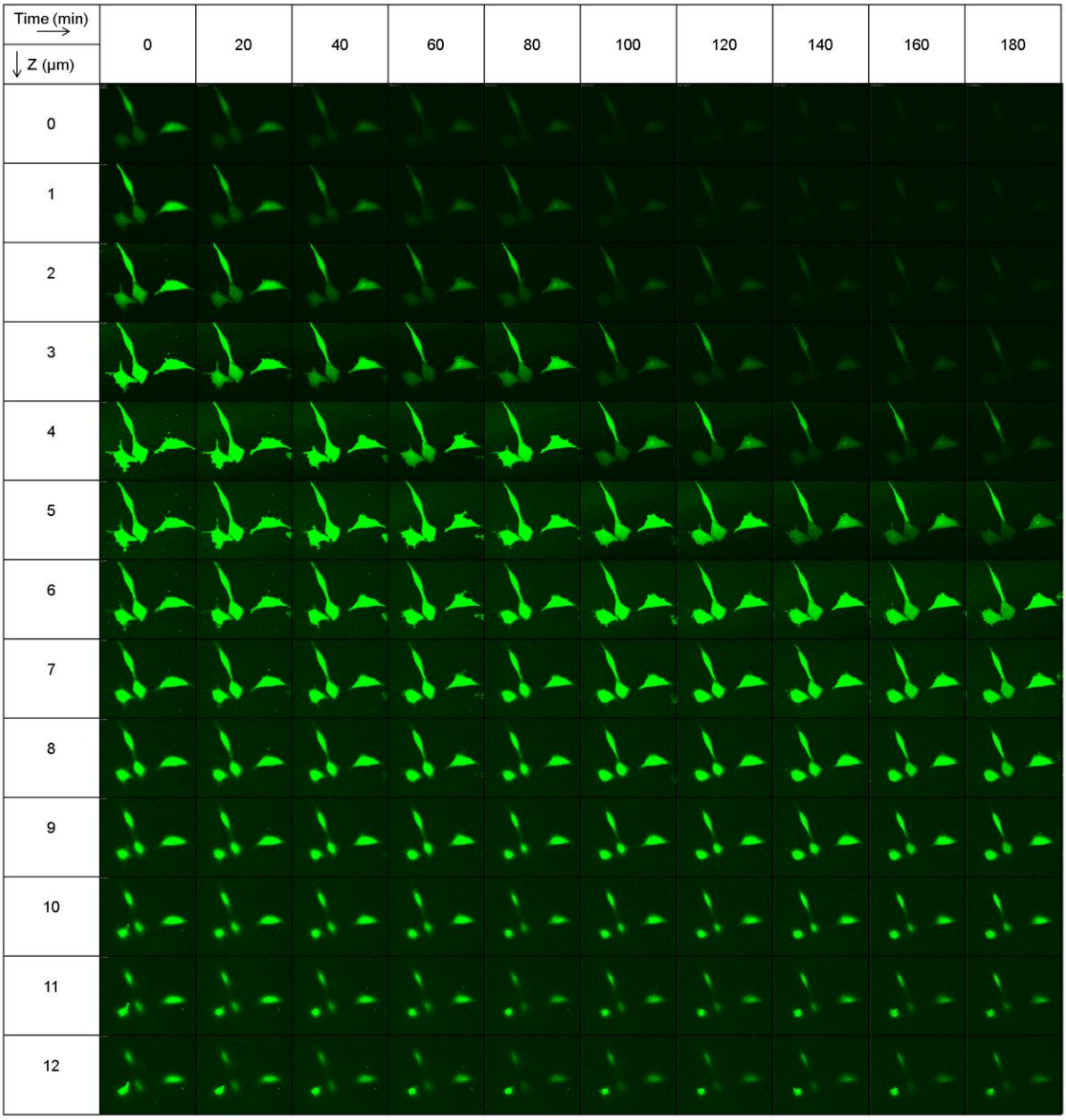

Figure 3-16: Time-lapse imaging of cells cultured in collagen with concentration of 2.5mg/ml.

3.2.3 Concluding remarks

Since collagen is a natural biopolymer, it had the potential to be a suitable option for studying cell mechanical interaction with their ECM. However, complicated mechanical behaviour and complexities

regarding time lapse imaging, including challenges with visualizing cell migration inside 3D collagen constructs, discouraged its use in the current research.

3.3 Polyacrylamide (PAAm)

Polyacrylamide is a synthetic polymer that was first used for mechanotransduction studies by Pelham and Wang in late 1990s [112]. It is fabricated through polymerization of acrylamide monomers by its crosslinker, bis-acrylamide (Figure 3-17). In this reaction, Tetramethylethylenediamine (TEMED) and ammonium persulfate are initiators that accelerate the polymerization process by increasing free radical formation rate.

PAAm has many advantages for this particular application. Not only is it easy to manipulate for fabricating polymers with versatile properties, it also is optically clear, chemically inert, and shows linear elastic mechanical behaviour over a wide range of stresses [243].

There is also a disadvantage to using PAAm in mechanotransduction studies. Recently, Trappmann et al. [244] showed that when elastic modulus of PAAm changes, porous structure on the surface of the membrane changes and this, in turn, affects ECM molecule tethering to the surface. They believed that the responses of cells could be due to this effect as opposed to changes in mechanical properties. It is worth mentioning that another recent study by Wen et al. [245] supports the idea that cells actually do sense the elastic modulus and that ECM molecule tethering is not the main parameter controlling cellular behaviour. The controversy over this aspect of PAAm substrate has not yet been resolved and this was considered a disadvantage of using this polymer in the current studies.

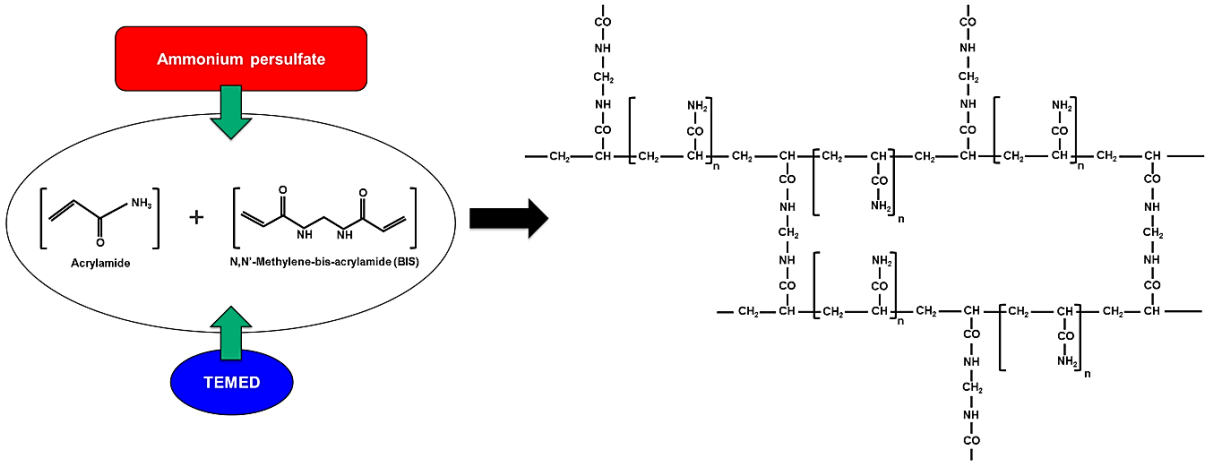

Figure 3-17: Schematic showing polymerization reaction for PAAm fabrication, adapted from [243].

3.3.1 Materials and methods

3.3.1.1 Sample preparation

PAAm samples were fabricated by mixing different concentrations of acrylamide (40% w/v, Bio-rad, CA, USA) and bis-acrylamide (2% w/v, Bio-rad, CA, USA) monomer solutions with ultra-pure water. All sample concentrations are listed in Table 3-2. To prepare samples for simple compression tests, monomer solution mixtures were poured in Teflon molds and polymerization was allowed to occur for 30 minutes.

Table 3-2: PAAm sample concentrations

Sample	Concentrations (vol %)			
	Acrylamide	Bis-acrylamide	TEMED	APS
10 - 0.01	10	0.01	0.15	0.5
12 - 0.01	12	0.01		
15 - 0.01	15	0.01		
10 - 0.1	10	0.1		
12 - 0.1	12	0.1		
15 - 0.1	15	0.1		
10 - 0.3	10	0.3		
12 - 0.3	12	0.3		
15 - 0.3	15	0.3		

3.3.1.2 Bulk mechanical characterization

Simple compression test was performed to measure compression elastic modulus of bulk samples. Experiments were performed in water (Figure 3-1) with a strain rate of 0.5mm/s. Simple compression was also used for stress relaxation experiments. Samples were kept at constant load at 20% strain and stress responses were plotted over time.

To calculate Poisson's ratio, lateral deformation was measured by taking images of simple compression test at 10 frame per second (fps) with high resolution charged-coupled device (CCD) camera (1028×1008 pixels) (STC-CL202A, SENTECH), through a camera link (NI PCIe-1427, National Instrument). Images were then processed using ImageJ (National Institute of Health (NIH), USA).

3.3.2 Results and discussion

3.3.2.1 Simple compression test

To investigate the effect of base polymer and crosslinker concentrations on mechanical behaviour of polymer, simple compression tests were performed on cylindrical samples and elastic modulus was calculated (Figure 3-18). Although the effect of crosslinker seems to be more substantial, it seems that increasing both base polymer (acrylamide) and crosslinker (bis-acrylamide) concentrations increased elastic modulus. This increase has been previously reported by Tse and Engler [246] as well.

In these experiments, since compression test was performed in water, there was very low friction between indenter and the samples. Because of this low friction, lateral bulging of the test samples did not occur.

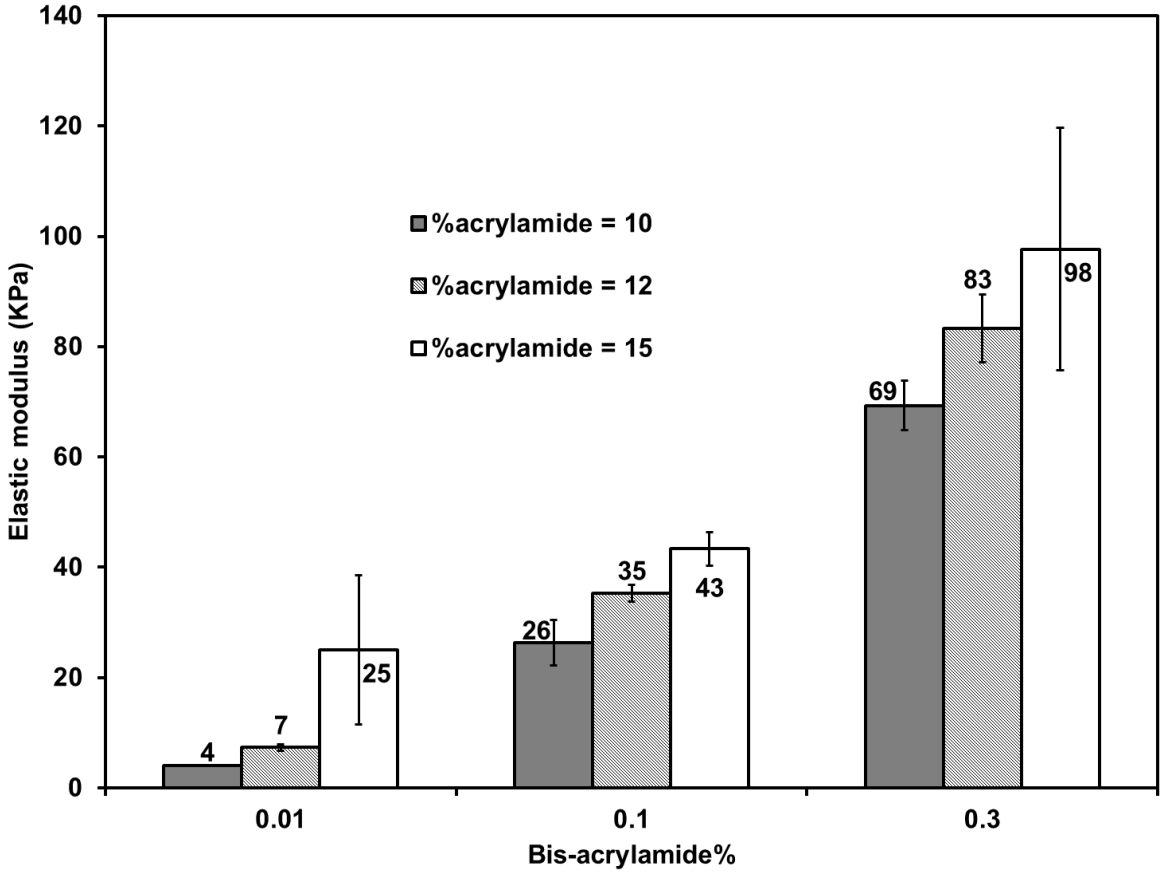

Figure 3-18: Elastic modulus of PAAm samples fabricated by various base polymer (acrylamide) and crosslinker (bis-acrylamide) concentrations.

Figure 3-19 shows a typical stress strain curve for a 10-0.01 sample. As previously mentioned, compression tests were performed in water to avoid samples from drying out. The other advantage of aqueous medium for compression test was decreasing friction on the interface of the probe and sample. However, there was a disadvantage to this as well. Samples slid off after certain amount of strain. As highlighted in Figure 3-19, the small step, in the otherwise almost linear curve, is believed to occur due to this sliding and sample movement.

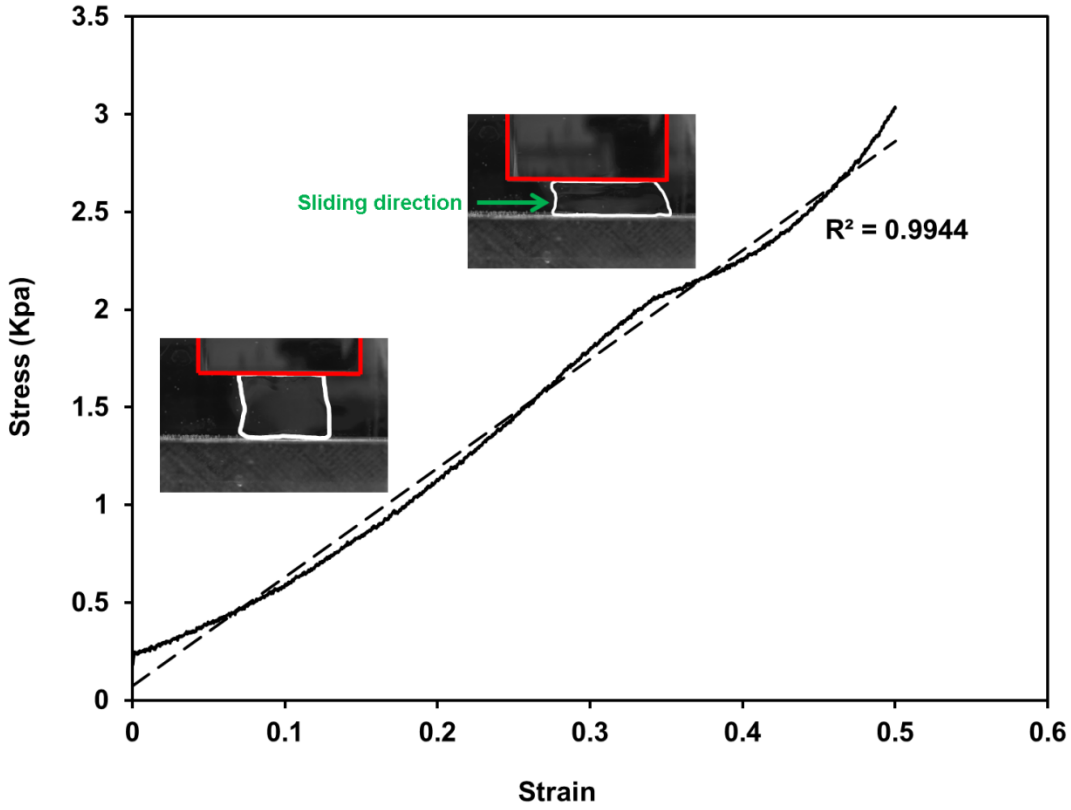

Figure 3-19: Compressive stress strain curve of a 10-0.01 sample and sample sliding at larger strains (~ 35%).

3.3.2.2 Stress relaxation

When a load is applied to a material (σ_0) (Figure 3-20a), an elastic material shows an instantaneous strain response, ε_0, (Figure 3-20b), which stays constant as long as the load is being applied. When it is unloaded, strain is released immediately. On the other hand, in a viscous fluid (Figure 3-20c), upon loading, strain increases with time, and after unloading strain does not decrease. A viscoelastic material shows both aspects; after loading, for small values of t, there is an immediate response for strain and as time t increases, strain gradually increases (Figure 3-20d). This means that if a viscoelastic material is

exposed to a constant stress, strain will increase with time. Furthermore, when unloading occurs, a large portion of stain (elastic part) is released instantaneously and then the rest of the strain decreases with time. Therefore, a phase difference exists between stress and strain.

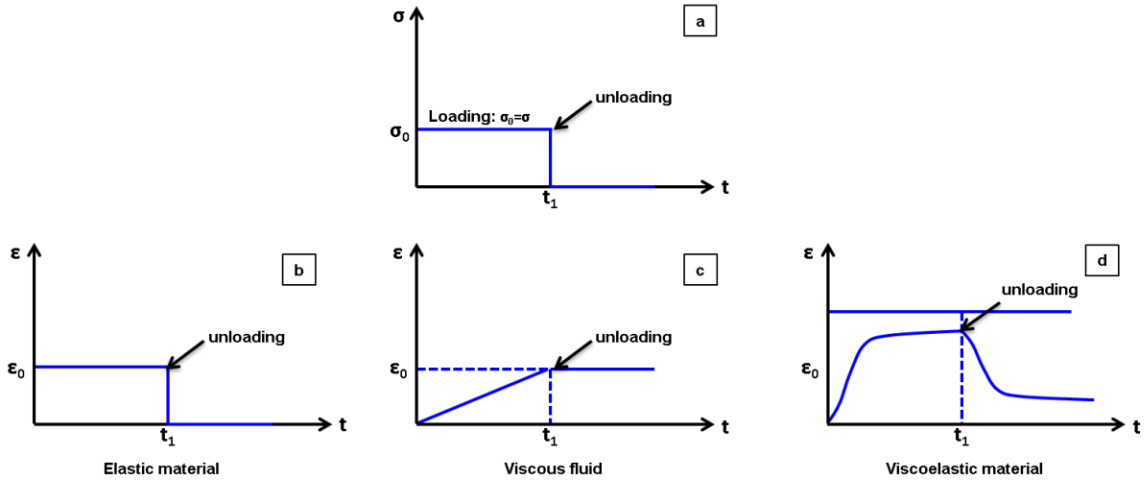

Figure 3-20: Different strain responses for different material, a) stress profile b) elastic material c) viscous fluid d) viscoelastic material, adapted from [247]

Another phenomenon in viscoelastic materials is stress relaxation (Figure 3-21). When a viscoelastic material is under a constant strain, stress decreases with time.

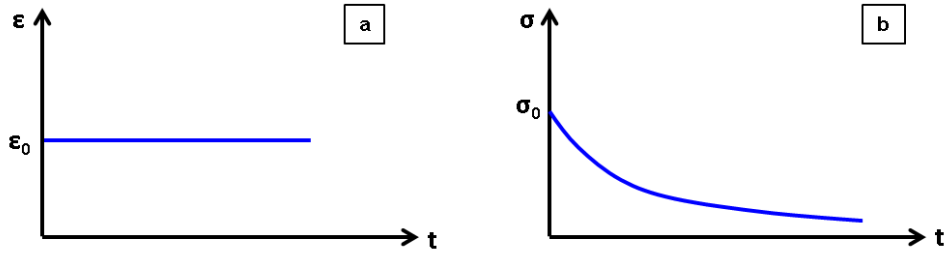

Figure 3-21: a) applied strain b) stress relaxation in a viscoelastic material, adapted from [247].

To investigate whether PAAm samples show viscoelastic behaviour, a stress relaxation test was performed. In these tests, load was kept constant (at 20% strain) for extended periods of time and the response of samples were plotted against time (Figure 3-22).

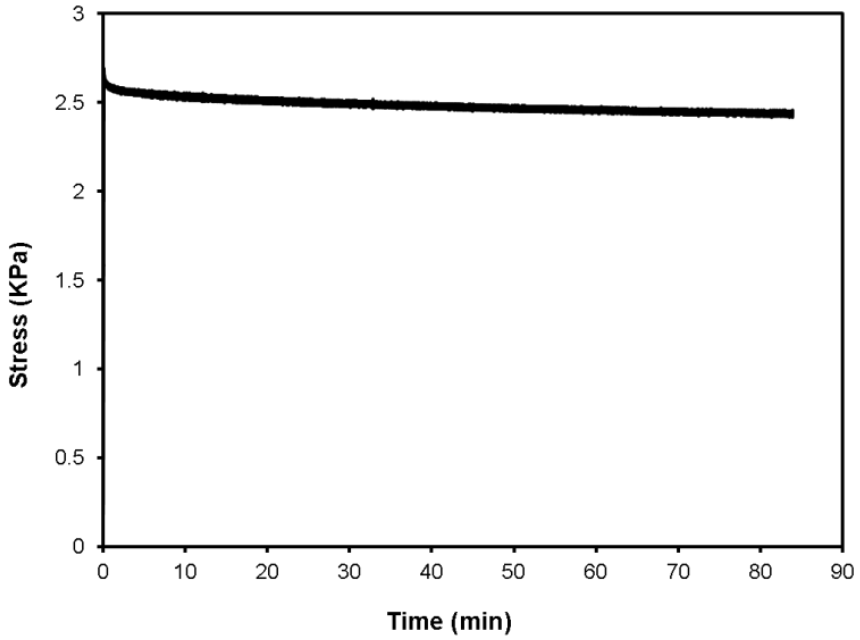

Figure 3-22: Stress relaxation plot for a 15-0.01 sample.

3.3.3 Concluding remarks

PAAm was found to be a material that can be tailored to have different elastic moduli with minimal stress relaxation and thus mainly elastic rather than viscoelastic behaviour. This elastic behaviour provided a simple characterization of substrate stiffness which was convenient in the eventual study of the influence of substrate stiffness on cell migration, which was one of the goals of the present thesis. PAAm also fulfills the other requirements such as optical clarity and chemical inertness. Thus, PAAm was chosen as the substrate for the investigations in the rest of the present thesis..

Chapter 4: Biological responses of human corneal epithelial cells

Mechanotransduction studies have generally focused on stem cells to understand the role of environmental mechanical stimuli in differentiation and on fibroblasts in wound healing and scar formation. Little is currently known on how a mechanical stimulus affects corneal epithelial cells, which can be relevant to ocular diseases such as keratoconus (KC), where high enzyme activities result in a mechanically weaker cornea [248,249]. While some studies suggest that corneal epithelial cells have more elongated morphology in keratoconic corneas [250], it is not clear how the decrease in mechanical stability of the cornea during the disease can affect these cells.

To thoroughly investigate mechanical interaction of corneal epithelial cells with their environment, both cellular biological responses[1] and their mechanical responses induced by a mechanical stimulus were assessed. The mechanical stimulus chosen for this study was substrate stiffness (elastic modulus) and the mechanical impact of cells on their environment consisted of the deformation they produced on the substrate during migration. In the current chapter biological responses are discussed.

To perform this study, human corneal epithelial cells (HCECs) were chosen and polyacrylamide (PAAm) substrates were used as substrates with varying elastic moduli. Pelham and Wang [112] first used polyacrylamide (PAAm) gels for mechanotransduction in late 1990s. Since then, PAAm gels have

[1] A modified version of this chapter was published as a journal paper in Acta Biomaterialia [339].

been extensively studied and used in mechanobiology research [251–253] because of their optical clarity, chemical inertness, and wide range of mechanical properties.

4.1 Materials and methods

4.1.1 Sample preparation

Several steps were involved in preparing PAAm membranes for cell culture and were adapted from Aratyn-Schaus *et al.* [254]: coverslip activation, membrane fabrication, surface functionalization, and ECM protein conjugation to the surface (Figure 4-1).

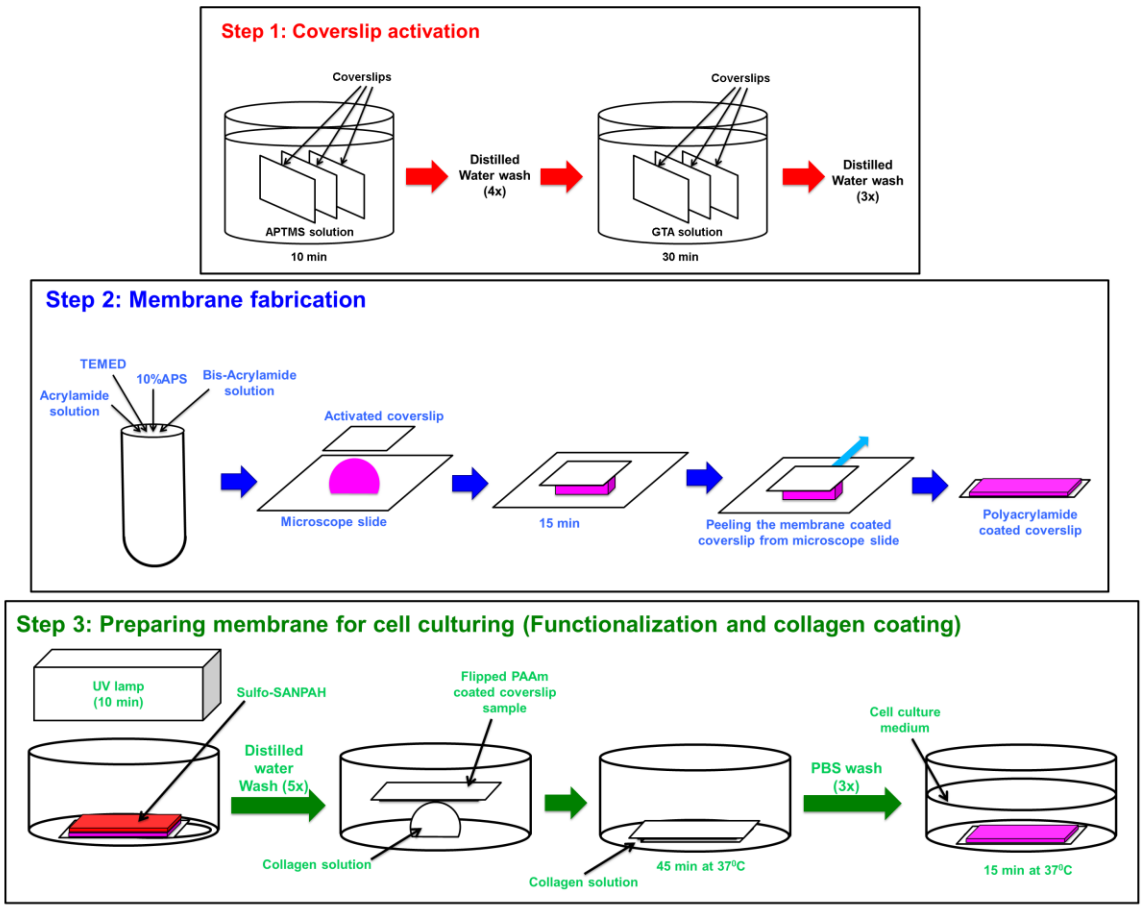

Figure 4-1: Schematic showing different steps of PAAm sample preparation.

4.1.1.1 Step 1: Coverslip activation

In order to fabricate PAAm-coated coverslips (Figure 4-1), glass coverslips (No. 1, 22 ×22 mm, VWR, Radnor, PA, USA) were chemically activated to allow the polymer to covalently bond to them.

Coverslips were first rinsed with ethanol. After drying, they were immersed in 2% (3-aminopropyl) trimethoxysilane (APTMS) solution (Sigma-Aldrich Canada Co. Oakville, ON, Canada) in isopropanol for 10 minutes. After four washes in distilled water, coverslips were placed in 1% glutaraldehyde solution (Sigma-Aldrich Canada Co. Oakville, ON, Canada) in distilled water for 30 minutes. Coverslips were then washed three times with distilled water and air-dried before membrane fabrication.

4.1.1.2 Step 2: Polyacrylamide (PAAm) membrane fabrication

Membrane fabrication was started with mixing different concentration of acrylamide (40% w/v, Bio-rad, Hercules, CA, USA) and bis-acrylamide (2% w/v, Bio-rad, Hercules, CA, USA) monomers and ultra-pure water (Figure 4-1). Variation in elastic modulus was achieved through changing the concentration of acrylamide in the final specimen. The following samples concentrations were used in this study (all concentrations are vol%): (1) compliant: 7% acrylamide – 0.01% bis-acrylamide, (2) medium: 10% acrylamide – 0.01% bis-acrylamide, (3) stiff: 15% acrylamide – 0.01% bis-acrylamide. To initiate the polymerization reaction, 10% ammonium persulfate (APS) (Bio-rad, Hercules, CA, USA) solution in water and tetramethylethylenediamine (TEMED) (Bio-rad, Hercules, CA, USA) were added to the monomer mixture. A small volume of each solution (15 µl) was placed on a microscope slide (VWR, Radnor, PA, USA) immediately following the addition of 10% APS solution and TEMED. An activated coverslip was placed on top of the drop so that the solution spread over the coverslip. These assemblies were left for 15-20 minutes (depending on concentration; lower concentration samples need more time for polymerization). Following polymerization, assemblies were left in ultra-pure water for 30 minutes before peeling the PAAm-coated coverslip from the microscope slide. To remove any unreacted monomer, all membranes were soaked in ultra-pure water overnight before surface functionalization.

4.1.1.3 Step 3: Surface functionalization of membranes and ECM coupling to the surface

In order to conjugate the ECM protein (in this study, collagen type I) to PAAm membranes, the surface of the samples was functionalized with a heterobifunctional crosslinker, sulfosuccinimidyl-6-(4'-azido-2'-nitrophenylamino) hexanoate (sulfo-SANPAH). Sample surfaces were covered with 2mg/ml solutions of sulfo-SANPAH (Thermo Scientific, Rockford, IL, USA) in water and membranes were exposed to a UV light source for 10 minutes. Samples were then thoroughly washed with distilled water to clean the surface from excess sulfo-SANPAH. Following functionalization, membranes were incubated with 0.05 mg/ml rat tail collagen type I (Sciencell, Carlsbad, CA, USA) solution at 37 $^{\circ}$C for 45 minutes.

4.1.2 Atomic Force Microscopy

Force spectroscopy method using atomic force microscope (AFM) (XE-100, Park Systems, Korea) was employed to measure the elastic modulus of the membranes as an indication of their stiffness. Measurements were performed in water, in contact mode, to prevent drying of the membranes. A spherical-tipped indenter (with a radius of less than 10 nm) was used, and a force-displacement curve was obtained for loading and unloading paths. Then, the Hertzian model was applied to the curve to determine the elastic modulus, based on the assumption that the material is purely elastic [255,256]. Since PAAm was known to exhibit essentially elastic behaviour [256] in the deformation range applied in the present study, this assumption was considered reasonable.

4.1.3 Cell culture

HPV-immortalized HCECs, kindly provided by Dr. Griffith, were maintained in an incubator with keratinocyte medium (KM) (Sciencell, Carlsbad, CA, USA) supplemented with keratinocyte growth supplement (KGS) (Sciencell, Carlsbad, CA, USA) and penstrep (Sciencell, Carlsbad, CA) at 37 $^{\circ}$C, 5% CO_2 and 95% humidity. Cell culture medium was replaced every 2 to 3 days. After the PAAm-coated coverslips had been prepared, functionalized and collagen-coated, 4×10^4 HCECs were seeded on these surfaces. Samples were kept in 6 well culture plates at 37 $^{\circ}$C, 5% CO_2 and 95% humidity.

Swiss Albino 3T3 fibroblasts (used as control cells in some experiments) were kept in Dulbecco's modified Eagle's medium (DMEM) supplemented with fetal bovine serum (FBS) and penstrep at 37 °C, 5% CO_2, and 95% humidity incubator. Cell culture medium was changed every two to three days. These fibroblasts were cultured on PAAm samples in the same manner as HCECs.

4.1.4 MTT assay

Using 3-(4,5-dimethylthiazol-2-yl)-2,5-diphenyltetrazolium bromide (MTT) (Biotium, Hayward, CA, USA), the HCECs viability and proliferation were determined when cells were cultured on the substrates with different elastic moduli. Following 48 h incubation of HCECs on various stiffness substrates, PAAm-coated coverslips were transferred to a new 6-well culture plate (BD Flacon, San Jose, CA, USA) to ensure that only cells on the samples were tested. Cells on both substrates and the initial culture plate wells were incubated overnight at 37 $^{\circ}$C with 0.5 mg/ml MTT solution in warm KM/KGS cell culture medium. To dissolve formazan crystals, isopropanol was added and absorbance was read at 595 and 650

nm using a Microplate Photometer (Thermo Scientific, Hudosn, NH, USA). Cell viability on the substrates is reported as relative viability compared to cells cultured on tissue culture polystyrene (TCPS).

4.1.5 Immunofluorescent staining of cytoskeleton structure

Cytoskeleton structure was studied through immunofluorescent staining after 48 h incubation of cells on the substrates. Cells were fixed using 2% paraformaldehyde and permeabilized with -20 $^{\circ}$C acetone. Actin filaments were then stained using Alexafluor-488 phalloidin (Invitrogen, Carlsbad, CA). Images were taken with an inverted laser scanning confocal microscope (LSM 510 meta, Carl Zeiss, Germany) using an argon laser (488 nm).

4.1.6 Flow cytometry

4.1.6.1 Membrane receptors

Expression of the integrin-$\alpha_3\beta_1$ and of the intercellular adhesion molecule-1 (ICAM-1) was studied by flow cytometry (BD FACSCalibur, BD Biosciences, San Jose, CA, USA). Following 48 h incubation, cells were detached from PAAm gels using TrypLE™ Express (Invitrogen, Grand Island, NY, USA). To ensure that just cells on the substrates were gathered, samples were transferred to a new culture plate before cell detachment. Cells were then washed and incubated with fluorescently-labeled antibodies against integrin-β_1 (CD29), integrin-α_3 (CD49c) and ICAM-1 (CD54) (BD Biosciences, Mississauga, ON, Canada) for 30 minutes at room temperature in the dark [257]. Samples were then diluted and fixed using 1% paraformaldehyde (final concentration) and analyzed by flow cytometry within five days.

4.1.6.2 Caspase

Caspase mediated apoptosis was also studied by flow cytometry using a caspase detection kit (Immunochemistry Technologies, Bloomington, MN, USA). After 48 h incubation, cells were detached from the substrates using TrypLE™ Express (Invitrogen, Grand Island, NY, USA), washed, and then incubated with the polycaspase enzyme probe (FAM-VAD-FMK). After one hour at 37 $^{\circ}$C, cells were washed three times and propidium iodide (PI) was added immediately prior to flow cytometry analysis to differentiate apoptotic from necrotic cells following the manufacturer's protocol. Apoptosis has been previously studied using flow cytometry [257–259].

4.1.7 Time lapse imaging by optical microcopy for migration studies

To study HCECs migration, cells were cultured both on the PAAm substrates and collagen-coated glass coverslips. As a positive control, to promote migration, TGFβ was also added to glass coverslip samples. Migration experiments were performed 48 h after cell seeding. Time lapse imaging was performed using a Nikon inverted optical microscope with a 40X objective lens. To provide an appropriate cell environment, a micro-incubator (Biosciences tools, San Diego, CA, USA) was mounted on the microscope stage to hold the temperature at 37 $^{\circ}$C. For migration speed calculation, cells were imaged for at least 1 h and tracking was performed by ImageJ (US National Institute of Health, NIH) and MTrackJ plugin (www.imagescience.org/meijering/software/mtrackj/). To track cells, nucleus movement was measured at 10 minute intervals.

4.1.8 Statistical Analysis

Statistical analysis was performed using STATISTICA V8 (StatSoft, Tulsa, OK, USA). Analysis of variance (ANOVA), followed by a multiple pair-wise comparisons using the Fisher's Least Significant Differene (LSD) test, was used to calculate statistical significance. The significance level was set at 0.05. All experiments were performed at least 3 times with different cell passages.

4.2 Results and discussion

4.2.1 Substrate elastic modulus

To have clear results about the mechanical behaviour of the substrates, at the same scale as cells would potentially feel, the force-spectroscopy method using AFM was implemented to further measure the elastic moduli of PAAm substrates. AFM has been previously used for measuring PAAm stiffness [256]. The Hertzian model [255] was used to estimate the elastic moduli of PAAm substrates from force-displacement data. The variations of elastic modulus with the change of acrylamide concentration are presented in Table 4-1. Consistent with previous reports [246], increasing acrylamide concentration increased the elastic modulus of PAAm.

Table 4-1: Elastic moduli of PAAm membranes with different acrylamide concentrations measured by AFM in contact mode. n = 3, Average ± standard deviation (SD).

Sample	Concentration (acrylamide – bis-acrylamide)	Elastic modulus (kPa)
Compliant	7% – 0.01%	1.3 ± 0.2
Medium	10% – 0.01%	3.2 ± 0.3*
Stiff	15% – 0.01%	9.2 ± 1.3*#

* significantly different from compliant substrate, $p < 0.01$, # significantly different from the medium substrate, $p < 0.01$.

In the present study, the acrylamide concentration, and hence the elastic moduli of PAAm substrates were carefully selected to match with those of cornea layers. The cornea consists of different layers; each layer having its unique structure and properties. Elastic moduli of these different layers can vary widely from less than 5 kPa for the basement membrane to more than 60 kPa for the Descemet's membrane (at older ages) [260]. As mentioned previously, during keratoconus, corneal elasticity and therefore stiffness decreases [261]. The elastic modulus of the medium substrate was tuned to the low end of the overall elastic moduli of the corneal layers. Then, it was varied to be higher (stiff substrate) and lower (compliant substrate) to investigate the effect of elastic modulus on HCECs behaviour.

4.2.2 Cell viability

MTT assay was used to measure metabolic activity of HCECs as an indication for cell viability and proliferation. Since the PAAm substrates size was smaller than that of culture plate wells, some of the cells still grew on the bottom of the well despite our effort to mostly seed cells onto the substrates. This was taken into account and thus Figure 4-2 presents both the percentage of metabolically active cells on PAAm substrates and total active cells (substrates and wells combined). Viability is reported as a percentage relative to the viability of control cells whereby control cells were cultured in a 6-well culture plate (TCPS). The high percentage of viable cells on the substrates indicated that PAAm substrates were not toxic to cells and provided a suitable environment for proliferation. A small increase in viability seemed to occur for the stiff substrates compared with the compliant substrates but this increase was not statistically significant ($p = 0.83$).

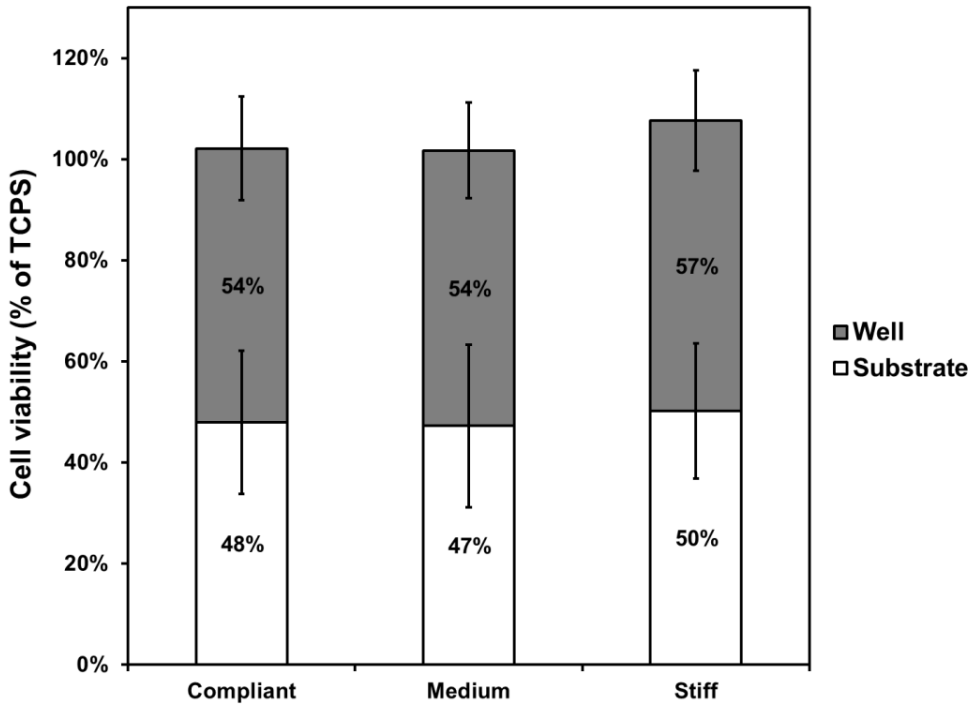

Figure 4-2: Effect of substrate stiffness on cell viability over 48 h. HCEC viability was measured by MTT assay with substrates and culture wells assessed separately, n=4, average ± SD.

4.2.3 Intercellular adhesion molecule-1 expression

Intercellular adhesion molecule-1 (ICAM-1 or CD54) is a transmembrane adhesion molecule. It is not only related to cytoskeleton components [262], but also upregulated by pro-inflammatory cytokines in corneal epithelial cells [263], and therefore, can be used as an indication of cell activation and inflammatory marker. Although there was a slight upregulation, no significant changes in ICAM-1 expression were found (Table 4-2). These results suggested that HCECs were not activated on the substrates and thus PAAm could be considered as an appropriate biomaterial to study the corneal cell response to change in elastic modulus. These results also suggested that changes in stiffness did not induce cell activation as measured by ICAM-1 expression.

Table 4-2: Effect of substrate stiffnes on ICAM-1 (CD54) expression. HCECs were cultured on the PAAm substrates having different elastic moduli. Following 48 h-interactions, cells were removed from the substrates and analysed by flow cytometry. n=4, average ± SD.

Sample	ICAM-1 (CD54) expression (arbitrary fluorescent unit)
TCPS	11.5 ± 3.4
Compliant	12.2 ± 2.6
Medium	12.0 ± 3.5
Stiff	11.9 ± 3.4

4.2.4 Apoptosis

Apoptosis or programmed cell death is a multi-step process consisting of membrane blebbing, nuclear dissociation and at the end DNA fragmentation [264]. Apoptosis is one of the cell death mechanisms that the human body uses to control cell count in organs as well as their size. Apoptosis also serves as a defense mechanism in the removal of damaged cells [265]. In comparison, necrosis is considered to be accidental or inappropriate, and occurs under extremely unfavorable conditions such as serious injuries and diseases [266]. In the context of the cornea, apoptosis has been previously reported to occur for keratocytes[1] in keratoconic corneas [267]. Apoptosis can occur by two different molecular pathways: intrinsic (or mitochondrial) and extrinsic (or death-receptor activated) [268]. Cysteine-aspartic proteases or caspases are enzymes that are key players in the apoptotic pathways [268,269]. They can both can start the disassembly process (be initiator) and help in progression of the process (be effector).

[1] Keratocytes are fibroblast-like cells residing in corneal stroma.

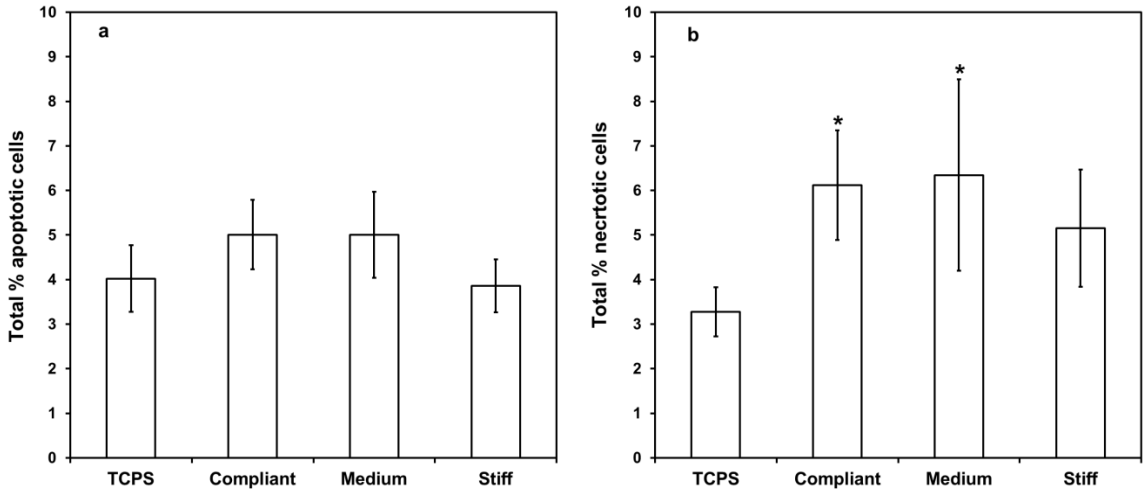

Figure 4-3: Effect of substrate stiffness on (a) cell apoptosis and (b) necrosis, * $p<0.05$ compared to TCPS. n = 4, average ± SD.

In the present study, caspase-mediated apoptosis of HCECs cultured on the substrates with different elastic moduli (compliant, medium and stiff) was studied using flow cytometry to investigate whether changes in mechanical properties could induce apoptosis in these cells. Also, propidium iodide (PI) was used as a secondary marker to study cell death by necrosis. Figure 4-3 shows total number of cells that stained for apoptosis or necrosis. Further details on the caspase and PI positive cell population are provided in Table 4-3. Cell death (by both mechanisms of apoptosis and necrosis) increased in samples with lower elastic modulus. This increase was statistically significant for PI positive cells. On a stiff substrate, with stiffness characteristics approaching that of TCPS, the percentage of apoptotic cells decreased and approached that of the TCPS.

Table 4-3: Effect of substrate stiffness on percentage cell death and apoptosis. Following 48 h incubation of HCECs on substrates with different elastic moduli, cells were detached from substrates and percentage cell death and apoptosis were measured by flow cytometry using the pan caspase marker, FITC-VAD-FMK for investigating apoptosis, while PI staining was used to assess necrosis, n=4, average ± SD.

Sample	Casp-/PI+ (necrosis)	Casp+/PI- (early apoptosis)	Casp+/PI+ (late apoptosis)
TCPS	1.56+0.81	2.31+1.02	1.71+0.30
Compliant	3.55+1.44	2.45+0.79	2.56+0.85
Medium	3.89+2.85	2.54+1.04	2.46+1.01
Stiff	3.24+1.60	1.95+0.74	1.91+0.48

Apoptosis in corneal epithelial cells has been previously correlated to generation of reactive oxygen species (ROS) [270]. Higher oxidative damage due to ROS [271] and higher apoptosis are other features in keratoconic eyes [249]. To investigate ROS generation in HCECs cultured on substrates with different elastic modulus, dihydrodichlorofluorescein diacetate (DCF) expression was measured using flow cytometry. DCF has been previously used for measuring oxidative stress in cells [272]. No statistically significant changes were found among our samples (Table 4-4), suggesting that ROS may not be responsible for inducing apoptosis and that changes in elastic modulus of the substrate might be directly responsible for triggering the mechanism of apoptosis in HCECs.

Table 4-4: Generation of reactive oxygen species (ROS) in HCECs was studied by investigating DCF expression of cells cultured on PAAm substrates with varying elastic modulus. HCECs were cultured on different PAAm substrates for 48 h and their DCF expression was measured by flow cytometry, n = 5 Average ± SD.

Sample	DCF expression (arbitrary fluorescent unit)
TCPS	146 ± 22
Compliant	135 ± 17
Medium	145 ± 21
Stiff	153 ± 30

4.2.5 Cytoskeleton structure

Cytoskeleton structure plays an important role in different cellular functions including cell shape, growth, division and also migration. It also allows cells to mechanically interact with their environment. Actin filaments, as one of the three main constituents of the cytoskeleton, are believed to act not only as a mediator in mechanotransduction, but also as direct mechanosensors [273].

The cytoskeleton structure was studied by fluorescent staining of the actin filaments of cells cultured on membranes with different elastic moduli. Confocal microscopy revealed that actin filaments, and thus cytoskeleton structure, were affected by the elastic modulus of the substrate (Figure 4-4). HCECs, when cultured on compliant substrates, lacked visible actin filaments (Figure 4-4a-1 and Figure 4-4a-2); bright fluorescent spots (white arrows) and only sparse number of short filaments (Figure 4-4a-2), mostly gathered around the perimeter of cells and not in the cytoplasm. Increasing the elastic modulus to 3.2 kPa (medium substrate; Figure 4-4b) led to the formation of more filaments (white arrows). HCECs adherent to the stiff substrate (Figure 4-4c-1), exhibited highly visible, stretched and organized actin filaments. Figure 4-4c-2 further highlights the organized structure of the actin filaments (white arrows) seeded on the stiff substrate.

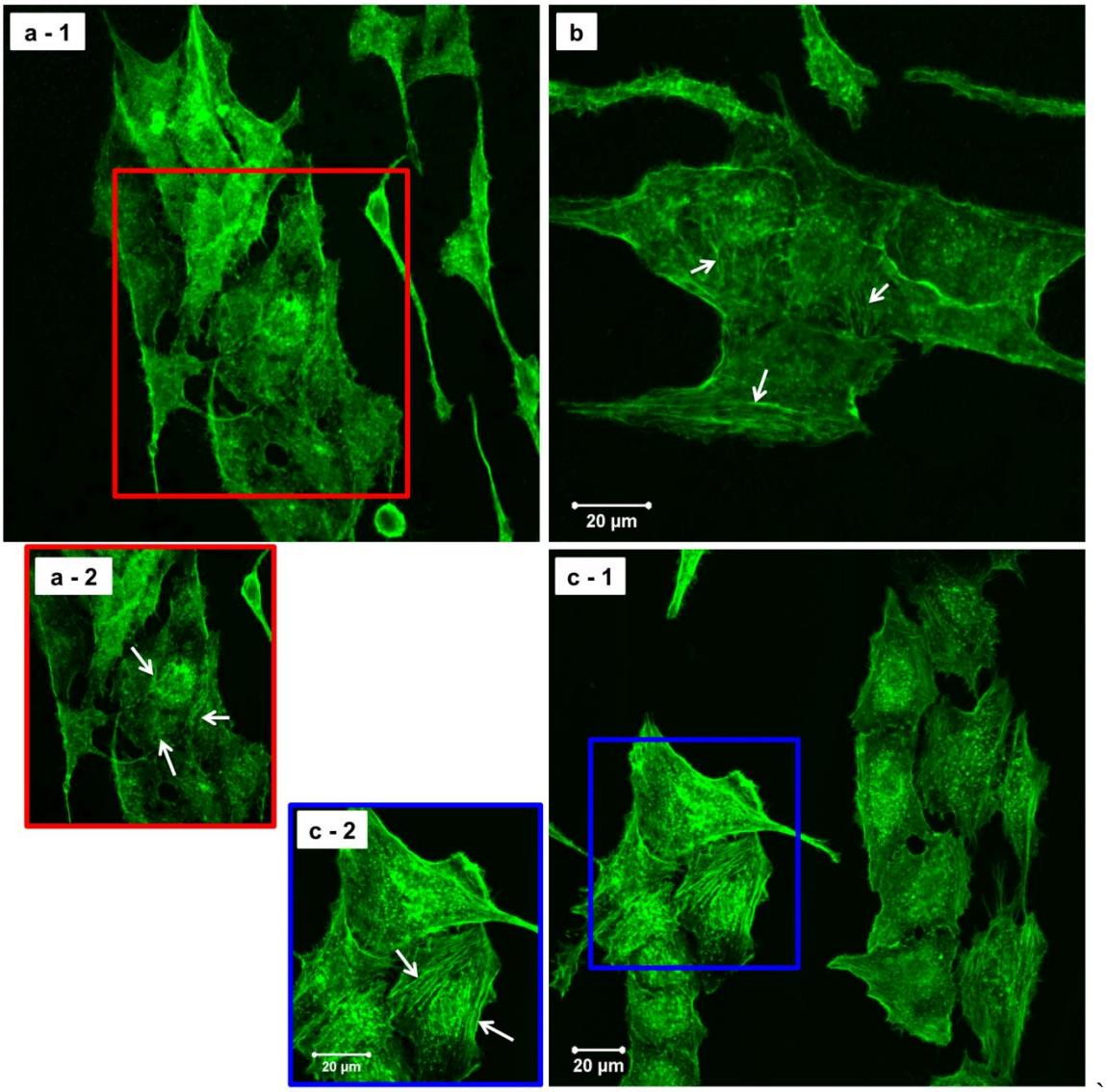

Figure 4-4: Actin filaments of HCECs cultured on PAAm substrates with different stiffness: a-1) compliant; a-2) magnified view of the rectangle shown on a-1; b) medium; c-1) stiff; c-2) magnified view of the rectangular region in c-1. Images were taken with laser scanning confocal microscope (Zeiss) with a 40X objective lens. White arrows highlight the actin filament organization. These images are representative results from n = 2 to 3 experiments.

Since cytoskeleton plays an important role in cell migration, actin filament disruption might adversely affect migration behaviour of HCECs on compliant substrate [274]. Actin filament buckling has been previously reported with fibroblasts cultured on compliant substrates [117]. While these characteristics were observed using 3T3 fibroblasts on the compliant PAAm substrate (see Figure 4-5a), actin filament buckling did not occur with HCECs. Both corneal and fibroblast immortalized cell lines responded to

mechanical cues but in significantly different manner. In 3T3 fibroblasts seeded on compliant PAAm substrate (Figure 4-5a), actin filaments formed but showed buckling (white arrows) but in HCECs seeded on compliant substrates (Figure 4-4a-1 and Figure 4-4a-2), there was a lack of filament formation. It's is worth noting that, 3T3 fibroblasts on stiff substrates showed organized and stretched actin filaments (Figure 4-5b, white arrows) similar to HCECs cultured on stiff substrate (Figure 4-4c-1 and Figure 4-4c-2).

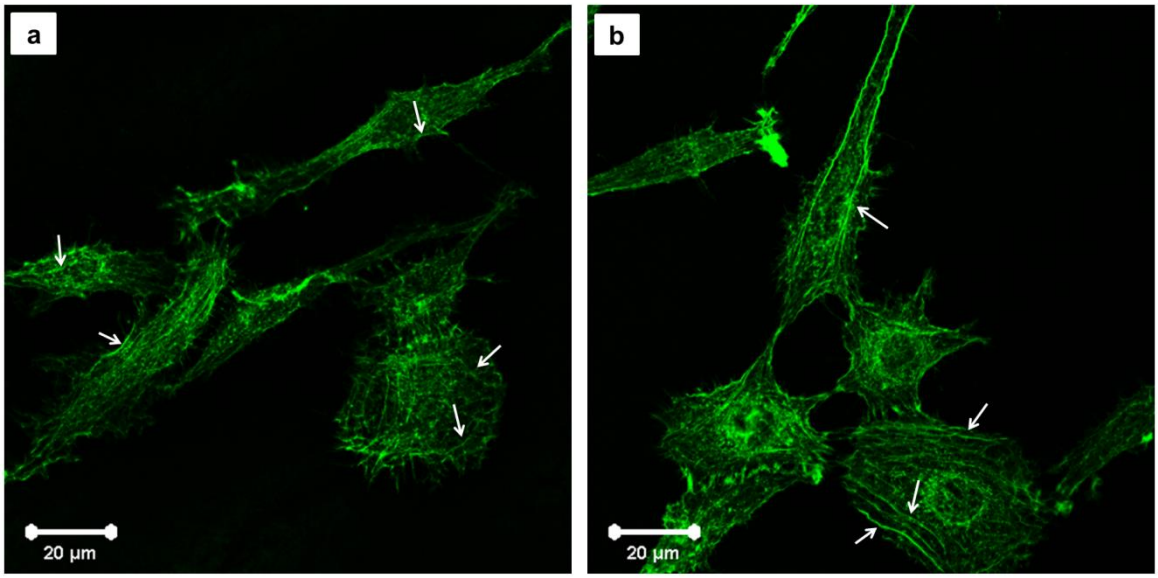

Figure 4-5: Actin filaments of 3T3 fibroblasts cultured on a) compliant (buckling of actin filaments can be seen on cells cultured on compliant PAAm matrix, white arrows) b) stiff PAAm substrate. Images were taken with laser scanning confocal microscope, 40X objective lens. White arrows highlight the actin filament organization. Reprinted from [275], with permission from ASME.

4.2.6 Integrin expression

In order to gain a better understanding of the effect of elastic modulus on cell adhesion, the integrin expression of HCECs seeded on PAAm substrates were also studied using flow cytometry. Integrin-α_3 and β_1 are two important membrane receptors involved in epithelial cell adhesion and spreading [276]. In epithelial cells, integrin-α_3 exclusively heterodimerizes with β_1 and integrin-$\alpha_3\beta_1$ plays an important role in cell migration during wound healing [277].

Although preliminary studies indicated an upregulation in integrin-α_3 [275], in the present study, seeding HCECs on substrates with different elastic moduli did not induce any statistically significant changes in integrin expression (Figure 4-6). While a small downregulation was observed with α_3 and β_1 when comparing the compliant substrate with stiffer substrates (medium, stiff or TCPS), these differences

failed to reach statistical significance. Since increasing number of replicates of experiments was coincident with increasing cell passage, these would tend to indicate that changes in integrin expression may be more sensitive to cell passage than substrate stiffness.

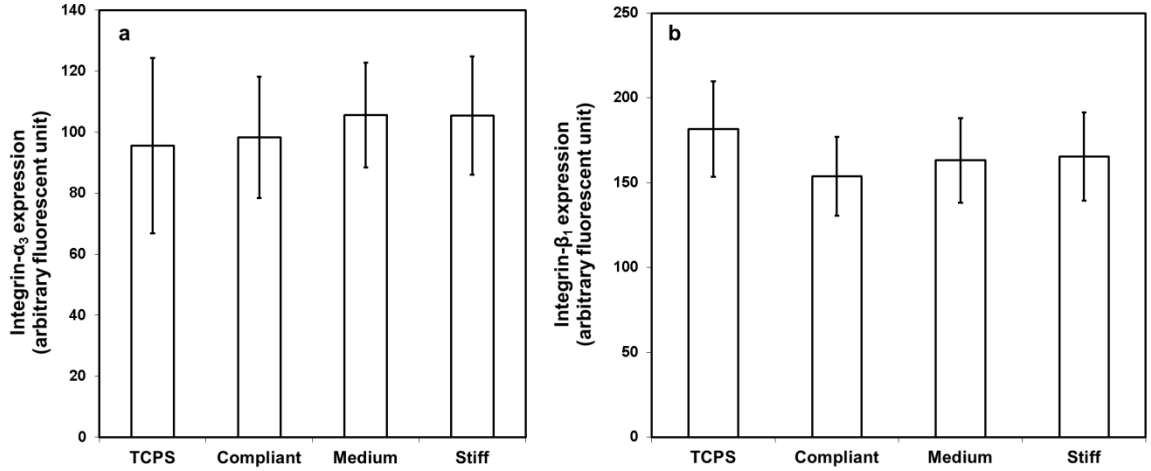

Figure 4-6: Effect of substrate stiffness on a) Integrin-α_3 and b) Integrin-β_1 expression of HCECs, n=9.

It has been previously shown that integrin-ligand bond has the ability to change its state and switch from a "relaxed" to a "tensioned" state by external mechanical force [278]. Our results tend to suggest that increasing stiffness of the substrate may not upregulate or downregulate the integrin expression; however, higher stiffness can apply higher external force and possibly induce changes in integrin-ligand bind state. At the same time, it is known that integrin molecules connect ECM ligands to cell cytoskeleton filaments [279]. Therefore, while only subtle changes in integrin expression were observed, these changes may or may not be playing a role in the cytoskeleton structure changes observed by confocal microscopy (Figure 4-4). Further studies will be required to determine the exact mechanisms.

4.2.7 HCECs migration

One of the main duties of corneal epithelial cells is migration during wound healing in corneal epithelium [280,281]. At the same time, migration is one of the biological processes controlled by the cytoskeleton (more specifically actin). Since the HCECs cytoskeleton was disrupted after seeding and interacting with the compliant matrices (Figure 4-4a), we hypothesized that migration behaviour of cells also changed on compliant substrates. To investigate these changes, migration behaviour was studied, including the migration speed of cells cultured on substrates with different moduli. Figure 4-7 shows cells

migrating on a glass coverslip (+TGFβ) and demonstrates tracking scheme for migration speed calculation.

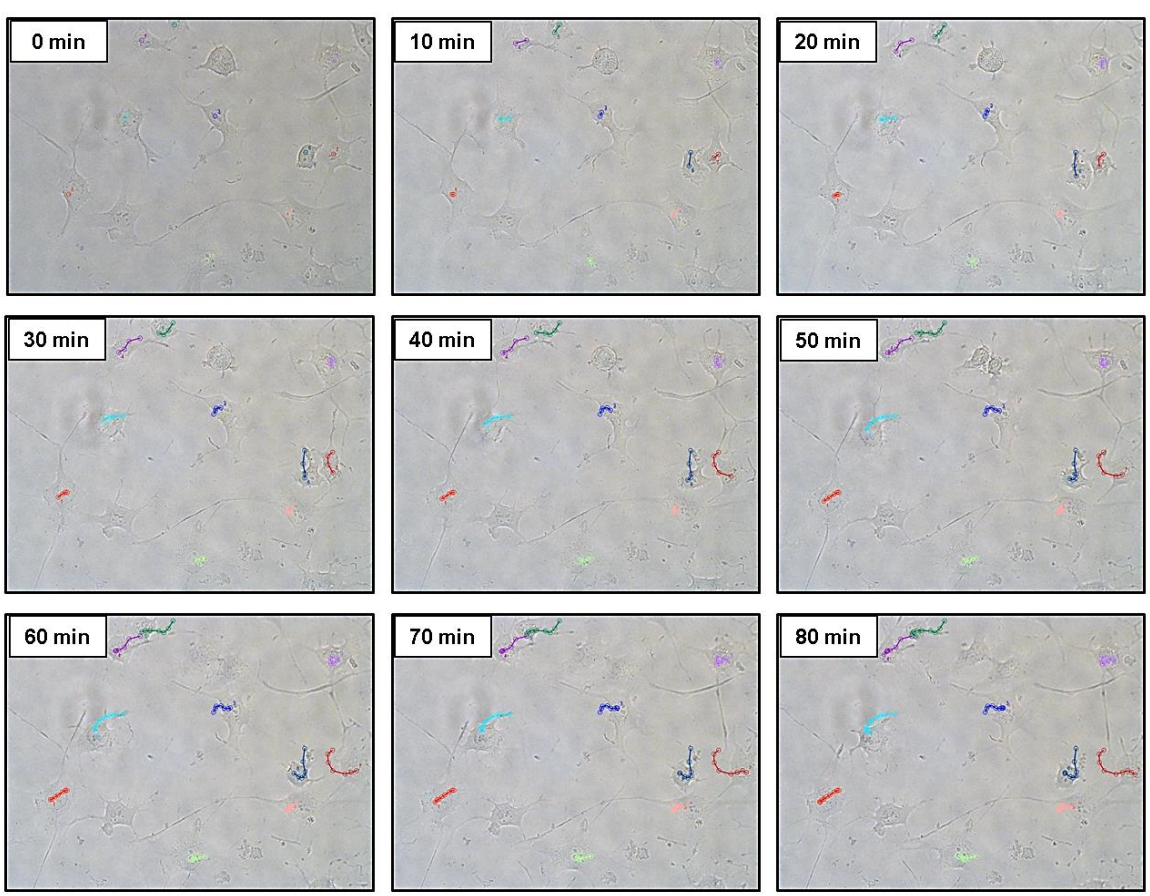

Figure 4-7: Tracking scheme used for measuring HCECs migration speed. Cells in this figure are cultured on a glass coverslip and TGFβ was added to them for positive control.

The migrating cells on various substrates were individually tracked using an optical microscope for at least an hour. The migration speed of cells on various substrates (Figure 4-8) showed that cells on medium and stiff substrate migrated with significantly higher speed than on compliant substrate ($p < 0.05$).

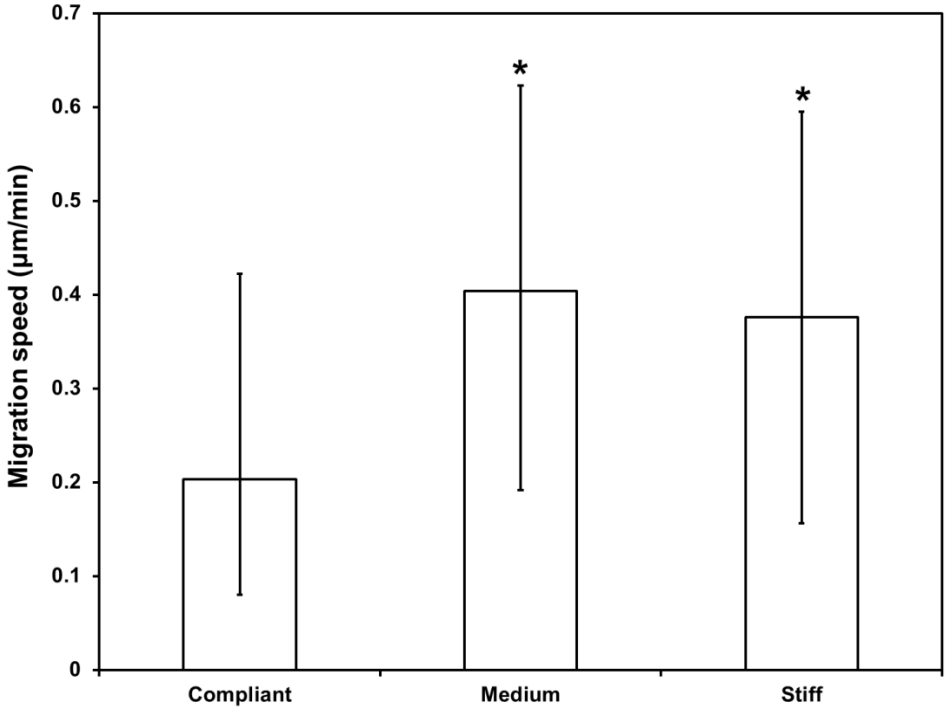

Figure 4-8: Migration speed of HCECs cultured on PAAm substrates with different elastic moduli. Cells were cultured on substrates for 48 h before time lapse imaging experiments. n = 3 to 5 **significantly different from compliant substrate, $p<0.05$.*

It has been previously shown that migration speed of cells on a 2D substrate has a biphasic relationship with substrate stiffness [131], which means that there is an optimum stiffness where cells show maximum migration speed. This optimum stiffness was reported to depend on the ECM ligand density on the surface [131]. Therefore, depending on substrate stiffness, increasing elastic modulus might lead to increase [112] or decrease [282] in cell migration speed. In the current research, elastic modulus was changing from 1.3kPa to 9.2kPa (Table 4-1) and in this range, HCECs displayed an increase in cell migration speed when increasing substrate stiffness.

The significant reduction in migration speed of cells cultured on compliant matrices is likely to be related to the impaired cytoskeleton structure and crumbled actin fibers. During cell migration, following cell polarization, protrusions called lamellipodia and filopodia are formed in the cell membrane. Lamellipodia are flat protrusions containing network of actin filaments whereas filopodia contain parallel fibers of actin filaments. Lamellipodia are mostly involved in directional migration while the role of filopodia is to explore the environment around the cell [190]. Formation of both protrusions is usually

driven by actin polymerization in a dynamic process [190]. Therefore, actin polymerization and filament formation plays a crucial role in migration.

For the positive control, where transforming growth factor β (TGFβ) was added to cells cultured on collagen-coated glass coverslip, a migration speed of 0.79 ± 0.39 μm/min was observed. It is believed that TGFβ affects different biological processes including cell migration [283,284]. Accordingly in our studies, TGFβ increased filopodia and lamellipodia activity in HCECs resulting in the observed higher exploratory behaviour of cells. The fact that such exploratory behaviour was not observed for cells migrating on the compliant substrates further confirmed the disrupted actin filaments observed in confocal microscopy.

4.3 Concluding remarks

This chapter presented results on the experiments regarding the cellular responses to elastic modulus as the mechanical stimulus. The substrates used were not toxic to cells and decreasing elastic modulus did not appear to induce activation (measured by ICAM-1 (CD54) expression of cells). However, a higher number of cells appear to undergo apoptosis and necrosis on the compliant substrates. While no statistically significant changes in integrin-$\alpha_3\beta_1$ were found, cytoskeleton and cell migration was significantly affected on the compliant substrates. Cells on substrate with the lower elastic modulus had fewer visible actin filaments, which in turn appear to impair their migratory behaviour. Statistically significant decreased migration speed was found for HCECs on the compliant substrates. The current investigation demonstrated that corneal epithelial cells are sensitive to changes in substrate stiffness, which may have direct implications in keratoconus where lower collagen stiffness has been observed.

Chapter 5: Mechanical responses of human corneal epithelial cells

Besides the expected biological behavior of cells, mechanical interaction of cells with their environment can also be observed. This includes the forces that they apply on their substrate and its resulting deformation. In the current research, this is classified as the "mechanical response" of the cells.

As mentioned before, cells have dynamic interactions with their substrate, the ECM. Our focus in this thesis is on migrating anchorage-dependent cells. Traction force microscopy is the method of choice for studying the mechanical responses of cells. In the present study, cells were cultured on 2D polyacrylamide substrates with varying elastic modulus and 3D cell-induced displacements and strains were measured. To facilitate these measurements, the substrates were loaded with fluorescent microbeads. During cell spreading and also migration, cells exert forces and deform the substrate and this deformation can be visualized by imaging fluorescent microbeads using a confocal or fluorescent microscope. Images obtained from the microscopy study can then be processed to perform deformation measurements and using substrate elastic properties, forces may also be calculated.

As previously explained, cell traction force measurement can be performed in three distinct levels of complexity. The first and easiest level is when cells are cultured on a 2D substrate and responses are measured in 2D as well. The second level of complexity is when cells are cultured on a 2D substrate but

3D responses are measured. The third and most complicated level is when cells are cultured inside a 3D matrix and 3D responses are also measured.

In the current research, the second level of complexity is chosen for studying the mechanical interaction of cells with their environment. As a first step in assessing the mechanical response of cells, HCECs were cultured on polyacrylamide substrates and deformation (displacements and strains) patterns were studied. Laser scanning confocal microscope was used for bead tracking and digital volume correlation (DVC) was used for the image processing to obtain displacements.

5.1 Materials and methods

5.1.1 Time lapse imaging by confocal microscopy for mechanical measurements

To measure cell induced deformation, PAAm substrates preparation and cell culturing methods were similar to sections 4.1.1 and 4.1.3 except that PAAm substrates were loaded with 10 vol% fluorescent microspheres (0.5 μm diameter, excitation/emission wavelengths of 580/605 nm; Invitrogen, Carlsbad, CA). Beads were directly added to the monomer mixtures and the solutions were vortexed for 10s for uniform distribution of the beads. Substrate thicknesses were kept between 30 μm to 70 μm, so that cells did not feel the rigid glass coverslip instead of PAAm substrates [223]. Cells were seeded on PAAm substrates and incubated for 48 h prior to confocal microcopy.

To prepare samples for confocal microscopy, the bottom of 35 mm Petri dishes (Corning, NY, USA) were machined to create a 20 mm diameter hole. A ring of double sided adhesive sheet (Grace Bio-Labs, OR, USA) was fixed to the rim of the hole and PAAm coated coverslips (with cells) were then placed on top, so as to have the uncoated glass underside of the coverslip directly above the microscope objective lens (Figure 5-1).

Live cell imaging was performed using an inverted laser scanning confocal microscope (LSM 510 meta, Carl Zeiss, Germany) equipped with a micro-incubator (Biosciences tools, San Diego, CA, USA) to maintain the temperature at 37 $^{\circ}$C (Figure 3-6). For the experiments, a 40x/1.3 oil objective lens was used. Migrating single cells were tracked and the 3D images of the substrates were taken every ~ 30 minutes for at least 1.5 h. A cell was considered single if there were no other cells within a surrounding of 100 μm × 100 μm square. Voxel sizes were kept at ~ 0.2 μm ×0.2 μm × 0.2 μm. Reported results are from one to two cells per substrate.

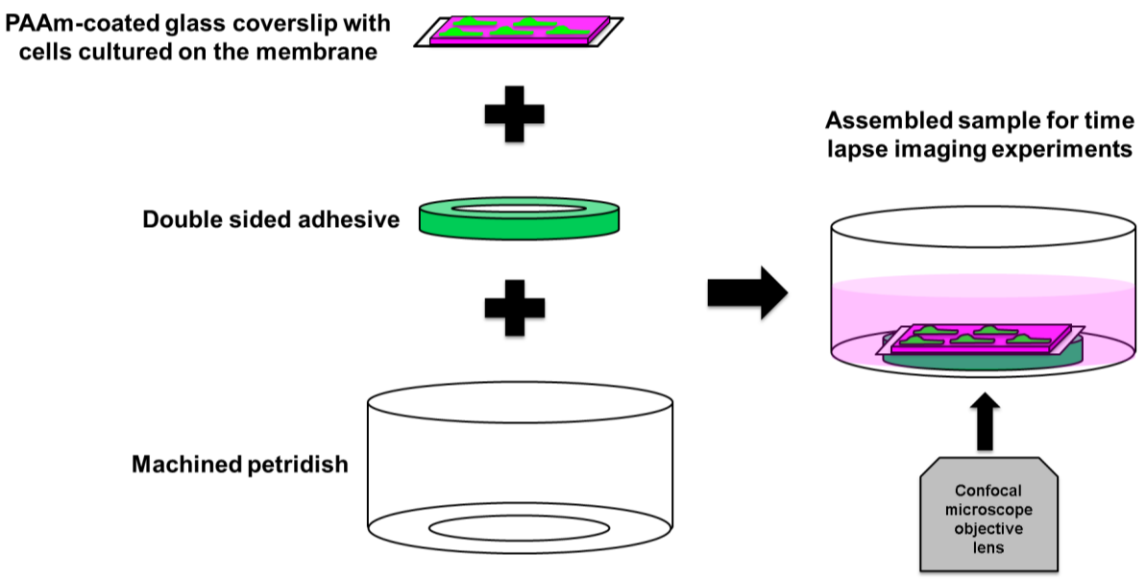

Figure 5-1: Schematic showing sample preparation for live cell imaging performed by confocal microscopy.

5.1.2 Confocal microscope

The most important advantage of the confocal microscope over a conventional wide field microscope is its ability to take 3D images. Higher resolution is also another advantage of using the confocal microscope. In a conventional wide field microscope, the camera receives both in-focus and out-of-focus rays (Figure 5-2a), while in a confocal microscope, the out-of-focus rays are eliminated by a pinhole that is placed in front of photomultiplier (PMT) [285]. Only in-focus rays can reach the detector and, after optical sectioning, series of point-by-point local images can be obtained and then assembled into a full 3D image [285] (Figure 5-2b).

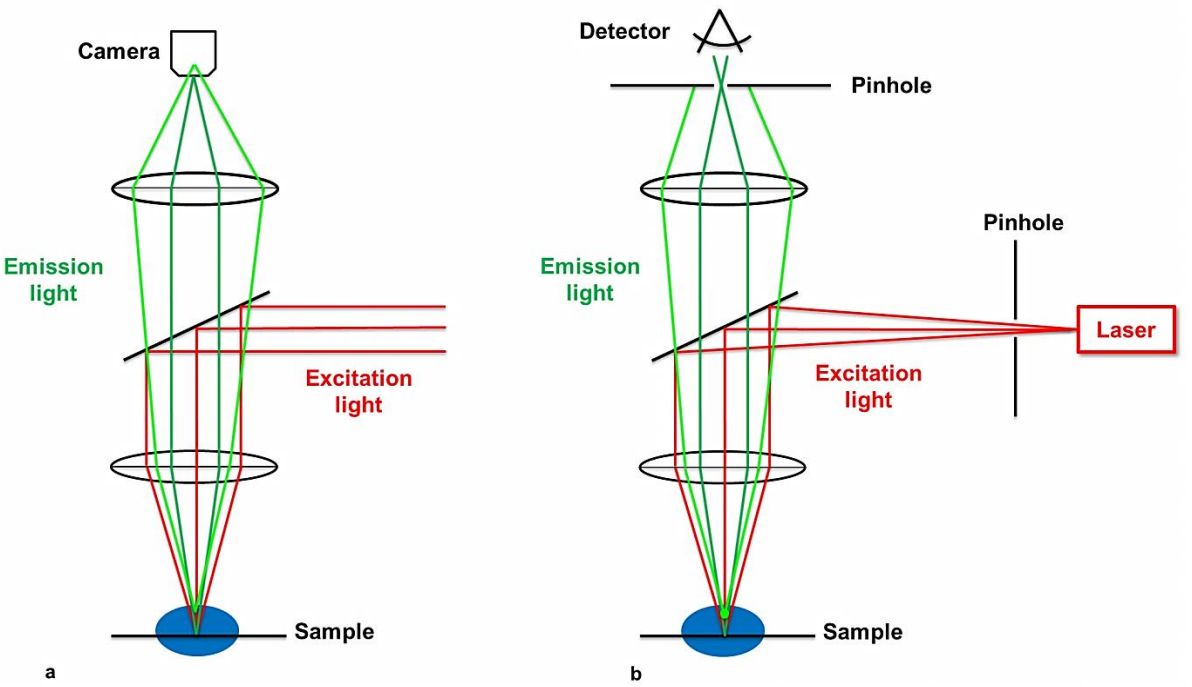

Figure 5-2: Optical path for a) conventional wide field microscope b) confocal microscope. Adapted from [285].

Since the resolution can be increased by decreasing the field of view [286], the point-by-point formation of the image results in both higher resolution and 3D image acquisition in confocal microscopes. In order for the pinhole to eliminate the out-of-focus rays, it has to be at the focal plane that corresponds to the plane of the objective lens [285]. This is why this microscope is called con-focal (both the image and the sample are in focal planes). In the confocal microscope, instead of white light or lights with different wavelengths, lasers with specific wavelengths are used to increase coherency of the excitation light. Although scanning can be performed by either moving the laser beam on the sample or moving the sample under the stationary laser, the preferred method is the laser scanning microscope due to increased speed. Rotating mirrors move the laser across the sample and the light coming from the sample also hits the same mirror at the same angle, which eliminates the necessity of moving the pinhole. The heart of a confocal microscope is its objective lens. The objective lens both focuses excitation laser light and collects the emitted light from the sample. Objective lenses that are used in confocal microscopes are immersion lenses. Using immersion lens increases the numerical aperture (NA) of the objective lens which is defined as [285]:

$$NA = n \times sin\alpha \qquad 5\text{-}1$$

where n is the refractive index of the immersion medium and α is the angle of the ray relative to the optic axis. NA shows the resolving power of the lens, so, the higher the NA, the higher the resolving power of the lens.

5.1.3 Digital volume correlation (DVC), basics[1] and principles

Digital volume correlation (DVC) is a 3D pattern recognition technique that is often used for measuring the full 3D deformation field of a matrix. It is an extension of digital image correlation (DIC) that is a signal processing technique for measuring surface deformations using digital images of the surface [287–290]. In DIC, deformation measurement is performed by tracking multiple small regions in the images before and after deformation. These regions normally contain speckles that either originate from the natural texture of the material or are added to the surface intentionally for tracking purposes [287,289]. Sum-of-squared differences (SSD), optical flow [291], cross-correlation [292], and fast normalized cross-correlation [293] are some of the tracking algorithms that have been used before.

DVC follows the same concept as DIC to measure 3D displacements and strains, and since measurements are performed in 3D, it can successfully measure the internal strains as well as surface ones. In DVC, similar to DIC, measurements can be performed by tracking small regions (subsets) containing microbeads that were intentionally added to the samples. Tracking can also be done without addition of microbeads by just tracking the texture of the material, if it has enough features.

For full-field measurements, two 3D images of the matrix, one before and one after the deformation are compared (Figure 5-3a). To do the comparison, a 3D grid, which can be as fine as one voxel, is placed on the stacks to divide them into smaller subsets (Figure 5-3b). Voxel is the unit of 3D volume image and is an equivalent of pixel in 2D images. Following grid formation, cross-correlation of corresponding subsets can result in deformation field [11,12,223].

[1] This section explains the basics of DVC. The code used here is not developed by the present author. It has been developed and published previously [287,340]. Use of this code for the current set up with 3D confocal microscope images is studied here.

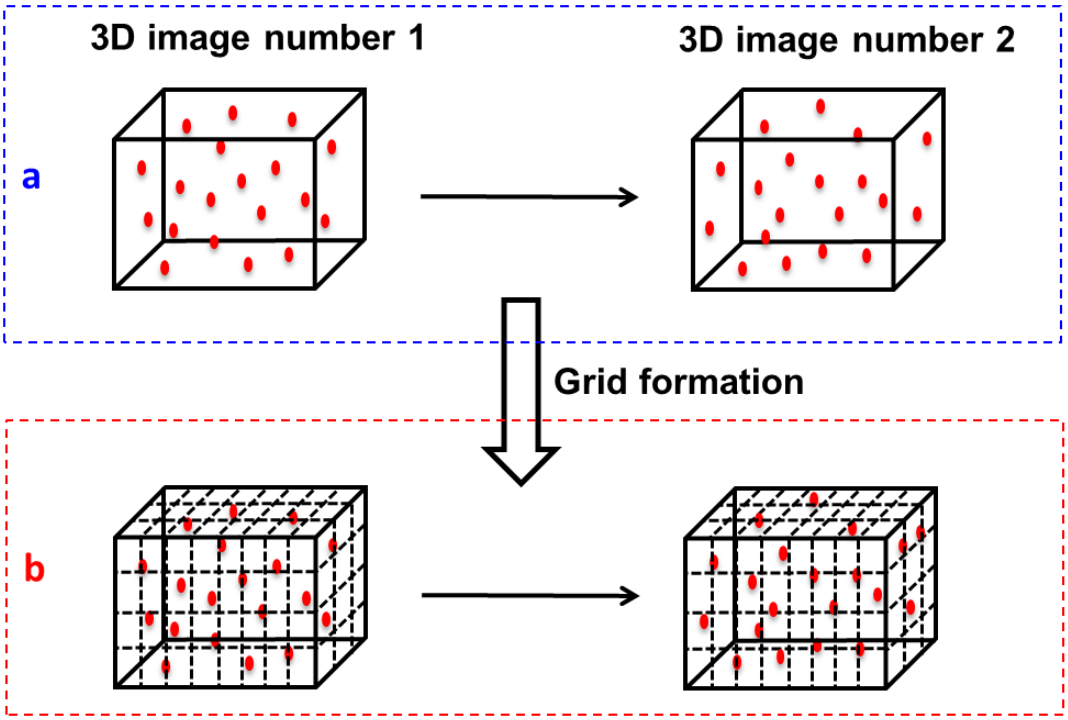

Figure 5-3: Schematic showing grid formation during the first steps of DVC.

Cross-correlation is a mathematical technique used for measuring the similarity of two data sets [294]. The higher the cross-correlation value, the higher the degree of similarity. For continuous functions f and g, it is defined as [294]:

$$f(x) \circ g(x) = \int_{-\infty}^{\infty} f^*(\alpha) g(x+\alpha) d\alpha \qquad 5\text{-}2$$

where ° denotes the cross-correlation between the two functions, * represents complex conjugate and α is a dummy variable of the integration. If g is the result of translation of f in one direction, then α measures the amount of translation [294].

Convolution is the other mathematical technique that is mostly used for modifying an image and it is defined as [294]:

$$f(x) \star g(x) = \int_{-\infty}^{\infty} f(\alpha) g(x-\alpha) d\alpha \qquad 5\text{-}3$$

in which ⋆ denotes the convolution and α is again a dummy variable of the integration.

Images are originally defined in a spatial domain and image transforms are techniques that map an image from one domain to another. The use of this transform leads to better resolution of a particular feature of picture or decreases the computational load [295]. Fourier transform is an image processing

tool that maps images from the spatial domain to the frequency domain. In this case, it can decrease computational load significantly [295]. It is defined as [296]:

$$F(\omega) = \int_{-\infty}^{+\infty} f(x) e^{-i2\pi\omega x} dx \qquad 5\text{-}4$$

Also, the inverse Fourier transform is defined as [296]:

$$f(x) = \int_{-\infty}^{+\infty} F(\omega) e^{i2\pi\omega x} d\omega \qquad 5\text{-}5$$

Since images are discrete functions, discrete Fourier transform is defined as

$$F(\omega) = \sum_{x=0}^{N-1} f(x) e^{\frac{-i2\pi\omega x}{N}} \qquad 5\text{-}6$$

for $\omega = 0,1,2, \dots, N-1$.

And thus, inverse Fourier transforms can also be defined in the same manner:

$$f(x) = \frac{1}{N} \sum_{\omega=0}^{N-1} F(\omega)\, e^{\frac{i2\pi\omega x}{N}} \qquad 5\text{-}7$$

The Fourier transform has many properties and which the Convolution theorem is one of the most important ones in digital image processing. It can be proven that[1] if *F(ω)* is the Fourier transform of *f(x)* and *G(ω)* is the Fourier transform of *g(x)* [296]

$$F(f(x) \star g(x)) = F(\omega)G(\omega) \Rightarrow f(x) \star g(x) = F^{-1}[F(\omega)G(\omega)] \qquad 5\text{-}8$$

According to the definitions of correlation and convolution, correlation of *f(x)* and *g(x)* is equal to convolution of *f(x)* and *g(-x)*. Therefore, the convolution theorem can be written as:

$$F(f(x) \circ g(x)) = F^*(\omega)G(\omega) \Rightarrow f(x) \circ g(x) = F^{-1}[F^*(\omega)G(\omega)] \qquad 5\text{-}9$$

In the current research, the algorithm chosen for running cross-correlation is fast normalized cross correlation (FNCC) [293]. A few modifications to the cross-correlation (Equation 4-2) can lead to more accurate and efficient computation [293].

For further explanations of DVC, consider the following specifications:

- $g(x, y)$ is the intensity value of the image at point (x, y)
- $t(x, y)$ is the template that has to be matched to the image[2]
- $g(x, y)$ has the size of $M_x \times M_y$ and $t(x, y)$ has the size of $N_x \times N_y$

[1] Proof of the theorem can be found in Appendix B.

[2] In our case, $g(x, y)$ is the second image and $t(x, y)$ is the subset chosen from $f(x)$, the first image.

– By moving $t(x,y)$ for u and v the best match can be found. In this case, the best match occurs when the correlation value is highest. To put this in the context of the current research, rigid body translation is assumed to be the only deformation present.

The first step is the calculation of averages of each function over specific regions. For example, the average of $g(x,y)$ over the region of $t(x,y)$ is calculated and denoted by $g_{avg(u,v)}$. Then, the average value of each function is subtracted from the original function so that the effect of illumination inconsistencies, such as abnormal bright or dark spots, on the images is eliminated. The correlation values calculated after this are independent of image contrast and brightness [297]. For the two images with discrete functions of $f(x)$ and $g(x)$, both having the size of N, cross-correlation can be written as [297]:

$$CC = \sum_{x,y}\left[g(x,y) - g_{avg(u,v)}\right]\left[t(x-u,y-v) - t_{avg}\right] \quad 5\text{-}10$$

To increase accuracy, the cross-correlation function can be normalized:

$$NCC = \frac{\sum_{x,y}\left[g(x,y)-g_{avg(u,v)}\right]\left[t(x-u,y-v)-t_{avg}\right]}{\left[\sum_{x,y}\left[\left(g(x,y)-g_{avg(u,v)}\right)^2\left(t(x-u,y-v)-t_{avg}\right)^2\right]\right]^{0.5}} \quad 5\text{-}11$$

This function is called the normalized cross-correlation (NCC). The NCC value is 1 for identical signals and 0 for functions that do not have any similarity. Despite being accurate, evaluation of this function requires considerable computational load. To alleviate this to some extent, another algorithm called fast normalized cross-correlation was developed. Looking at the numerator of Equation 5-11:

$$\sum_{x,y}\left[g(x,y) - g_{avg(u,v)}\right]\left[t(x-u,y-v) - t_{avg}\right]$$

$$= \sum_{x,y} g(x,y)t(x-u,y-v) - t_{avg}\sum_{x,y} g(x,y) \quad 5\text{-}12$$

Note that $g_{avg(u,v)}\sum_{x,y}\left[t(x-u,y-v) - t_{avg}\right] = 0$ [293].

The denominator can also be simplified as:

$$\sum_{x,y}\left(g(x,y) - g_{avg(u,v)}\right)^2 = \sum_{x,y} g^2(x,y) + \sum_{x,y} g^2_{avg(u,v)} - 2\sum_{x,y} g(x,y)g_{avg(u,v)} = \sum_{x,y} g^2(x,y) - \frac{1}{N_x N_y}\left(\sum_{x,y} g(x,y)\right)^2 \quad 5\text{-}13$$

To further simplify the computation, Lewis [293] suggested the FNCC algorithm. In this algorithm, pre-computing two sum tables of $s(u,v)$ and $s^2(u,v)$ can help in reducing the computational load. The two-sum tables are then defined as [297]:

$$s(u,v) = g(u,v) + s(u-1,v) + s(u,v-1) - s(u-1,v-1) \quad 5\text{-}14$$

$$s^2(u,v) = g^2(u,v) + s^2(u-1,v) + s^2(u,v-1) - s^2(u-1,v-1) \quad 5\text{-}15$$

Calculating these two-sum tables, although time consuming, decreases the computational load for finding numerator and denominator of Equation 4.11.

It is crucial to note that all equations discussed here are for 2D images but 3D images are fabricated by stacking 2D images and so these equations can be easily expanded to cover them as well.

The result from FNCC is discrete displacement field at the center of each subset [298]. To achieve a continuous displacement field, with acceptable sub-voxel accuracy, interpolation algorithms can be used. Both quadratic [12] and cubic interpolation [299] functions, paired with different minimization techniques, such as Gaussian-Newton, have been previously used [299].

In the current research, a quadratic interpolation function paired with the least squared solution was used to find the continuous displacement field [287]. This quadratic function can be written as[1]:

$$d(x,y) = \alpha_0 + \alpha_1 x + \alpha_2 y + \alpha_{12} xy + \alpha_{11} x^2 + \alpha_{22} y^2 + \varepsilon \quad 5\text{-}16$$

where ε is the error that should be minimized. Function L is defined as:

$$L = \left(\alpha_0 + \alpha_1 x + \alpha_2 y + \alpha_{12} xy + \alpha_{11} x^2 + \alpha_{22} y^2 - d(x,y)\right)^2 \quad 5\text{-}17$$

and to write the least square solution and find the coefficients, L should be minimized with respect to all $\alpha_{i,j}$ coefficients:

$$\frac{\partial L}{\partial \alpha_{i,j}}|_{i,j=1,2} = 0 \quad 5\text{-}18$$

It is worth noting that, here, the polynomial is fitted to the points with highest correlation value and maximum similarity.

Strain calculations are performed based on the linear theory of elasticity and infinitesimal strains are found from displacement the based on the following equation:

$$\varepsilon_{ij} = \frac{1}{2}\left(\frac{\partial u_i}{\partial x_j} + \frac{\partial u_j}{\partial x_i}\right) \quad 5\text{-}19$$

5.1.4 Running DVC code

The parameters involved in getting results from this code can be divided to two main groups:

1. **Processing parameters:** The most accurate results from FNCC algorithm are obtained by careful selection of the processing parameters. Grid spacing (GS) is the first parameter that can affect results [300]. While extremely small GS increases the computational load, it is important that GS is small

[1] This function can be categorized under linear regression models [341].

enough so that no signal is lost and adequate spatial resolution exists [301,302]. In the current study, GS is generally kept at 5 pixels (~ 1 μm).

Another parameter affecting the results is correlation size (CS), which is an indication for subset size. In Figure 5-4[1], assuming the grid spacing of 5 pixels, the green square shows a CS of 10. This green area moves over to the second image and correlation is performed over this area. CS is inversely related to noise level, meaning that smaller CS tends to increase noise level. At the same time, increasing CS increases computational load.

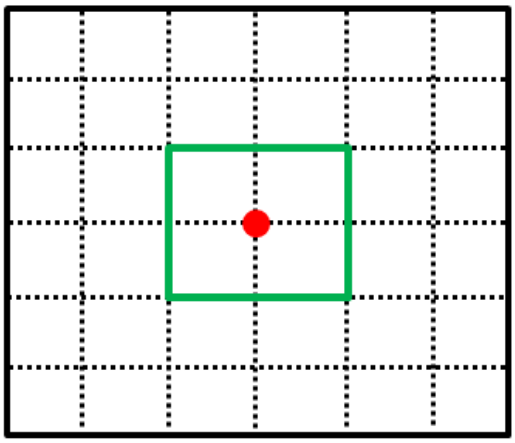

Figure 5-4: Schematic showing CS. Grid spacing is 5 and the green square shows CS of 10.

The final processing parameter affecting the results is search ratio (SR; a similar concept has been used before and named "overlapping" [302]). SR, as the name suggests, is an indication of the area where the subset size is moved over and searches for the highest correlation value. SR, combined with the initial subset size, or CS, determines the search window over the second image. In case large deformations are expected, such as a large focus drift or stage movements, search ratio was chosen higher. Figure 5-5 shows two examples of SR values. Figure 5-5a shows one image of the 3D stack and the subset is the green square. When SR is 1 (Figure 5-5b), the search window (blue square) is the same as the subset size. When SR is 2 (Figure 5-5c), the search window is twice the size of subset. A SR of 2 is used in the current research because it has been previously used and yielded acceptable results [302].

[1] To make it easier to demonstrate the parameter values, just one 2D image of a 3D stack is shown.

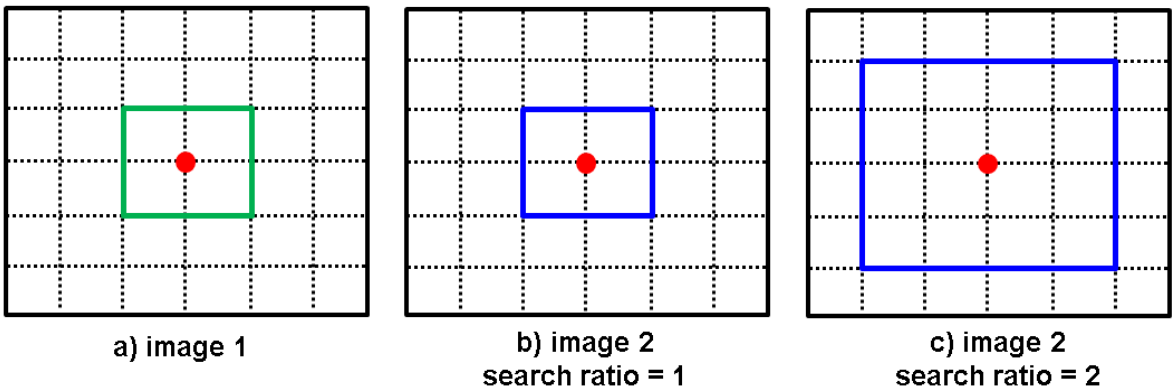

Figure 5-5: Demonstration of SR, a) first 3D stack b) second 3D stack and search window when SR = 1, c) second 3D stack and search window when SR = 2.

The effect of three parameters (GS, CS and SR) on computational load and deformation features are summarized in Table 5-1. As mentioned, smaller GS increases computational load but increases the resolution of deformation field. At the same time, larger CS increases computational load and decreases noise level. It is important to keep in mind that very large CS can lead to loss of subtle patterns. Larger SR, and therefore larger search window, allows for detection of larger deformation range.

Table 5-1: DVC processing parameters and their effect on computational load and various deformation features.

Input parameter	Computational load	Deformation feature
GS ↓	↑	Resolution ↑
CS ↑	↑	Noise ↓
SR ↑	↑	Range ↑

A flowchart of running DVC MATLAB code is depicted in Figure 5-6. Once the two images were loaded, DVC was run with initial settings of rough grid (large grid spacing), small CS and large SR to obtain an initial estimate of the measurements. It is important to note that sources of displacement on images are not all from cells. Due to the instability of the confocal microscope stage, not only the stage can move in the x and y direction, but large displacements in the z direction can also be detected by DVC because of the focus drift of the confocal microscope stage. It is important to estimate this initial displacement and enter it as estimated values to DVC. This allows DVC to detect the smaller deformations related to the cell interaction with the substrate. Once initial estimates were entered into DVC, the code was run again with a finer grid, larger CS and smaller SR. This step was repeated until a

balance between accuracy and computational load was reached. The main parameter that was changed was CS. Smaller CS can allow for better detection of delicate patterns that might be lost in case of large CS.

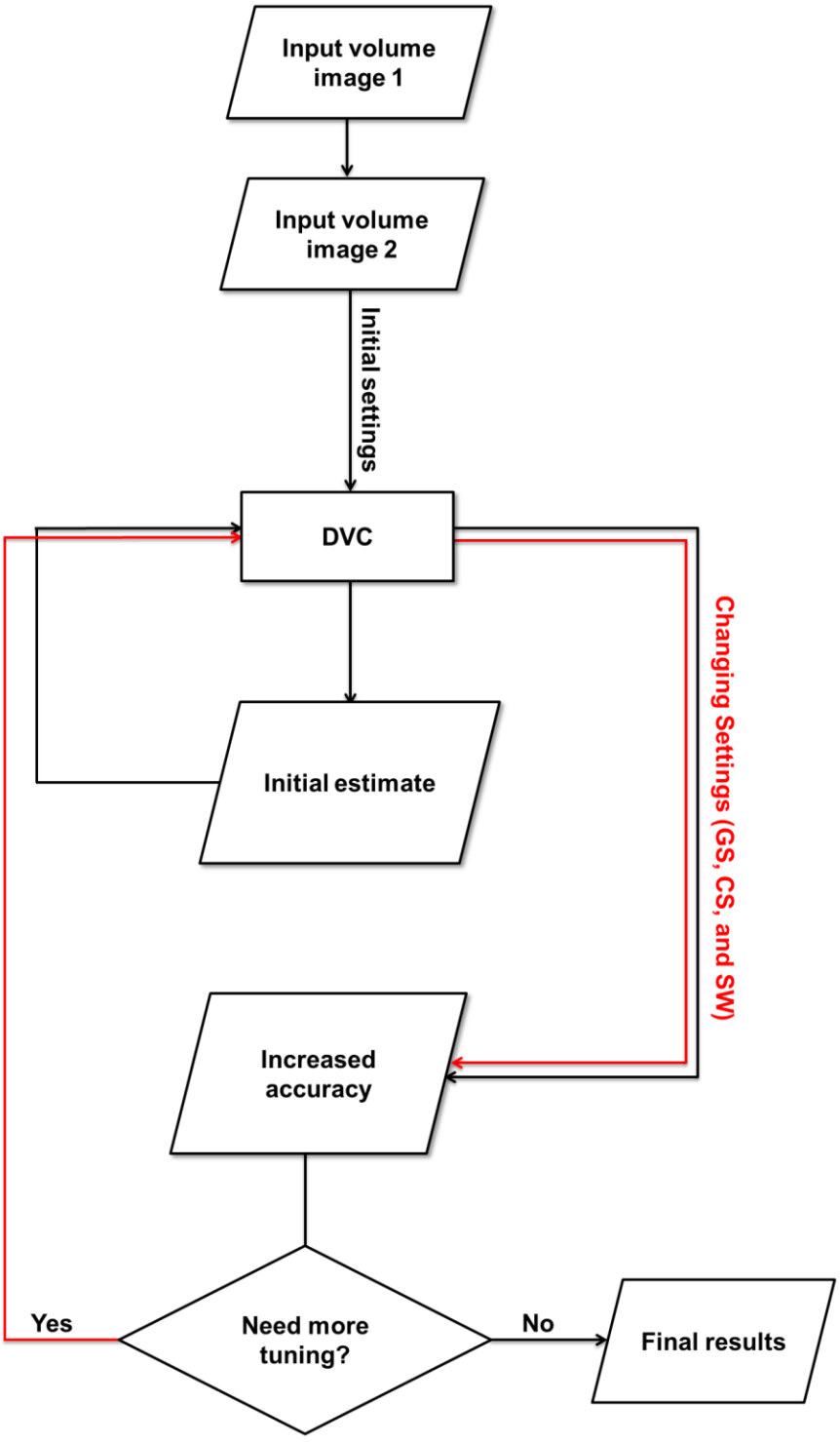

Figure 5-6: Flowchart for running DVC code.

2. Post processing parameters: Post processing parameters are involved with plotting the results. These parameters do not affect accuracy of the results, but rather affect the demonstration of the results.

5.2 Results and discussion

5.2.1 DVC verification

In order to verify the DVC code and determine whether the code was being used properly, a cell free section of the substrate was chosen from the images and displacements and strains were measured[1]. It was important to choose an area that was quite far from the cell, so that cell deformation field did not affect the results. Figure 5-7 shows an image of a cell on a substrate. In this image, the square shows the cell-free area used for DVC verification. In this case, the displacements measured are expected to be somewhat uniform, and may also provide information on the movement of the stage.

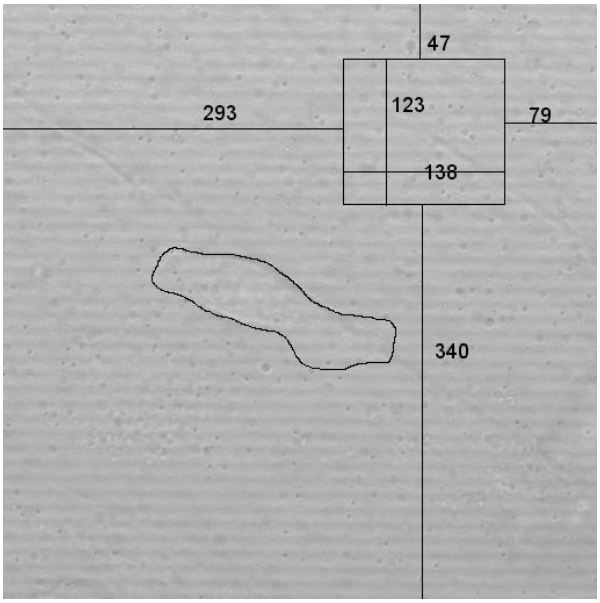

Figure 5-7: Image of a cell on the surface of a PAAm substrate. A cell free area of the image (the square) was chosen for DVC validation. All measurements are in pixels.

Results from DVC on all x (Figure 5-8a), y (Figure 5-8b), and z (Figure 5-8c) directions showed fairly uniform displacements. The variations on each image were smaller than one pixel (~ 0.2 μm) in the x-direction (Figure 5-8a) and the y-direction (Figure 5-8b) directions and about three pixels in the z direction (Figure 5-8c).

[1] Further DVC verification using collagen samples is presented in Appendix C.

Although this experiment is not an accurate verification of the measurement and calculation system, it provides us with a point of comparison where no cell is present and deformation should be zero. It is also important to understand the experimental challenges and sources of error involved in the process. The before and after images have to be taken from the same exact spot, any interruption and slight movement of the stage can induce large errors. Therefore, any procedure for verification would be very difficult in our microscope and micro-incubator setup.

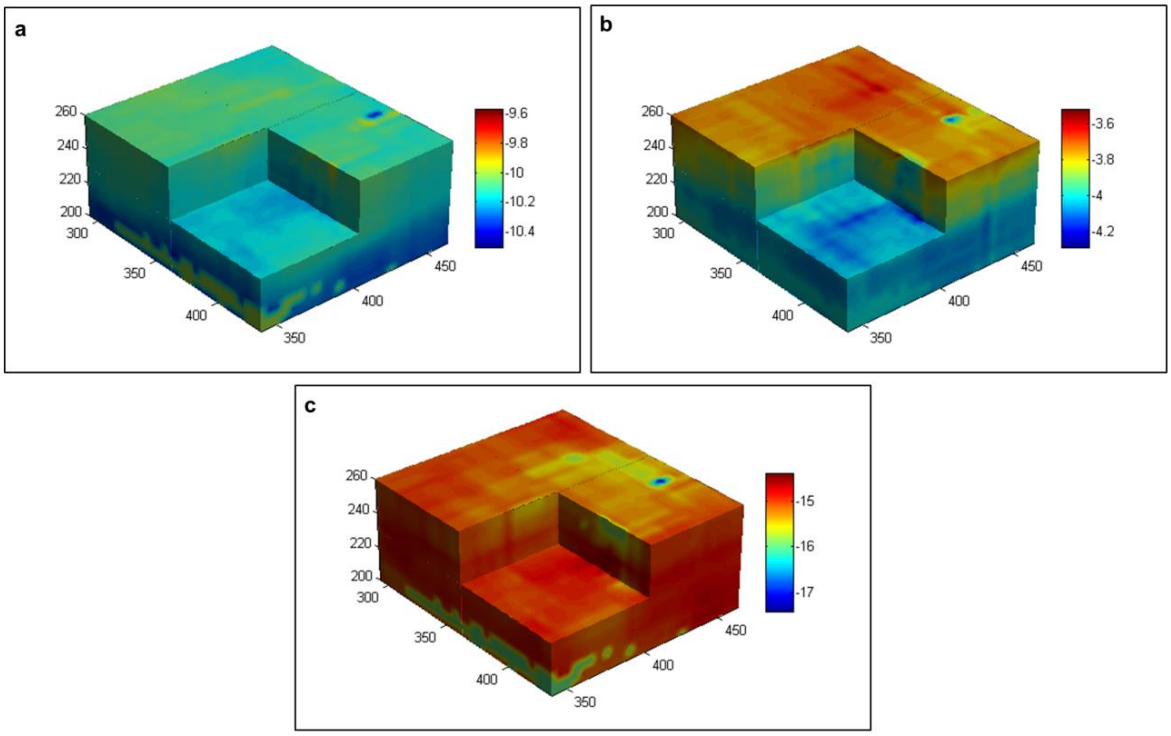

Figure 5-8: Displacement results for verification of DVC code on a) x, b) y, c) z direction. Color bars indicate displacement values in pixels (1 pixel ~ 0.2 μm). For these results, GS = 2, CS = 20, and SR = 2, no smoothing was done, no initial estimate was given (Figure 5-6), and the color bars as chosen by MATLAB were not adjusted.

It is also worth mentioning that DVC has been previously used for processing confocal microscope images where fluorescent microbeads were used as speckles for tracking deformation [12,303].

5.2.2 DVC results of migrating cells

Following verification of the code, images gathered from time lapse imaging experiments were processed by DVC. The main goals of these investigations were to find displacements and, in some cases, strains induced by cells on the substrate. The displacements are a direct result of the forces applied by the cell on the substrate. In traction force microscopy, the published protocols suggest that cells should be

removed from the substrate so that deformation is released and strains and force measurements are performed by comparing images before and after deformation [11,15].

In the current research, it was very difficult to detach the cells from the substrate mainly because it was challenging to access the sealed chamber while maintaining microscope stage stability. To compensate for the fact that there was not an “after” image, which is just an image of the substrate that included cell-free areas, images were divided to smaller sections. Although DVC was run on all sections, strain calculation was performed only on sections where a cell had migrated from and left the area, which could then be considered as a deformation-free area. Figure 5-9 shows images of a cell before and after migration for an hour. The section shown on Figure 5-9a and Figure 5-9b is one where the cell completely left the area, therefore, all displacements and strains were measured, while Figure 5-9c and Figure 5-9d shows the same cell before and after migration for an hour but the chosen section still contains the cell. Strains are not reported for these latter sections.

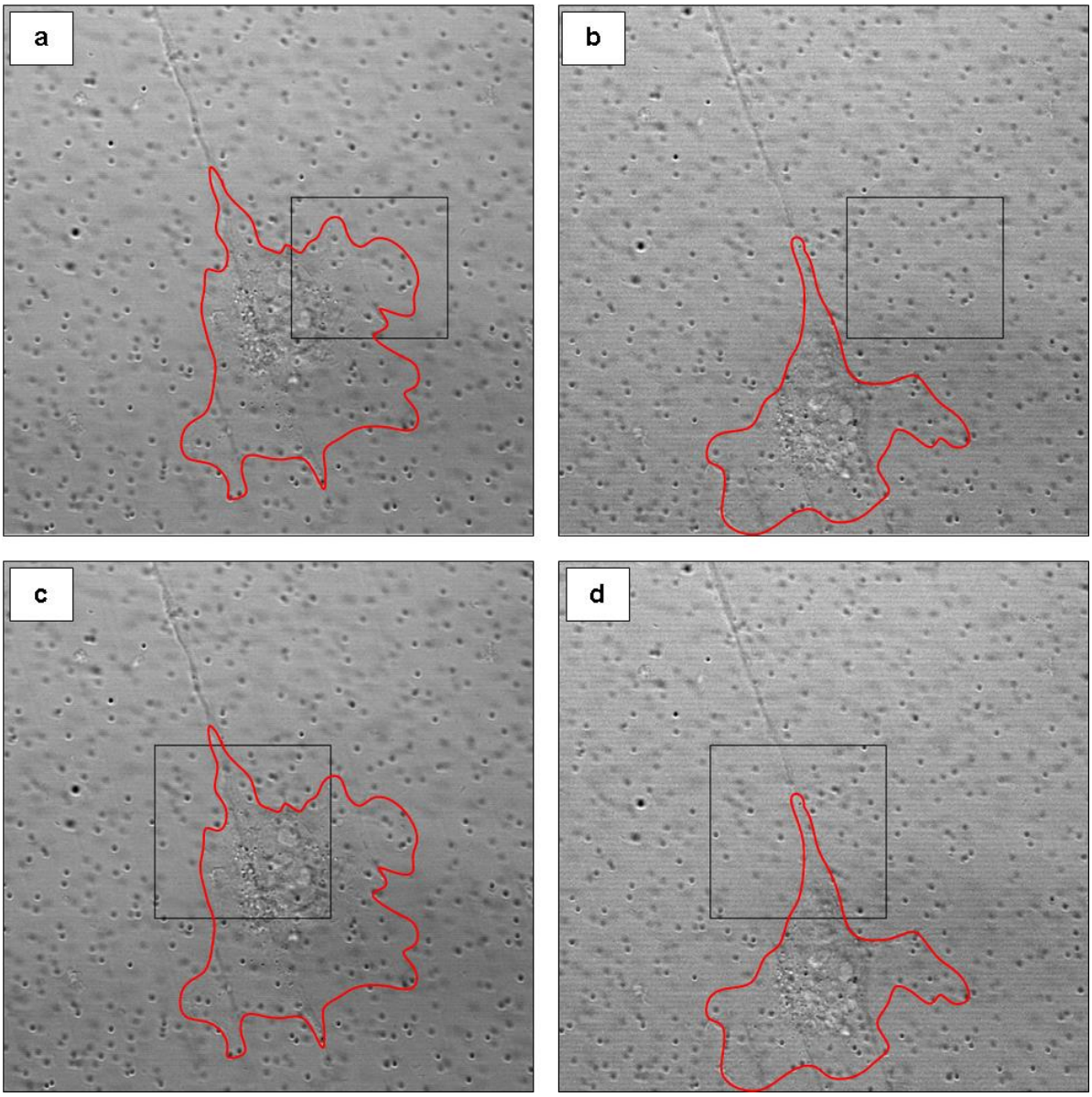

Figure 5-9: Images of a cell cultured on a medium substrate, a) before b) after images of the section used for both displacements and strains measurement, c) and d) show before and after images of the section used for just displacements measurement. On the two later images, cell did not completely leave the area. Duration of experiment was 90 minutes.

5.2.2.1 Out of plane deformations

Figure 5-10 shows the result of out of plane (z direction) displacement and out of plane (z direction) strain induced by the cell on the section shown in Figure 5-9a and Figure 5-9b. The cell not only exerted forces (and therefore induced displacement and strain) in the x and y directions, it also exerted forces in

the z direction as well. This is in agreement with recent reports [11,14,15,225]. The z-direction displacements were smaller than the in-plane ones and, thus, the color bar range was decreased to ensure that the patterns were visible.

Correlation values for different grid points were also calculated and it was found that for most of the grid points, correlation value was above 0.9 which indicates that DVC can detect substrate deformation and results can be considered reliable. However, around the points where large displacements occur, correlation value could drop as low as 0.1. In this case, although the value of displacement is not reliable, the pattern may still provide some qualitative information. For example, the regions of high displacement can be identified, even if the actual deformation values are not known.

It is worth mentioning that all results for migrating cells were obtained following the flowchart shown in Figure 5-6. The results from the initial estimate roughly calculates the movement of stage and when the movement of stage was entered as initial values for displacement, the pattern related to deformation induced by cells could be revealed more accurately.

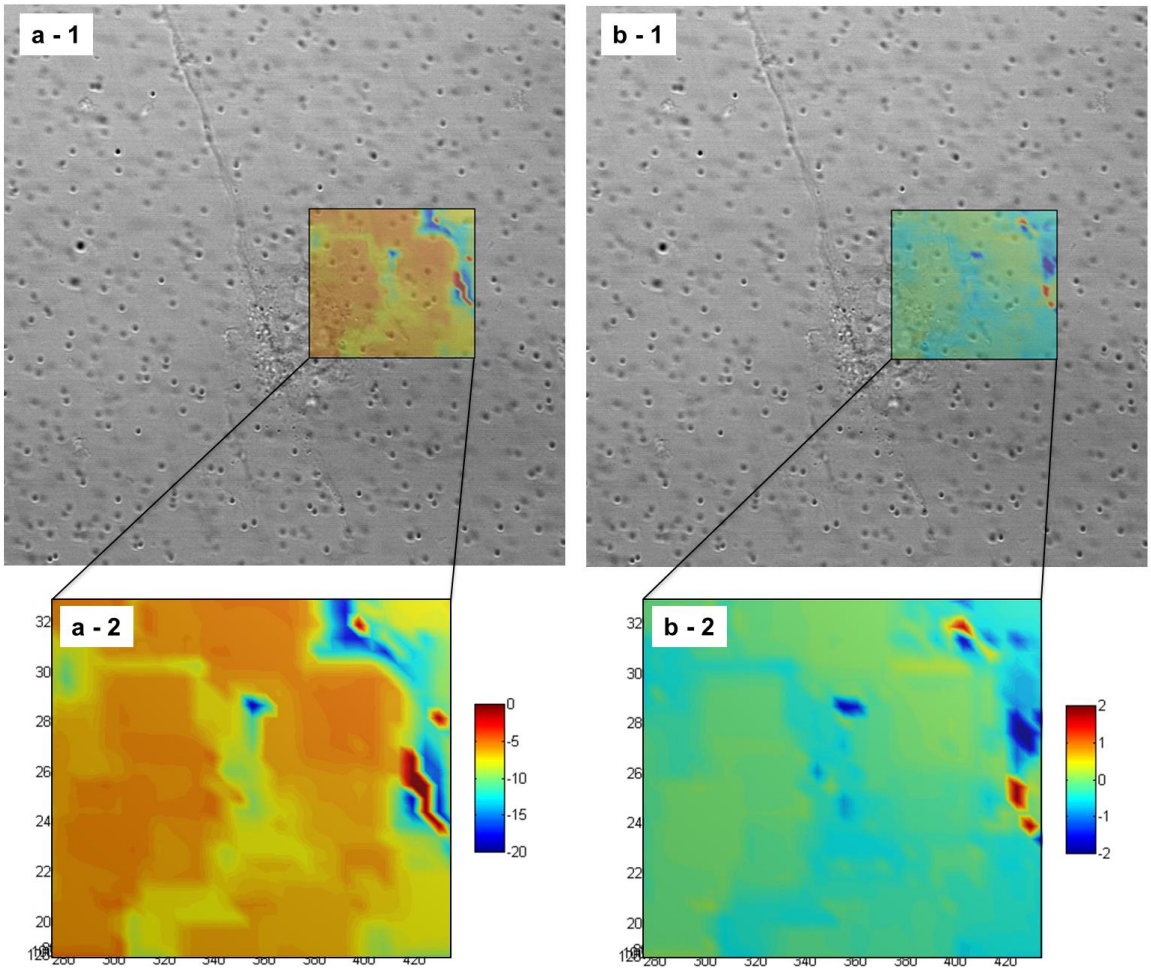

Figure 5-10: a-1) Out of plane (z direction) displacement and b-1) Out of plane (z direction) strain induced by cells on a medium stiffness substrate (3.2 kPa). a-2 and b-2 show magnified view of z displacement and z strain contour plots, respectively. GS is 5, CS is 15 and SR is 2. Color bar on the left contour plot indicate displacement values in pixels (1 pixel = 0.19 μm). On the right contour plot, strain color bar shows the values of strain. Both contour plots, and contour plots overlaid on the image of the cell, are shown for more clear demonstration of results. Displacements and strains in x and y directions for this cell can be found in supplementary information in Appendix D (Figure D - 1).

Although existence of forces in the z direction has been previously reported, the directions of these forces are still controversial. Franck *et al.* [11] has reported that a migrating fibroblast exerts upward pulling force in the trailing edge, while forces on the leading edge are downward pushing forces. However, Legant *et al.* [15] showed upward forces under the leading edge. Also, Delanoë-Ayari *et al.* [14] and Hur *et al.* [13] associated the push-pull behaviour to the cell nucleus. Our results (Figure 5-11) show similar trend to Franck *et al.* [11], where cells appear to "peel off" their trailing end from the

substrate, while the front is trying to “grab” the matrix. The process, both experimental and numerical, seems to be extremely sensitive to the cell lines used, and also the different substrates with different range of properties that can also directly affect cell responses and measurements.

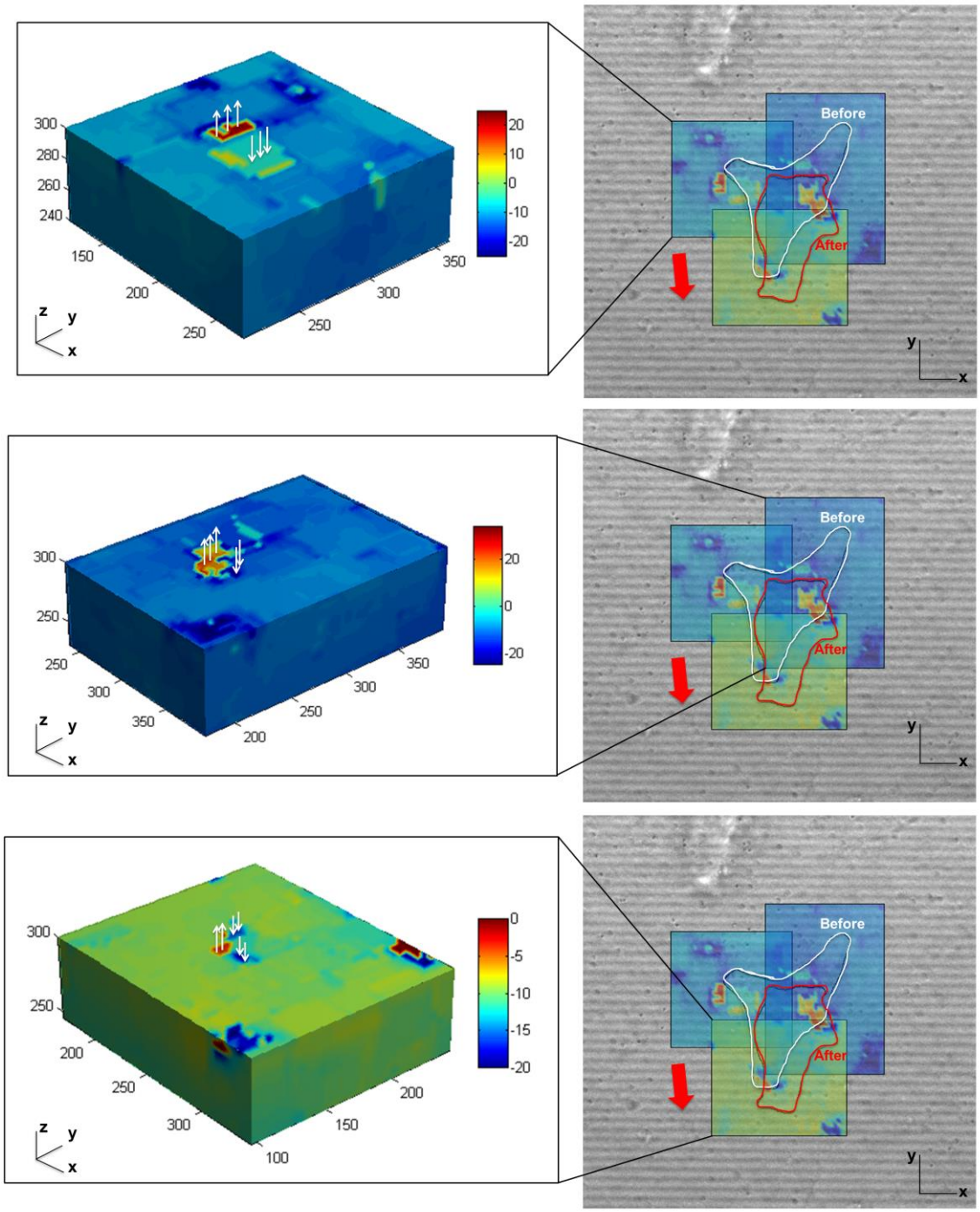

Figure 5-11: Out of plane displacements for a cell cultured on a compliant substrate (1.3 kPa) on three overlapping regions. Possible coupled forces are indicated by white arrows. The red arrow shows migration direction. GS = 5, CS = 15 and SR = 2. Color bars indicate displacement values in pixels (1 pixel = 0.19 μm). Both contour plots and contour plots overlaid on the image of the cell are shown for more clear demonstration of results.

It is important to note that the direction of the red arrow in Figure 5-11 shows the general direction of cell movement (based on the migration of nucleus). Investigating the displacements more locally, close to the cell edges, indicates that cells cause paired regions of substantial local displacement. These displacements could represent a combination of a normal force in one direction and a moment (force couple) acting on the substrate at the cell boundaries. Figure 5-12 further illustrates how these moments might act both on the leading and the trailing edges. It was noted that at the leading edge of the cell, the two regions of local displacement are found to be negative (Figure 5-11) but since one is larger than the other this does not contradict the idea that some combination of normal force and moment are acting.

When taking into consideration the accuracy of the displacement measurements and the limited number of samples, the idea proposed above that moments occur must be considered somewhat speculative at this time. However, Legant *et al.* [15] have recently reported similar "rotational moments" induced on a substrate by mouse embryonic fibroblasts. All these observations suggest that mechanical interactions of cells with their substrate may be more complicated in nature, but further investigation is needed to fully understand and quantify these interactions.

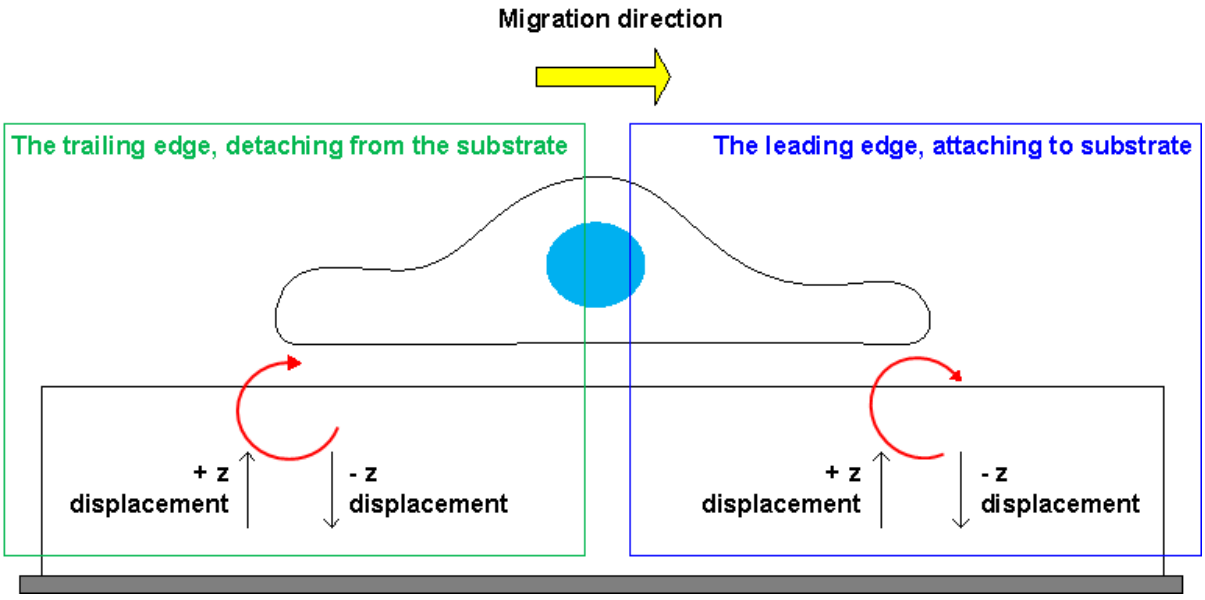

Figure 5-12: Schematic showing displacements and moments induced by cells acting on the substrate.

The depth of the deformations applied by cells was also assessed and it was found that these were rather large on compliant substrates (Figure 5-13). Our measurements indicated a depth of ~ 2.8 μm to ~ 5 μm for different sections. This depth has been previously reported to be around 10 to 15 μm for 3T3

fibroblasts [11]. The difference between our measurements and Maskarinec *et al* [11] can be due to differences in cell type (HCECs vs. 3T3 fibroblasts) or in the elastic modulus of the substrate.

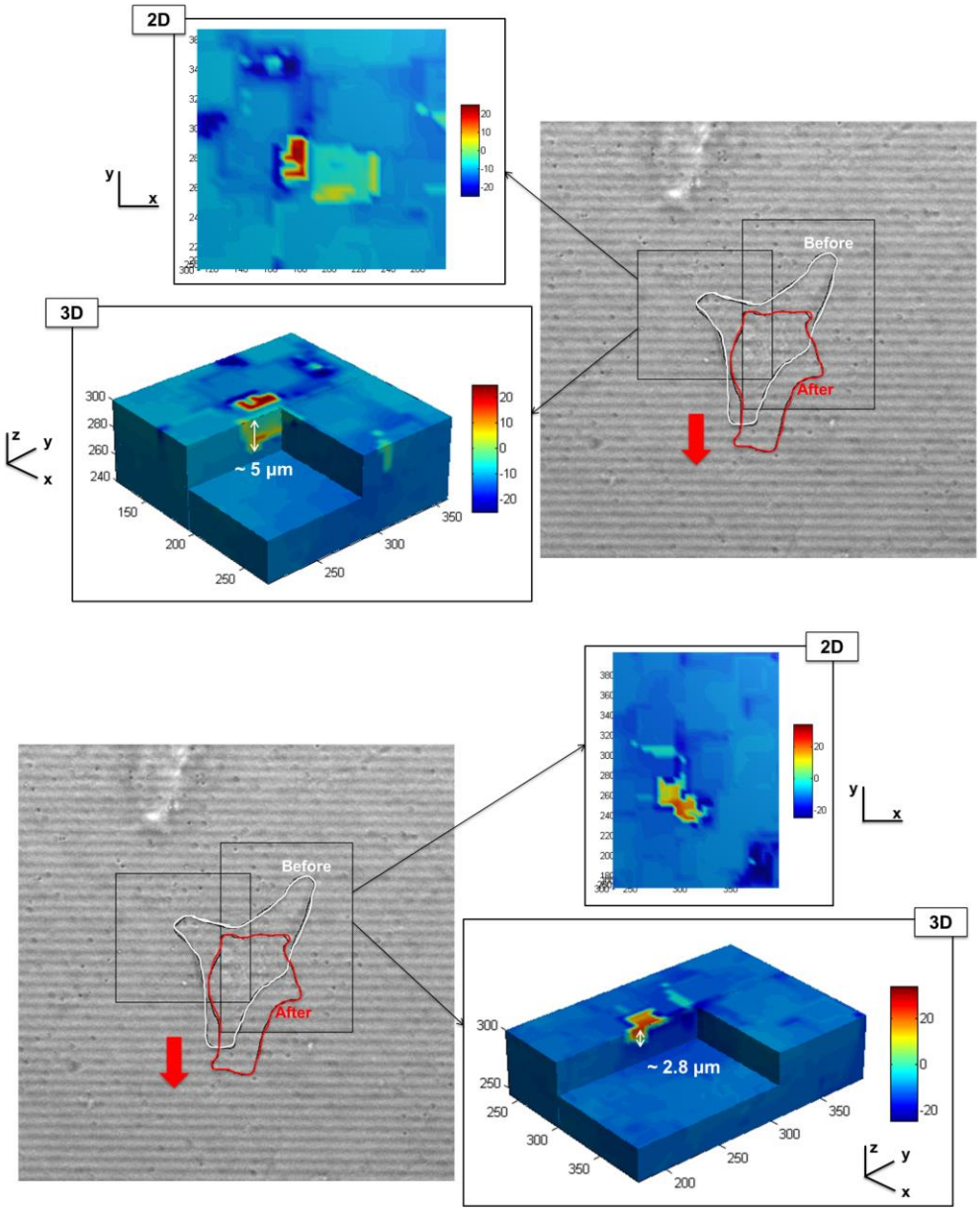

Figure 5-13: Depth of deformation field for a cell cultured on a compliant substrate. Both 2D and 3D views of displacement in the z direction are shown in two different sections. GS = 5, CS = 15 and SR = 2. All axes units are pixel. Color bars indicate displacement values in pixels (1 pixel = 0.19 µm). Both contour plots and contour plots overlaid on the image of the cell are shown for more clear demonstration of results. Displacements in the x and y directions for another cell cultured on a compliant substrate can be found in Appendix D (Figure D - 2 and Figure D - 3, respectively).

5.2.2.2 Compliant vs. stiff substrate

Displacements induced by cells on different substrates were measured and it was found that while cells could induce noticeable displacements on both surfaces, deformation by cells on compliant substrate appeared to be exerted over a larger area (~75 μm^2 on compliant substrate vs. ~ 9 μm^2 on stiff substrate). Figure 5-14 shows displacements induced by cells cultured on compliant and stiff substrates in the z direction. In 0, we speculated that integrin-ligand bond of cells cultured on stiff substrate was in a "tensioned" state as opposed to a "relaxed" state of this bond for cells cultured on compliant substrates [278]. We also speculated that this relaxed state could cause a "crumbled" cytoskeleton (Figure 4-4) and lower migration speed (Figure 4-8). The relaxed state of this integrin-ligand bond on compliant matrices, and therefore the impaired cytoskeleton structure, could also lead to the inefficient force exertion in focal adhesion and cause the forces to be applied over larger areas.

It has been previously reported that cells on stiffer substrates exert larger forces [304]. In the current thesis forces are not accurately calculated, but, the displacement directions and the areas they are applied over, can still give some indication of the forces applied by cells. Assuming this is true and taking into account that forces on the stiffer substrates are applied over smaller areas, it is likely that higher normal stresses are exerted on the stiffer substrates.

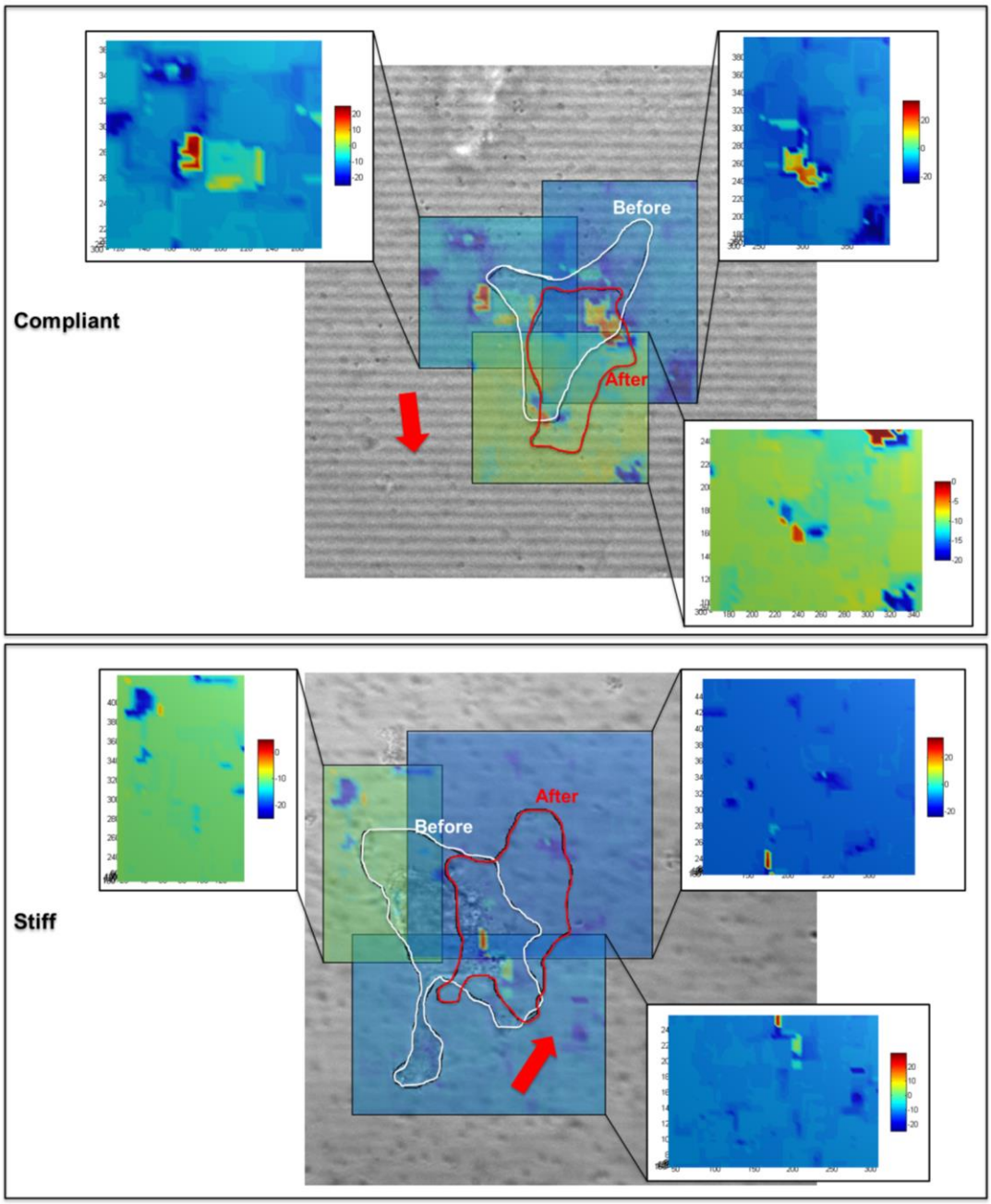

Figure 5-14: Out of plane (z direction) displacements induced by HCECs cultured on a compliant and a stiff substrate on three different sections. Displacements in the x and y directions for cells cultured on compliant and stiff substrates can be found in Appendix D (Figure D - 4 and Figure D - 5, respectively). Larger area over which the cell traction forces are exerted can be seen. Also, Figure D - 6 shows another cell cultured on compliant matrix and larger areas of force exertion can be seen on this image as well. Color bars indicate displacement values in pixels (1 pixel = 0.19 μm). Red arrow shows migration direction. GS = 5, CS = 15 and SR = 2. Both contour plots and contour plots overlaid on the image of the cell are shown for more clear demonstration of results.

5.2.2.3 Deformation pattern underneath the cell

It has been previously reported that the deformations that cells induce on the substrate have a pattern. Large forces in the leading edge of migrating cells were previously shown to exist [10,11]. However, in the present results, the displacement magnitudes were about the same in all x (Figure 5-15), y (Figure 5-16) and z (Figure 5-17) directions. This could be due to the difference in cell line used (HCECs vs. 3T3 fibroblasts) or calculation inaccuracies, which may arise from the fact that correlation values are typically small close to the areas where forces are detected. Assuming that cells exert traction forces at focal adhesions [305], localized deformations at these spots lead to large deformations that DVC might not be able to accurately follow. While patterns may be reliable, displacement magnitudes may not be accurate.

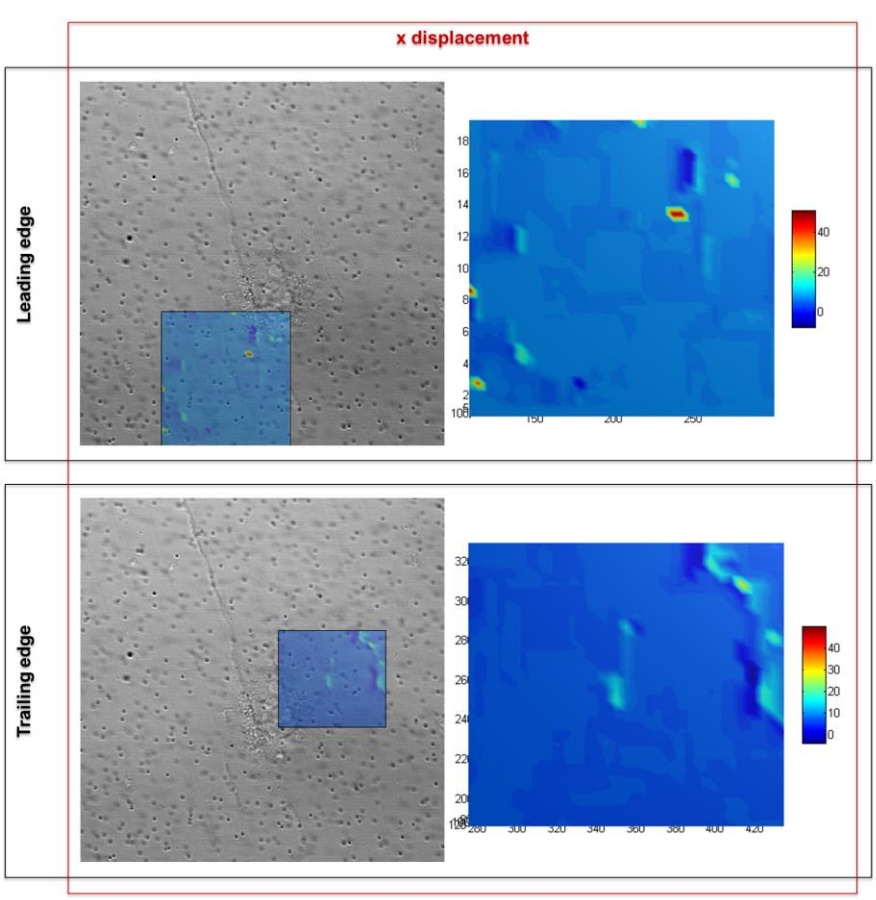

Figure 5-15: Displacements in the x direction for comparison of magnitude and patterns in the leading and trailing edge of an HCEC cultured on a medium substrate. GS = 5, CS = 15 and SR = 2. Color bars indicate displacement values in pixels (1 pixel = 0.19 μm). Both contour plots and contour plots overlaid on the image of the cell are shown for more clear demonstration of results.

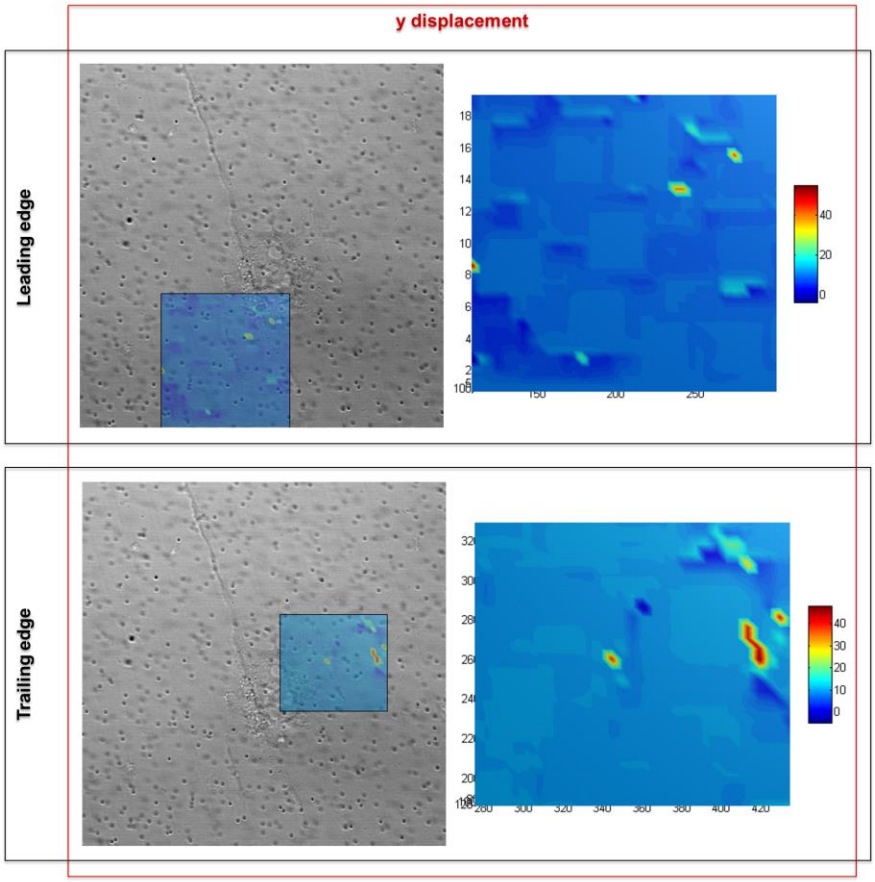

Figure 5-16: Displacements in the y direction for comparison of magnitude and patterns in the leading and trailing edge of an HCEC cultured on a medium substrate. GS = 5, CS = 15 and SR = 2. Color bars indicate displacement values in pixels (1 pixel = 0.19 μm). Both contour plots and contour plots overlaid on the image of the cell are shown for more clear demonstration of results.

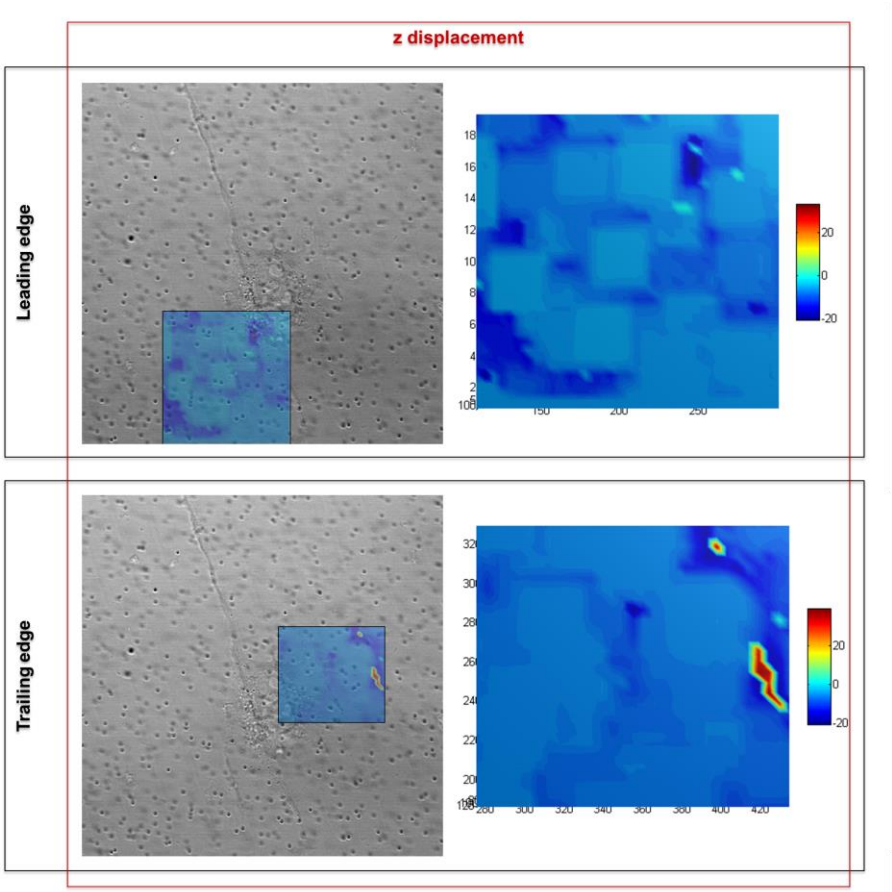

Figure 5-17: Displacements in the z direction for comparison of magnitude and patterns in the leading and trailing edge of an HCEC cultured on a medium substrate. GS = 5, CS = 15 and SR = 2. Color bars indicate displacement values in pixels (1 pixel = 0.19 μm). Both contour plots and contour plots overlaid on the image of the cell are shown for more clear demonstration of results.

Deformation under the nucleus is another matter that has been a subject of discussion before. Although 2D studies confirmed that insignificant forces are present under the nucleus of migrating cells [35,201], earlier 3D force calculations have reported substantial forces under the nucleus [11,14,223]. Interestingly, Legant *et al.* [15] have recently shown that for fully spread cells, no displacements were detected under the nucleus. They also reported that, following initial adhesion formation and before full spreading of the cells, there were forces present under the nucleus but these forces did not exist for fully spread cells. They further speculated that forces were usually present when cells had a round morphology. Figure 5-18 shows our results of displacements under the nucleus for the compliant, medium and stiff samples. While the cell on the medium substrate (Figure 5-18b) did not induce significant deformation under the nucleus, cells on the compliant (Figure 5-18a) and stiff (Figure 5-18c) substrates did indeed deform the substrate

under the nucleus. The medium substrate has an elastic modulus of 3.2 kPa, which is similar to that of Legant *et al*. [15], who found no deformation under the nucleus. At the same time, the stiff substrate with 9.2 kPa elastic modulus has closer properties to the research by Franck *et al*. [223] and Maskarinec *et al*. [11]. The different range of substrate properties and the fact that cells are capable of detecting and responding to these differences may be one of the sources responsible for these inconsistencies. It is also important to note that in the case of the compliant and stiff substrates, the nucleus did not fully move and leave the search window. The more consistent pattern seen on the substrates was that cells induced larger displacements around the perimeter of the cell rather than under nucleus.

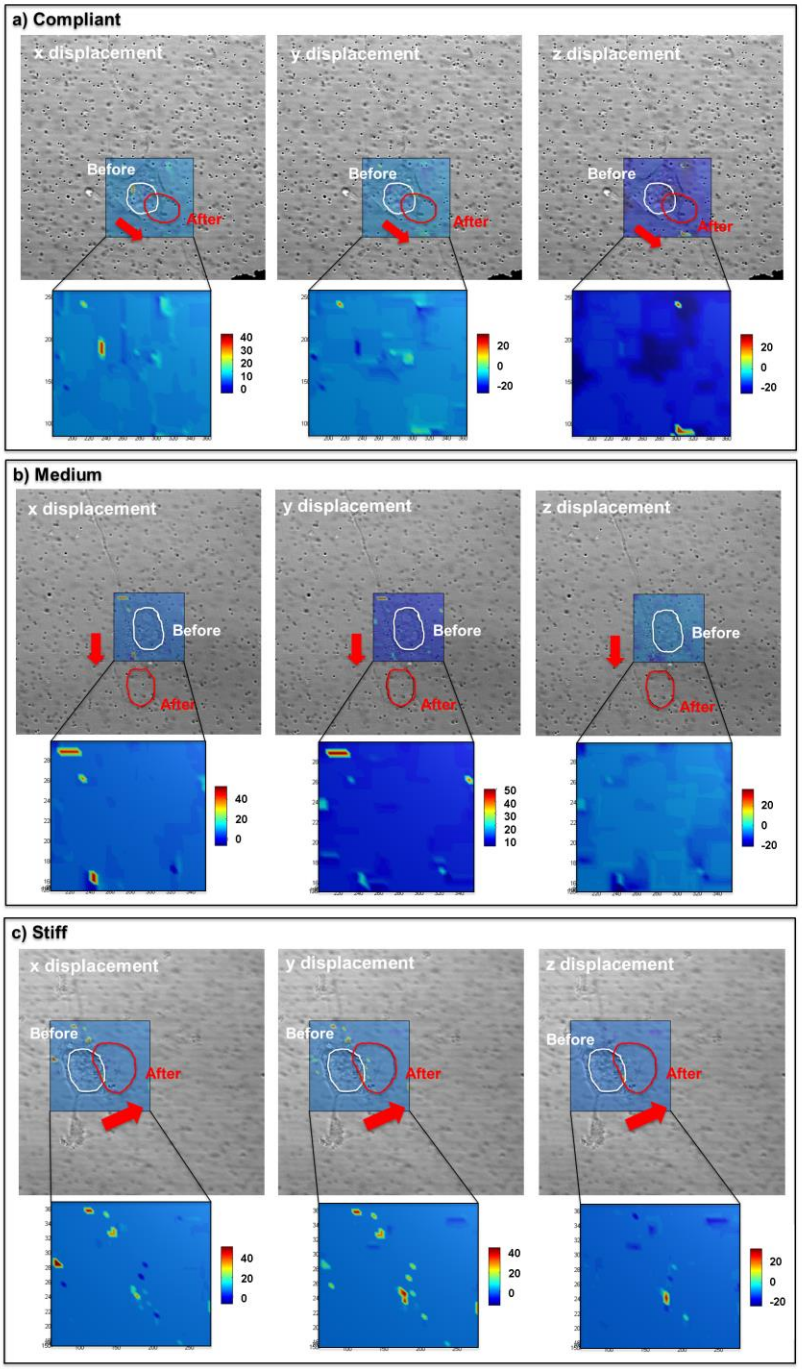

Figure 5-18: Displacements induced by nucleus of single cell on a) compliant, b) medium, and c) stiff substrates. Two circles on the top row images show nucleus before and after migration of cells for an hour. GS = 5, CS = 15 and SR = 2. Color bars indicate displacement values in pixels (1 pixel = 0.19 μm). Both contour plots and contour plots overlaid on the image of the cell are shown for more clear demonstration of results.

5.2.3 Experimental challenges

Time lapse imaging is a delicate and time consuming process involving many parameters. In this section, a few of the challenges encountered during these experiments are discussed.

1. **Phototoxicity**: It is believed that excited fluorophores can induce Reactive Oxygen Species (ROS) formation. As mentioned before, ROS are reactive molecules containing oxygen and can induce oxidative damage in cells [306]. Formation of these molecules during microscopy can be harmful to cells and lead to changes in cell cycle and even cell death (through apoptosis) [307]. To decrease phototoxicity during confocal microscopy, laser intensity was significantly reduced. This had to be balanced with the need to have an acceptable signal to noise (S/N) ratio when decreasing laser intensity. For example, Argon laser (with 488 nm wavelength and rather high energy levels) intensity was decreased to 2% while usually it is used at 50% and HeNe laser (with 543 nm wavelength and much lower energy levels, known as a "weak" laser) was used at 15%. Keeping the HeNe laser at higher intensity was critical as it was used for imaging fluorescent microbeads. To further decrease the effect of phototoxicity, cells were not fluorescently-labelled, instead, phase contrast images of the cells were taken while the set up was switched to confocal microscopy for taking 3D stacks of the substrate loaded with fluorescent microbeads.

2. **Photobleaching**: Diminishing fluorescent intensity after specific number of cycles of excitation emission is called photobleaching. It is believed that fluorescent molecules go through an irreversible change and start to lose their properties [308]. It has been reported that controlling excitation exposure can reduce this problem [307]. Decreasing laser intensity in our experiments not only helped with phototoxicity, it also helped with photobleaching. Furthermore, images of beads were taken at higher speeds to decrease the exposure as much as possible. Since fluorescent beads have a strong signal, decreasing laser intensity and increasing image acquisition speed were a feasible solution.

3. **Focus-drift**: Focus drift in confocal microscopy can occur due to the microscope focus mechanism [309]. It is more prominent in systems equipped with a micro-incubator for controlled environment [310]. The micro-incubator, not only can add extra weight and thus can exacerbate the drift, but it can also cause thermal instability in the system due to higher temperature [311]. It has been suggested that even the environment of the microscope space (such as air conditioning units) can affect focus drift [312]. It has been recommended that in order to decrease the effect of

thermal instability, the micro-incubator should be installed on the microscope stage at least two hours prior to the imaging session to allow the microscope to equilibrate at 37 ^{0}C.

5.3 Concluding remarks

The current study shows that our algorithm is capable of detecting out-of-plane displacements that result from out of plane forces as well as in plane displacements and forces. It was also found that the mechanical response of cells could be more complex than expected and that cells might be capable of exerting moments on the substrates. No changes in magnitude and pattern of displacements were found in the leading edge compared to the trailing edge of the cell. Deformation under the nucleus was seen for compliant and stiff substrates but not for cells cultured on the medium stiffness substrate. Cells on the compliant substrate induced displacements over larger areas when compared to cells cultured on the stiff substrates.

It is important to note that observations are based on a maximum of two experiments. Therefore, the conclusions drawn require further investigation to extend the current work and to test the generality of the present findings.

Chapter 6: Conclusions and recommendations for future work

As the title of this thesis indicates “Investigating some of the mechanical interactions of cells with their environment”, this work mainly focuses on the various aspects of cellular responses to mechanical stimuli. Specifically, elastic modulus was chosen as the mechanical stimulus affecting cellular behaviour and characterized responses were the cell biological responses, such as viability, expression of adhesion molecule, and migration behaviour, and the cell mechanical responses such as deformations induced on the substrate and strains and types of traction forces. Cell induced deformation as a result of 2D migration was the main mechanical response from cells studied in this research. Generally, interaction of cells with their environment, whether chemical, physical or biological, can be done in three levels. In the current research, the second level was chosen whereby cells were cultured on a 2D substrate and migrating cells on a flat surface were studied. While cell migration was occurring in two-dimensions and biological responses were assessed in two-dimensions, 3D mechanical response of cells was evaluated.

The specific conclusions of the present thesis are given in the following section.

6.1 Summary and Conclusions

1. The first step in the present thesis was finding the proper biomaterial to be used as the model environment. This material required specific properties. Several different materials were tested and polyacrylamide (PAAm) was chosen as the most appropriate choice for this study.

2. One of the unique characteristics of PAAm was the ability to manipulate its mechanical properties by changing the chemical composition. PAAm samples with various chemical concentrations were fabricated. Mechanical behaviour was studied by a simple compression test. Specifically, compressive elastic modulus were measured and stress relaxation was investigated to provide a mechanical characterization of the substrates.

3. Three PAAm concentrations were chosen for further study as model materials for cell culture and substrates were fabricated in a three-step process. Using atomic force microscopy (AFM) and nano-indentation, compressive elastic moduli for these substrates were further measured to provide information more relevant to what cells would feel when cultured on these substrates. Using these PAAm substrates, both biological and mechanical aspects of cellular behaviour were successfully studied.

4. The biological responses studied on the different substrates were cell viability, cytoskeleton structure, adhesion molecule expression, apoptosis and migration behaviour. PAAm was found to be not cytotoxic for human corneal epithelial cells (HCECs) and it also did not activate cells as measured by expression of ICAM-1.

5. In the cell studies, while adhesion molecule (integrin-$\alpha 3\beta 1$) expression did not change, HCECs cytoskeleton, specifically actin filaments, did not form properly on the compliant substrates. On the other hand, cells showed visible, prominent actin filaments on stiff substrates. HCECs migration was also affected by substrate elastic modulus. Cells on compliant substrates showed significantly lower migration speed, compared to the ones cultured on stiff substrate. All these results further emphasize that substrate elastic modulus, as mechanical stimulus, affects HCECs responses in a significant way and needs to be studied closely.

6. To further investigate the mechanical responses of cells, confocal microscopy was used in conjunction with the image processing technique, digital volume correlation (DVC). Our measurements not only showed out of plane displacements, it also highlighted a new level of complexity regarding the cell mechanical responses during migration. It was found that cells may induce moments as well as forces on the substrates. The direction of forces and moments revealed that cells tend to grab the substrate in the leading edge and release it in the trailing edge.

7. Our measurements did not show any differences in terms of the magnitude of the displacement in the front and back of the migrating cells. It was also found that HCECs tend to exert cell traction forces around the edges as opposed to under the nucleus.

8. Mechanical stimulus, specifically elastic modulus, can affect both biological and mechanical behaviour of HCECs. This effect can be substantial and can lead to visible changes observed with migration speed of cells, or it can lead to more subtle changes such as changes in the cell-induced deformation of the substrate. It is important to explore, study and understand these changes so as to develop more practical and clinical applications.

6.2 Contributions

Some studies in the more complex levels of cell-substrate interactions have been published recently but there are many more questions that need to be answered and more accurate methods need to be developed. The results from this thesis contributed knowledge to the cell biomechanics field, and more specifically, how different cell types can respond to mechanical stimuli. The specific contributions that this thesis has made to the cell biomechanics research field are as follows:

1. Human corneal epithelial cells (HCECs) have been shown to detect substrate stiffness as mechanical stimulus and respond to it, both biologically and mechanically.
2. The 3D deformation patterns, applied by HCECs, have been further established.
3. Some evidence has been found to support the idea that cells can apply moments to a substrate as well as normal forces.

The following two journal and one conference papers have been published from this research:

1. Molladavoodi S, Gorbet M, Medley J, Kwon HJ. Investigation of microstructure, mechanical properties and cellular viability of poly(L-lactic acid) tissue engineering scaffolds prepared by different thermally induced phase separation protocols. J Mech Behav Biomed Mater 2013;17:186–97.
2. Molladavoodi S, Kwon HJ, Medley J, Gorbet M. Human corneal epithelial cell response to substrate stiffness. Acta Biomaterialia. 201; 11, 324-32.
3. Molladavoodi S, Medley J, Gorbet M, Kwon HJ. Mechanotransduction in Corneal Epithelial Cells. Proc. ASME 2013 Int. Mech. Eng. Congr. Expo. IMECE2013, 2014, p. 1–5.

The results from the current research also emphasize the role of mechanics in cellular behaviour and show the necessity of studying mechanical behaviour of cells as well as biological behaviour when

studying processes like migration speed. It also highlights how these two types of responses can be intricately tangled and studying both aspects in parallel can provide a better understanding towards more real world and clinical applications.

6.3 Future work

The current research emphasizes the importance of mechanics in cell biology and cellular behaviour. The following recommendations for future work can further help with understanding the mechanical interaction of cells with their environment:

1. To get an even more complete picture of the processes, further experiments in biological responses of cells will help with better understanding the underlying mechanisms of how cells are capable of detecting mechanical stimuli.
2. Since the DVC method used is independent of the cell type used here, using different cell lines, such as tumor and cancer cells, with the same protocols can help further gain knowledge on the effect of mechanical behaviour of cells in various contexts.
3. Although the correlation algorithm used for image processing technique, DVC, is the most efficient and accurate one currently available, the code can still benefit from optimization. There are a few ways to increase accuracy of this code:
    a. Preprocessing of images to decrease noise level and thus increase accuracy.
    b. Using higher levels of interpolation.
4. Accurate cell traction force calculation is the next step for characterizing mechanical behaviour of cells. Magnitude, direction and pattern of forces are the parameters that need to be studied. More accurate cell traction force magnitudes and directions can further reveal the complicated mechanical responses of cells and therefore moments applied by cells can be studied more effectively.
5. The current study focuses on how cells interact with a surface of a substrate in 2D. However, rather than a substrate, to better mimic the *in vivo* situation, a 3D matrix is needed within which cells can both grow and move. The matrix must have specific controlled properties including a fibrous morphology. it would then potentially be possible to measure 3D displacements and strains.

6. To use a 3D matrix with a complex morphology, more complicated continuum mechanics theories are needed to relate displacements and strains to cell traction forces.
7. It is important to also start translating these results to more clinical applications. The following suggestions can open up a way to the former:
    a. Depending on the cell type, it is important to implement more relevant biomaterial substrates and matrices. For example, in case of HCECs and the connection of their behaviour to keratoconus (KC), it is more relevant to use collagen as the material. This can lead to more applied results.
    b. Again, depending on the cell type and the condition they are related to, the effect of drug on cell behaviour, both mechanical and biological can lead to further optimization of therapeutic strategies.

Appendix A: Investigation of microstructure, mechanical properties and cellular viability of poly(L-lactic acid) tissue engineering scaffolds prepared by different thermally induced phase separation protocols

Sara Molladavoodi, Maud Gorbet, John Medley, Hyock Ju Kwon

Journal of the Mechanical Behavior of Biomedical Materials [313]

Introduction

Tissue engineering is an approach for repairing or replacing damaged tissue with new functional natural tissue. One type of tissue engineering involves the introduction of a cell-loaded synthetic scaffold. In this method, the cells initiate tissue growth and the synthetic scaffold provides structural support but gradually degrades while the new tissue grows and replaces it. Since the microstructure of ECM is fibrous [229], fabricating a fibrous-structured substrate to mimic the ECM has been considered important. The scaffold should also be fabricated from a biocompatible material so that the degradation products do not stimulate the immune system [314]. Furthermore, the scaffold should have a highly interconnected porous structure so that cells can grow tissue and nutrients and biological waste can flow through to support cell growth [315,316].

One of the most difficult aspects of tissue engineering is the gradual transfer of load from the degrading scaffold to the newly grown natural tissue. Thus, the scaffold becomes a composite structure with changing properties and any optimization of the initial scaffold must consider this complexity [314]. The design of scaffolds for tissue engineering remains a challenging task involving much speculation, pilot studies and an overall iterative approach. It is important to have as much information as possible regarding the initial characteristics of the various material choices for the scaffold.

Several methods have been reported for fabricating tissue engineering scaffolds such as porogen leaching [317–319], gas foaming [320], 3D printing [321], electrospinning [322,323], and phase separation [231,324,325]. Various types of polymers have been used as scaffold materials; these polymers can be either natural or synthetic. Although natural materials can provide a better cell attachment and function, synthetic materials have the advantage of permitting a better control over the properties of the scaffold.

Poly(lactic acid) (PLA) is one of the synthetic polymers that is used extensively in tissue engineering [232]. This polymer is one of the aliphatic polyesters with chiral molecule which has four isomers: poly(L-lactic acid), poly(D-lactic acid), poly(D,L-lactic acid), and meso-poly(lactic acid) [314]. The first of these, PLLA, is a biodegradable and biocompatible polymer that is approved by the US Food and Drug Administration (FDA) for clinical use [229].

Generally, biodegradation of polymers can be caused either by enzymes present in the human body or by water through hydrolysis [314]. PLA is degraded by random hydrolysis of ester bonds and the main product is lactic acid which normally exists in the human body. The lactic acid formed in the body enters the tricarboxylic acid cycle and breaks down to water and carbon dioxide [326].

Phase separation is one of the methods used for fabricating PLA scaffolds. Phase separation, can happen by cooling the polymer solutions to low temperature [232] in a process known as thermally induced phase separation (TIPS). In TIPS, a uniform mixture of two elements (e.g. a solution) is quenched to a low temperature where the two components in the mixture are immiscible [227]. Immiscibility is the direct consequence of decreasing temperature and so thermal energy is the driving force during this process. Control over the microstructure and properties can be achieved by adjusting quenching temperature, solvent type, and polymer concentration [227,230]. Although TIPS is a more common method, phase separation can also be induced by addition of a non-solvent to reduce the miscibility of the polymer and solvent [232].

While there are several studies on how to perform TIPS, there is a lack of information regarding the relationship between these final properties (e.g. the final microstructure) and subsequent cell viability. In the present study, two different TIPS protocols were used to fabricate fibrous (F-TIPS) and porous (P-TIPS) scaffolds from PLLA polymer. Mechanical properties were evaluated by both simple and cyclic compression tests. These tests were performed dry and also in the presence of water to determine its influence on mechanical properties. Furthermore, in order to explore the effect of microstructure and mechanical properties on cellular viability, human osteosarcoma fibroblasts were cultured in various scaffolds and cell viability was measured. The results of these cellular viability assays were confirmed by using live/dead staining observed by laser scanning confocal microscope. Finally, simple compression tests were performed following the incubation of specimens in cell culture medium to estimate the effect of scaffold biodegradation on mechanical properties.

Materials and methods

Specimen Preparation

PLLA specimens were fabricated by dissolving the Poly(L-lactic acid) (PLLA) in appropriate solvent for both F-TIPS and P-TIPS methods[1]. Resomer grade PLLA with inherent viscosity of 1.5 - 2 dl/g and molecular weight of 190,000 - 200,000 Daltons (Boehringer Ingelheim, Germany) was used in this study. As shown in Table A - 1 specimens were fabricated in concentrations of 3, 5 and 7 wt% of PLLA (where these values are the percent of the weight of the entire solution). Specimens had a simple cylindrical shape with 10 mm diameter and 10 mm height.

Table A - 1: Summary of specimens used in this study

Fabrication method	PLLA concentration (wt%)	Descriptive specimen name	Water content
F-TIPS	3	3F-TIPS	Wet
			Dry
	5	5F-TIPS	Wet
			Dry
	7	7F-TIPS	Wet
			Dry
P-TIPS	3	3P-TIPS	Wet
			Dry
	5	5P-TIPS	Wet
			Dry
	7	7P-TIPS	Wet
			Dry

F-TIPS method

PLLA was dissolved in Tetrahydrofuran (THF) (Sigma Aldrich, Canada) at 50-60 ^{o}C. The solution was poured in a 100 mm Pyrex® glass petridish (Sigma-Aldrich, Canada) and then immediately placed in a freezer (Norlake Scientific, Hudson, WI) at -25 ^{o}C for two hours. Cooling was performed under conditions of natural convection. The frozen specimens were then punched from the PLLA frozen sheet and placed in deionized water for two days to allow the solvent to be replaced with water. The water was changed twice a day. After the exchange process, specimens were either freeze-dried for another two days to prepare the dry specimens or kept immersed in water to prepare the wet specimens. Protocol for this method was adopted from other studies [229,230,327].

[1] Method designation was based on the final microstructure and will be discussed further in the results and discussion section.

P-TIPS method

PLLA was dissolved at 60-70 ^{o}C in a mixture of 1,4-dioxane (Sigma Aldrich, Canada) and distilled water (the ratio of 1,4-dioxane to distilled water was 87/13) [227]. The solutions were poured into aluminum molds and then immediately placed into liquid nitrogen. After the specimens had been in liquid nitrogen for two hours, they were placed in ethanol for two days to allow the solvent to be replaced with ethanol. The ethanol was changed twice a day. In the same way as for the F-TIPS, the specimens were either freeze-dried for another two days or immersed in deionized water to produce the dry or wet versions. Protocol for this method was adopted from other studies [227,233,234].

SEM investigations

The microstructures of all freeze-dried specimens were investigated using a JSM-6460 (JEOL, Japan) scanning electron microscopy (SEM) at 20 kV. For SEM observations, all specimens (including the specimens after the compression test) were fractured in liquid nitrogen and coated with a 10 nm layer of gold.

Pore size and fiber diameter measurements

From the SEM micrographs, one hundred fiber diameters were estimated for each F-TIPS specimens and fifty pore sizes[1] were estimated for each P-TIPS specimen. For each specimen, these data values were consolidated into their average plus or minus the standard deviation.

Mechanical behaviour characterization

In general, simple compression tests were used to characterize the mechanical behaviour of all the PLLA specimens. However, 5F-TIPS specimens were subjected to cyclic compression testing and simple compression testing after various times of biodegradation (incubation in cell culture medium).

Simple Compression Test

The effects of PLLA concentration, fabrication method, and presence of water in the specimens on the stress-strain behaviour were investigated by simple uniaxial compression tests (Figure A - 1). These tests were performed on three specimens of each type using a universal material testing machine (Texture analyser.xt Plus, Stable Micro Systems, New Jersey) with a 49.05 N (5 kgf) load cell. Dry specimens

[1] Pore diameter was measured and reported as pore size.

were placed directly on a stiff flat aluminum substrate and compressed with an acrylic cylindrical indenter of larger diameter, whereas wet specimens were placed in a polycarbonate cubic container filled with deionized water. To evaluate the lateral deformation of specimen, images of the specimen were captured by a high resolution charged-coupled device (CCD) camera (1028×1008 pixels) (STC-CL202A, SENTECH), through a camera link (NI PCIe-1427, National Instrument). To help produce clear and high contrast images, an LED light panel was placed behind the specimen. The mechanical testing and image capture were synchronized by LabVIEW (V. 8.5) software (National Instruments, Austin , TX).

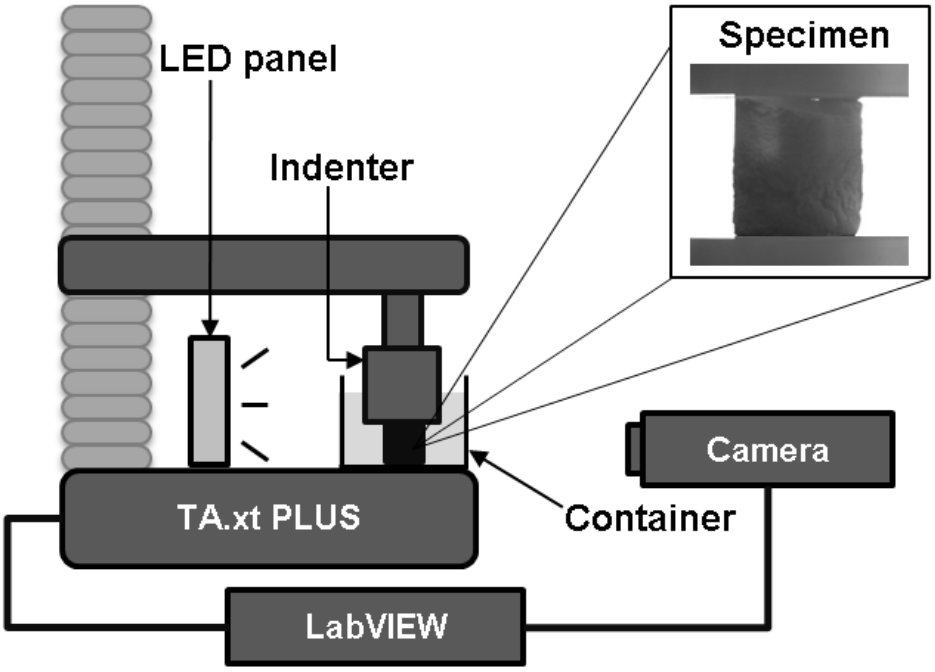

Figure A - 1: Schematic of the layout for compression test.

Upon confirming negligible specimen "bulging", engineering stress and engineering strain were calculated as

$$\sigma = \frac{F}{A_0}, \ \varepsilon = \frac{\Delta L}{L_0} \qquad \text{A-1}$$

where F is compressive force measured by the load cell, A_0 initial cross-sectional area, ΔL change of specimen height, and L_0 initial specimen height. Specimens were loaded up to 20 % strain with a

cross-head speed of 0.2 mm/s, and then unloaded to zero load at the same speed while force, displacement and images were recorded.

Cyclic Compression Test

Cyclic compression tests were performed on 5F-TIPS specimens. The same test setup was used as for the simple compression tests (Figure A - 1). Tests were performed by repeating "loading-unloading-recovery cycles" four times at a constant cross-head speed of 0.2 mm/s. In the first cycle, the cross-head was moved downwards until 20% engineering strain was achieved, and then moved up until the load reached zero. Then, specimen recovery was allowed for 30 minutes. In the following cycles, the same specimen was compressed up to 80 % of its recovered height (20% engineering strain), and then the unloading-recovery cycles were repeated. Since permanent deformation took place after each cycle, starting position of the crosshead decreased.

Cell Culture, viability assay, and microscopy

In order to study the effect of microstructure on cell viability, MG63 cell line (human osteosarcoma fibroblast) (ATCC, Manassas, VA), derived from a 14 year old male was used in this study. Cells were maintained in MEM medium (Minimum Essential Medium Eagle, ATCC, Manassas, VA) supplemented with 10 % FBS, and 1 % penstrep at 37 ^{o}C, 5 % CO_2, and 95 % humidity incubator. Cell culture medium was changed every two to three days.

Prior to cell culturing, all the scaffolds were cut in half and left in 70% ethanol overnight and then placed in sterile phosphate buffer saline (PBS) (VWR, Radnor, PA) for another day (changing PBS several times to make sure that the ethanol had been removed from the scaffolds). Cell suspension was cultured on the top of the sterilized scaffolds. To make sure cells attached to the scaffold, the cell/scaffold construct was left in incubator at 37°C for 1.5 hours before adding the cell culture medium.

Using 3-(4,5-dimethylthiazol-2-yl)-2,5-diphenyltetrazolium bromide (MTT; Biotium, Hayward, CA) assay, cellular viability was measured for all concentrations of specimens prepared by both methods, i.e. 3F-TIPS, 5F-TIPS, 7F-TIPS, 3P-TIPS, 5P-TIPS, and 7P-TIPS. For each set, three specimens were used (n=3). Cell viability and proliferation were measured during a period of 8 days. On the day of the assay, scaffolds were transferred to a new cell culture plate (to ensure that only cells on the scaffolds were tested), and incubated with MTT solution in cell culture medium (0.5 mg/mL) for 3 hours at 37 °C. Enough MTT solution was added to fully cover the entire specimen. Then, isopropanol was added to

dissolve the formazan crystals and absorbance was read at 595 nm using a microplate photometer (Thermo Scientific, Hudosn, NH). Cell viability percentage was reported as relative viability compared to cells which were cultured in a well of a tissue-culture treated cell culture plate.

To further confirm the viability of cells cultured on 5F-TIPS scaffolds, cells were stained with a Live\Dead Viability Kit for mamalian cells (Invitrogen, Carlsbad, CA) according to manufacturer's protocol. This kit provides an assay to simultaneously visualize both live and dead cells. Cells were then imaged by an inverted laser scanning confocal microscope (LSM 510 meta, Carl Zeiss, Germany) using an argon laser (488nm) and an HeNe laser (543nm).

Biodegradation

To investigate the effect of biodegradation on mechanical properties of PLLA, 5F-TIPS specimens were incubated at 37 ^{o}C, 5 % CO_2, and 95 % humidity condition in Dulbecco's Modified Eagle Medium (DMEM) (Invitrogen, Carlsbad, CA) supplemented with 10 % FBS (VWR, Radnor, PA), and 1 % penstrep (mixture of 5,000 units of penicillin (base) and 5,000 µg of streptomycin (base)/ml) (Invitrogen, Carlsbad, CA). Over the period of two months, simple compression tests were performed on several different incubated specimens. During the first month, one specimen was tested each week. The last specimen was tested by the end of the second month.

Statistical analysis

To evaluate the significance of the differences, an analysis of variance (ANOVA) was performed followed by a multiple pair-wise comparisons using the Tukey HSD test using STATISTICA V8 (StatSoft, Tulsa, OK). Significance level was considered to be 0.05.

Results and discussion

Microstructural investigations

Typical SEM images of 3, 5 and 7 wt% specimens showed that microstructures resulting from F-TIPS and P-TIPS methods were significantly different (Figure A - 2). F-TIPS yielded fibrous structures that better resemble the natural ECM microstructure, whereas P-TIPS produced foam like porous microstructures. Similar morphological microstructures have been reported by others for F-TIPS [229,230] and P-TIPS [227].

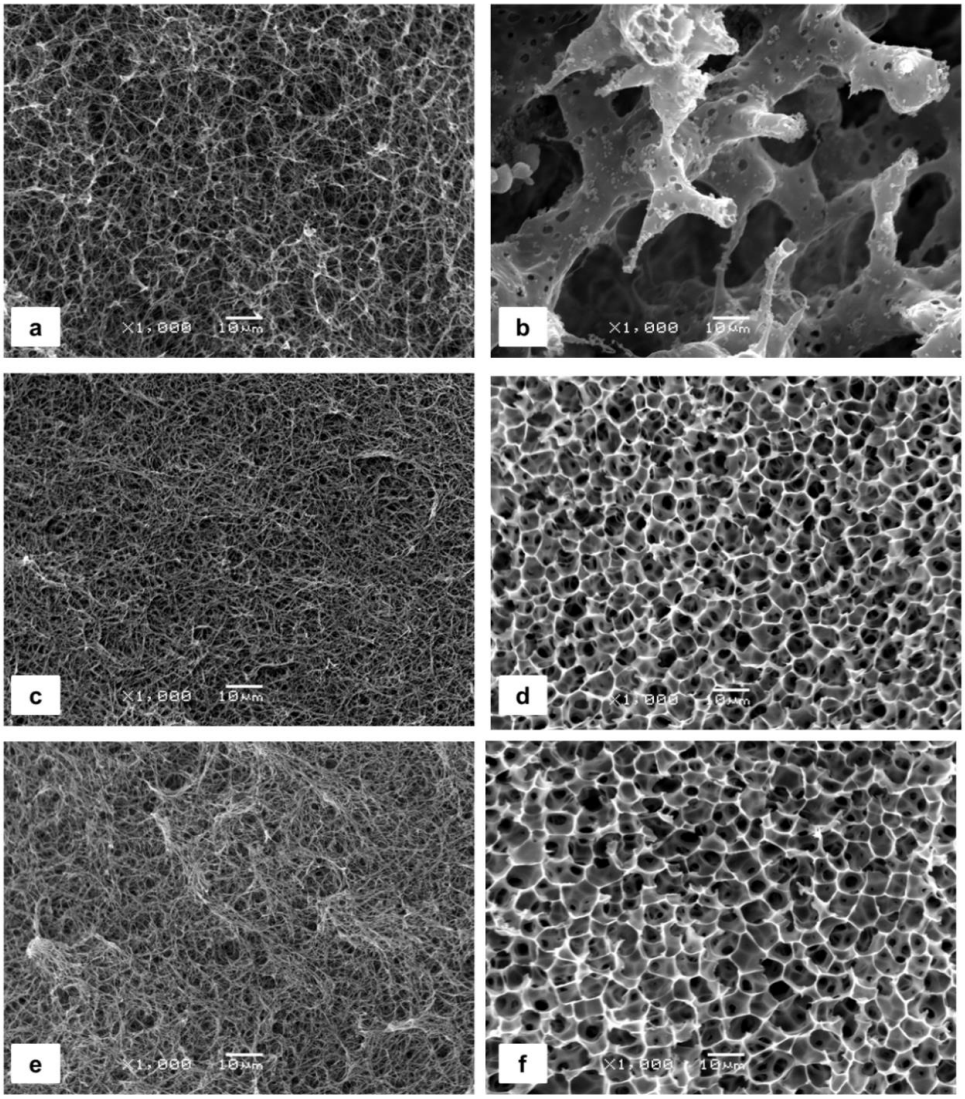

Figure A - 2: SEM micrographs: a) 3F-TIPS, b) 3P-TIPS, c) 5F-TIPS, d) 5P-TIPS,e) 7F-TIPS, f) 7P-TIPS.

As previously noted, TIPS consisted of the following major steps: i) dissolving PLLA in a suitable solvent, ii) freezing the solution, iii) exchanging the solvent with a non-solvent, and iv) finally drying the specimen (usually by freeze-drying) [228]. Phase separation of a polymer solution was described by Ma [328] as a self-assembly process. In this process, instead of short molecules aggregating into long chains, polymer's long chains were reorganized. It has been reported that the polymer solution goes through liquid-liquid phase separation during synthesis by both F-TIPS [229,230] and P-TIPS [231–235] methods. However, the difference in structure is probably a result of the different mechanisms during phase

separation. Different cooling temperatures and solvents used in these two methods might be the main reason of different phase separation mechanisms.

The microstructures of typical 5P-TIPS and 5F-TIPS specimens were viewed at higher magnification (Figure A - 3) to more clearly show the fibrous structure of the F-TIPS compared with the porous structures of the P-TIPS.

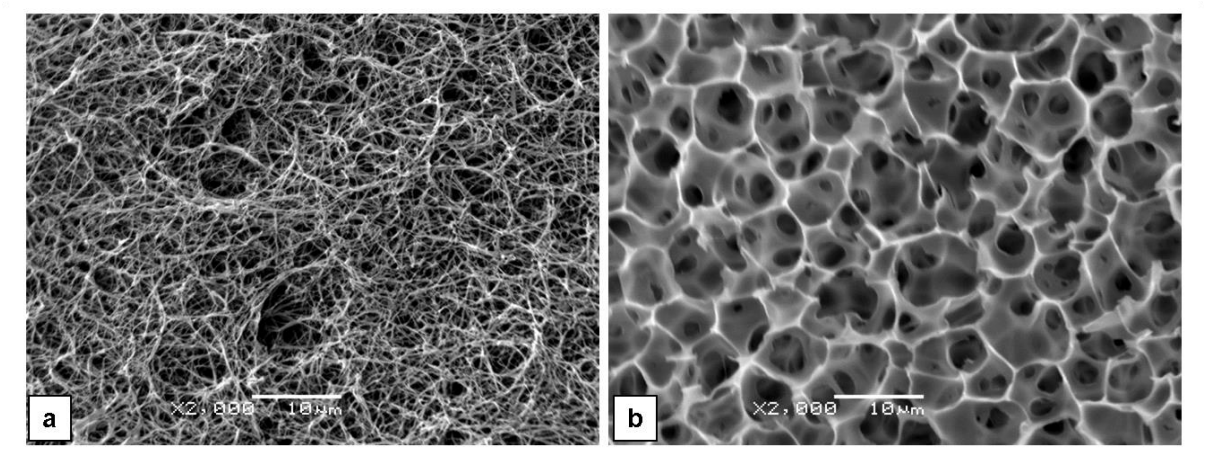

Figure A - 3: PLLA (5 wt %) specimens prepared by a) F-TIPS, b) P-TIPS.

From the SEM images, one hundred fiber diameters were measured on SEM images of the three polymer concentrations prepared by F-TIPS (Figure A - 4). It was found that there is a general trend of increasing fiber diameter with increasing polymer concentration. However, increasing polymer concentration from 3 to 5 wt% did not result in a significant increase in fiber diameter ($p = 0.06$). At the same time, a significant increase was detected when the concentration increased from 5 to 7 wt% ($p < 0.001$). Similar results had been reported by others [229,230].

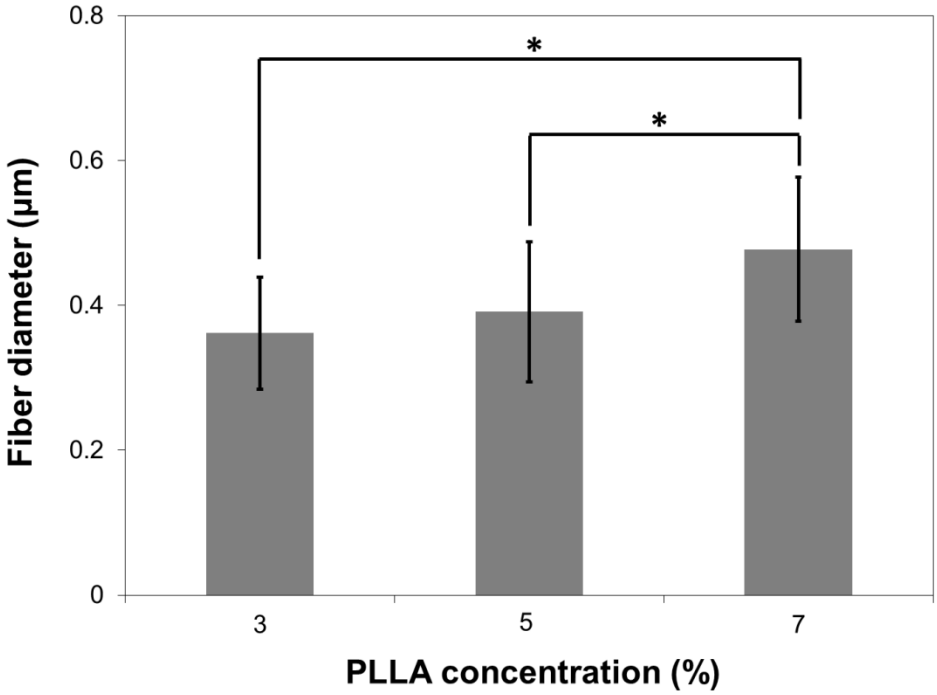

Figure A - 4: Fiber diameters of F-TIPS specimens, *p < 0.001.

Fifty pore size measurements were made on SEM images of the three polymer concentrations prepared by P-TIPS (Figure A - 5). The 3 wt% specimens had significantly larger pore sizes than the other two specimens that had higher polymer concentrations ($p < 0.001$). This might be attributed to the incomplete microstructure formation at this low concentration. Due to the scarcity of polymer chains, pores were formed locally and nonuniformly, as shown in Figure A - 2 which resulted in the large standard deviation of the pore sizes. Nonuniformly distributed pores for low polymer concentrations had been reported by Schugens *et al.* [329]. This was in contrast to the uniform and completely formed pores observed when PLLA concentrations were 5 or 7 wt%. Pore size increase was not statistically significant ($p = 0.7$) when the concentration went from 5 to 7 wt%. The increase in polymer concentration might have resulted in thicker pore walls which then subsequently increased mechanical properties of 7 wt% specimens.

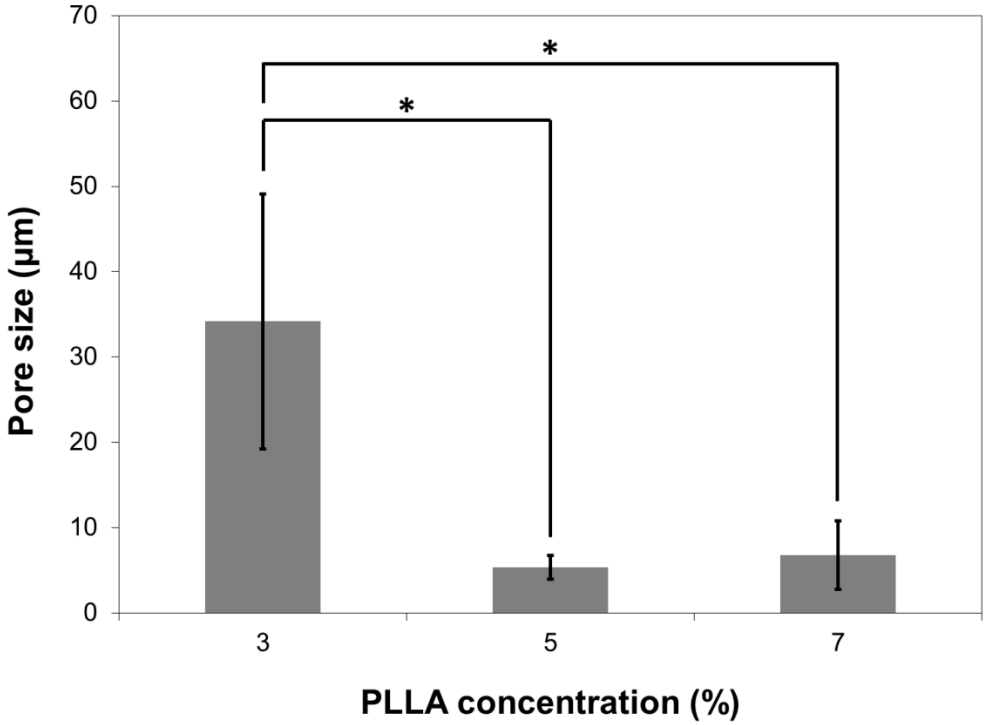

Figure A - 5: Pore size of P-TIPS specimens, *p < 0.001.

Pore size distribution across the surface of P-TIPS specimens was also investigated (Figure A - 6). Comparison between Figure A - 6a and Figure A - 6b indicates that the pores close to the wall of the mold were finer than the ones formed in the middle of the specimen. This might be attributed to the different cooling rates, which near the wall was higher than in the middle of the specimen. Hence, pores close to the mold wall formed faster than those in the middle. Note that the region with finer pore size is limited to the vicinity of the wall, which suggested that rapid cooling occurred locally.

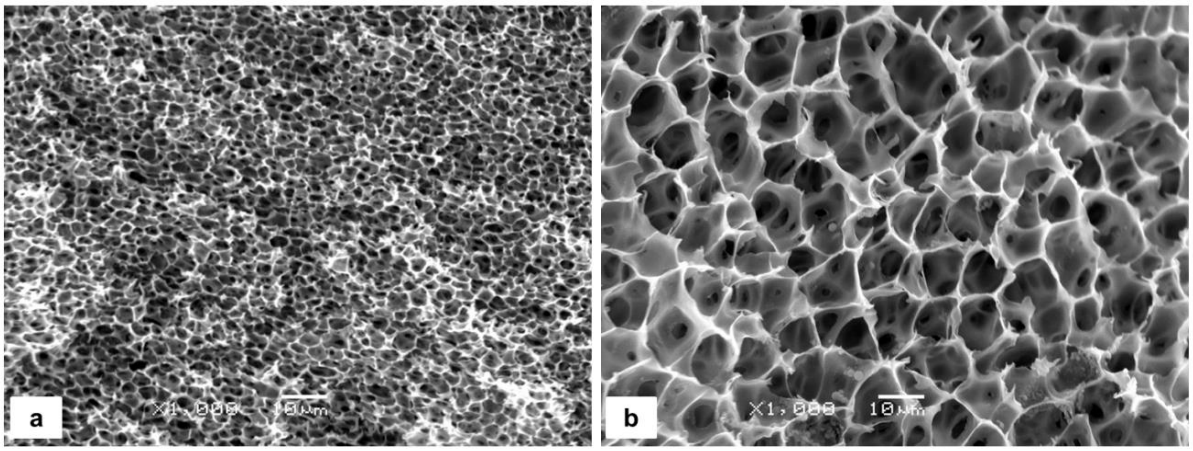

Figure A - 6: PLLA (7 wt %) specimens prepared by P-TIPS, microstructure a) near the wall of the mold b) in the middle.

Mechanical behaviour characterization

Simple Compression Test

Typical engineering stress-strain curves from loading and unloading cycles of compression test on 5F-TIPS and 5P-TIPS are shown in Figure A - 7. The specimens exhibited some relatively small-scale viscoelastic behaviour but their response could be approximated by an elastic-plastic type representation with the following three regions: 1) linear elastic, 2) transition, and 3) plastic. A somewhat similar approach was reported by Park and Todo [330] for much stiffer PLLA scaffolds that had been designed for bone tissue engineering.

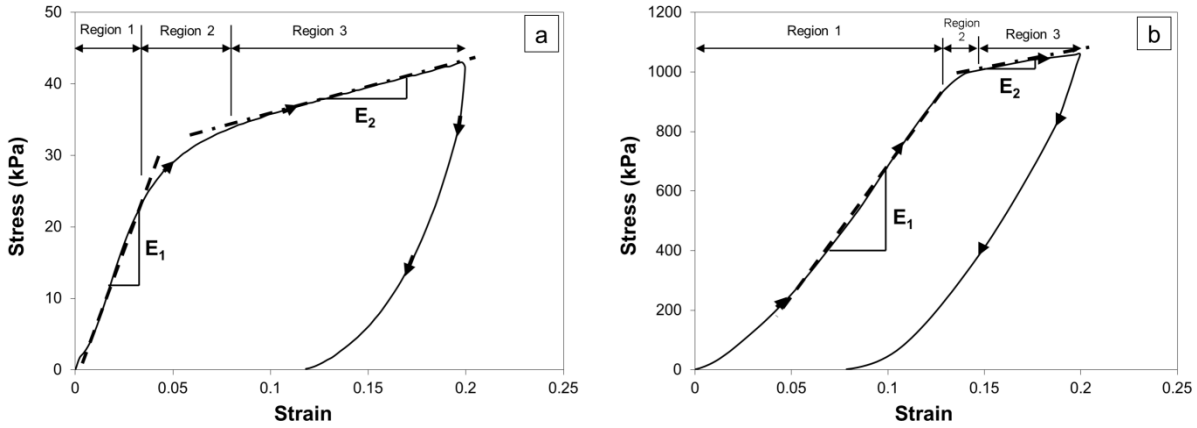

Figure A - 7: Typical compression stress-strain curves of 5 wt% PLLA specimens fabricated by a) F-TIPS, b) P-TIPS methods.

A typical stress-strain curve of the F-TIPS specimens (Figure A - 7a) demonstrated almost linear increase of stress with strain in region 1 below 4 % strain. Since no permanent strain was observed after unloading, the deformation behaviour in this region can be approximated as linear elastic with an elastic modulus designated as E_1.

Upon further loading and after a narrow transition (region 2), another approximately linear stress-strain relationship occurred in region 3 (Figure A - 7a). If the specimen was unloaded from this region, the stress-strain relationship followed an unloading path (as indicated by the arrow), that was almost linear with about the same slope as in Region 1, to leave the permanent deformation. Thus, this region can be regarded as plastic deformation region with a "plastic" modulus designated as E_2. When the specimen was unloaded from 20 % strain, a permanent strain of about 13 % remained.

A typical stress-strain curve for P-TIPS specimens (Figure A - 7b) showed slightly different deformation behaviour compared with the F-TIPS specimens. The same three regions could be identified but the moduli of the P-TIPS specimens were much higher. Also, permanent strain upon unloading from the 20 % strain deformation was reduced to about 8 %.

For the three specimens of each type listed in Table A - 1 elastic moduli (E_1) were determined for comparison purposes (Figure A - 8). Statistical analysis revealed that all the elastic moduli were significantly affected by fabrication method and polymer concentration but not existence of water. The elastic moduli of the P-TIPS specimens were significantly higher than those of F-TIPS specimens at the same concentration ($p < 0.001$) and the elastic moduli increased significantly with polymer concentration in both F-TIPS and P-TIPS specimens ($p < 0.001$) which agreed with other studies [229,316]. However, no significant differences were detected for the effect of wet or dry specimens ($p = 0.076$). Dry specimens did show the trend of having slightly higher elastic moduli than wet specimens. This might be attributed to a lubrication effect of water in F-TIPS specimens, resulting in decreased internal friction. During deformation of dry specimens, besides material resistance to deformation, additional force had to be applied to overcome the friction caused by fiber rotation and slip in F-TIPS specimens and pore wall deformation in P-TIPS specimens (as will be discussed further in the next sections).

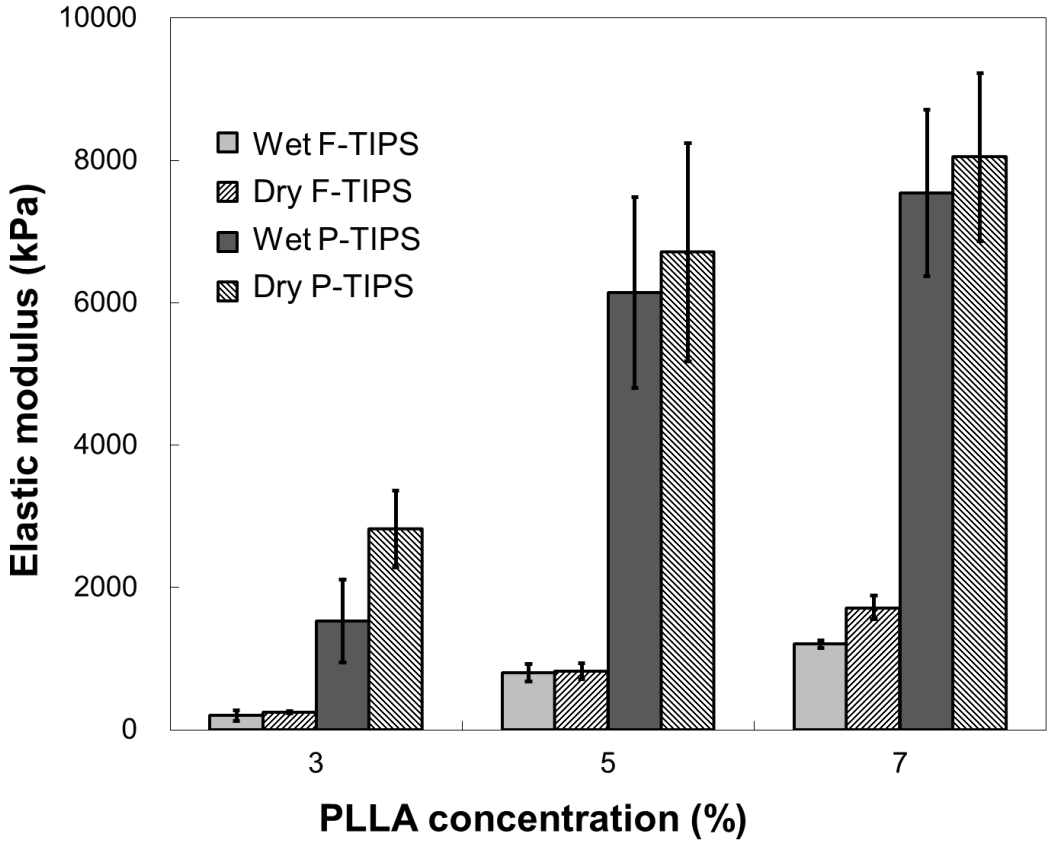

Figure A - 8: Elastic moduli of wet and dry PLLA specimens fabricated by F- TIPS and P-TIPS methods, n=3.

Microstructural deformation

The differences of elastic moduli between F-TIPS and P-TIPS specimens could be attributed to differences in microstructural deformation mechanism. As shown in Figure A - 2 the F-TIPS specimens had fibrous structures that were easier to deform in compression than the more solid porous-structured P-TIPS specimens because fiber diameters were smaller and more flexible than pore wall thicknesses. Furthermore, fibers were loosely connected by flexible junctions as opposed to pore walls rigidly interconnected together. As a result, the elastic moduli of F-TIPS specimens were less than 15 % of those of the same type of P-TIPS specimens (Table A - 2).

Table A - 2: Elastic and plastic moduli of various PLLA specimens, n=3

Polymer conc. (wt%)	Fabrication method	Dry/Wet	Elastic modulus E_1 Avg ± Std Dev (kPa)	Plastic modulus E_2 Avg ± Std Dev (kPa)
3	F-TIPS	Wet	202 ± 75	30 ± 5.2
		Dry	245 ± 17	38 ±8.3
	P-TIPS	Wet	1527 ± 580	210 ± 35
		Dry	2824 ± 538	325 ± 43
5	F-TIPS	Wet	780 ± 97	75 ± 14
		Dry	822 ± 108	90 ± 15
	P-TIPS	Wet	6145 ± 1338	1050 ± 214
		Dry	6710 ± 1533	1220 ± 186
7	F-TIPS	Wet	1204 ± 51	147 ± 28
		Dry	1717 ± 166	180 ± 19
	P-TIPS	Wet	7541 ± 1166	1430 ± 168
		Dry	8048 ± 1180	905 ± 106

The plastic moduli of the specimens were also listed in Table A - 2. The relationships between the plastic moduli and the microstructure were examined more rigorously by also considering SEM micrographs.

The change of microstructure caused by plastic deformation was investigated using the SEM micrographs taken from the surface of the PLLA specimens after compression test. The compression test was performed with the same setup shown in Figure A - 1. A typical SEM micrograph of a F-TIPS specimen after plastic deformation in the simple compression test (Figure A - 9) revealed that, even though overall structure looked similar to the undeformed structure, broken fibers were present (as highlighted within the circles) which had not been previously observed in any of the uncompressed specimens. Therefore, fiber breakage was likely to be a microstructural feature of the plastic deformation. Also, as shown in Figure A - 9, there were junctions of entangled fibers that must have helped holding the

F-TIPS specimen together [331]. Since these junctions were relatively loose, it was considered likely that fiber disentanglements, slip and rotation occurred in the junctions during compression. Thus, in addition to fiber deformation, it was likely that microstructural damage, such as junction disentanglement, also contributed to permanent deformation of the F-TIPS specimens.

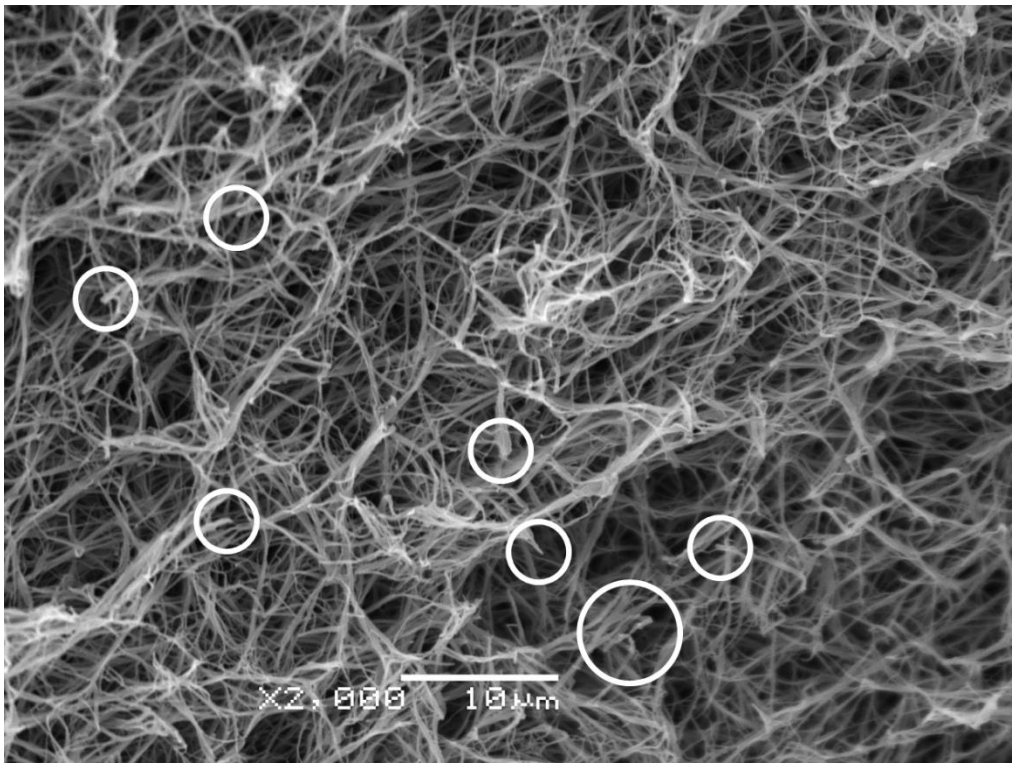

Figure A - 9: SEM micrograph from surface of a 3F-TIPS specimen after simple compression test. Circles highlight areas of broken fibers.

Similar microstructural damage after deformation was not found in porous structured P-TIPS specimens (Figure A - 10). However, compared to uncompressed specimens (shown in Figure A - 2), deformed as well as collapsed pores were observed (deformed pores were highlighted within circles). Thus, the microstructural mechanism of plastic deformation in porous P-TIPS specimens was likely to be buckling and rupture of wall structure. Since this wall buckling and rupture process require higher forces than the plastic deformation mechanism in fibrous structure, the plastic moduli (E_2) of porous P-TIPS specimens was higher than that of the fibrous F-TIPS specimens as shown in Table A - 2.

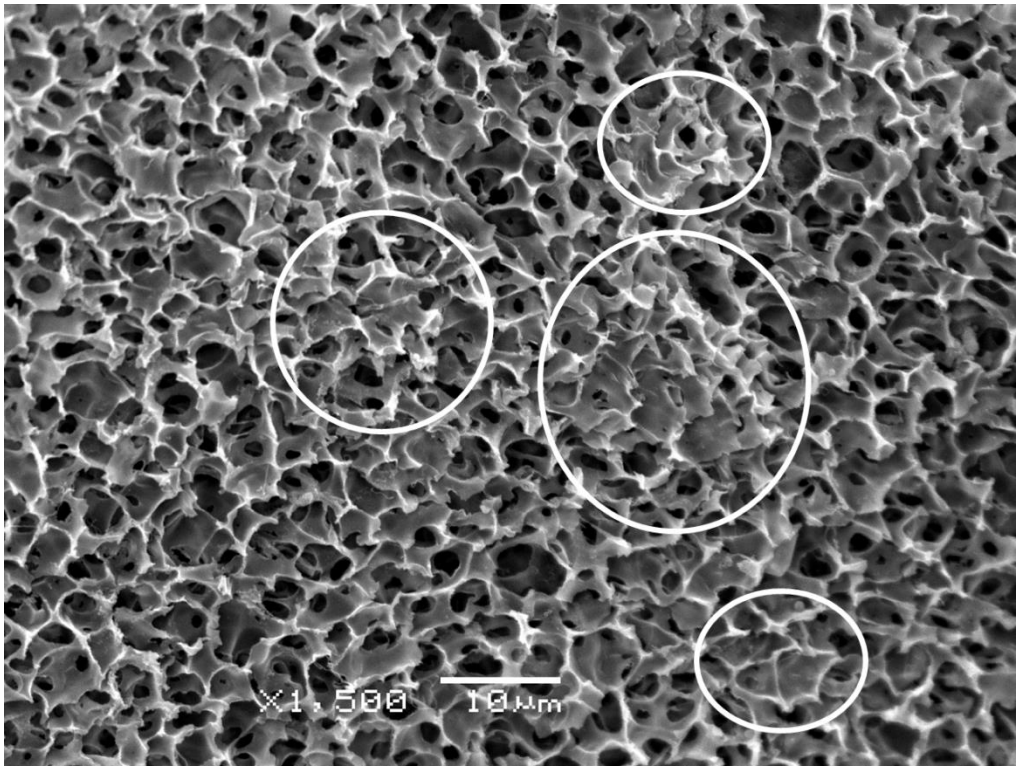

Figure A - 10: SEM micrograph from surface of a 5P-TIPS specimen after simple compression test. Circles highlight areas of deformed pores.

Lateral Deformation

The calculation of stress for all of the compression testing (Equation A-1) depended on the uniaxial compression of the specimens. This meant that any bulging of the specimens at the midpoint of their height in the lateral direction would indicate that the ends contacting the test machine had been constrained by friction. Fortunately, this did not occur and there was also very little lateral deformation of any kind (Figure A - 11). Thus, the use of Equation A-1 to calculate stress was justified.

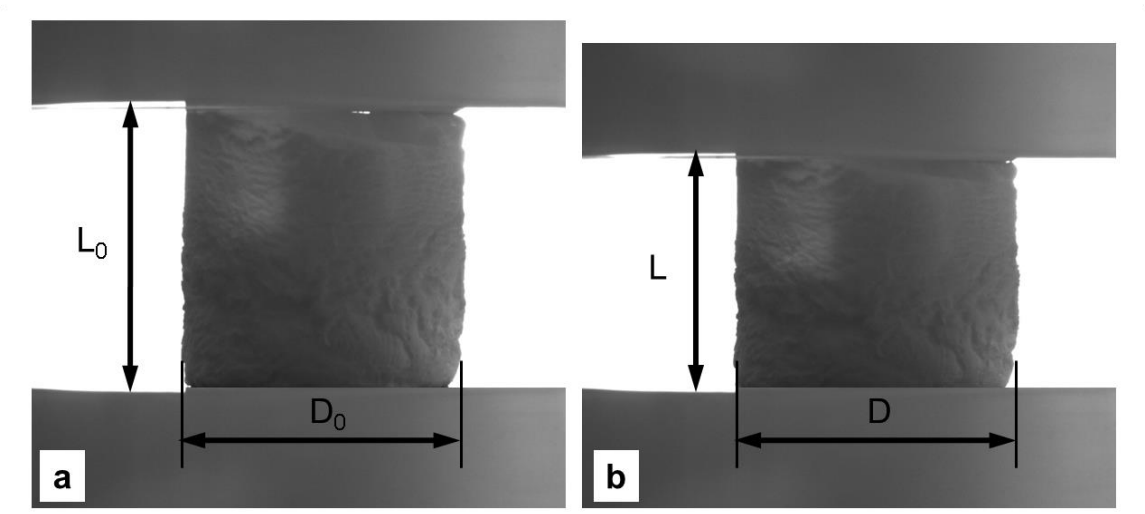

Figure A - 11: Variation of diameter of a typical 5F-TIPS specimen during compression test: (a) zero strain (b) at 20% strain.

In order to qualitatively assess the lateral deformation, Poisson's ratio of different specimens was calculated from the images taken by the CCD camera by

$$\upsilon = -\frac{\varepsilon_{lat}}{\varepsilon_{long}} \qquad \text{A-2}$$

$$\varepsilon_{lat} = \frac{D_0 - D}{D_0} \qquad \text{A-3}$$

$$\varepsilon_{long} = \frac{L_0 - L}{L_0} \qquad \text{A-4}$$

Where υ is Poisson's ratio**,** ε_{lat} lateral strain, ε_{long} longitudinal strain, D_0 initial specimen diameter, D final specimen diameter, L_0 initial specimen height and L final specimen height (Figure A - 11).

Poisson's ratio would have a value of 0.5 if the volume remained constant and the lateral strain was small [332] but for these scaffolds, since little lateral deformation occurred, Poisson's ratio was very small. Poisson's ratio, calculated from Equation A-2 to A-4, varied from 0.05 to 0.15 for different specimens.

Cyclic Compression Test

If a material were to be used as a tissue scaffold, repeated loadings at various amplitudes would be applied and this might cause a change in mechanical properties. Stress-strain curves from the cyclic compression tests of a typical 5F-TIPS specimen is presented for strain based on the initial height (Figure A - 12).

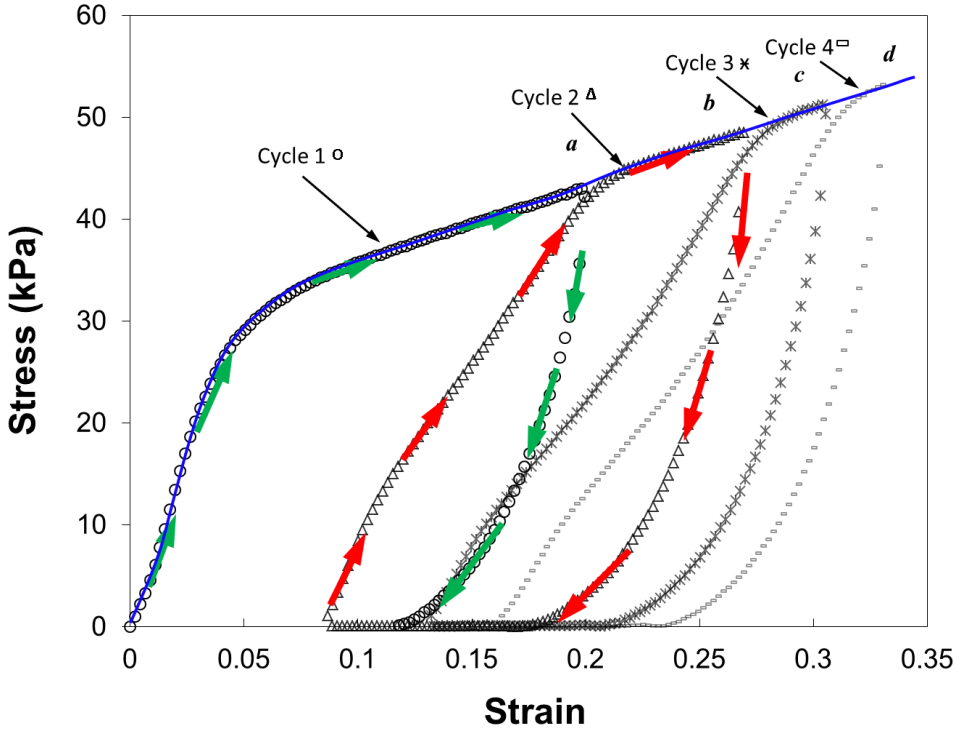

Figure A - 12: Cyclic stress-strain curve for a typical 5F-TIPS specimen.

The shapes of stress-strain curves from successive cycles were similar and they each had elastic, transition and plastic regions. However, elastic moduli decreased as the cyclic loading was repeatedly applied and permanent plastic deformation accumulated. This might be attributed to the microstructural damage caused by plastic deformation that was discussed in the previous section. After loading was removed, this microstructural damage remained and thus the fibrous scaffold lost part of its resistance to deformation, which caused a reduction in elastic modulus.

A particularly notable feature in Figure A - 12 was the so-called “memory effect” as described in conventional plasticity theory [333]. When an elastic-plastic material was loaded higher than its yield strength to be plastically deformed, then unloaded and reloaded again, a small loop would be formed (as shown by arrows in Figure A - 12). After this, the stress-strain path would rejoin the original path and

proceed as if the small loop had never occurred. The stress-strain curves of PLLA from multiple cycles as shown in Figure A - 12 clearly demonstrated this memory effect.

A curve from the origin that passes through the upper portion of each curve, (solid trend line in Figure A - 12) may be used to characterize the cyclic stress-strain behaviour. In an ideal material, this cyclic stress-strain curve would be the same as that found in a simple compression test. This did indeed occur in the present study (Figure A - 12). Therefore, for a fibrous PLLA scaffold, the stress-strain curve determined from a simple compression test can provide insight into the cyclic stress-strain behaviour.

Cell Viability Analysis

Cellular viability is one of the crucial factors that has to be evaluated for tissue engineering scaffolds. In the present study, human osteosarcoma fibroblasts were cultured on the scaffolds prepared by both F-TIPS and P-TIPS methods and MTT assay was used to study cell viability and proliferation. This assay gives an indication of metabolically active cells compared to the control, which is based on the reduction of the yellow tetrazolium salt to purple formazan precipitate in mitochondria of active cells. Since during MTT assay, the MTT containing solution covers the entire specimen, measured cell viability percentage is an indication of cells both on the surface of scaffold and inside it.

Since microstructure of natural extracellular matrix (ECM) had been reported as fibrous [229], it was expected that specimens with fibrous structure would better support cell growth. However, the results (Figure A - 13) show the opposite trend. Cell viability was more persistent and remained higher during an 8 day period for P-TIPS specimens with porous structure (Figure A - 13b and Figure A - 2b, d and f) but there was a drop from 90% to about 50% in cell viability for F-TIPS specimens with fibrous structure (Figure A - 13a and Figure A - 2a, c, and e). For P-TIPS specimens, increasing optical densities (OD) were observed (data not shown) and thus are an indication of cell proliferation [334]. However, for F-TIPS specimens, OD started to decrease after day 5 suggesting that cells were not proliferating and were also dying as compared to day 5. Microstructure was found to have a significant effect on cell viability ($p < 0.001$).

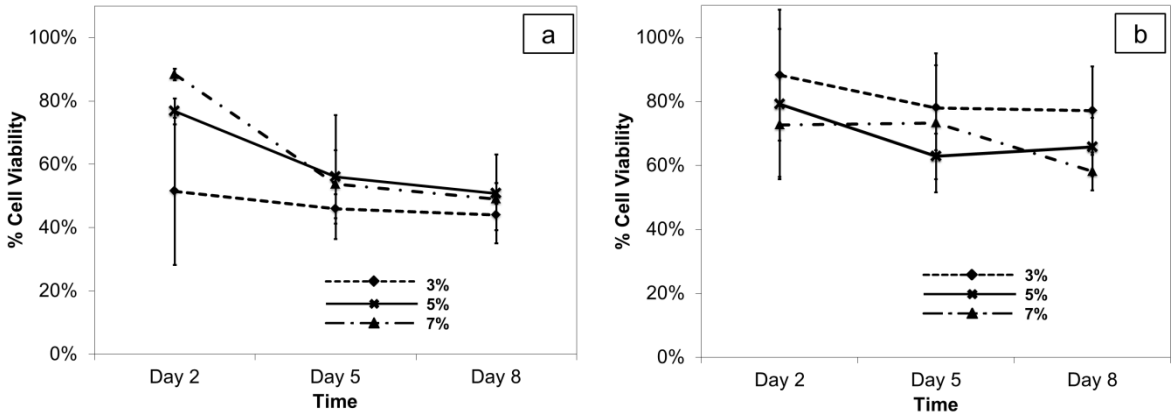

Figure A - 13: Human osteosarcoma fibroblast viability results from MTT assay for a) F-TIPS specimens b) P-TIPS specimens.

It is well-known that mechanical properties of the substrate can affect cell behaviour [2,6,112,122]. Also, the effect of interconnectivity, pore size and microstructure on cell viability had been previously reported and emphasized [316,335,336]. The fibrous microstructure (of F-TIPS specimens) and its associated lower elastic modulus might be the reason for lower cell viability in F-TIPS specimens. The microstructure of F-TIPS specimens consisted of entangled fibers with much smaller pore size. Therefore, although there was more viability at day 2 for F-TIPS specimens, the cells then stopped proliferating. Tu *et al.* [316] has also seen the effect of interconnectivity on Mouse 3T3 fibroblast cells. In this study, it was found that after 4 weeks, cell viability was higher for scaffolds with higher interconnectivity [316]. However, Hu *et al.* [327] found that when the similar protocol for fabricating PLLA scaffolds was used, MC-3T3 fibroblastic cells had proliferated in fibrous PLLA specimens for up to 7 days. This difference in response might be a consequence of using different cell lines or perhaps because of subtle differences in their microstructure compared with that of the present study. We have also tested Swiss Albino 3T3 fibroblast cells and obtained the similar results (data not shown).

Cell viability was further investigated using the Live\Dead Viability Kit for mamalian cells with a confocal microscope for a 5P-TIPS and a 5F-TIPS specimen. For this test, human osteosarcoma cells were cultured in the scaffolds and then labelled and imaged on day 3. Calcein AM labels live cells in green and Ethidium Homodimer labels dead cells in red.

As shown in Figure A - 14 simultaneous imaging of live and dead cells revealed that although dead cells were observed in the structure, a majority of cells were alive (green stain), which confirmed the viability status of cells cultured in the P-TIPS scaffolds. It can also be seen that on day 3, more viable cells can be seen in the F-TIPS scaffold. However, according to MTT assay results, beyond day 5 cell

proliferation rate is reduced in the F-TIPS structure. Based on the results of these two tests, P-TIPS scaffolds are anticipated to show better long-term cell viability under unloaded conditions.

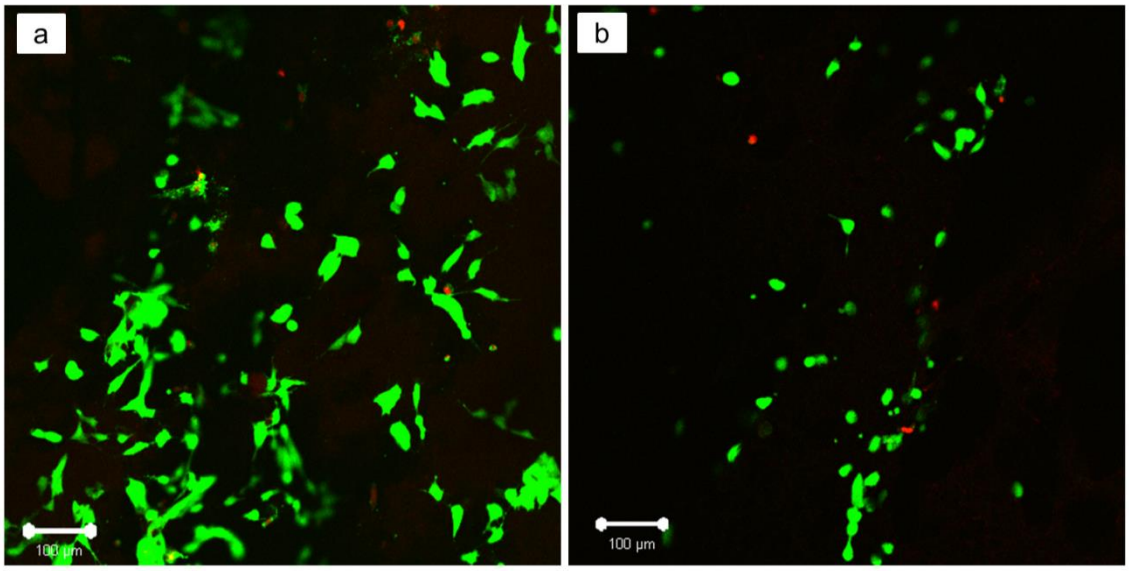

Figure A - 14: Confocal micrographs of human osteosarcoma cells in a) 5F-TIPS, b) 5P-TIPS specimen, live cells are green and dead cells are red, (10X).

Biodegradation

Biodegradation of mechanical properties is one of the essential characteristics to be considered for the application as a tissue engineering scaffold. The stress-strain curves from a simple compression test for a typical 5F-TIPS specimen, after various amounts of biodegradation in cell culture medium were plotted after being normalized with maximum stress before biodegradation (Figure A - 15). Three observations can be made from the curves. i) The Elastic modulus remained constant until the third week, after which a significant decrease was observed. After 2 months, the elastic modulus was only around 10% of the initial value (9.5 kPa initially vs. 1.0 kPa after 2 months). ii) The transition zone strain decreased until the third week but then increased drastically while the corresponding stress levels decreased. After 2 months, the transition from elastic to plastic deformation was so “smooth” that it was difficult to identify. iii) Stress level in the plastic region had decreased with the biodegradation time, while the plastic modulus showed little change.

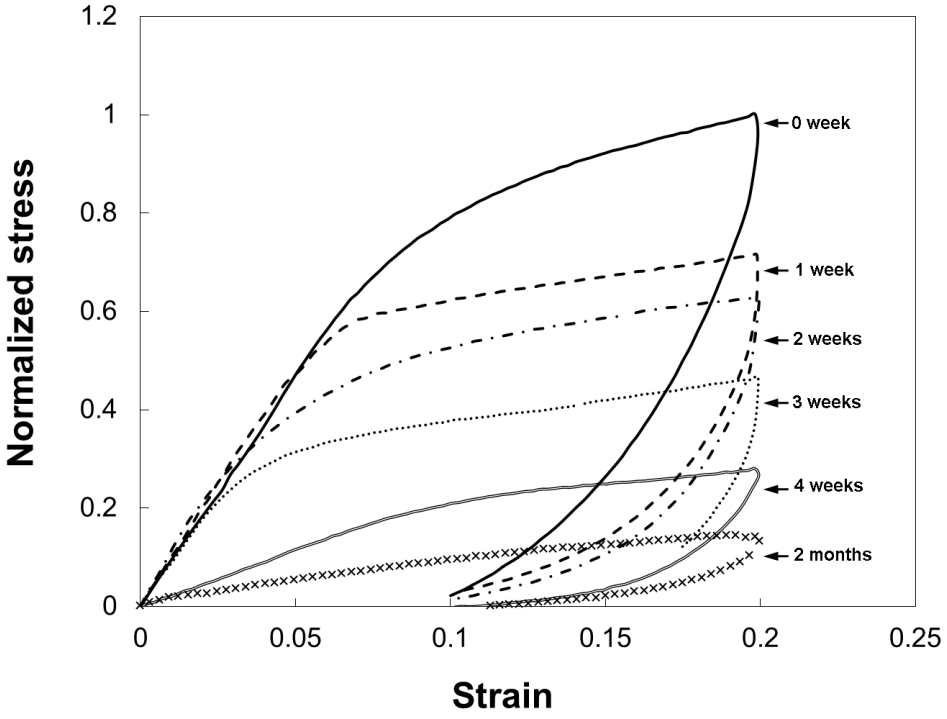

Figure A - 15: Stress-strain curves of a typical 5F-TIPS specimen during biodegradation.

Observations i) and ii) suggested that biodegradation mechanisms had a significant impact on mechanical properties after the third week. In fibrous structured PLLA, microstructural integrity was maintained by the fibers connected by junction entanglement; so both fibers and junctions sustained the material strength. Kim *et al.* [337] reported that fibers in electrospun PLLA based scaffolds were melted by the biodegradation process. As a result, fibers were losing volume and thus strength in the culture medium. This might be a reason for continual reduction of the transition zone stress and strain for the first three weeks of the study. On the other hand, biodegradation at the junctions might progress at a much slower rate because entanglements and friction between fibers would be relatively insensitive to the fiber size reduction. However, eventually junction biodegradation would start which would cause a drop in the elastic modulus.

The loss of microstructural integrity might also be involved in observation (iii) since microstructural damage such as fiber breakage and junction disentanglement would continue to occur in the plastic region with the increase of strain. Therefore, the deformation behaviour in plastic region was not changed much by biodegradation, except that it occurred at a reduced stress level. This is supported by the consistent permanent strains of about 10% that were left after unloading, regardless of biodegradation time.

Conclusions

The present study provides more insight into mechanical properties and biocompatibility of PLLA scaffolds. PLLA specimens were successfully fabricated by two different TIPS methods. It was found that liquid-liquid TIPS can result in two distinct fibrous (F-TIPS) and porous (P-TIPS) microstructures. The viscoelastic behaviour of the PLLA was minimal and thus a relatively simple elastic-plastic representation for the mechanical behaviour was possible. The differences in microstructures affected the mechanical properties; specimens fabricated by F-TIPS method tended to have lower elastic moduli than the specimens prepared by P-TIPS. Both elastic and plastic moduli increased substantially with polymer concentration but the presence of water made little difference. A memory effect in plastic deformation region was found from the cyclic compression test, and the cyclic stress-strain curve was almost identical to that obtained from a simple compression test. Although it was expected to see higher cell viability in F-TIPS specimens (due to its fibrous microstructure), higher cell viability was observed in the P-TIPS specimens. However, the cell viability tests were not cultured under loaded conditions and thus might not represent many *in vivo* situations. Biodegradation decreased elastic modulus and generally altered the shape of the stress strain curve. In order to understand the effect of microstructure on cell viability in detail, a more systematic study is needed which will be further developed in the future.

Appendix B: Convolution theorem proof

$$k(w) = F^{-1}\big(F(w)G(w)\big) = \frac{1}{N}\sum_{w=0}^{N-1} F(w)G(w)e^{\frac{i2\pi wx}{N}}$$

$$= \frac{1}{N}\sum_{w=0}^{N-1}\sum_{n=0}^{N-1} f(n)e^{\frac{-i2\pi wn}{N}} G(w)e^{\frac{i2\pi wx}{N}}$$

$$= \sum_{n=0}^{N-1}\frac{1}{N} f(n)\sum_{w=0}^{N-1} G(w)e^{\frac{i2\pi w(x-n)}{N}}$$

$$= \sum_{n=0}^{N-1} f(n)\frac{1}{N}\sum_{w=0}^{N-1} G(w)e^{\frac{i2\pi w(x-n)}{N}}$$

$$= \sum_{n=0}^{N-1} f(n)g(x-n) = f(x) * g(x)$$

Appendix C: DVC verification

In order to further verify DVC code, two experiments were performed using collagen samples, prepared as described in 3.2.1.1:

1. The first test was pure translation. In this test, collagen sample was placed on a glass bottom dish (Figure 3-4) and two confocal micrographs of collage fibers were taken before and after moving microscope stage in y direction. CRM was the method of choice for imaging collagen fibers.
2. The second test was simultaneous simple compression test and confocal microscopy. In this test a motorized linear stage (Zaber Technologies Inc, BC, Canada) (Figure C - 1a) with control over the probe displacement was used and three-dimensional micrographs of collagen fibers, with CRM technique, were taken before and after deformation. In this experiment, collagen sample was placed on a glass bottom dish (Figure 3-4) on the microscope stage and the probe of the linear stage was moved down for 200 μm and compressed the sample (Figure C - 1b).

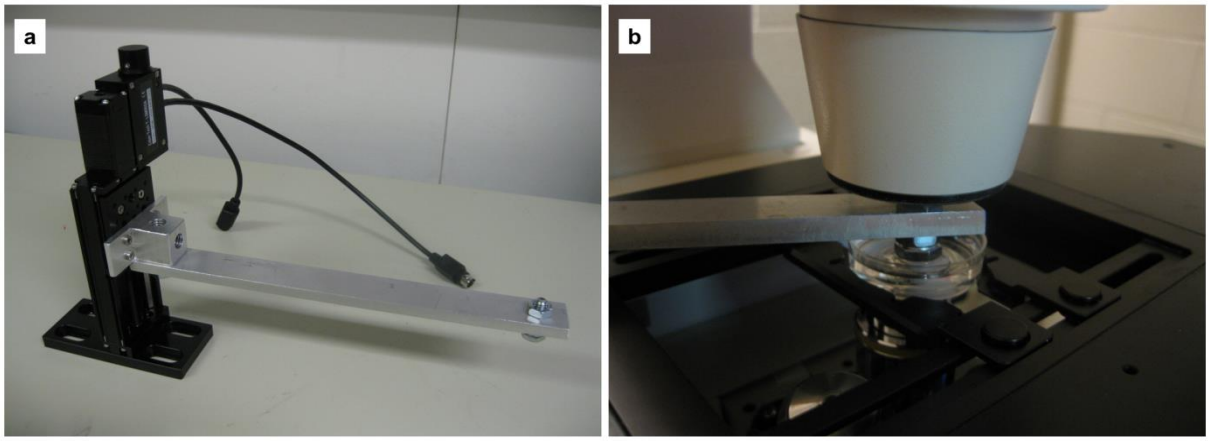

Figure C - 1: a) Motorized linear stage used for compression test DVC b) Linear stage setup on confocal microscope stage.

Figure C - 2 shows displacement results from pure translation test. It can be seen that the y displacement has been detected and displacements in y and z direction are negligible.

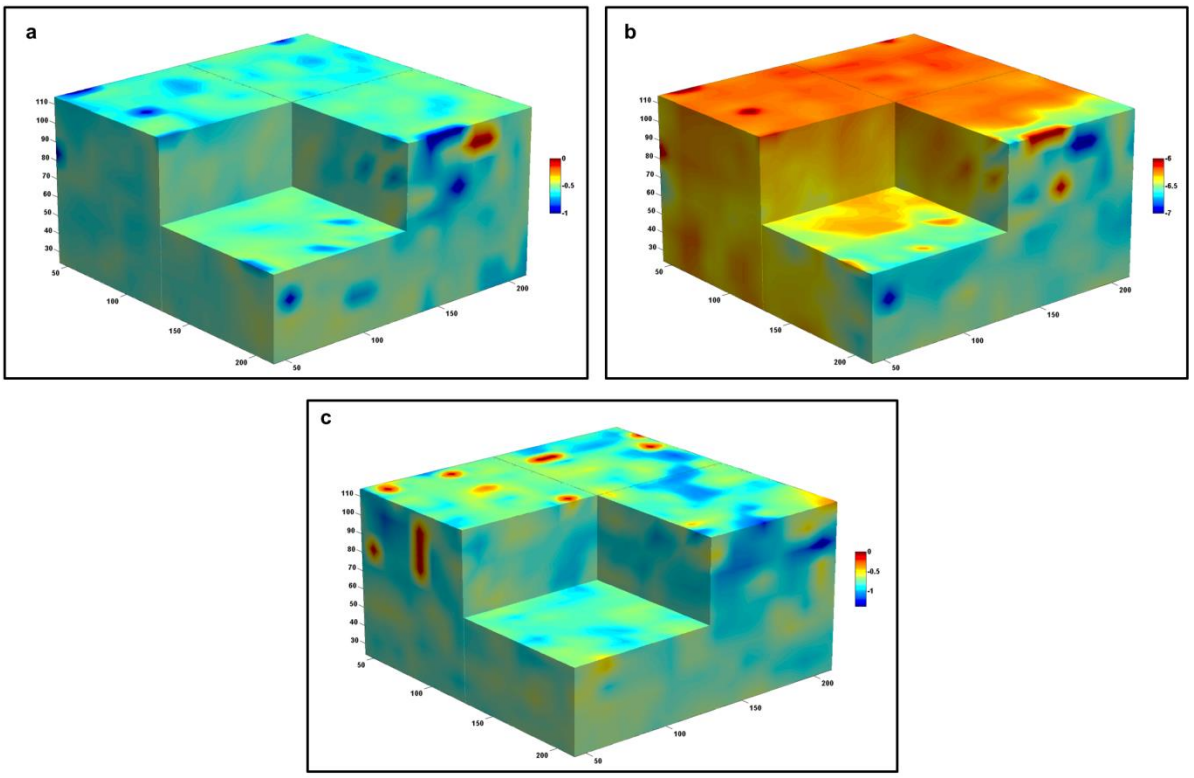

Figure C - 2: a) x, b) y and c) z displacements measured from 3D confocal images of collagen fibers for verifying DVC by pure translation experiment. All values are in pixels (1 pixel = 0.5 μm).

In simple compression test, 3D confocal micrographs taken from before and after compression test were analyzed by DVC and displacements were calculated (Figure C - 3). It can be seen that DVC can detect larger displacement and strain in z direction compared to the ones in x and y directions.

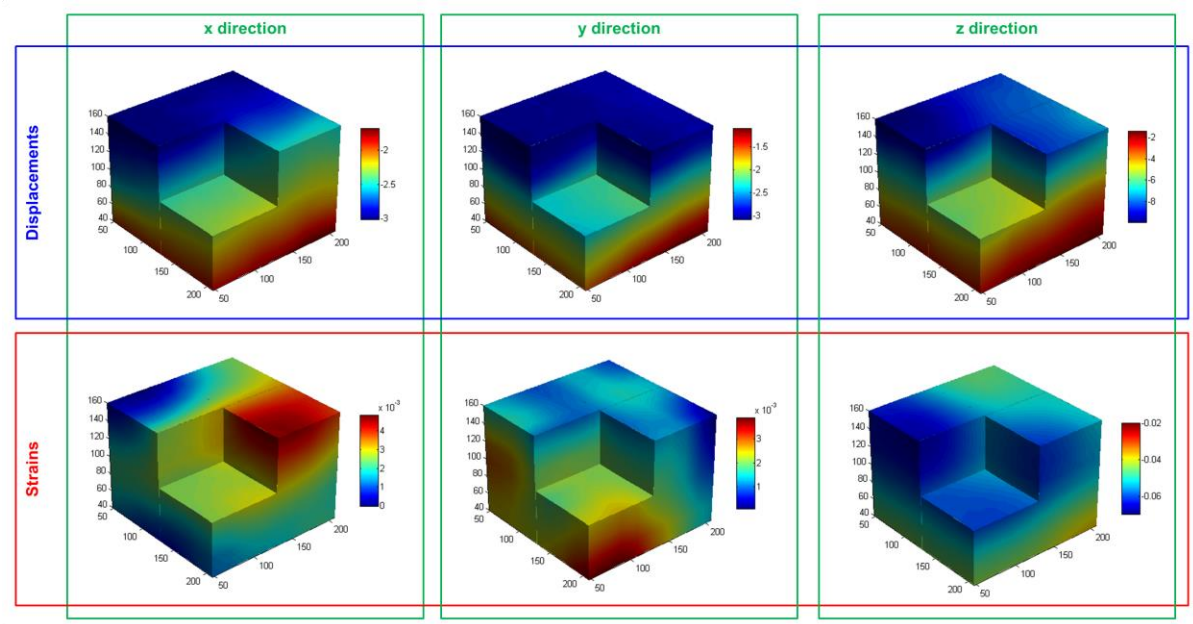

Figure C - 3: Displacements and strains measured from 3D confocal microscope images of collagen fibers for verifying DVC by simultaneous compression and microscopy experiment. All values are in pixels (1 pixel = 0.5 μm).

Here, the displacement induced on the sample is 200 μm, having the original height of the sample which was 5 mm, total strain induced on the sample can be calculated:

$$\varepsilon_t = \frac{\Delta l}{l_i} = \frac{200}{5000} = 0.04$$

Also, from z displacement measured by DVC (Figure C - 3), average strain on the sample can be calculated:

$$\varepsilon_c = \frac{\Delta l}{l_i} = \frac{9-2}{120} = 0.058$$

This 5.8 % of strain is comparable to the z strain measured by DVC (Figure C - 3). At the same time, both these strains are rather larger than the total strain of the sample. Here, CRM directly images the collagen microstructure and DVC measures deformations based on inherent microstructural features of the sample. This microstructure is inconsistent and complicated network of fibers which can vary from spot to spot and local higher strain measurements are expected.

Also, the cubic section of collagen sample that was imaged and processed by DVC during simple compression test is close to the bottom of the sample where the sample touches the dish (Figure C - 4). Therefore, it is confined and cannot deform freely. Thus, as expected, the maximum displacement on the

upper surface of this section is smaller than the displacement induced on the sample and decreases close to the bottom of the dish.

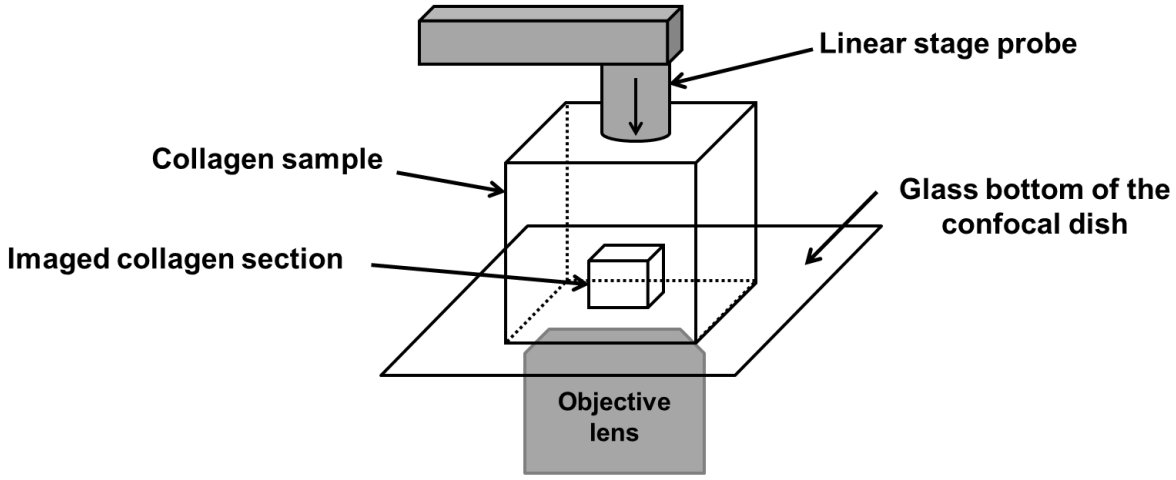

Figure C - 4: Schematic of simultaneous compression and microscopy experiment setup for verifying DVC.

Appendix D: Supplementary information for Chapter 5

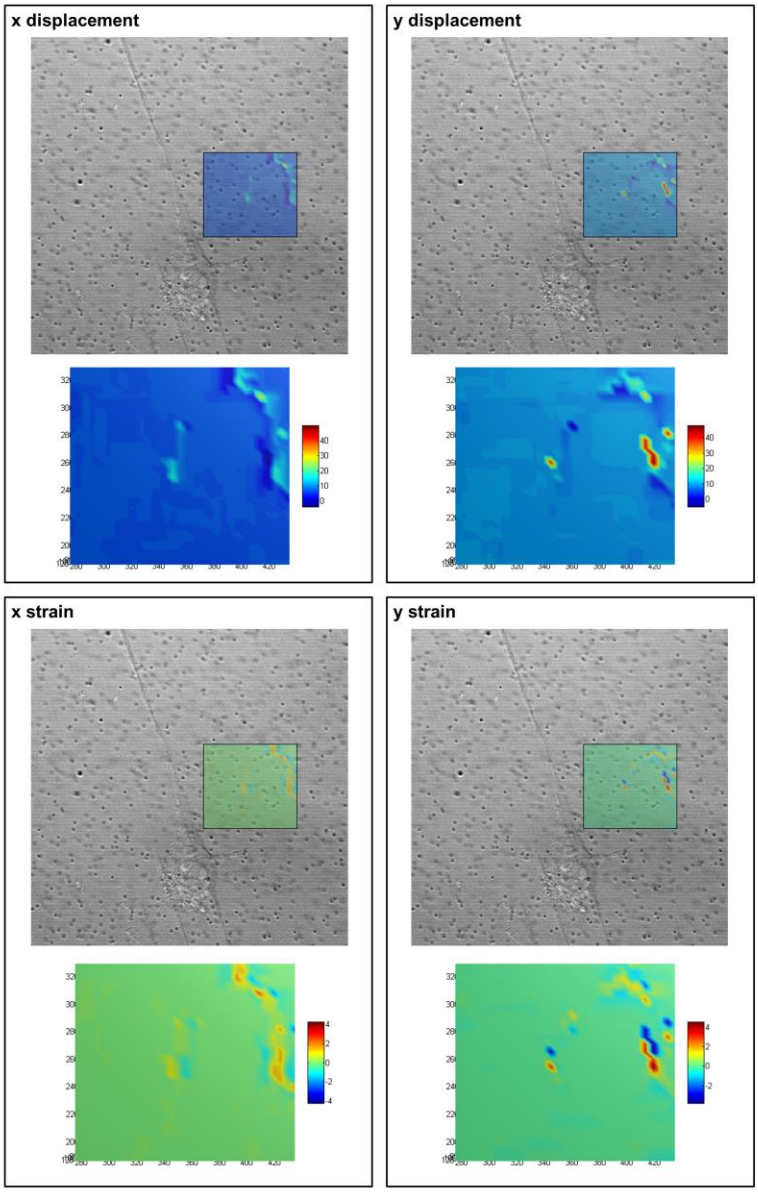

Figure D - 1: Displacements and strains in the x and y directions for a cell seeded on a medium substrate, before and after migration for an hour. Supplementary information to Figure 5-10. GS = 5, CS = 15 and SR = 2. Color bars indicate displacement values in pixels (1 pixel = 0.19 μm). Both contour plots and contour plots overlaid on the image of the cell are shown for more clear demonstration of results.

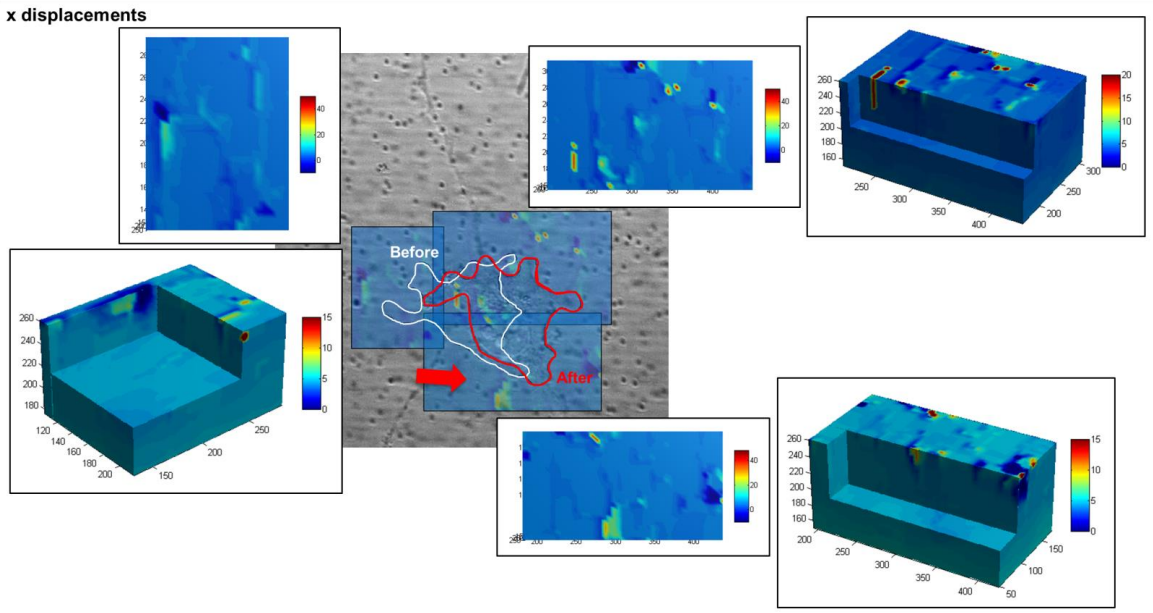

Figure D - 2: Displacements in the x direction for a cell seeded on a compliant substrate, before and after migration for 90 minutes. Supplementary information to Figure 5-13. GS = 5, CS = 15 and SR = 2. Red arrow shows migration direction. Red arrow shows migration direction. Color bars indicate displacement values in pixels (1 pixel = 0.19 μm). Both contour plots and contour plots overlaid on the image of the cell are shown for more clear demonstration of results.

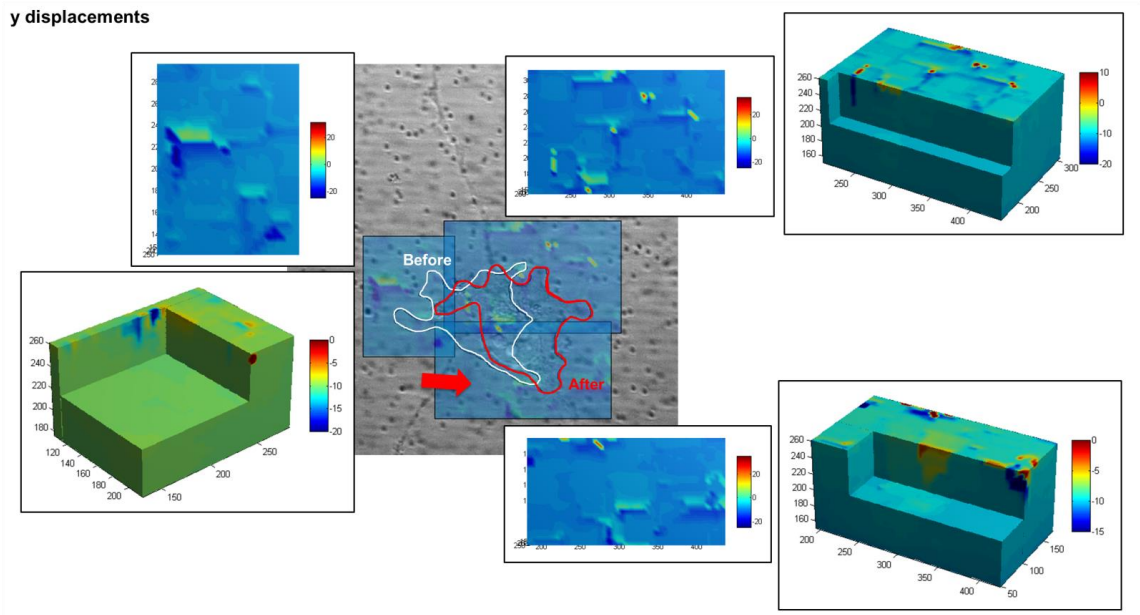

Figure D - 3: Displacements in y direction for a cell seeded on a compliant substrate, before and after migration for 90 minutes. Supplementary information to Figure 5-13. GS = 5, CS = 15 and SR = 2. Red arrow shows migration direction. Red arrow shows migration direction. Color bars indicate displacement values in pixels (1 pixel = 0.19 μm). Both contour plots and contour plots overlaid on the image of the cell are shown for more clear demonstration of results.

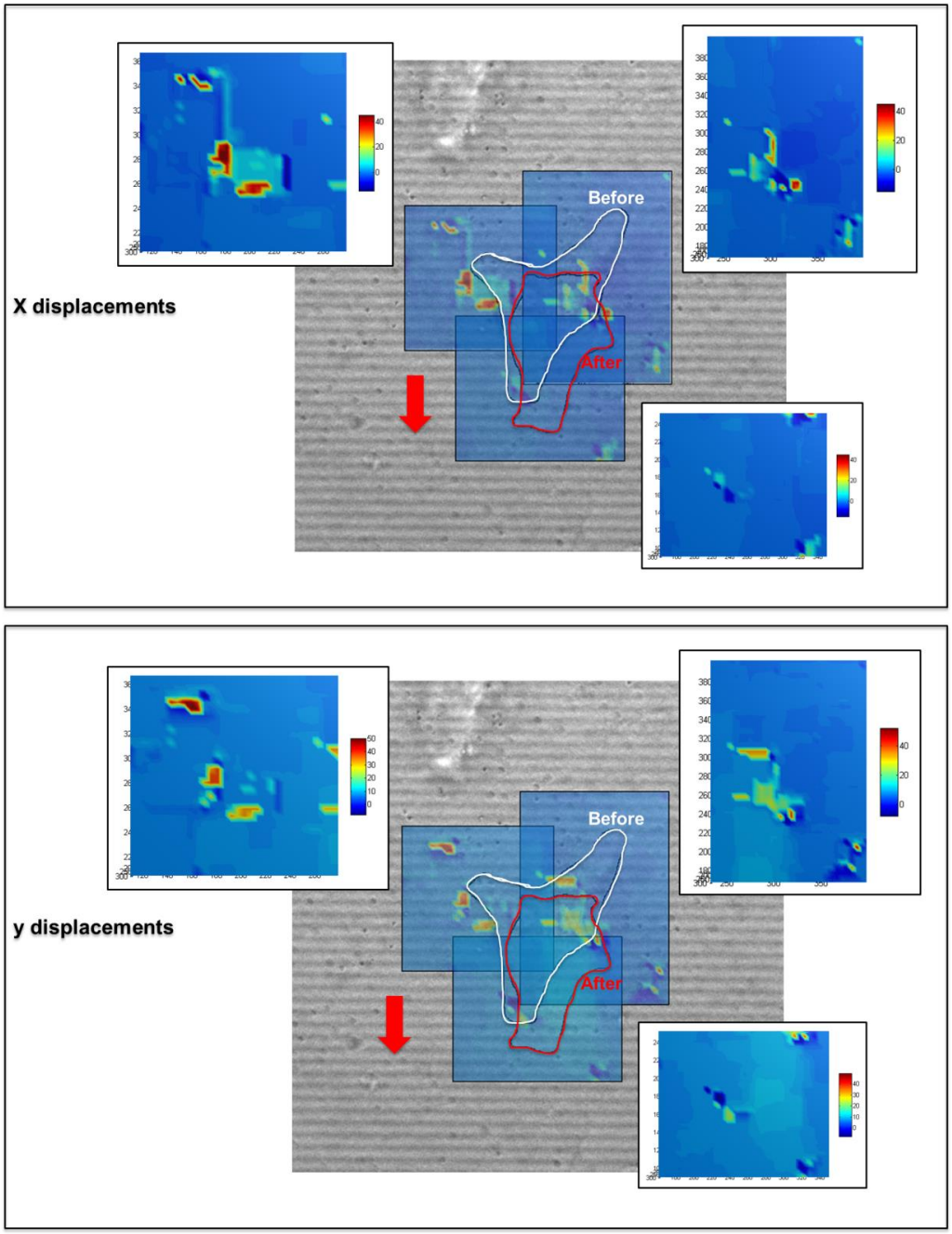

Figure D - 4: In plane displacements (x and y directions) of a cell cultured on a compliant substrate, before and after migration for an hour. Supplementary information to Figure 5-14. GS = 5, CS = 15 and SR = 2. Red arrow shows migration direction. Color bars indicate displacement values in pixels (1 pixel = 0.19 μm). Both contour plots and contour plots overlaid on the image of the cell are shown for more clear demonstration of results.

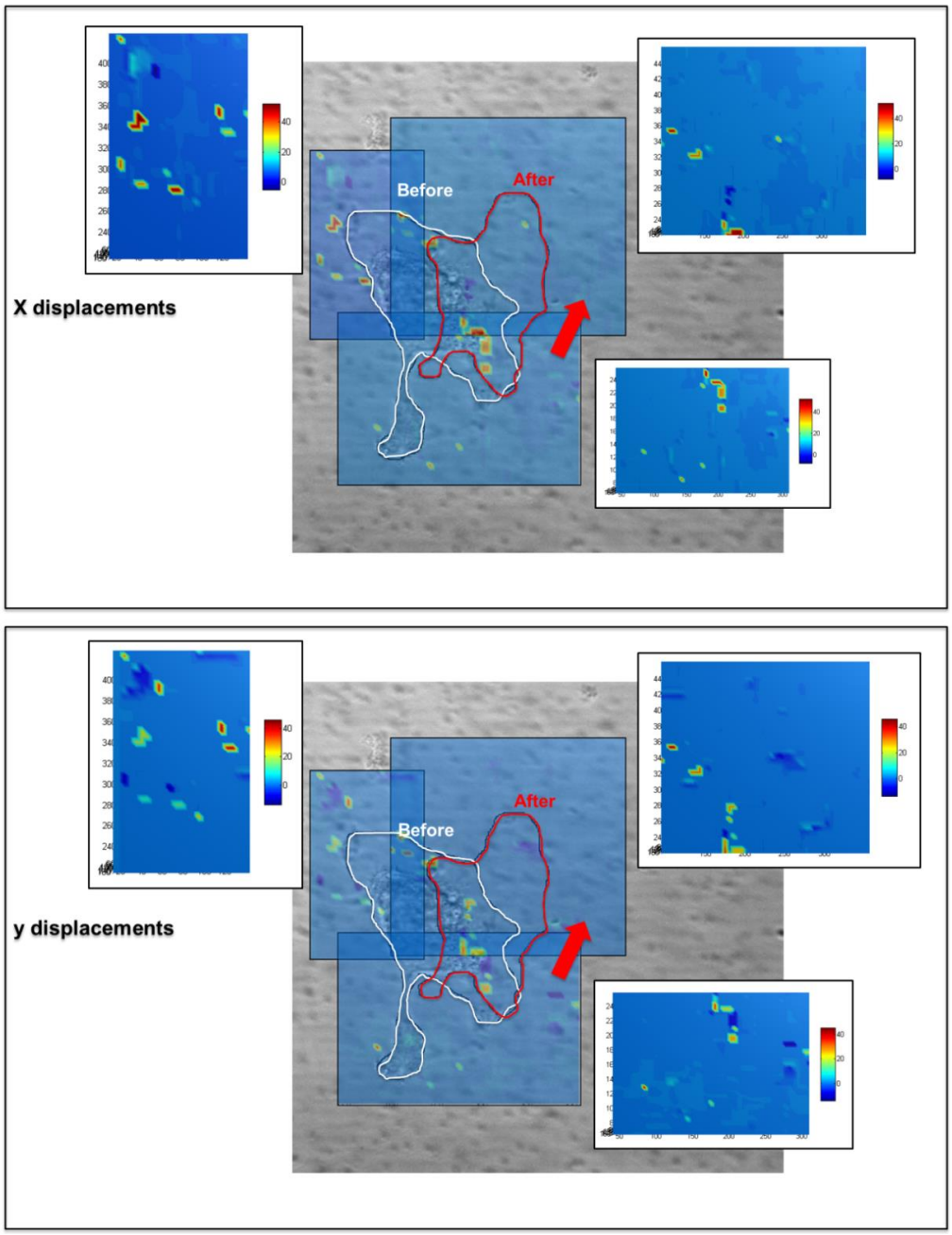

Figure D - 5: In plane displacements (x and y directions) of a cell cultured on a stiff substrate, before and after migration for an hour. Supplementary information to Figure 5-14. GS = 5, CS = 15 and SR = 2. Red arrow shows migration direction. Color bars indicate displacement values in pixels (1 pixel = 0.19 μm). Both contour plots and contour plots overlaid on the image of the cell are shown for more clear demonstration of results.

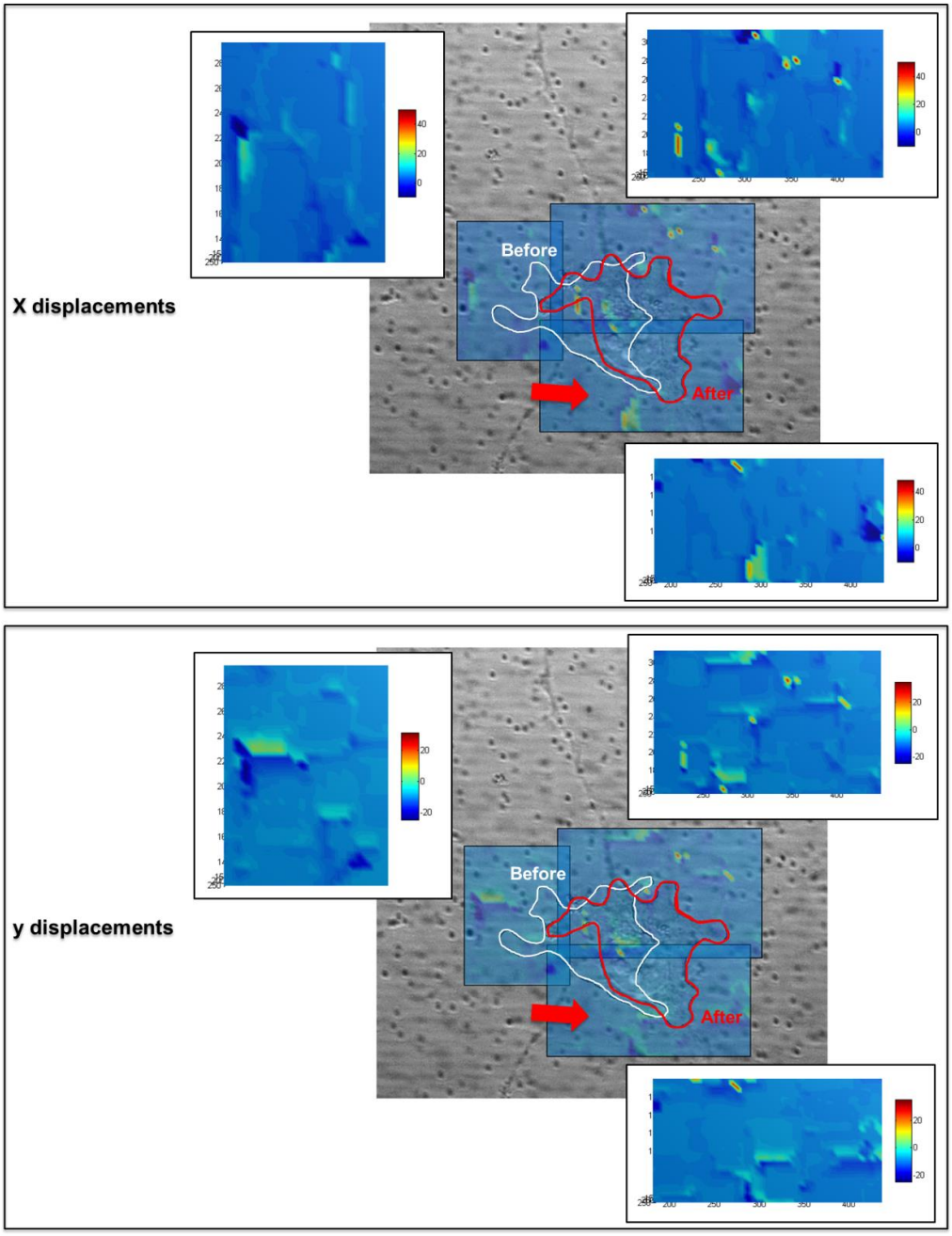

Figure D - 6: Displacements and strains in x and y directions for a cell seeded on a soft substrate, before and after migration for 90 minutes. Supplementary information to Figure 5-14. GS = 5, CS = 15 and SR = 2. Red arrow shows migration direction. . Red arrow shows migration direction. Color bars indicate displacement values in pixels (1 pixel = 0.19 μm). Both contour plots and contour plots overlaid on the image of the cell are shown for more clear demonstration of results.

Copyright Permissions

ELSEVIER LICENSE
TERMS AND CONDITIONS

Jan 14, 2015

This is a License Agreement between Sara Molladavoodi ("You") and Elsevier ("Elsevier") provided by Copyright Clearance Center ("CCC"). The license consists of your order details, the terms and conditions provided by Elsevier, and the payment terms and conditions.

All payments must be made in full to CCC. For payment instructions, please see information listed at the bottom of this form.

Supplier	Elsevier Limited The Boulevard,Langford Lane Kidlington,Oxford,OX5 1GB,UK
Registered Company Number	1982084
Customer name	Sara Molladavoodi
Customer address	Mechanical and Mechatronics Engineering Waterloo, ON N2L 3G1
License number	3547670170480
License date	Jan 14, 2015
Licensed content publisher	Elsevier
Licensed content publication	Journal of the Mechanical Behavior of Biomedical Materials
Licensed content title	Investigation of microstructure, mechanical properties and cellular viability of poly(L-lactic acid) tissue engineering scaffolds prepared by different thermally induced phase separation protocols
Licensed content author	None
Licensed content date	January 2013
Licensed content volume number	17
Licensed content issue number	n/a
Number of pages	12
Start Page	186
End Page	197
Type of Use	reuse in a thesis/dissertation
Portion	full article
Format	both print and electronic
Are you the author of this Elsevier article?	Yes

Will you be translating?	No
Title of your thesis/dissertation	Investigating Mechanical Interactions of Cells with Their Environment
Expected completion date	Jan 2015
Estimated size (number of pages)	200
Elsevier VAT number	GB 494 6272 12
Permissions price	0.00 CAD
VAT/Local Sales Tax	0.00 CAD / 0.00 GBP
Total	0.00 CAD

ELSEVIER LICENSE
TERMS AND CONDITIONS

Jan 14, 2015

This is a License Agreement between Sara Molladavoodi ("You") and Elsevier ("Elsevier") provided by Copyright Clearance Center ("CCC"). The license consists of your order details, the terms and conditions provided by Elsevier, and the payment terms and conditions.

All payments must be made in full to CCC. For payment instructions, please see information listed at the bottom of this form.

Supplier	Elsevier Limited The Boulevard,Langford Lane Kidlington,Oxford,OX5 1GB,UK
Registered Company Number	1982084
Customer name	Sara Molladavoodi
Customer address	Mechanical and Mechatronics Engineering Waterloo, ON N2L 3G1
License number	3547670355800
License date	Jan 14, 2015
Licensed content publisher	Elsevier
Licensed content publication	Acta Biomaterialia
Licensed content title	Human corneal epithelial cell response to substrate stiffness
Licensed content author	None
Licensed content date	1 January 2015
Licensed content volume number	11
Licensed content issue number	n/a
Number of pages	9
Start Page	324
End Page	332
Type of Use	reuse in a thesis/dissertation
Intended publisher of new work	other
Portion	full article
Format	both print and electronic
Are you the author of this Elsevier article?	Yes
Will you be translating?	No

Title of your thesis/dissertation	Investigating Mechanical Interactions of Cells with Their Environment
Expected completion date	Jan 2015
Estimated size (number of pages)	200
Elsevier VAT number	GB 494 6272 12
Permissions price	0.00 CAD
VAT/Local Sales Tax	0.00 CAD / 0.00 GBP
Total	0.00 CAD

Bibliography

[1] Alberts B, Johnson, Alexander, Lewis, Julian, Raff, Martin C., Roberts, K., Walter, Peter, Wilson, John Hunt T. Molecular biology of the cell. 5th ed. CN. New York: Garland Science; 2008.

[2] Discher DE, Janmey P, Wang Y-L. Tissue cells feel and respond to the stiffness of their substrate. Science 2005;310:1139–43.

[3] Shiu Y-T, Li S, Marganski WA, Usami S, Schwartz MA, Wang Y-L, et al. Rho mediates the shear-enhancement of endothelial cell migration and traction force generation. Biophys J 2004;86:2558–65.

[4] Zaidel-Bar R, Kam Z, Geiger B. Polarized downregulation of the paxillin-p130CAS-Rac1 pathway induced by shear flow. J Cell Sci 2005;118:3997–4007.

[5] Simmons CA, Matlis S, Thornton AJ, Chen S, Wang C-Y, Mooney DJ. Cyclic strain enhances matrix mineralization by adult human mesenchymal stem cells via the extracellular signal-regulated kinase (ERK1/2) signaling pathway. J Biomech 2003;36:1087–96.

[6] Evans ND, Minelli C, Gentleman E, LaPointe V, Patankar SN, Kallivretaki M, et al. Substrate stiffness affects early differentiation events in embryonic stem cells. Eur Cells Mater J 2009;18:1–13.

[7] Nam J, Johnson J, Lannutti JJ, Agarwal S. Modulation of embryonic mesenchymal progenitor cell differentiation via control over pure mechanical modulus in electrospun nanofibers. Acta Biomater 2011;7:1516–24.

[8] Lo CM, Wang HB, Dembo M, Wang Y. Cell movement is guided by the rigidity of the substrate. Biophys J 2000;79:144–52.

[9] Harris AK, Wild P, Stopak D. Silicone rubber substrata: a new wrinkle in the study of cell locomotion. Sci 1980;208 :177–9.

[10] Dembo M, Wang YL. Stresses at the cell-to-substrate interface during locomotion of fibroblasts. Biophys J 1999;76:2307–16.

[11] Maskarinec S a, Franck C, Tirrell D a, Ravichandran G. Quantifying cellular traction forces in three dimensions. Proc Natl Acad Sci U S A 2009;106:22108–13.

[12] Franck C, Hong S, Maskarinec S a., Tirrell D a., Ravichandran G. Three-dimensional Full-field Measurements of Large Deformations in Soft Materials Using Confocal Microscopy and Digital Volume Correlation. Exp Mech 2007;47:427–38.

[13] Hur SS, Zhao Y, Li Y-S, Botvinick E, Chien S. Live Cells Exert 3-Dimensional Traction Forces on Their Substrata. Cell Mol Bioeng 2009;2:425–36.

[14] Delanoë-Ayari H, Rieu JP, Sano M. 4D Traction Force Microscopy Reveals Asymmetric Cortical Forces in Migrating Dictyostelium Cells. Phys Rev Lett 2010;105:248103.

[15] Legant WR, Choi CK, Miller JS, Shao L, Gao L, Betzig E, et al. Multidimensional traction force microscopy reveals out-of-plane rotational moments about focal adhesions. Proc Natl Acad Sci U S A 2013;110:881–6.

[16] Rozario T, DeSimone DW. The extracellular matrix in development and morphogenesis: a dynamic view. Dev Biol 2010;341:126–40.

[17] Badylak SF. The extracellular matrix as a biologic scaffold material. Biomaterials 2007;28:3587–93.

[18] Mow VC, Huiskes R, Ovid Technologies I. Basic orthopaedic biomechanics & mechano-biology. 3rd ed. CN. Philadelphia, PA: Lippincott Williams & Wilkins; 2005.

[19] Mow VC, Ateshian G a, Spilker RL. Biomechanics of diarthrodial joints: a review of twenty years of progress. J Biomech Eng 1993;115:460–7.

[20] Badylak SF, Freytes DO, Gilbert TW. Extracellular matrix as a biological scaffold material: Structure and function. Acta Biomater 2009;5:1–13.

[21] Kim S-H, Turnbull J, Guimond S. Extracellular matrix and cell signalling: the dynamic cooperation of integrin, proteoglycan and growth factor receptor. J Endocrinol 2011;209:139–51.

[22] Wipff P-J, Rifkin DB, Meister J-J, Hinz B. Myofibroblast contraction activates latent TGF-beta1 from the extracellular matrix. J Cell Biol 2007;179:1311–23.

[23] Kan M, Wu X, Wang F, McKeehan WL. Specificity for Fibroblast Growth Factors Determined by Heparan Sulfate in a Binary Complex with the Receptor Kinase. J Biol Chem 1999;274:15947–52.

[24] Nagel M, Tahinci E, Symes K, Winklbauer R. Guidance of mesoderm cell migration in the Xenopus gastrula requires PDGF signaling. Development 2004;131:2727–36.

[25] Bronner-Fraser M. Distribution and function of tenascin during cranial neural crest development in the chick. J Neurosci Res 1988;21:135–47.

[26] Gao Y, Xiao Q, Ma H, Li L, Liu J, Feng Y, et al. LKB1 inhibits lung cancer progression through lysyl oxidase and extracellular matrix remodeling. Proc Natl Acad Sci U S A 2010;107:18892–7.

[27] Kakkad SM, Solaiyappan M, O'Rourke B, Stasinopoulos I, Ackerstaff E, Raman V, et al. Hypoxic Tumor Microenvironments Reduce Collagen I Fiber Density. Neoplasia 2010;12:608–17.

[28] Mecham RP. The extracellular matrix: an overview. Berlin: Springer; 2011.

[29] Brightman a O, Rajwa BP, Sturgis JE, McCallister ME, Robinson JP, Voytik-Harbin SL. Time-lapse confocal reflection microscopy of collagen fibrillogenesis and extracellular matrix assembly in vitro. Biopolymers 2000;54:222–34.

[30] Halper J. Progress in heritable soft connective tissue diseases. Dordrecht: Springer; 2014.

[31] Friedl P, Wolf K. Plasticity of cell migration: a multiscale tuning model. J Cell Biol 2010;188:11–9.

[32] Zaman MH, Trapani LM, Sieminski AL, Siemeski A, Mackellar D, Gong H, et al. Migration of tumor cells in 3D matrices is governed by matrix stiffness along with cell-matrix adhesion and proteolysis. Proc Natl Acad Sci U S A 2006;103:10889–94.

[33] Ehrbar M, Sala A, Lienemann P, Ranga A, Mosiewicz K, Bittermann A, et al. Elucidating the role of matrix stiffness in 3D cell migration and remodeling. Biophys J 2011;100:284–93.

[34] Friedl P, Wolf K. Proteolytic interstitial cell migration: a five-step process. Cancer Metastasis Rev 2009;28:129–35.

[35] Reinhart-King CA, Dembo M, Hammer DA. Endothelial Cell Traction Forces on RGD-Derivatized Polyacrylamide Substrata. Langmuir 2002;19:1573–9.

[36] Mierke CT, Rösel D, Fabry B, Brábek J. Contractile forces in tumor cell migration. Eur J Cell Biol 2008;87:669–76.

[37] Friedl P, Zänker KS, Bröcker EB. Cell migration strategies in 3-D extracellular matrix: differences in morphology, cell matrix interactions, and integrin function. Microsc Res Tech 1998;43:369–78.

[38] Indra I, Undyala V, Kandow C, Thirumurthi U, Dembo M, Beningo K a. An in vitro correlation of mechanical forces and metastatic capacity. Phys Biol 2011;8:015015.

[39] Sottile J. Regulation of angiogenesis by extracellular matrix. Biochim Biophys Acta 2004;1654:13–22.

[40] Lochter A, Bissell MJ. Involvement of extracellular matrix constituents in breast cancer. Semin Cancer Biol 1995;6:165–73.

[41] Ingber DE, Folkman J. Mechanochemical switching between growth and differentiation during fibroblast growth factor-stimulated angiogenesis in vitro: role of extracellular matrix. J Cell Biol 1989;109:317–30.

[42] Roeder B a., Kokini K, Sturgis JE, Robinson JP, Voytik-Harbin SL. Tensile Mechanical Properties of Three-Dimensional Type I Collagen Extracellular Matrices With Varied Microstructure. J Biomech Eng 2002;124:214.

[43] Watt FM, Huck WTS. Role of the extracellular matrix in regulating stem cell fate. Nat Rev Mol Cell Biol 2013;14:467–73.

[44] Alves M, Martins A, Costa-pinto A, Correlo V, Sol P, Faria S, et al. Chondrogenic differentiation of human bone marrow mesenchymal stem cells in chitosan-based scaffolds using a flow-perfusion bioreactor. J Tissue Eng Regen Med 2011;5:722–32.

[45] Gumbiner BM. Cell adhesion: the molecular basis of tissue architecture and morphogenesis. Cell 1996;84:345–57.

[46] Abercrombie M, Heaysman JEM, Pegrum SM. The locomotion of fibroblasts in culture: IV. Electron microscopy of the leading lamella. Exp Cell Res 1971;67:359–67.

[47] Geiger B, Spatz JP, Bershadsky AD. Environmental sensing through focal adhesions. Nat Rev Mol Cell Biol 2009;10:21–33.

[48] Campbell ID, Humphries MJ. Integrin structure, activation, and interactions. Cold Spring Harb Perspect Biol 2011;3:1–14.

[49] Arnaout M a, Mahalingam B, Xiong J-P. Integrin structure, allostery, and bidirectional signaling. Annu Rev Cell Dev Biol 2005;21:381–410.

[50] Karp G. Cell and molecular biology : concepts and experiments. 3rd ed. CN. New York: John Wiley & Sons; 2003.

[51] Margadant C, Sonnenberg A. Integrin-TGF-beta crosstalk in fibrosis, cancer and wound healing. EMBO Rep 2010;11:97–105.

[52] Tamkun JW, DeSimone DW, Fonda D, Patel RS, Buck C, Horwitz a F, et al. Structure of integrin, a glycoprotein involved in the transmembrane linkage between fibronectin and actin. Cell 1986;46:271–82.

[53] Mofrad MRK, Kamm RD. Cellular mechanotransduction: diverse perspectives from molecules to tissues. Cambridge: Cambridge University Press; 2010.

[54] Larson, Richard S, Corbi Angel L, Berman Lisa and ST. Primary structure of the leukocyte function-associated molecule-1 alpha subunit: an integrin with an embedded domain defining a protein superfamily. J Cell Biol 1989;108:703–12.

[55] Janet A. Askari, Patrick A. Buckley APM and MJH. Linking integrin conformation to function. J Cell Sci 122 2009;122:165–70.

[56] Litvinov RI, Shuman H, Bennett JS, Weisel JW. Binding strength and activation state of single fibrinogen-integrin pairs on living cells. Proc Natl Acad Sci U S A 2002;99:7426–31.

[57] Chigaev A, Blenc AM, Braaten J V, Kumaraswamy N, Kepley CL, Andrews RP, et al. Real time analysis of the affinity regulation of alpha 4-integrin. The physiologically activated receptor is intermediate in affinity between resting and Mn(2+) or antibody activation. J Biol Chem 2001;276:48670–8.

[58] Takagi J, Petre BM, Walz T, Springer TA. Global Conformational Rearrangements in Integrin Extracellular Domains in Outside-In and Inside-Out Signaling. Cell 2002;110:599–611.

[59] Luo B-H, Carman C V, Springer T a. Structural basis of integrin regulation and signaling. Annu Rev Immunol 2007;25:619–47.

[60] Beglova N, Blacklow SC, Takagi J, Springer T a. Cysteine-rich module structure reveals a fulcrum for integrin rearrangement upon activation. Nat Struct Biol 2002;9:282–7.

[61] Nishida N, Xie C, Shimaoka M, Cheng Y, Walz T, Springer T a. Activation of leukocyte beta2 integrins by conversion from bent to extended conformations. Immunity 2006;25:583–94.

[62] Margadant C, Monsuur HN, Norman JC, Sonnenberg A. Mechanisms of integrin activation and trafficking. Curr Opin Cell Biol 2011;23:607–14.

[63] Tadokoro S, Shattil SJ, Eto K, Tai V, Liddington RC, de Pereda JM, et al. Talin binding to integrin beta tails: a final common step in integrin activation. Science 2003;302:103–6.

[64] Jiang G, Giannone G, Critchley DR, Fukumoto E, Sheetz MP. Two-piconewton slip bond between fibronectin and the cytoskeleton depends on talin. Nature 2003;424.

[65] Calderwood D a, Ginsberg MH. Talin forges the links between integrins and actin. Nat Cell Biol 2003;5:694–7.

[66] Brown NH, Gregory SL, Rickoll WL, Fessler LI, Prout M, White RAH, et al. Talin Is Essential for Integrin Function in Drosophila. Dev Cell 2002;3:569–79.

[67] Shi X, Ma Y-Q, Tu Y, Chen K, Wu S, Fukuda K, et al. The MIG-2/integrin interaction strengthens cell-matrix adhesion and modulates cell motility. J Biol Chem 2007;282:20455–66.

[68] Moser M, Nieswandt B, Ussar S, Pozgajova M, Fässler R. Kindlin-3 is essential for integrin activation and platelet aggregation. Nat Med 2008;14:325–30.

[69] Ye F, Snider AK, Ginsberg MH. Talin and kindlin: the one-two punch in integrin activation. Front Med 2014;8:6–16.

[70] Xiao T, Takagi J, Coller BS, Wang J-H, Springer T a. Structural basis for allostery in integrins and binding to fibrinogen-mimetic therapeutics. Nature 2004;432:59–67.

[71] Adair BD, Xiong J-P, Maddock C, Goodman SL, Arnaout MA, Yeager M. Three-dimensional EM structure of the ectodomain of integrin {alpha}V{beta}3 in a complex with fibronectin. J Cell Biol 2005;168:1109–18.

[72] Luo B-H, Strokovich K, Walz T, Springer T a, Takagi J. Allosteric beta1 integrin antibodies that stabilize the low affinity state by preventing the swing-out of the hybrid domain. J Biol Chem 2004;279:27466–71.

[73] Shi M, Foo SY, Tan S-M, Mitchell EP, Law SKA, Lescar J. A structural hypothesis for the transition between bent and extended conformations of the leukocyte beta2 integrins. J Biol Chem 2007;282:30198–206.

[74] Tiwari S, Askari J a, Humphries MJ, Bulleid NJ. Divalent cations regulate the folding and activation status of integrins during their intracellular trafficking. J Cell Sci 2011;124:1672–80.

[75] Grzesiak JJ, Davis GE, Kirchhofer D, Pierschbacher MD. Regulation of alpha 2 beta 1-mediated fibroblast migration on type I collagen by shifts in the concentrations of extracellular Mg2+ and Ca2+ [published erratum appears in J Cell Biol 1992 Jul;118(1):219]. J Cell Biol 1992;117:1109–17.

[76] Xiong J-P, Stehle T, Zhang R, Joachimiak A, Frech M, Goodman SL, et al. Crystal structure of the extracellular segment of integrin alphaVbeta3 in complex with an Arg-Gly-Asp ligand. Science 2002;296:151–5.

[77] Takagi J, Erickson HP, Springer TA. C-terminal opening mimics “inside-out” activation of integrin α5β1. Nat Struct Biol 2001;8:531–3.

[78] Chiquet M. Regulation of extracellular matrix gene expression by mechanical stress. Matrix Biol 1999;18:417–26.

[79] Humphries JD, Wang P, Streuli C, Geiger B, Humphries MJ, Ballestrem C. Vinculin controls focal adhesion formation by direct interactions with talin and actin. J Cell Biol 2007;179:1043–57.

[80] Zimerman B, Volberg T, Geiger B. Early molecular events in the assembly of the focal adhesion-stress fiber complex during fibroblast spreading. Cell Motil Cytoskeleton 2004;58:143–59.

[81] Alexandrova AY, Arnold K, Schaub S, Vasiliev JM, Meister J-J, Bershadsky AD, et al. Comparative dynamics of retrograde actin flow and focal adhesions: formation of nascent adhesions triggers transition from fast to slow flow. PLoS One 2008;3:e3234.

[82] Choi CK, Vicente-Manzanares M, Zareno J, Whitmore L a, Mogilner A, Horwitz AR. Actin and alpha-actinin orchestrate the assembly and maturation of nascent adhesions in a myosin II motor-independent manner. Nat Cell Biol 2008;10:1039–50.

[83] Gardel ML, Sabass B, Ji L, Danuser G, Schwarz US, Waterman CM. Traction stress in focal adhesions correlates biphasically with actin retrograde flow speed. J Cell Biol 2008;183:999–1005.

[84] Nobes CD, Hall A. Rho, Rac, and Cdc42 GTPases regulate the assembly of multimolecular focal complexes associated with actin stress fibers, lamellipodia, and filopodia. Cell 1995;81:53–62.

[85] Geiger B, Bershadsky a. Assembly and mechanosensory function of focal contacts. Curr Opin Cell Biol 2001;13:584–92.

[86] Choi CK, Zareno J, Digman MA, Gratton E, Horwitz AR. Cross-correlated fluctuation analysis reveals phosphorylation-regulated paxillin-FAK complexes in nascent adhesions. Biophys J 2011;100:583–92.

[87] Webb DJ, Donais K, Whitmore L a, Thomas SM, Turner CE, Parsons JT, et al. FAK-Src signalling through paxillin, ERK and MLCK regulates adhesion disassembly. Nat Cell Biol 2004;6:154–61.

[88] Zaidel-Bar R, Ballestrem C, Kam Z, Geiger B. Early molecular events in the assembly of matrix adhesions at the leading edge of migrating cells. J Cell Sci 2003;116:4605–13.

[89] Grashoff C, Hoffman BD, Brenner MD, Zhou R, Parsons M, Yang MT, et al. Measuring mechanical tension across vinculin reveals regulation of focal adhesion dynamics. Nature 2010;466:263–6.

[90] Zhang X, Jiang G, Cai Y, Monkley SJ, Critchley DR, Sheetz MP. Talin depletion reveals independence of initial cell spreading from integrin activation and traction. Nat Cell Biol 2008;10:1062–8.

[91] Watanabe N, Madaule P, Reid T, Ishizaki T, Watanabe G, Kakizuka A, et al. p140mDia, a mammalian homolog of Drosophila diaphanous, is a target protein for Rho small GTPase and is a ligand for profilin. EMBO J 1997;16:3044–56.

[92] Amano M, Fukata Y, Kaibuchi K. Regulation and functions of Rho-associated kinase. Exp Cell Res 2000;261:44–51.

[93] Nakano K, Takaishi K, Kodama A, Mammoto A, Shiozaki H, Monden M, et al. Distinct actions and cooperative roles of ROCK and mDia in Rho small G protein-induced reorganization of the actin cytoskeleton in Madin-Darby canine kidney cells. Mol Biol Cell 1999;10:2481–91.

[94] Watanabe N, Kato T, Fujita A, Ishizaki T, Narumiya S. Cooperation between mDia1 and ROCK in Rho-induced actin reorganization. Nat Cell Biol 1999;1:136–43.

[95] Riveline D, Zamir E, Balaban NQ, Schwarz US, Ishizaki T, Narumiya S, et al. Focal contacts as mechanosensors: externally applied local mechanical force induces growth of focal contacts by an mDia1-dependent and ROCK-independent mechanism. J Cell Biol 2001;153:1175–86.

[96] Galbraith CG, Yamada KM, Sheetz MP. The relationship between force and focal complex development 2002;159:695–705.

[97] Balaban NQ, Schwarz US, Riveline D, Goichberg P, Tzur G, Sabanay I, et al. Force and focal adhesion assembly: a close relationship studied using elastic micropatterned substrates. Nat Cell Biol 2001;3:466–72.

[98] Harunaga JS, Yamada KM. Cell-matrix adhesions in 3D. Matrix Biol 2011;30:363–8.

[99] Fraley SI, Feng Y, Krishnamurthy R, Kim D-H, Celedon A, Longmore GD, et al. A distinctive role for focal adhesion proteins in three-dimensional cell motility. Nat Cell Biol 2010;12:598–604.

[100] Tamariz E, Grinnell F. Modulation of Fibroblast Morphology and Adhesion during Collagen Matrix Remodeling. Mol Biol Cell 2002;13 :3915–29.

[101] Zhou X, Rowe RG, Hiraoka N, George JP, Wirtz D, Mosher DF, et al. Fibronectin fibrillogenesis regulates three-dimensional neovessel formation. Genes Dev 2008;22:1231–43.

[102] Kubow KE, Horwitz AR. Reducing background fluorescence reveals adhesions in 3D matrices. Nat Cell Biol 2011;13:3–5; author reply 5–7.

[103] Hakkinen KM, Harunaga JS, Doyle AD, Yamada KM. Direct comparisons of the morphology, migration, cell adhesions, and actin cytoskeleton of fibroblasts in four different three-dimensional extracellular matrices. Tissue Eng Part A 2011;17:713–24.

[104] Provenzano PP, Inman DR, Eliceiri KW, Keely PJ. Matrix density-induced mechanoregulation of breast cell phenotype, signaling and gene expression through a FAK-ERK linkage. Oncogene 2009;28:4326–43.

[105] Henstock JR, Rotherham M, Rose JB, El Haj AJ. Cyclic hydrostatic pressure stimulates enhanced bone development in the foetal chick femur in vitro. Bone 2013;53:468–77.

[106] Wang JH-C. Mechanobiology of tendon. J Biomech 2006;39:1563–82.

[107] Kaverina I, Krylyshkina O, Beningo K, Anderson K, Wang Y-L, Small JV. Tensile stress stimulates microtubule outgrowth in living cells. J Cell Sci 2002;115:2283–91.

[108] Trache A, Meininger G a. Atomic force-multi-optical imaging integrated microscope for monitoring molecular dynamics in live cells. J Biomed Opt 2014;10:064023.

[109] Giannone G, Jiang G, Sutton DH, Critchley DR, Sheetz MP. Talin1 is critical for force-dependent reinforcement of initial integrin-cytoskeleton bonds but not tyrosine kinase activation. J Cell Biol 2003;163:409–19.

[110] Wang N, Suo Z. Long-distance propagation of forces in a cell. Biochem Biophys Res Commun 2005;328:1133–8.

[111] Mack PJ, Kaazempur-Mofrad MR, Karcher H, Lee RT, Kamm RD. Force-induced focal adhesion translocation: effects of force amplitude and frequency. Am J Physiol Cell Physiol 2004;287:C954–62.

[112] Pelham RJ, Wang Y -l. Cell locomotion and focal adhesions are regulated by substrate flexibility. Proc Natl Acad Sci 1997;94:13661–5.

[113] Cameron AR, Frith JE, Cooper-White JJ. The influence of substrate creep on mesenchymal stem cell behaviour and phenotype. Biomaterials 2011;32:5979–93.

[114] Hadjipanayi E, Mudera V, Brown RA. Guiding cell migration in 3D: a collagen matrix with graded directional stiffness. Cell Motil Cytoskeleton 2009;66:121–8.

[115] Vincent LG, Choi YS, Alonso-Latorre B, del Álamo JC, Engler AJ. Mesenchymal stem cell durotaxis depends on substrate stiffness gradient strength. Biotechnol J 2013;8:472–84.

[116] Keogh MB, O'Brien FJ, Daly JS. Substrate stiffness and contractile behaviour modulate the functional maturation of osteoblasts on a collagen-GAG scaffold. Acta Biomater 2010;6:4305–13.

[117] Ghosh K, Pan Z, Guan E, Ge S, Liu Y, Nakamura T, et al. Cell adaptation to a physiologically relevant ECM mimic with different viscoelastic properties. Biomaterials 2007;28:671–9.

[118] Byfield FJ, Reen RK, Shentu T-P, Levitan I, Gooch KJ. Endothelial actin and cell stiffness is modulated by substrate stiffness in 2D and 3D. J Biomech 2009;42:1114–9.

[119] Kasas S, Wang X, Hirling H, Marsault R, Huni B, Yersin A, et al. Superficial and deep changes of cellular mechanical properties following cytoskeleton disassembly. Cell Motil Cytoskeleton 2005;62:124–32.

[120] Cai S, Pestic-Dragovich L, O'Donnell ME, Wang N, Ingber D, Elson E, et al. Regulation of cytoskeletal mechanics and cell growth by myosin light chain phosphorylation. Am J Physiol 1998;275:C1349–56.

[121] Coughlin MF, Fredberg JJ. Changes in cytoskeletal dynamics and nonlinear rheology with metastatic ability in cancer cell lines. Phys Biol 2013;10:065001.

[122] Hadjipanayi E, Mudera V, Brown RA. Close dependence of fibroblast proliferation on collagen scaffold matrix stiffness. J Tissue Eng Regen Med 2009:77–84.

[123] Miron-Mendoza M, Seemann J, Grinnell F. The differential regulation of cell motile activity through matrix stiffness and porosity in three dimensional collagen matrices. Biomaterials 2010;31:6425–35.

[124] Guo W, Frey MT, Burnham NA, Wang Y. Substrate rigidity regulates the formation and maintenance of tissues. Biophys J 2006;90:2213–20.

[125] McGrail DJ, Kieu QMN, Dawson MR. The malignancy of metastatic ovarian cancer cells is increased on soft matrices through a mechanosensitive Rho–ROCK pathway. J Cell Sci 2014;127 :2621–6.

[126] Deeg J a, Louban I, Aydin D, Selhuber-Unkel C, Kessler H, Spatz JP. Impact of local versus global ligand density on cellular adhesion. Nano Lett 2011;11:1469–76.

[127] Elias DR, Poloukhtine A, Popik V, Tsourkas A. Effect of ligand density, receptor density, and nanoparticle size on cell targeting. Nanomedicine 2013;9:194–201.

[128] Richert L, Vetrone F, Yi J-H, Zalzal SF, Wuest JD, Rosei F, et al. Surface Nanopatterning to Control Cell Growth. Adv Mater 2008;20:1488–92.

[129] Anselme K, Davidson P, Popa AM, Giazzon M, Liley M, Ploux L. The interaction of cells and bacteria with surfaces structured at the nanometre scale. Acta Biomater 2010;6:3824–46.

[130] Chaudhuri O, Koshy ST, Branco da Cunha C, Shin J-W, Verbeke CS, Allison KH, et al. Extracellular matrix stiffness and composition jointly regulate the induction of malignant phenotypes in mammary epithelium. Nat Mater 2014;13:970–8.

[131] Peyton SR, Putnam AJ. Extracellular matrix rigidity governs smooth muscle cell motility in a biphasic fashion. J Cell Physiol 2005;204:198–209.

[132] Hoyer J, Distler A, Haase W, Gogelein H. Ca2+ influx through stretch-activated cation channels activates maxi K+ channels in porcine endocardial endothelium. Proc Natl Acad Sci U S A 1994;91:2367–71.

[133] Hoyer J, Kohler R, Haase W, Distler A. Up-regulation of pressure-activated Ca(2+)-permeable cation channel in intact vascular endothelium of hypertensive rats. Proc Natl Acad Sci U S A 1996;93:11253–8.

[134] Popp R, Hoyert J, Meyer J, Galla H-J, Gogelein H. Stretch-activated non-selective cation channels in the antiluminal membrane of porcine cerebral capillaries. J Physiol 1992;454:435–49.

[135] Blumenthal DK, Stull JT. Activation of skeletal muscle myosin light chain kinase by calcium(2+) and calmodulin. Biochemistry 1980;19:5608–14.

[136] Liedert A, Kaspar D, Blakytny R, Claes L, Ignatius A. Signal transduction pathways involved in mechanotransduction in bone cells. Biochem Biophys Res Commun 2006;349:1–5.

[137] Schwarz G, Droogmans G, Nilius B. Shear stress induced membrane currents and calcium transients in human vascular endothelial cells. Pflügers Arch 1992;421:394–6.

[138] Jacobs E, Cheliakine C, Gebremedhin D, Birks E, Davies P, Harder D. Shear activated channels in cell-attached patches of cultured bovine aortic endothelial cells. Pflügers Arch 1995;431:129–31.

[139] Barakat a. I, Leaver E V., Pappone P a., Davies PF. A Flow-Activated Chloride-Selective Membrane Current in Vascular Endothelial Cells. Circ Res 1999;85:820–8.

[140] Gether U. Uncovering molecular mechanisms involved in activation of G protein-coupled receptors. Endocr Rev 2000;21:90–113.

[141] Zhang M, Chen Y-J, Ono T, Wang J-J. Crosstalk between integrin and G protein pathways involved in mechanotransduction in mandibular condylar chondrocytes under pressure. Arch Biochem Biophys 2008;474:102–8.

[142] Gudi SRP, Clark CB, Frangos JA. Fluid Flow Rapidly Activates G Proteins in Human Endothelial Cells: Involvement of G Proteins in Mechanochemical Signal Transduction. Circ Res 1996;79:834–9.

[143] Hunyady L, Turu G. The role of the AT1 angiotensin receptor in cardiac hypertrophy: angiotensin II receptor or stretch sensor? Trends Endocrinol Metab 2004;15:405–8.

[144] Jaalouk DE, Lammerding J. Mechanotransduction gone awry. Nat Rev Mol Cell Biol 2009;10:63–73.

[145] Zou Y, Akazawa H, Qin Y, Sano M, Takano H, Minamino T, et al. Mechanical stress activates angiotensin II type 1 receptor without the involvement of angiotensin II. Nat Cell Biol 2004;6:499–506.

[146] Gudi S, Nolan JP, Frangos JA. Modulation of GTPase activity of G proteins by fluid shear stress and phospholipid composition. Proc Natl Acad Sci 1998;95:2515–9.

[147] Haidekker MA, L'Heureux N, Frangos JA. Fluid shear stress increases membrane fluidity in endothelial cells: a study with DCVJ fluorescence. Am J Physiol Hear Circ Physiol 2000;278:H1401–6.

[148] Montagne K, Uchiyama H, Furukawa KS, Ushida T. Hydrostatic pressure decreases membrane fluidity and lipid desaturase expression in chondrocyte progenitor cells. J Biomech 2014;47:354–9.

[149] White CR, Frangos J a. The shear stress of it all: the cell membrane and mechanochemical transduction. Philos Trans R Soc Lond B Biol Sci 2007;362:1459–67.

[150] Sawada Y, Tamada M, Dubin-Thaler BJ, Cherniavskaya O, Sakai R, Tanaka S, et al. Force sensing by mechanical extension of the Src family kinase substrate p130Cas. Cell 2006;127:1015–26.

[151] Yee KL, Weaver VM, Hammer D a. Integrin-mediated signalling through the MAP-kinase pathway. IET Syst Biol 2008;2:8–15.

[152] Kim T-J, Seong J, Ouyang M, Sun J, Lu S, Hong JP, et al. Substrate rigidity regulates Ca2+ oscillation via RhoA pathway in stem cells. J Cell Physiol 2009;218:285–93.

[153] Fukata M, Watanabe T, Noritake J, Nakagawa M, Yamaga M, Kuroda S, et al. Rac1 and Cdc42 Capture Microtubules through IQGAP1 and CLIP-170. Cell 2002;109:873–85.

[154] Siegrist SE, Doe CQ. Microtubule-induced cortical cell polarity. Genes Dev 2007;21:483–96.

[155] Guilak F, Tedrow JR, Burgkart R. Viscoelastic properties of the cell nucleus. Biochem Biophys Res Commun 2000;269:781–6.

[156] Vaziri A, Mofrad MRK. Mechanics and deformation of the nucleus in micropipette aspiration experiment. J Biomech 2007;40:2053–62.

[157] Caille N, Thoumine O, Tardy Y, Meister J-J. Contribution of the nucleus to the mechanical properties of endothelial cells. J Biomech 2002;35:177–87.

[158] Dahl KN, Kahn SM, Wilson KL, Discher DE. The nuclear envelope lamina network has elasticity and a compressibility limit suggestive of a molecular shock absorber. J Cell Sci 2004;117:4779–86.

[159] Pajerowski JD, Dahl KN, Zhong FL, Sammak PJ, Discher DE. Physical plasticity of the nucleus in stem cell differentiation. Proc Natl Acad Sci U S A 2007;104:15619–24.

[160] Brangwynne CP, MacKintosh FC, Kumar S, Geisse NA, Talbot J, Mahadevan L, et al. Microtubules can bear enhanced compressive loads in living cells because of lateral reinforcement. J Cell Biol 2006;173:733–41.

[161] Ingber DE. Tensegrity: the architectural basis of cellular mechanotransduction. Annu Rev Physiol 1997;59:575–99.

[162] Fernández P, Pullarkat PA, Ott A. A master relation defines the nonlinear viscoelasticity of single fibroblasts. Biophys J 2006;90:3796–805.

[163] Mills JP, Qie L, Dao M, Lim CT, Suresh S. Nonlinear elastic and viscoelastic deformation of the human red blood cell with optical tweezers. Mech Chem Biosyst 2004;1:169–80.

[164] Crisp M, Liu Q, Roux K, Rattner JB, Shanahan C, Burke B, et al. Coupling of the nucleus and cytoplasm: role of the LINC complex. J Cell Biol 2006;172:41–53.

[165] Maniotis a J, Chen CS, Ingber DE. Demonstration of mechanical connections between integrins, cytoskeletal filaments, and nucleoplasm that stabilize nuclear structure. Proc Natl Acad Sci U S A 1997;94:849–54.

[166] Deguchi S, Maeda K, Ohashi T, Sato M. Flow-induced hardening of endothelial nucleus as an intracellular stress-bearing organelle. J Biomech 2005;38:1751–9.

[167] Mathur AB, Reichert WM, Truskey G a. Flow and high affinity binding affect the elastic modulus of the nucleus, cell body and the stress fibers of endothelial cells. Ann Biomed Eng 2007;35:1120–30.

[168] Lee JSH, Chang MI, Tseng Y, Wirtz D. Cdc42 mediates nucleus movement and MTOC polarization in Swiss 3T3 fibroblasts under mechanical shear stress. Mol Biol Cell 2005;16:871–80.

[169] Thomas CH, Collier JH, Sfeir CS, Healy KE. Engineering gene expression and protein synthesis by modulation of nuclear shape. Proc Natl Acad Sci U S A 2002;99:1972–7.

[170] Dahl KN, Ribeiro AJS, Lammerding J. Nuclear shape, mechanics, and mechanotransduction. Circ Res 2008;102:1307–18.

[171] Zlatanova J, Leuba SH. Stretching and imaging single DNA molecules and chromatin. J Muscle Res Cell Motil 2002;23:377–95.

[172] Dupont S, Morsut L, Aragona M, Enzo E, Giulitti S, Cordenonsi M, et al. Role of YAP/TAZ in mechanotransduction. Nature 2011;474:179–83.

[173] Calvo F, Ege N, Grande-Garcia A, Hooper S, Jenkins RP, Chaudhry SI, et al. Mechanotransduction and YAP-dependent matrix remodelling is required for the generation and maintenance of cancer-associated fibroblasts. Nat Cell Biol 2013;15:637–46.

[174] Ingber D. Mechanobiology and diseases of mechanotransduction. Ann Med 2003;35:564–77.

[175] McKnight AL, Kugel JL, Rossman PJ, Manduca A, Hartmann LC, Ehman RL. MR elastography of breast cancer: preliminary results. AJR Am J Roentgenol 2002;178:1411–7.

[176] Kraning-Rush CM, Carey SP, Califano JP, Smith BN, Reinhart-King C a. The role of the cytoskeleton in cellular force generation in 2D and 3D environments. Phys Biol 2011;8:015009.

[177] Munevar S, Wang Y, Dembo M. Traction force microscopy of migrating normal and H-ras transformed 3T3 fibroblasts. Biophys J 2001;80:1744–57.

[178] Dunn MG, Silver FH, Swann DA. Mechanical Analysis of Hypertrophic Scar Tissue: Structural Basis for Apparent Increased Rigidity. J Investig Dermatol 1985;84:9–13.

[179] Georges PC, Hui J-J, Gombos Z, McCormick ME, Wang AY, Uemura M, et al. Increased stiffness of the rat liver precedes matrix deposition: implications for fibrosis. Am J Physiol Gastrointest Liver Physiol 2007;293:G1147–54.

[180] Takahashi K, Kakimoto Y, Toda K, Naruse K. Mechanobiology in cardiac physiology and diseases. J Cell Mol Med 2013;17:225–32.

[181] Janmey P a, Miller RT. Mechanisms of mechanical signaling in development and disease. J Cell Sci 2011;124:9–18.

[182] Engler AJ, Carag-Krieger C, Johnson CP, Raab M, Tang H-Y, Speicher DW, et al. Embryonic cardiomyocytes beat best on a matrix with heart-like elasticity: scar-like rigidity inhibits beating. J Cell Sci 2008;121:3794–802.

[183] Al-Haque S, Miklas JW, Feric N, Chiu LLY, Chen WLK, Simmons C a, et al. Hydrogel substrate stiffness and topography interact to induce contact guidance in cardiac fibroblasts. Macromol Biosci 2012;12:1342–53.

[184] Li Z, Dranoff J a, Chan EP, Uemura M, Sévigny J, Wells RG. Transforming growth factor-beta and substrate stiffness regulate portal fibroblast activation in culture. Hepatology 2007;46:1246–56.

[185] Delmas P. Polycystins: from mechanosensation to gene regulation. Cell 2004;118:145–8.

[186] Ressler B, Lee RT, Randell SH, Drazen JM, Kamm RD. Molecular responses of rat tracheal epithelial cells to transmembrane pressure. Am J Physiol Lung Cell Mol Physiol 2000;278:L1264–72.

[187] Swartz M a, Tschumperlin DJ, Kamm RD, Drazen JM. Mechanical stress is communicated between different cell types to elicit matrix remodeling. Proc Natl Acad Sci U S A 2001;98:6180–5.

[188] Friedl P. Prespecification and plasticity: shifting mechanisms of cell migration. Curr Opin Cell Biol 2004;16:14–23.

[189] Friedl P, Bröcker E-B. The biology of cell locomotion within three-dimensional extracellular matrix. Cell Mol Life Sci C 2000;57:41–64.

[190] Ridley AJ, Schwartz MA, Burridge K, Firtel RA, Ginsberg MH, Borisy G, et al. Cell Migration: Integrating Signals from Front to Back. Sci 2003;302 :1704–9.

[191] Poincloux R, Collin O, Lizárraga F, Romao M, Debray M, Piel M, et al. Contractility of the cell rear drives invasion of breast tumor cells in 3D Matrigel. Proc Natl Acad Sci U S A 2011;108:1943–8.

[192] Beningo KA, Dembo M, Wang Y. Responses of fibroblasts to anchorage of dorsal extracellular matrix receptors. Proc Natl Acad Sci U S A 2004;101:18024–9.

[193] DeSimone DW, Horwitz AR. Many modes of motility. Sci 2014;345 :1002–3.

[194] Petrie RJ, Gavara N, Chadwick RS, Yamada KM. Nonpolarized signaling reveals two distinct modes of 3D cell migration. J Cell Biol 2012;197:439–55.

[195] Wolf K, Müller R, Borgmann S, Bröcker E-B, Friedl P. Amoeboid shape change and contact guidance: T-lymphocyte crawling through fibrillar collagen is independent of matrix remodeling by MMPs and other proteases. Blood 2003;102:3262–9.

[196] Lemmon CA, Chen CS, Romer LH. Cell traction forces direct fibronectin matrix assembly. Biophys J 2009;96:729–38.

[197] Reinhart-King C a, Dembo M, Hammer D a. The dynamics and mechanics of endothelial cell spreading. Biophys J 2005;89:676–89.

[198] James DW, Taylor JF. The stress developed by sheets of chick fibroblasts in vitro. Exp Cell Res 1969;54:107–10.

[199] Burton K, Taylor DL. Traction forces of cytokinesis measured with optically modified elastic substrata. Nature 1997;385:450–4.

[200] Lee J, Leonard M, Oliver T, Ishihara a, Jacobson K. Traction forces generated by locomoting keratocytes. J Cell Biol 1994;127:1957–64.

[201] Du Roure O, Saez A, Buguin A, Austin RH, Chavrier P, Silberzan P, et al. Force mapping in epithelial cell migration. Proc Natl Acad Sci U S A 2005;102:2390–5.

[202] Tymchenko N, Wallentin J, Petronis S, Bjursten LM, Kasemo B, Gold J. A novel cell force sensor for quantification of traction during cell spreading and contact guidance. Biophys J 2007;93:335–45.

[203] Bell E, Ivarsson B, Merrill C. Production of a tissue-like structure by contraction of collagen lattices by human fibroblasts of different proliferative potential in vitro. Proc Natl Acad Sci 1979;76:1274–8.

[204] Delvoye P, Wiliquet P, Leveque J-L, Nusgens B V, Lapiere CM. Measurement of Mechanical Forces Generated by Skin Fibroblasts Embedded in a Three-Dimensional Collagen Gel. J Investig Dermatol 1991;97:898–902.

[205] Sun S, Cho M. Human fibroblast migration in three-dimensional collagen gel in response to noninvasive electrical stimulus. II. Identification of electrocoupling molecular mechanisms. Tissue Eng 2004;10:1558–65.

[206] Campbell BH, Clark WW, Wang JH-C. A multi-station culture force monitor system to study cellular contractility. J Biomech 2003;36:137–40.

[207] Zheng X, Zhang X. An optical Moiré technique for cell traction force mapping. J Micromechanics Microengineering 2008;18:125006.

[208] Heetz MIPS. A micromachined device provides a new bend on fibroblast traction forces. Proc Natl Acad Sci U S A 1997;94:9114–8.

[209] Tan JL, Tien J, Pirone DM, Gray DS, Bhadriraju K, Chen CS. Cells lying on a bed of microneedles: an approach to isolate mechanical force. Proc Natl Acad Sci U S A 2003;100:1484–9.

[210] Yang MT, Reich DH, Chen CS. Measurement and analysis of traction force dynamics in response to vasoactive agonists. Integr Biol (Camb) 2011;3:663–74.

[211] Ricart BG, Yang MT, Hunter CA, Chen CS, Hammer DA. Measuring Traction Forces of Motile Dendritic Cells on Micropost Arrays. Biophysj 2011;101:2620–8.

[212] Doyle AD, Wang FW, Matsumoto K, Yamada KM. One-dimensional topography underlies three-dimensional fibrillar cell migration. J Cell Biol 2009;184:481–90.

[213] Merkel R, Kirchgessner N, Cesa CM, Hoffmann B. Cell force microscopy on elastic layers of finite thickness. Biophys J 2007;93:3314–23.

[214] Fournier MF, Sauser R, Ambrosi D, Meister J-J, Verkhovsky AB. Force transmission in migrating cells. J Cell Biol 2010;188:287–97.

[215] Hyland C, Mertz AF, Forscher P, Dufresne E. Dynamic peripheral traction forces balance stable neurite tension in regenerating Aplysia bag cell neurons. Sci Rep 2014;4:1–8.

[216] Koch TM, Münster S, Bonakdar N, Butler JP, Fabry B. 3D Traction forces in cancer cell invasion. PLoS One 2012;7:e33476.

[217] Hall MS, Long R, Hui C-Y, Wu M. Mapping Three-Dimensional Stress and Strain Fields within a Soft Hydrogel Using a Fluorescence Microscope. Biophys J 2014;102:2241–50.

[218] Feng X, Hall MS, Wu M, Hui C-Y. An adaptive algorithm for tracking 3D bead displacements: application in biological experiments. Meas Sci Technol 2014;25:055701.

[219] Sabass B, Gardel ML, Waterman CM, Schwarz US. High resolution traction force microscopy based on experimental and computational advances. Biophys J 2008;94:207–20.

[220] Hall MS, Long R, Feng X, Huang Y, Hui C-Y, Wu M. Toward single cell traction microscopy within 3D collagen matrices. Exp Cell Res 2013;319:2396–408.

[221] Yang Z, Lin J-S, Chen J, Wang JH-C. Determining substrate displacement and cell traction fields--a new approach. J Theor Biol 2006;242:607–16.

[222] Toyjanova J, Bar-Kochba E, López-Fagundo C, Reichner J, Hoffman-Kim D, Franck C. High Resolution, Large Deformation 3D Traction Force Microscopy. PLoS One 2014;9:e90976.

[223] Franck C, Maskarinec S a, Tirrell D a, Ravichandran G. Three-dimensional traction force microscopy: a new tool for quantifying cell-matrix interactions. PLoS One 2011;6:e17833.

[224] Lesman A, Notbohm J, Tirrell D a, Ravichandran G. Contractile forces regulate cell division in three-dimensional environments. J Cell Biol 2014;205:155–62.

[225] Legant WR, Miller JS, Blakely BL, Cohen DM, Genin GM, Chen CS. Measurement of mechanical tractions exerted by cells in three-dimensional matrices. Nat Methods 2010;7.

[226] Zeng D, Ferrari A, Ulmer J, Veligodskiy A, Fischer P, Spatz J, et al. Three-dimensional modeling of mechanical forces in the extracellular matrix during epithelial lumen formation. Biophys J 2006;90:4380–91.

[227] Nam YS, Park TG. Porous biodegradable polymeric scaffolds prepared by thermally induced phase separation. J Biomed Mater Res 1999;47:8–17.

[228] Smith LA, Ma PX. Nano-fibrous scaffolds for tissue engineering. Colloids Surfaces B Biointerfaces 2004;39:125–31.

[229] Ma PX, Zhang R. Synthetic nano-scale fibrous extracellular matrix. J Biomed Mater Res 1999;46:60–72.

[230] Yang F, Murugan R, Ramakrishna S, Wang X, Ma YX, Wang S. Fabrication of nano-structured porous PLLA scaffold intended for nerve tissue engineering. Biomaterials 2004;25:1891–900.

[231] La Carrubba V, Pavia FC, Brucato V, Piccarolo S. PLLA/PLA scaffolds prepared via Thermally Induced Phase Separation (TIPS): tuning of properties and biodegradability. Int J Mater Form 2008;1:619–22.

[232] He L, Zhang Y, Zeng X, Quan D, Liao S, Zeng Y, et al. Fabrication and characterization of poly (L-lactic acid) 3D nanofibrous scaffolds with controlled architecture by liquid-liquid phase separation from a ternary polymer-solvent system. Polymer (Guildf) 2009;50:4128–38.

[233] Budyanto L, Goh YQ, Ooi CP. Fabrication of porous poly (L-lactide)(PLLA) scaffolds for tissue engineering using liquid–liquid phase separation and freeze extraction. J Mater Sci Mater Med 2009;20:105–11.

[234] Schugens C, Maquet V, Grandfils C, Jérôme R, Teyssie P. Polylactide macroporous biodegradable implants for cell transplantation. II. Preparation of polylactide foams by liquid-liquid phase separation. J Biomed Mater Res 1996;30:449–61.

[235] Hua FJ, Kim GE, Lee JD, Son YK, Lee DS. Macroporous poly (L-lactide) scaffold 1. Preparation of a macroporous scaffold by liquid–liquid phase separation of a PLLA–dioxane–water system. J Biomed Mater Res 2002;63:161–7.

[236] Iordan A, Duperray A, Gérard A, Grichine A, Verdier C. Breakdown of cell-collagen networks through collagen remodeling. Biorheology 2010;47:277–95.

[237] Storm C, Pastore JJ, MacKintosh FC, Lubensky TC, Janmey PA. Nonlinear elasticity in biological gels. Nature 2005;435:191–4.

[238] Chen DTN, Wen Q, Janmey P a., Crocker JC, Yodh AG. Rheology of Soft Materials. Annu Rev Condens Matter Phys 2010;1:301–22.

[239] Onck PR, Koeman T, van Dillen T, van der Giessen E. Alternative Explanation of Stiffening in Cross-Linked Semiflexible Networks. Phys Rev Lett 2005;95:178102.

[240] Ethier CR, Simmons CA. Introductory biomechanics: from cells to organisms. Cambridge: Cambridge University Press; 2007.

[241] Murphy G, Nagase H. Progress in matrix metalloproteinase research. Mol Aspects Med 2008;29:290–308.

[242] Gelse K. Collagens—structure, function, and biosynthesis. Adv Drug Deliv Rev 2003;55:1531–46.

[243] Wang Y, Discher DE. Methods in Cell Biology. Cell Mechanics. Vol 83. Amsterdam: Elsevier Academic Press; 2007.

[244] Trappmann B, Gautrot JE, Connelly JT, Strange DGT, Li Y, Oyen ML, et al. Extracellular-matrix tethering regulates stem-cell fate. Nat Mater 2012;11:642–9.

[245] Wen JH, Vincent LG, Fuhrmann A, Choi YS, Hribar KC, Taylor-Weiner H, et al. Interplay of matrix stiffness and protein tethering in stem cell differentiation. Nat Mater 2014;13.

[246] Tse JR, Engler AJ. Preparation of Hydrogel Substrates with Tunable Mechanical Properties. Curr. Protoc. Cell Biol., John Wiley & Sons, Inc.; 2001.

[247] Haddad YM. Viscoelasticity of engineering materials. 1st ed. London: Chapman & Hall; 1995.

[248] Zhou L, Sawaguchi S, Twining SS, Sugar J, Feder RS, Yue BY. Expression of degradative enzymes and protease inhibitors in corneas with keratoconus. Investig Ophthalmol Vis Sci 1998;39 :1117–24.

[249] Cristina Kenney M, Brown DJ. The cascade hypothesis of keratoconus. Cont Lens Anterior Eye 2003;26:139–46.

[250] Efron N, Hollingsworth JG. New perspectives on keratoconus as revealed by corneal confocal microscopy. Clin Exp Optom 2008;91:34–55.

[251] Engler AJ, Sen S, Sweeney HL, Discher DE. Matrix elasticity directs stem cell lineage specification. Cell 2006;126:677–89.

[252] Shih Y-R V, Tseng K-F, Lai H-Y, Lin C-H, Lee OK. Matrix stiffness regulation of integrin-mediated mechanotransduction during osteogenic differentiation of human mesenchymal stem cells. J Bone Miner Res 2011;26:730–8.

[253] Jacot JG, McCulloch AD, Omens JH. Substrate stiffness affects the functional maturation of neonatal rat ventricular myocytes. Biophys J 2008;95:3479–87.

[254] Aratyn-Schaus Y, Oakes PW, Stricker J, Winter SP, Gardel ML. Preparation of Complaint Matrices for Quantifying Cellular Contraction. J Vis Exp 2010:e2173.

[255] Domke J, Radmacher M. Measuring the Elastic Properties of Thin Polymer Films with the Atomic Force Microscope. Langmuir 1998;14:3320–5.

[256] Solon J, Levental I, Sengupta K, Georges PC, Janmey PA. Fibroblast adaptation and stiffness matching to soft elastic substrates. Biophys J 2007;93:4453–61.

[257] Tanti NC, Jones L, Gorbet MB. Impact of Multipurpose Solutions Released from Contact Lenses on Corneal Cells. Optom Vis Sci 2011;88.

[258] Darzynkiewicz Z, Bruno S, Del Bino G, Gorczyca W, Hotz M a, Lassota P, et al. Features of apoptotic cells measured by flow cytometry. Cytometry 1992;13:795–808.

[259] Pubhshers ES, Pagliacci C. A rapid and simple method for measuring thymocyte apoptosis by propidium iodide staining and flow cytometry. J Immunol Methods 1991;139:271–9.

[260] Last JA, Liliensiek SJ, Nealey PF, Murphy CJ. Determining the mechanical properties of human corneal basement membranes with atomic force microscopy. J Struct Biol 2009;167:19–24.

[261] Spoerl E, Huhle M, Seiler T. Induction of cross-links in corneal tissue. Exp Eye Res 1998;66:97–103.

[262] Carpen O. Association of intercellular adhesion molecule-1 (ICAM-1) with actin- containing cytoskeleton and alpha-actinin. J Cell Biol 1992;118:1223–34.

[263] Yannariello-brown J, Hallberg CK, Häberle H, Brysk MM, Jiang Z, Patel JA, et al. Cytokine modulation of human corneal epithelial cell ICAM-1 (CD54) expression. Exp Eye Res 1998;67:383–93.

[264] Brodie C, Blumberg PM. Regulation of cell apoptosis by protein kinase c δ. Apoptosis 2003;8:19–27.

[265] Hengartner MO. The biochemistry of apoptosis. Nature 2000;407:770–6.

[266] Schwartzman RA, Cidlowski JA. Apoptosis: The Biochemistry and Molecular Biology of Programmed Cell Death. Endocr Rev 1993;14:133–51.

[267] Kim WJ, Rabinowitz YS, Meisler DM, Wilson SE. Keratocyte apoptosis associated with keratoconus. Exp Eye Res 1999;69:475–81.

[268] Riedl SJ, Shi Y. Molecular mechanisms of caspase regulation during apoptosis. Nat Rev Mol Cell Biol 2004;5:897–907.

[269] Thornberry NA, Lazebnik Y. Caspases: Enemies Within. Sci 1998;281 :1312–6.

[270] Shi L, Yu X, Yang H, Wu X. Advanced Glycation End Products Induce Human Corneal Epithelial Cells Apoptosis through Generation of Reactive Oxygen Species and Activation of JNK and p38 MAPK Pathways. PLoS One 2013;8:e66781.

[271] Buddi R, Lin B, Atilano SR, Zorapapel NC, Kenney MC, Brown DJ. Evidence of Oxidative Stress in Human Corneal Diseases. J Histochem Cytochem 2002;50 :341–51.

[272] Shin YJ, Seo JM, Chung TY, Hyon JY, Wee WR. Effect of Cysteamine on Oxidative Stress-induced Cell Death of Human Corneal Endothelial Cells. Curr Eye Res 2011;36:910–7.

[273] Risca VI, Wang EB, Chaudhuri O, Chia JJ, Geissler PL, Fletcher DA. Actin filament curvature biases branching direction. Proc Natl Acad Sci U S A 2012;109:2913–8.

[274] Gardel ML, Schneider IC, Aratyn-Schaus Yvonne, Waterman CM. Mechanical Integration of Actin and Adhesion Dynamics in Cell Migration. Annu Rev Cell Dev Biol 2010;26:315–33.

[275] Molladavoodi S, Medley J, Gorbet M, Kwon HJ. Mechanotransduction in Corneal Epithelial Cells. Proc. ASME 2013 Int. Mech. Eng. Congr. Expo. IMECE2013, 2014, p. 1–5.

[276] Stepp MA. Corneal integrins and their functions. Exp Eye Res 2006;83:3–15.

[277] Goldfinger LE, Hopkinson SB, deHart GW, Collawn S, Couchman JR, Jones JC. The alpha3 laminin subunit, alpha6beta4 and alpha3beta1 integrin coordinately regulate wound healing in cultured epithelial cells and in the skin. J Cell Sci 1999;112 :2615–29.

[278] Friedland JC, Lee MH, Boettiger D. Mechanically Activated Integrin Switch Controls α5β1 Function. Sci 2009;323 :642–4.

[279] Bouaouina M, Lad Y, Calderwood DA. The N-terminal Domains of Talin Cooperate with the Phosphotyrosine Binding-like Domain to Activate β1 and β3 Integrins. J Biol Chem 2008;283 :6118–25.

[280] Watanabe M, Kondo S, Mizuno K, Yano W, Nakao H, Hattori Y, et al. Promotion of Corneal Epithelial Wound Healing In Vitro and In Vivo by Annexin A5. Investig Ophthalmol Vis Sci 2006;47 :1862–8.

[281] Lu L, Reinach PS, Kao WW-Y. Corneal Epithelial Wound Healing. Exp Biol Med 2001;226 :653–64.

[282] Lautscham LA, Lin CY, Auernheimer V, Naumann CA, Goldmann WH, Fabry B. Biomembrane-mimicking lipid bilayer system as a mechanically tunable cell substrate. Biomaterials 2014;35:3198–207.

[283] Boudreau HE, Casterline BW, Rada B, Korzeniowska A, Leto TL. Nox4 involvement in TGF-beta and SMAD3-driven induction of the epithelial-to-mesenchymal transition and migration of breast epithelial cells. Free Radic Biol Med 2012;53:1489–99.

[284] Platten M, Wick W, Wild-Bode C, Aulwurm S, Dichgans J, Weller M. Transforming growth factors beta(1) (TGF-beta(1)) and TGF-beta(2) promote glioma cell migration via Up-regulation of alpha(V)beta(3) integrin expression. Biochem Biophys Res Commun 2000;268:607–11.

[285] Muller M. Introduction to confocal fluorescence microscopy. 2nd ed. CN. Bellingham, Wash.: SPIE Press; 2006.

[286] Fujimoto JG, Farkas DL. Biomedical optical imaging. Oxford: Oxford University Press; 1986.

[287] Han Y, Rogalsky AD, Zhao B, Kwon HJ. The application of digital image techniques to determine the large stress–strain behaviors of soft materials. Polym Eng Sci 2012;52:826–34.

[288] Berfield TA, Patel JK, Shimmin RG, Braun P V, Lambros J, Sottos NR. Micro- and Nanoscale Deformation Measurement of Surface and Internal Planes via Digital Image Correlation. Exp Mech 2007;47:51–62.

[289] Zhang D, Arola DD. Applications of digital image correlation to biological tissues. J Biomed Opt 2004;9:691–9.

[290] Thompson MS, Schell H, Lienau J, Duda GN. Digital image correlation: a technique for determining local mechanical conditions within early bone callus. Med Eng Phys 2007;29:820–3.

[291] Papanikolopoulos N. Selection of features and evaluation of visual measurements during robotic visual servoing tasks. J Intell Robot Syst 1995;13:279–304.

[292] Lucas BD. An iterative image registration technique with an application to stereo vision. Imaging 1981;130:121–9.

[293] Lewis JP. Fast Template Matching. Vis. interface, Quebec City, Canada: 1995, p. 120–3.

[294] Gonzalez RC. Digital image processing using MATLAB. Upper Saddle River, N.J.: Pearson Prentice Hall; 2004.

[295] Qidwai U. Digital image processing : an algorithmic approach with MATLAB. Boca Raton: CRC Press; 2010.

[296] Niblack W. An introduction to digital image processing. Englewood Cliffs, N.J.: Prentice-Hall International; 1986.

[297] Briechle K, Hanebeck UD. Template Matching using Fast Normalized Cross Correlation 2001:95–102.

[298] Bay BK. Methods and applications of digital volume correlation. J Strain Anal Eng Des 2008;43:745–60.

[299] Bay BK, Smith TS, Fyhrie DP, Saad M. Digital volume correlation: Three-dimensional strain mapping using X-ray tomography. Exp Mech 1999;39:217–26.

[300] Liu L, Morgan EF. Accuracy and precision of digital volume correlation in quantifying displacements and strains in trabecular bone. J Biomech 2007;40:3516–20.

[301] Yaofeng S, Pang JHL. Study of optimal subset size in digital image correlation of speckle pattern images. Opt Lasers Eng 2007;45:967–74.

[302] Gillard F, Boardman R, Mavrogordato M, Hollis D, Sinclair I, Pierron F, et al. The application of digital volume correlation (DVC) to study the microstructural behaviour of trabecular bone during compression. J Mech Behav Biomed Mater 2014;29:480–99.

[303] Kwon HJ. Application of Digital Volume Correlation Algorithm to cell mechanics. ASME 2009 Int. Mech. Eng. Congr. Expo. Vol. 11 Mech. Solids, Struct. Fluids, vol. C, Lake Buena Vista, Florida: ASME; 2009, p. 1–7.

[304] Kong HJ, Polte TR, Alsberg E, Mooney DJ. FRET measurements of cell-traction forces and nano-scale clustering of adhesion ligands varied by substrate stiffness. Proc Natl Acad Sci U S A 2005;102:4300–5.

[305] Schwarz US, Balaban NQ, Riveline D, Bershadsky a, Geiger B, Safran S a. Calculation of forces at focal adhesions from elastic substrate data: the effect of localized force and the need for regularization. Biophys J 2002;83:1380–94.

[306] Apel K, Hirt H. Reactive Oxygen Species: Metabolism, Oxidative Stress, and Signal Transduction. Annu Rev Plant Biol 2004;55:373–99.

[307] Hoebe RA, Van Oven CH, Gadella TWJ, Dhonukshe PB, Van Noorden CJF, Manders EMM. Controlled light-exposure microscopy reduces photobleaching and phototoxicity in fluorescence live-cell imaging. Nat Biotech 2007;25:249–53.

[308] Ditlbacher H, Krenn JR, Felidj N, Lamprecht B, Schider G, Salerno M, et al. Fluorescence imaging of surface plasmon fields. Appl Phys Lett 2002;80:404.

[309] Price JH, Gough D a. Comparison of phase-contrast and fluorescence digital autofocus for scanning microscopy. Cytometry 1994;16:283–97.

[310] Kreft M, Stenovec M, Zorec R. Focus-Drift Correction in Time-Lapse Confocal Imaging. Ann N Y Acad Sci 2005;1048:321–30.

[311] Mason DC, Green DK. Automatic Focusing of a Computer-Controlled Microscope. Biomed Eng IEEE Trans 1975;BME-22:312–7.

[312] Stephens DJ, Allan VJ. Light Microscopy Techniques for Live Cell Imaging. Sci 2003;300 :82–6.

[313] Molladavoodi S, Gorbet M, Medley J, Kwon HJ. Investigation of microstructure, mechanical properties and cellular viability of poly(L-lactic acid) tissue engineering scaffolds prepared by different thermally induced phase separation protocols. J Mech Behav Biomed Mater 2013;17:186–97.

[314] Cheung HY, Lau KT, Lu TP, Hui D. A critical review on polymer-based bio-engineered materials for scaffold development. Compos Part B Eng 2007;38:291–300.

[315] Liu X, Smith L, Wei G, Won Y, Ma PX. Surface engineering of nano-fibrous poly (L-lactic acid) scaffolds via self-assembly technique for bone tissue engineering. J Biomed Nanotechnol 2005;1:54–60.

[316] Tu C, Cai Q, Yang J, Wan Y, Bei J, Wang S. The fabrication and characterization of poly (lactic acid) scaffolds for tissue engineering by improved solid–liquid phase separation. Polym Adv Technol 2003;14:565–73.

[317] Guan L, Davies JE. Preparation and characterization of a highly macroporous biodegradable composite tissue engineering scaffold. J Biomed Mater Res Part A 2004;71:480–7.

[318] Wei G, Ma PX. Partially nanofibrous architecture of 3D tissue engineering scaffolds. Biomaterials 2009;30:6426–34.

[319] Liu X, Smith LA, Hu J, Ma PX. Biomimetic nanofibrous gelatin/apatite composite scaffolds for bone tissue engineering. Biomaterials 2009;30:2252–8.

[320] Mooney DJ, Baldwin DF, Suh NP, Vacanti JP, Langer R. Novel approach to fabricate porous sponges of poly (-lactic-co-glycolic acid) without the use of organic solvents. Biomaterials 1996;17:1417–22.

[321] Xu H, Han D, Dong JS, Shen GX, Chai G, Yu ZY, et al. Rapid prototyped PGA/PLA scaffolds in the reconstruction of mandibular condyle bone defects. Int J Med Robot Comput Assist Surg 2010;6:66–72.

[322] Inai R, Kotaki M, Ramakrishna S. Structure and properties of electrospun PLLA single nanofibres. Nanotechnology 2005;16:208.

[323] Yang F, Murugan R, Wang S, Ramakrishna S. Electrospinning of nano/micro scale poly (L-lactic acid) aligned fibers and their potential in neural tissue engineering. Biomaterials 2005;26:2603–10.

[324] Goh YQ, Ooi CP. Fabrication and characterization of porous poly (l-lactide) scaffolds using solid–liquid phase separation. J Mater Sci Mater Med 2008;19:2445–52.

[325] Chen VJ, Ma PX. Nano-fibrous poly (L-lactic acid) scaffolds with interconnected spherical macropores. Biomaterials 2004;25:2065–73.

[326] Gunatillake PA, Adhikari R. Biodegradable synthetic polymers for tissue engineering. Eur Cells Mater 2003;5:1–16.

[327] Hu J, Liu X, Ma PX. Induction of osteoblast differentiation phenotype on poly (L-lactic acid) nanofibrous matrix. Biomaterials 2008;29:3815–21.

[328] Ma PX. Scaffolds for tissue fabrication. Mater Today 2004;7:30–40.

[329] Schugens C, Maquet V, Grandfils C, Jérôme R, Teyssie P. Biodegradable and macroporous polylactide implants for cell transplantation: 1. Preparation of macroporous polylactide supports by solid-liquid phase separation. Polymer (Guildf) 1996;37:1027–38.

[330] Park JE, Todo M. Development and characterization of reinforced poly (l-lactide) scaffolds for bone tissue engineering. J Mater Sci Mater Med 2011;22:1171–82.

[331] Ramzi M, Rochas C, Guenet JM. Structure-properties relation for agarose thermoreversible gels in binary solvents. Macromolecules 1998;31:6106–11.

[332] Kwon HJ, Rogalsky AD, Kovalchick C, Ravichandran G. Application of digital image correlation method to biogel. Polym Eng Sci 2010;50:1585–93.

[333] Dowling NE. Mechanical behavior of materials : engineering methods for deformation, fracture, and fatigue. Englewood Cliffs, N.J.: Prentice Hall; 2007.

[334] Sharma S, Mohanty S, Gupta D, Jassal M, Agrawal AK, Tandon R. Cellular response of limbal epithelial cells on electrospun poly-ε-caprolactone nanofibrous scaffolds for ocular surface bioengineering: a preliminary in vitro study. Mol Vis 2011;17:2898.

[335] Yang J, Shi G, Bei J, Wang S, Cao Y, Shang Q, et al. Fabrication and surface modification of macroporous poly (L-lactic acid) and poly (L-lactic-co-glycolic acid)(70/30) cell scaffolds for human skin fibroblast cell culture. J Biomed Mater Res 2002;62:438–46.

[336] Maquet V, Martin D, Malgrange B, Franzen R, Schoenen J, Moonen G, et al. Peripheral nerve regeneration using bioresorbable macroporous polylactide scaffolds. J Biomed Mater Res 2000;52:639–51.

[337] Kim K, Yu M, Zong X, Chiu J, Fang D, Seo YS, et al. Control of degradation rate and hydrophilicity in electrospun non-woven poly (D,L-lactide) nanofiber scaffolds for biomedical applications. Biomaterials 2003;24:4977–85.

[338] Wang JH-C, Lin J-S. Cell traction force and measurement methods. Biomech Model Mechanobiol 2007;6:361–71.

[339] Molladavoodi S, Kwon H-J, Medley J, Gorbet M. Human corneal epithelial cell response to substrate stiffness. Acta Biomater 2015;11:324–32.

[340] Han Y, Kim D-W, Kwon H-J. Application of digital image cross-correlation and smoothing function to the diagnosis of breast cancer. J Mech Behav Biomed Mater 2012;14:7–18.

[341] Montgomery DC. Design and analysis of experiments. 7th edi. Hoboken, NJ: John Wiley & Sons, Inc.; 2009.